A METHODOLOGY TO ASSESS SEISMIC RISK FOR POPULATIONS OF UNREINFORCED MASONRY BUILDINGS

BY

ÖMER ONUR ERBAY

B.S., Middle East Technical University, 1997
M.S., Middle East Technical University, 1999

REPORT   07-10

Mid-America Earthquake Center
Civil and Environmental Engineering
University of Illinois at Urbana-Champaign, 2004

Urbana, Illinois

ABSTRACT

**A METHODOLOGY TO ASSESS SEISMIC RISK FOR
POPULATIONS OF UNREINFORCED MASONRY BUILDINGS**

A regional risk/loss assessment methodology that utilizes easily obtainable physical properties of clay brick unreinforced masonry buildings is developed.

The steps of the proposed risk/loss assessment methodology are based on comprehensive sensitivity investigations that are conducted on building as well as region specific parameters. From these investigations, the most significant factors for regional risk/loss estimations are identified and the number of essential parameters that is required by the proposed methodology is reduced.

Parameter distributions for global and local properties of unreinforced masonry buildings at urban regions of the United States are defined. From these distributions building populations are generated and they are used in sensitivity investigations. A simple analytical model representing dynamic characteristics of unreinforced masonry buildings is utilized to carry out the sensitivity investigations. A procedure that utilizes response estimates from analytical calculations is laid out to evaluate building damage for in-plane and for out-of-plane actions. An example building evaluation is provided to illustrate the steps of the proposed procedure.

The developed regional risk/loss assessment methodology is demonstrated on a small town in Italy that was recently shaken by two moderate size earthquakes. From data collection to utilization of generated hazard-loss relationships, the steps of the methodology are demonstrated from the perspective of a stakeholder. Estimated losses are compared with the field data.

Analytical investigations have shown that due to total risk/loss concept, hazard-loss relationships that are unacceptably scattered for individual building loss calculations can be utilized to estimate risk/loss at regional level. This statement is proven to be valid especially for building populations that possess low-level correlation in terms of their dynamic response characteristics. Furthermore, sensitivity investigations on biased building populations have

shown that among investigated parameters, 1) ground motion categories, 2) number of stories, 3) floor aspect ratio and 4) wall area to floor area ratio are the most significant parameters in regional risk/loss calculations.

ACKNOWLEDGEMENTS

TABLE OF CONTENTS

LIST OF FIGURES

xi

xiv

LIST OF TABLES

CHAPTER 1 INTRODUCTION

1.1 Statement of the problem

Over the last century, the experience gained from past earthquakes and the knowledge acquired through ongoing research have significantly enhanced our understanding on earthquake design, evaluation, and mitigation. Throughout the course of this evolution, design codes and construction practices have been considerably updated to address deficiencies of the built environment. Such improvement resulted in better performing buildings and safer communities however, deficiencies and lack of seismic design in the existing buildings continue to threaten the safety of our societies and the economy.

The dilemma is to decide what to do with the existing built environment that was not designed for seismic actions either due to lack of knowledge or unawareness of the threat. To effectively address this issue, non-engineering decision makers need means to estimate the consequences that are associated with future earthquakes over a specific region. This requires simple yet accurate regional risk/loss assessment methodologies. Through such methodologies, decision makers may pose "what if" type questions to identify critical zones and components of their region. Determination of these critical zones and components are essential to layout effective and economical loss mitigation strategies.

One major effort in development of such risk/loss estimation tools was conducted in HAZUS earthquake loss estimation methodology that was funded by the Federal Emergency Management Agency, FEMA (1997). In this methodology, regional loss is estimated through utilizing vulnerability relationships that are defined for different classes of buildings. For most building classes these vulnerability relationships are empirically defined from expert opinions. Such opinion based vulnerability functions are highly static, *i.e.* do not provide flexibility for further development with advanced knowledge, and direct, *i.e.* do not possess information regarding intermediate steps that identify the hazard – damage relationships. These drawbacks hamper the evaluation of uncertainty and likewise the accuracy of loss estimates. To overcome these issues, vulnerability functions have to be developed through rational analyses that are conducted on robust and analytically sound models of buildings. Such investigations allow identification of the significant building parameters for loss

calculations. Furthermore, being explicit in terms of intermediate steps, they allow understanding of the level of uncertainties at various stages of calculations. Through incorporation of new knowledge, these uncertainties can be reduced to improve the accuracy of loss estimates.

Among construction types, unreinforced masonry buildings need special attention primarily because of their high seismic vulnerability as observed in numerous past earthquakes (Abrams 2001, Bruneau 1994-1995, Bruneau and Lamontagne 1994). Prior to 1950's the majority of these buildings were designed only for gravity loads without considering the seismic effects. After this period, seismic design principles were introduced into building codes. The adaptation process to the new seismic provisions was quick in regions like the western coast of the United States in which earthquakes occur frequently. However, this was not the case for regions like the central and eastern United States where potential catastrophic seismic events occur infrequently. As a result, even after 1950's, many buildings were still engineered to support only the gravity actions. Currently, these buildings constitute approximately 30-40% of the existing building population in the United States, Canada, and similarly in other parts of the World.

Over the last few decades, significant knowledge has been gained on seismic response characteristics of unreinforced masonry buildings. However, a rational and comprehensive investigation to develop simple risk/loss assessment methodology for populations of unreinforced masonry buildings has been lacking.

1.2 Objectives and scope

The primary objective of this study is to develop a methodology that utilizes easily obtainable physical properties of unreinforced masonry buildings to assess their regional seismic risk/loss potential.

Research is focused towards old existing clay brick unreinforced masonry buildings that have material, configuration, and construction characteristics similar to the ones found in urban regions of the United States. In general, these buildings were constructed in the late 19th to early 20th century. Typically, these buildings contain wood floor construction that results in

2

flexible diaphragm response. Such flexible diaphragm response imposes increased demands on components that are orthogonal to the direction of shaking. Even though the focus is concentrated on unreinforced masonry buildings the approach is general and can be applied to develop similar risk/loss assessment methodologies for other construction types.

Within the scope of this study, a comprehensive sensitivity investigation is conducted on building as well as region specific parameters. Simple analytical models that have 3 horizontal degrees of freedom per each story are utilized to conduct these investigations. Nonlinear dynamic time history analysis is utilized to estimate the seismic response of buildings. Vulnerability of buildings is investigated for both in-plane and out-of-plane actions. Torsion, soil-structure interaction, and the affects of vertical accelerations are not considered.

Hazard level is represented by the spectral acceleration at the fundamental period of buildings. A suite of ground motions is used to represent the variations in ground shaking characteristics. These ground motions are selected from various combinations of PGA/PGV, distance, magnitude, and soil properties.

1.3 Organization of the report

In general, the chapters of the report can be grouped in to four: Chapter 2, Chapter 3-4-5, Chapter 6-7, and Chapter 8.

Chapter 2 provides background on vulnerability evaluation and risk/loss calculations. Different loss assessment approaches are summarized and contrasted with each other. The chapter then introduces the total loss/risk concept, the thrusting idea that is utilized to reduce the number of essential parameters for regional loss assessment calculations. Based on total risk/loss concept, a framework for sensitivity analyses is presented. Finally, the preliminary version of the proposed regional risk/loss assessment methodology is provided.

Chapters 3, 4, and 5 include theoretical derivations and investigations that provide the rational basis to simplify and fine tune the proposed methodology. First part of Chapter 3 provides background on analytical idealization, damage categorization, and loss estimation methods for unreinforced masonry buildings. Second part of Chapter 3 presents the theoretical derivations

for a generic loss evaluation procedure. Steps of this procedure is outlined and demonstrated at the end of Chapter 3. Chapter 4 gathers information about typical unreinforced masonry building properties at urban regions of the United States. Base on collected data, generic distributions representing important parameters of unreinforced masonry buildings are presented. This chapter also provides a randomization procedure and demonstrates likely outcomes with two building populations. Chapter 5 utilizes procedures that are developed in Chapters 3 and 4 to conduct sensitivity investigations on building and region parameters. The results of these sensitivity investigations are utilized to finalize the steps of the proposed methodology.

Chapter 6, introduces the final version of the proposed regional loss/risk assessment methodology. The steps are explained together with the key relationships and tools of the methodology. This chapter is written as independent as from rest of the report and, therefore, can be regarded as the user's manual of the developed methodology. In Chapter 7, the developed risk/loss estimation methodology is demonstrated on a small town in Italy. The demonstration is carried out from the perspective of a decision-maker. The calculated loss estimates are compared with the collected damage data from the field.

Chapter 8 summarizes the findings and conclusions of this study and provides suggestions for future research.

CHAPTER 2 SEISMIC RISK ASSESSMENT FOR POPULATIONS OF BUILDINGS

2.1 Introduction

The evaluation of seismic risk for building populations typically involves estimation and summation of expected losses due to all possible earthquakes within the region of the building population. For a given region the occurrence of earthquakes and their consequences are mutually exclusive and collectively exhaustive events. Therefore, the previous statement can be expressed in terms of the total probability theory as follows:

$$\text{Total Seismic Risk} = \sum_{\substack{\text{for all possible} \\ \text{hazard levels}}} E\left(\text{Loss} \mid \text{Hazard} = H_i\right) \cdot P\left(\text{Hazard} = H_i\right) \qquad (2.1)$$

In the above expression the term $E\left(\text{Loss} \mid \text{Hazard} = H_i\right)$ is the expected amount of losses, consequences, for a given level of hazard, H_i and the term $P\left(\text{Hazard} = H_i\right)$ is the probability of getting a hazard level of H_i. How to <u>quantify</u> the loss and the hazard terms and <u>estimate</u> the relationship between them would be the immediate questions that one might pose. The answer highly depends on the purpose of the investigation (stakeholder needs), the form of the available data, and level of accessible technology (Abrams et al 2002). For a scenario-based investigation, for a particular hazard level, the summation term in Eq 2.1 drops down since there is only one possible event. The resulting risk term will be the seismic risk for that particular scenario.

In the case of quantifying the level of seismic hazard, commonly two approaches have been utilized: 1) the use of scale measures, such as in the case of Modified Mercalli Intensity (MMI) and European Macroseismic Intensity (EMS-98) scales, 2) the use of quantitative parameter that represents the magnitude of a certain property of the seismic action, ground motion, such as the peak ground acceleration or velocity (PGA, PGV) and spectral acceleration or velocity at a specified period and damping (S_a, S_d). In the first approach the hazard level is defined in qualitative terms and therefore is susceptible to judgmental errors. The second approach eliminates these subjective errors however, it has its own limitations due

to incompleteness in the historic seismic data. In the absence of complete historic seismic data, a typical approach is to combine available data with analytical models that characterizes the fault mechanism and the attenuation relationships of the region. Over the last century, significant progress has been achieved both in data collection process and in analytical modeling of the hazard phenomena. United States Geological Survey, USGS (1997), uniform seismic hazard maps are the products of similar investigation in which extensive available seismic data is enhanced in view of the most current analytical models and simulation techniques. In these seismic maps, quantitative parameters of earthquakes for different regions are provided for different hazard levels. Each hazard level is represented by an earthquake having a different return period. The longer the return period (the lower the probability of getting the earthquake) is, the higher the hazard level. Owing to the information that these maps provide, they are highly suitable for regional seismic risk investigation studies and therefore will be utilized in this study. Through use of these maps, one can estimate the quantitative parameters of the seismic hazard for a given probability of occurrence, the second term in Eq. 2.1. The only remaining term is the quantification and estimation of losses for a given level of hazard, the first term in Eq. 2.1.

Depending on the stakeholder needs and the purpose of the risk investigation, the term "loss" can be represented by different measures (Abrams 2002, Gülkan 1992, Holmes 1996, 2000, Plessier 2002). These representations may include repair/replacement cost of the damaged buildings, number of people killed, number of homeless people, degree of environmental pollution, number of trucks necessary to remove the debris, and many other possible measures that might be useful in understanding the consequences of a seismic event and setting up proper mitigation strategies to reduce these consequences. As can be deduced from a wide range of different loss definitions, the task of estimating seismic risk can be very broad and implementation may require interactions of various disciplines. To isolate the interaction within structural engineering field, the focus, in this report, is concentrated on the losses that are represented by percent replacement cost of buildings. Typically, losses that are associated with direct building damage are approximately 25-35% of total regional losses.

The next section will summarize the earlier studies that have been conducted to estimate losses for a given hazard level. The following sections will discuss the differences in regional

and building specific seismic risk investigations and will introduce the proposed risk/loss assessment methodology and the verification framework. The verification framework will be utilized in Chapter 5 to investigate the sensitivity of certain parameters on regional seismic risk/loss estimations. The proposed methodology has been developed and refined in view of these sensitivity investigations.

2.2 Previous work on developing hazard – loss relationships

There are commonly two types of approaches in determining the relationship between hazard and loss: 1) empirical and 2) analytical. Empirical based hazard – loss relationships are determined through statistical investigation of observational data that is collected after each major earthquake (Gülkan et al 1992, Hassan and Sozen 1997, Kiremidjian1985). In the absence of observational data, which is usually the case for higher levels of seismicity and infrequent events, engineering judgments and expert opinions are consulted to fill the gap. ATC-13 (1985) is the first attempt to compile the knowledge gained from past earthquakes with expert opinions. The damage probability matrices are used to represent the hazard loss relationships for 78 different building classes. A following study, ATC-21 (1988), utilized these relationships to develop a rapid screening procedure to identify potentially weak buildings in existing building populations through a scoring process.

Even though empirical based approaches provide a direct relationship between hazard and loss, the results are subjective and limited to specific building type, hazard level, and geologic condition. Extension of the developed hazard – loss relationships to different building types, geologic conditions, and hazard levels is not easy and usually generate relationships that are hard to update in the case of additional supporting data and knowledge. To overcome these drawbacks, more recent studies are heading towards hazard-loss relationships that are developed through an analytical procedure. In such an approach, analytical models that represent buildings are analyzed with different levels of hazard to estimate a relationship between hazard and loss (Hwang and Jaw 1990). The observational data from previous earthquakes are commonly used as supporting evidence for the obtained relationships. One advantage of generating hazard – loss relationships through an analytical procedure is that the uncertainties associated with each component of the process can be investigated and if

necessary can be improved with more refined analytical investigations. Whereas, with empirical based hazard – loss relationships, uncertainty in relationships are implicit and therefore are difficult to quantify. Table 2.1 highlights and compares the main characteristics of hazard – loss relationships developed using either empirical or analytical procedures. Due to its flexibility and potential for future development and use, the focus is given to analytical based hazard – loss relationships.

Table 2.1. Comparison of hazard – loss relationships that are developed based on empirical and analytical methods

Empirical	Analytical
• Based on observational data and expert opinion.	• Based on analytical models. The resulting relationships are verified through observational data.
• Hazard level is typically represented in qualitative terms such as, scale measures (MMI, MSK98) and magnitude (M_s, M_m).	• Hazard level is represented in quantitative terms such as, the ground motion parameters (eg. PGA, S_a, S_d) and return period of the earthquake (eg. 2% in 50 yrs).
• Direct relationship between hazard and loss. Sources of uncertainty are implicit and hard to identify.	• May consist of intermediate relationships to define the relationship between hazard and loss. Intermediate relationships are useful in understanding the sources of uncertainty.
• Hard to update and refine with additional knowledge and data; since intermediate relationships are implicit.	• Easy to update and refine with additional knowledge and data; since intermediate relationships are explicit.

In the broadest sense, development of analytical based hazard – loss relationships consists of developing three key relationships, hazard-demand, demand-damage, and damage-loss. These probabilistic relationships are combined to generate the hazard-loss relationship. Figure 2.1 presents typical flowchart and the key steps that are followed to develop such relationships. The first step of the process is to select a set of representative ground motion time histories that will capture the characteristics of the seismic hazard (frequency content, duration, magnitude) over the region. One major problem in selecting these ground motions is the sparseness of the recorded ground motions, especially for larger seismic events. To

overcome this issue, Fischer *et al.* 2002, Dumova-Jovanoska 2000, Abrams *et al.* 1997, Singhal and Kiremidjian 1996, and Howard and Jaw 1990 generated synthetic ground motions to represent the hazard. As an alternative to synthetically generated ground motions, Bazzurro and Cornell 1994, Dymiotis *et al.* 1998, 1999 used recorded ground motions and scaled them to fill the gap between large and medium level events. In such an approach, quantitative parameters of ground motions (PGA, S_a, S_d) are scaled up or down accordingly in order to generate the desired level of hazard from the recorded ones. There are also cases where a combined approach, synthetic and recorded ground motions, is utilized to represent the hazard (Mwafy and Elnashai 2001).

Hazard

Select ground motion time histories that represent the seismicity over the site or region

Parameters

Identify typical building configurations

Determine typical range of material and component properties

Demand

Estimate the variation of response parameters (demand) through dynamic or static analyses

Develop analytical models for dynamic or static analysis

Damage

Estimate the damage state for different levels of response parameters

Loss

Estimate losses associated with each damage level

Develop vulnerability relationships for different building parameters

Calculate the hazard – loss relationships that will be used in risk assessment investigations

Figure 2.1. General steps of developing analytical based hazard-loss curves

The question of whether scaled ground motions would represent the characteristics of real earthquakes that might occur at the scaled level has been a concern for many researchers.

9

Shome and Cornell (1998) conducted a systematic investigation on different scaling measures and their effects on dynamic response parameters of building structures. They selected two different sets of ground motions from two magnitude and distance intervals, 1) M=5.25-5.75, R=5-25km, 2) M=6.7-7.3, R=10-30km. Each ground motion data set was scaled up or down accordingly to the same level as the other set. The dynamic response parameters calculated from the scaled set were compared with the results obtained from the set that was kept at the original level. Basically three different scaling measures were investigated, 1) peak ground acceleration, 2) spectral acceleration at the fundamental building period, and 3) average spectral acceleration for a range of periods in the vicinity of the building's fundamental period. Comparison of the results has shown that scaling of ground motions from one level to another has small effect on the nonlinear displacement demand estimates of buildings. Among the scaling measures, the scaling based on spectral acceleration at the fundamental period of buildings with 5% damping level was suggested to be the most convenient and best alternative method. With reference to this conclusion and applicability to USGS hazard maps, scaling method based on spectral acceleration is used throughout this study.

Once seismic hazard is characterized through the selection or synthetic generation of ground motion set, the parameter identification step starts. The goal of this step is to identify the characteristic properties of the building class that is of interest. These properties typically involve parameters that might influence the dynamic response characteristics of buildings and may include configuration, geometry, weight/mass, and structural properties (stiffness, strength, deformation capacity) of the components. Due to random nature of construction, each parameter is represented by a best estimate, mean, and an associated probability distribution. For robust and comprehensive hazard – loss investigation, the uncertainty in each parameter should be investigated and reflected in the final relationships (Dymiotis *et al*. 1998,1999, Singhal and Kiremidjian 1996, Hwang and Jaw 1994, Kishi *et al*. 1999). The parameters that are critical for unreinforced masonry buildings are introduced and discussed in Chapters 3 and 4.

The parameter identification step is followed by the demand estimation step, also known as the response estimation step. In this step, analytical idealization and structural analysis methods are utilized to estimate the demand parameters of buildings. Due to randomness in

ground motion properties and building parameters, demand estimates are also random. The goal of this step is to characterize the variation in demand parameters for different levels of seismic hazard, i.e. the hazard-demand relationship. The demand parameters that have good correlation with observed damage are typically used in these relationships. Among possible alternatives, building drift (Abrams *et al.* 1997, Lang and Bachmann 2003, Yun *et al.* 2002), interstory drift (Calvi 1999, Fisher *et al.* 2002, Yun *et al.* 2002), ductility ratio (Hwang and Jaw 1990), and a form of damage index such as Park and Ang (Singhal and Kiremidjian 1996, Dumova-Jovanoska 2000) are commonly used demand parameters.

Table 2.2. Advantages and disadvantages of different analysis methods.

Analysis Method	Advantages	Disadvantages
Linear Static	• Computationally faster and less demanding than the nonlinear static analysis • Displacement based demand parameters	• Poor accuracy in capturing nonlinear behavior • No information on velocity, acceleration, and dissipated energy
Linear Dynamic	• Computationally faster and less demanding than nonlinear dynamic analysis • Displacement, velocity and acceleration based response parameters	• Low accuracy in capturing nonlinear behavior • No information on dissipated energy due to nonlinear effects
Nonlinear Static (Pushover)	• Computationally faster and less demanding than nonlinear dynamic analysis • Nonlinear effects • Displacement based demand parameters	• Limited consideration of ground motion parameters • No information on velocity and acceleration • Nonlinear modes can only be considered in special analysis methods (e.g. adaptive pushover analysis)
Nonlinear Dynamic	• Nonlinear effects • Displacement, velocity, and acceleration based demand parameters	• Computationally the most demanding and time-consuming

Depending on the type of demand parameters and the dynamic response characteristics of buildings (e.g. failure modes), different analytical models and analysis methods have been

used by researchers. FEMA-356 (2000) Prestandard for Seismic Rehabilitation and Evaluation of Existing Buildings, provides a list of commonly used analysis and analytical idealization methods. The advantages and disadvantages of these methods are summarized in Tables 2.2 and 2.3. As can be deducted from these tables, better precision requires more detailed analytical models, more information about buildings, and more computation time.

Table 2.3. Advantages and disadvantages of two commonly used analytical models to represent the dynamic response characteristics of buildings.

Idealization Method	Advantages	Disadvantages
Single degree of freedom (SDOF)	• Computationally faster and less demanding. • Typically requires less parameters to define the model	• May not capture contribution of other modes in nonlinear analysis. • Approximation due to assumed mode shapes especially in nonlinear analysis. • Different failure modes are implicitly considered.
Multiple degree of freedom (MDOF)	• May capture the effects of higher modes. • Multiple failure mechanisms may be modeled explicitly.	• Computationally more demanding and time-consuming. • Typically requires more parameters to define the model

The common approach in selecting methods and models for seismic risk investigation studies is to optimize the use of available information and computational resources in order to achieve an acceptable accuracy and precision. For example, Fisher et al (2002) suggested two analytical models to carry out seismic risk investigations for two different levels of analyses. The first model is intended to represent populations of buildings. In this model, the behavior of each story is modeled with a single inelastic element and the story masses are lumped at each floor level. The idea is to capture the global response characteristics with limited information, as it would be unlikely and impractical to have detailed information on each building in a given building population. The second model is intended to analyze individual buildings for which more detailed information is available. An inelastic three-dimensional frame model is suggested to idealize the buildings. In this model, each structural component

of the building is modeled with a single finite element and the mass tributary to each component is lumped at the ends of the elements. The goal of this model is to represent the global as well as the local dynamic response characteristics of the buildings. In both models, the building response parameters are estimated through nonlinear dynamic time history analyses conducted for selected set of ground motions. The analytical models and analysis techniques for unreinforced masonry buildings are discussed in detail in Chapter 3.

Table 2.4. FEMA building performance levels (damage categories) (Definitions are taken from FEMA-356, 2000)

Damage Category	Damage Definition
Immediate Occupancy (light)	The damage state in which only very limited structural damage has occurred. The basic vertical- and lateral-force-resisting systems of the building retain nearly all of their pre-earthquake strength and stiffness. Some minor structural repairs may be appropriate, these would generally not be required prior to reoccupancy.
Damage Control Range	The continuous range of damage states between the Life Safety Structural Performance Level and the Immediate Occupancy Structural Performance Level.
Life Safety (moderate)	The damage state in which significant damage to the structure has occurred, but some residual strength and stiffness left in all stories. Gravity-load-bearing elements function. No out-of-plane failure of walls or tipping of parapets. Some permanent drift. Damage to partitions. Building may be beyond economical repair.
Limited Safety Range	The continuous range of damage states between the Life Safety Structural Performance Level and the Collapse Prevention Structural Performance Level.
Collapse Prevention (severe)	The damage state in which the building has little residual stiffness and strength, but load-bearing columns and walls function. Large permanent drifts. Some exits blocked. Infills and unbraced parapets failed or at incipient failure. Building is on the verge of partial or total collapse

The estimated demand parameters for a given hazard level are used to classify buildings into different damage categories. A damage category is a qualitative definition of possible damage patterns that may be observed for a particular structural state. Typical damage categories may range from no damage to collapsed state of buildings and may include sub divisions depending on the desired refinement. Most commonly used damage categorizations include the ones proposed in the ATC-13 (1985), ATC-38 (1996), FEMA-356 (2000), and EMS-98 (1998) documents. A summary of FEMA-356 and EMS-98 damage categories and their definitions are provided in Tables 2.4 and 2.5.

The classification of buildings into different damage categories requires development of a quantitative relationship between the damage states and the demand (response) parameters. In developing such relationships, measured demand parameters are correlated with damage observations gathered from field and laboratory investigations. Demand-damage relationships for unreinforced masonry buildings are discussed in Chapter 3.

Table 2.5. EMS-98 damage categories.

Damage Category	Damage Definition
Negligible (Grade 1)	No structural damage, slight non-structural damage. Hair-line cracks in very few walls. Fall of small pieces of plaster only. Fall of loose stones from upper parts of buildings in very few cases.
Moderate (Grade 2)	Slight structural damage, moderate non-structural damage. Cracks in many walls. Fall of fairly large pieces of plaster. Partial collapse of chimneys.
Substantial (Grade 3)	Moderate structural damage, heavy non-structural damage. Large and extensive cracks in most walls. Roof tiles detach. Chimneys fracture at the roof line; failure of individual non-structural elements (partitions, gable walls).
Heavy (Grade 4)	Heavy structural damage, very heavy non-structural damage. Serious failure of walls; partial structural failure of roofs and floors.
Collapse (Grade 5)	Very heavy structural damage. Total or near total collapse.

Once the damage categories are quantified in terms of the demand parameters, one may determine the variation of damage for a given level of hazard by using the estimated demand parameters. One common approach in representing the relationship between hazard and damage is through vulnerability curves (Hwang and Jaw 1994, Singhal and Kiremidjian 1996). In these curves the variation of damage for a given hazard level is expressed in terms of a cumulative probability distribution for each damage category. As shown in Fig. 2.2, the vertical axis shows the probability of attaining and exceeding a specified damage category.
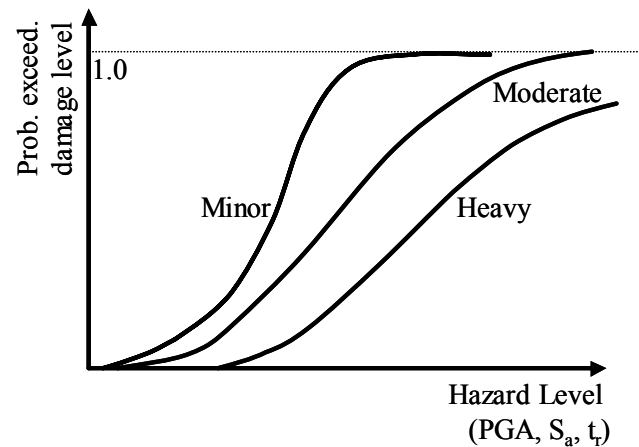
Figure 2.2. A typical hazard – damage, vulnerability, curve

In conjunction with vulnerability curves, damage – loss relationships have to be determined before generating the hazard – loss relationships. This final key relationship, damage – loss, quantifies the amount of loss for a given level of damage state. As discussed in the preceding sections the term loss can be expressed in many different forms depending on the purpose of the risk investigation and the stakeholder needs. One commonly used measure is the repair cost of damage as expressed in terms of building replacement cost (ATC-38, Abrams *et al.* 1997, Kishi *et al.* 2001, Hwang and Lin 2000, Stehle *et al.* 2002). As in the case of demand – damage relationship the development of damage – loss relationships highly depend on correlation of field observations. ATC-38 was one of the major investigation efforts that conducted a correlation analysis to identify damage – loss relationship in the aftermath of the 1994 Northridge earthquake. This field study gathered damage and replacement cost (estimated) database for over 300 buildings right after the event. After one year from this study, a mail survey was conducted to gather exact cost of repair of 61 buildings. The

estimate and exact repair costs were compared to provide the damage – replacement cost distributions in the ATC-38 report. Damage – replacement cost relationships for unreinforced masonry buildings are summarized in Chapter 3.
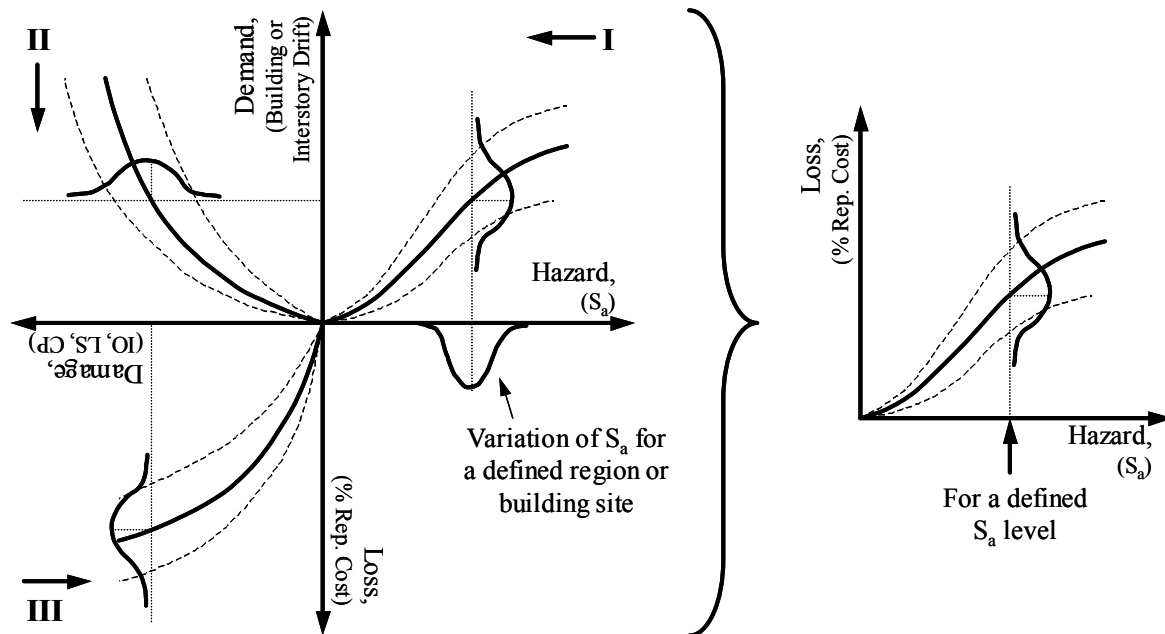
Figure 2.3. The three intermediate relationships to calculate hazard – loss relationship (adopted from Kishi et. al. 2001).

Once the three key relationships are developed, the relationship between hazard and loss can be directly generated by following the steps as shown in Fig 2.3. The axis names in Fig 2.3 are provided for illustration purposes and, in general, they may be represented with different measures. As can be seen from Fig. 2.3, uncertainties (scatter) in preceding relationships are affecting uncertainties in the next relationships. In other words, there is a propagation of uncertainty from one step to the other. In addition to this propagation, the variations in the internal parameters also add to uncertainties in the resulting relationships. For example a variation still exists in demand parameters due to uncertainties associated with building properties (stiffness, strength, material properties, geometric dimensions) and analytical models that idealize the structural response, even if the hazard level and time history data of the ground motions are precisely known. In developing hazard – loss relationships, the main goal is to identify the parameters and relationships that significantly contribute to the resulting

uncertainties and refine them to achieve better accuracy. Types of such parameters highly depend on the level of hazard – loss studies; building specific or regional. The following sections will discuss the basis of such sensitivity investigations in view of regional hazard – loss estimates. Differences between building specific and regional risk investigations will be highlighted and the thrusting ideas that will help to reduce uncertainties and number of parameters will be introduced.

2.3 Building specific versus populations of buildings

In the extreme case, the concepts of seismic risk assessment of individual buildings can be used to estimate the seismic risk of populations of buildings. In this approach, each building in a given population is investigated individually and the seismic risk over the region is determined by adding risks associated with each building. Even though the results will be highly accurate, it would be practically and economically unfeasible to carry out such an investigation with this "brute force" approach. Yet, non-engineering decision makers need simple and rapid estimates of anticipated losses to develop the proper judgment to execute their mitigation plans. In order to overcome issues related with impracticality and extravagance, the problem can be approached from a different angle. This perspective can be reflected through a simple analogy.

Assume a region is represented by a box, buildings in the region by different sizes of steel balls and the total seismic risk by the total weight of the steel balls in the box. In this case, the building population is analogous to the steel balls in the box. One possible way to estimate the total weight of steel balls is to weigh each ball and add the results. As one might imagine, this would be a highly tedious and time-consuming task, especially as the size of the box gets bigger and the number of steel balls becomes higher. Even though the end result would be highly accurate the process would be equally impractical. A possible alternative in estimating the total weight would be to investigate a smaller "representative" group of steel balls. From this investigation, an average representative weight for a steel ball can be determined. This value can be utilized to estimate the total weight by multiplying it by the number of steel balls in the box. Of course, the representative weight value will be higher or lower than the real weight of each steel ball. However, it is still possible to make an accurate estimation of the

total weight since the differences between the representative weight and the real weight of the steel balls will more or less cancel each other during the summation process.

The accuracy of the total weight estimation can be improved by dividing the steel ball population into subgroups that contain similar size steel balls. A representative weight value for each subgroup can be determined from small sized samples taken from each of the subgroups. The representative weight value of each group can be multiplied with the total number of steel balls in that group. The total weight can be determined by adding weight estimates from each group. Sub-grouping of similar size steel balls yields smaller difference between the representative and the real weight values, i.e. less scatter. The number of subgroups is a function of the variability in the sizes of the steel balls. As the variability gets higher, more subgroups are needed to improve the accuracy.

The concepts introduced in the preceding paragraphs can be applied to estimate the total seismic risk of populations of buildings for a defined region. As is in the analogy of total weight estimation of the steel balls, the key phrase is the "total" seismic risk over a defined region. Hazard – loss relationships representing building groups in sub-regions can be used to calculate the total loss over the whole region. The total seismic risk is the multiplication of this total loss estimate with the occurrence probability of the hazard level that is used in the total loss estimates.

In addition to error correcting advantage of the idea of total seismic risk, it can be statistically proven that the summation process reduces the scatter in the total risk estimates. In the most general sense, the summation process in estimating total loss can be considered as the addition of n random variables where n is the number of buildings in the population. Here, the random variable is the loss in a particular building for a given level of hazard. The resulting summation, total loss over the region, is also a random variable. With reference to the concepts in Ang and Tang (1975), the mean and the scatter of this summation can be expressed as:

$$\mu_{TL} = \sum_{i=1}^{n} \mu_{Li} \qquad\qquad (2.2)$$

$$\sigma_{TL}^2 = \sum_{i=1}^{n} \sigma_{Li}^2 + \sum_{i \neq j}^{n}\sum^{n} \rho_{ij}\sigma_{Li}\sigma_{Lj} \qquad\qquad (2.3)$$

here, μ_{TL}, μ_{Li} = mean values of the total loss and the loss in building i, respectively.

σ_{TL}, σ_{Li} = standard deviations of the total loss and the loss in building i, respectively.

ρ_{ij} = correlation coefficient between loss values in building i and j.

n = number of buildings in the population.
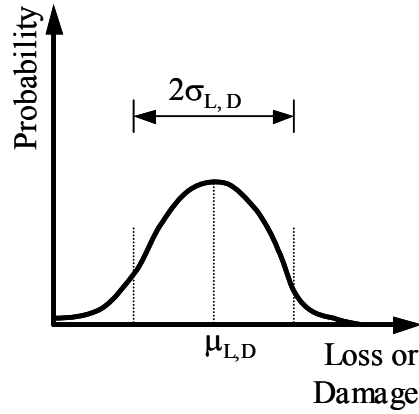
Figure 2.4. A typical distribution of building loss or damage for a given level of hazard

Depending on the loss correlation between two buildings, the term ρ_{ij} may range from 1.0, full positive correlation, to -1.0, full negative correlation. A value close to 0.0 means very light or no correlation. In reality, there is always some sort of correlation among observed losses in buildings especially, when there are similarities in construction types, material properties, and location. For highly different construction types and locations, the correlation tends to zero and the second summation term in Eq. 2.3 vanishes. Even though Eq. 2.3 suggests an increase for the overall scatter, the relative scatter, a better measure for uncertainty, tends to get smaller as n gets larger. Relative scatter is also known as the coefficient of variation and is defined as the ratio of the standard deviation to the mean value of the distribution. Even though the reduction in relative scatter is valid for any generic case, the idea can be demonstrated more easily with a simple example. Let for a particular level of

hazard, the buildings in a given building population is represented by the same loss distribution function as shown in Fig. 2.4. For constant correlation coefficient, ρ, the Eqs. 2.2 and 2.3 reduce to:

$$\mu_{TL} = n\mu_L \tag{2.4}$$

$$\sigma_{TL}^2 = n\sigma_L^2 + n(n-1)\rho\sigma_L^2 \tag{2.5}$$

and relative scatter can be expressed as:

$$\delta_{TL} = \frac{\sqrt{n\sigma_L^2 + n(n-1)\rho\sigma_L^2}}{n\mu_L} \tag{2.6}$$

note that for $\rho = 1.0$, full positive correlation, Eq. 2.6 reduces to

$$\delta_{TL} = \frac{\sigma_L}{\mu_L} = \delta_L \tag{2.7}$$

and similarly for uncorrelated case, $\rho = 0.0$,

$$\delta_{TL} = \frac{1}{\sqrt{n}}\frac{\sigma_L}{\mu_L} = \frac{1}{\sqrt{n}}\delta_L \tag{2.8}$$

As can be seen form Eq. 2.7, for full correlation, the relative scatter of the total loss estimate, δ_{TL}, is the same as the relative scatter of the individual loss estimate, δ_L. In this case, reduction in relative scatter may not be achieved through a summation process. Fortunately, in reality, finding building populations that have full correlation on loss estimates is very unlikely. Even if there exists some correlation, it is almost always less than 1.0. This concept is highly useful in setting the acceptable levels of uncertainties when developing hazard – loss or hazard – damage relationships for regional risk assessment investigations. As long as the mean value associated with these relationships can be determined accurately, the summation process can be relied on to reduce the relative scatter in the final total loss estimates. The scatter reduction and error correction concepts discussed in this section are used to develop broader and more generic hazard – damage and hazard – loss relationships.

2.4 Framework for sensitivity analysis

The concepts discussed so far should be systematically utilized to investigate the sensitivity of total risk/loss estimates to parameters that characterize a given region. Unlike building specific investigations, these sensitivity analyses should be carried out on building populations in order to fully utilize benefits of the regional risk/loss assessment concepts. This section lays out a generic procedure, framework, to conduct such sensitivity investigations on building populations. The laid out framework is utilized in Chapter 5 to conduct sensitivity analysis on populations of unreinforced masonry buildings.

The very first step of the framework is to define the building population on which the sensitivity investigations will be conducted. For this purpose, one may choose and gather information from a real (existing) building population. One limitation to this approach is the scarcity of information either in the inventory or in the recorded damage. Even though missing information may be filled with judgments and assumptions, the resulting data would lose its credibility. Yet, if such data can be gathered it would be specific to a certain region and primarily be useful for verification rather than development purposes.

An alternative approach for defining building populations is through synthetic generation of building populations from statistical distributions of parameters that characterize the region and the target building population. The parameters may involve number of stories, plan area, plan aspect ratio, wall-area-to-floor-area ratio, age, diaphragm type, and building function. The distribution of these parameters differs from one population type to another. For example, the characteristics of buildings in downtowns are expected to be different from a more uniform building population such as buildings owned by retail stores. Typical distributions representing different population types can be developed through field investigations and discussions with building owners, stakeholders. Such investigations and discussions also allow elimination of undesirable region-specific characteristics and may result in more generic and unbiased statistical representation of the building population. Once the statistical distributions of the parameters are determined, synthetic populations can be generated through a randomization process, such as the Monte Carlo or the Latin Hypercube Sampling techniques. The synthetic generation of unreinforced masonry building populations at urban regions is discussed in Chapter 4.

21
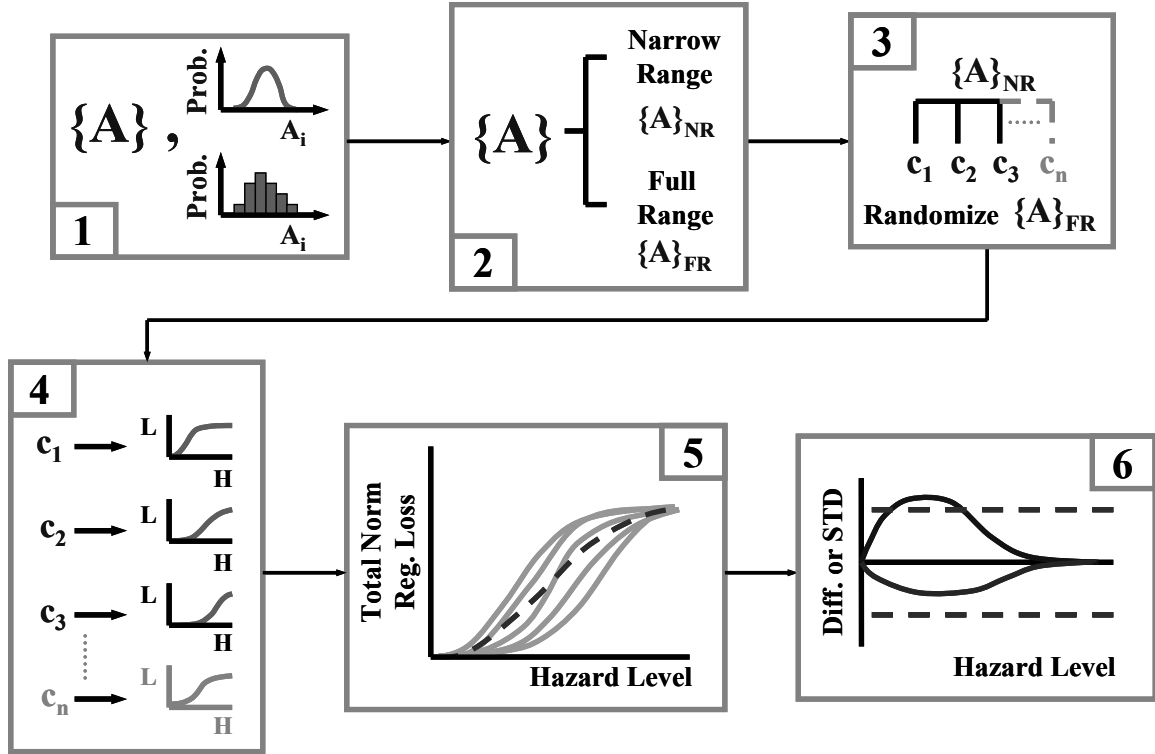
Figure 2.5. Flowchart to investigate the effect of parameters on total seismic loss estimates

Synthetically generated building populations can be utilized to investigate the influence of each parameter or combinations of parameters on total risk/loss estimations. These investigations can be systematically carried out by following the flowchart presented in Fig. 2.5. The steps of the flowchart can be explained as follows:

Step 1: Identify parameters (represented by the vector {A} in box 1) that are thought to be significant in regional loss/risk calculations. Based on the characteristics of the target building population, assign a distribution to each selected parameter. As discussed in earlier paragraphs, the parameter distributions are used to generate synthetic building populations.

Step 2: Divide selected parameters into two groups as represented by the vectors $\{A\}_{NR}$ and $\{A\}_{FR}$ in box 2. The vector $\{A\}_{NR}$ contains the parameters whose significance on regional loss/risk calculations will be investigated in the current sensitivity analysis. These parameters are randomized from smaller subintervals that are defined on the original distributions. The

parameters in vector $\{A\}_{FR}$ are left out from the current sensitivity investigation. These parameters are randomized at their full range.

Step 3: Define the limits of subintervals for all parameters in vector $\{A\}_{NR}$. One way of defining limits of subintervals is through dividing distributions into equal areas *i.e.* creating subintervals that have the same observance probability. Defined subintervals for all parameters in vector $\{A\}_{NR}$ are combined to create "cases" for the current sensitivity investigation. Each case represents a building population having one or more parameters that are biased towards a certain range. The analysis of these cases will provide answers to the following questions: 1) How much does unbiased hazard-loss relationship change if certain parameters are biased towards a specific interval? and 2) Are there any parameter combinations that result in similar hazard-loss relationships?

Step 4: Calculate hazard-loss relationship representing each "case" as well as the hazard-loss relationship representing the unbiased building population. For cases, the regional loss calculations are conducted on building populations that are generated by randomizing parameters according to the limits of subintervals. For the unbiased hazard-loss relationship, the regional loss calculations are conducted on building populations that are generated through randomizing all parameters at their full range. As can be expected the hazard-loss relationship needs to be calculated only once as it is independent of the parameter grouping in Step 2.

Steps 5 and 6: Normalize hazard-loss relationship for each "case" and plot them on the same graph. Compare curves among each other and with the unbiased hazard-loss relationship (the dotted curve in box 5 in Fig. 2.5). The comparison of curves among each other will provide answer to the second question in Step 3. Similarly, the comparison of curves with the unbiased hazard-loss relationship will provide answer to the first question in Step 3. Difference or standard deviation curves (as shown in box 6 in Fig. 2.5) can be utilized to evaluate the significance of each parameter or parameter combination with respect to a defined threshold error level. If the maximum deviation or difference is below the acceptable error level, then the parameter or parameter combination can be considered as insignificant in regional loss/risk estimations.

The flowchart is repeated until all desired parameter or parameter combinations are investigated.

2.5 The methodology: Preliminary

This section introduces the preliminary version of the seismic loss/risk assessment methodology that is intended to be developed in this report. The needs and the issues that are discussed in this preliminary methodology are used to guide investigations in Chapters 3, 4, and 5. The results of these investigations are used to revise and simplify the preliminary version of the loss/risk assessment methodology. The final version of the methodology is presented in Chapter 6.
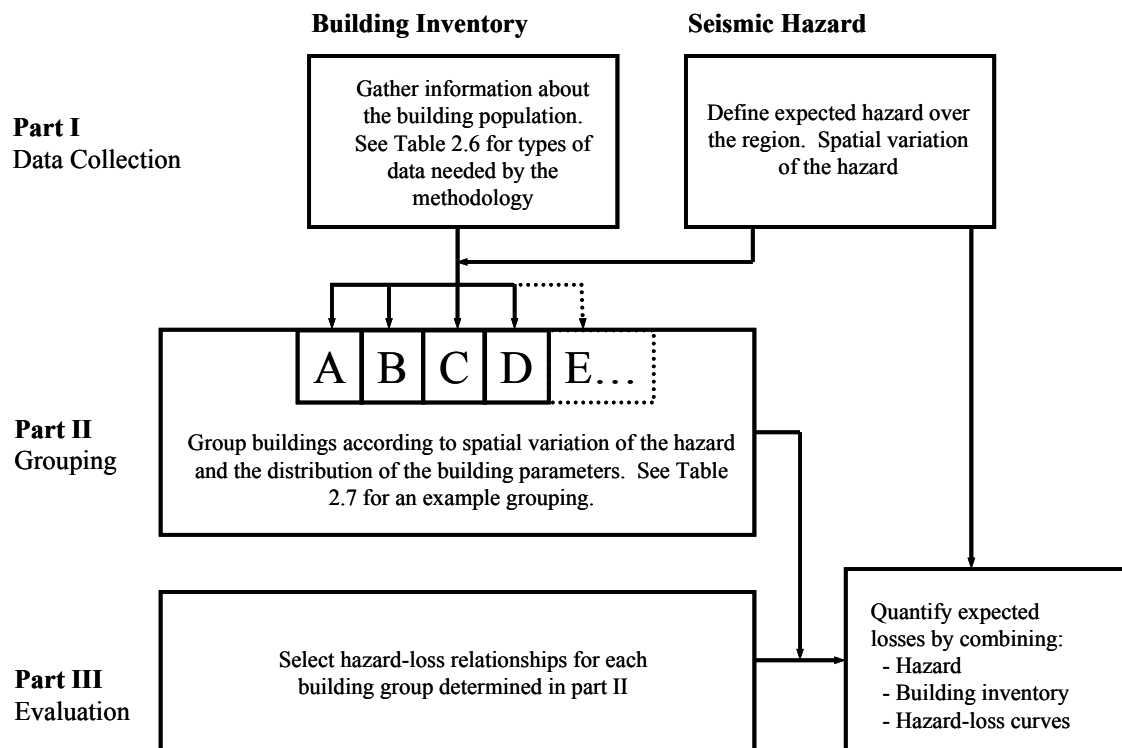
Figure 2.6 General layout and steps of the seismic risk/loss assessment methodology

City or state decision makers, insurance companies, and other building owners are intended to be the primary stakeholders to use the methodology. In the most general sense, the methodology can be divided into three parts: data collection, grouping, and evaluation. Fig 2.6 shows theses three parts of the methodology and their co-interaction among each other.

As the name implies, the first part is the data collection section of the methodology. This part has three primary steps in which the user gathers specific information about the seismicity, soil conditions, and the building inventory across the region. Table 2.6 lists parameters that are possibly significant for regional loss/risk calculations. A list of resources that can be referenced to collect these data is provided at the bottom of the same table. As can be expected this is the most tedious and time consuming part of any loss assessment methodology. To ease the applicability of the methodology, the parameters provided in Table 2.6 should be systematically investigated and the ones showing lower significance should be removed form the list. As discussed earlier, the primary goal of Chapter 5 is to conduct such sensitivity investigations on these parameters.

Table 2.6. Elements and resources of data collection

Seismic Hazard and Soil Conditions	Building Parameters
• Spectral acceleration, S_a and its spatial distribution within the building population. • Soil variation over the region	• Monetary value of the buildings • number of stories • plan area • plan aspect ratio • wall area / floor area (A_w/A_f) • story height • elastic modulus of masonry • elastic properties of diaphragms • average size of window/door openings • average height of piers • floor mass • aerial locations
<u>Possible resources</u>	<u>Possible resources</u>
• USGS Digital Hazard Maps (provides PGA and spectral values of the expected ground motion for a given location and return period of the earthquake)	• Existing city inventories • Tax assessor's or insurance database • New technologies (aerial photography) • Field surveys

After gathering information about the region and the building population, the grouping part begins. In this part, the goal is to organize building inventory data according to the distributions of the building parameters and the ground motion variability due to soil conditions. An example grouping is demonstrated in Table 2.7. Each group represents possible ranges of parameters that result in similar hazard-loss relationships. For example one-story buildings on stiff soil may have similar hazard-loss characteristics as four-story buildings on softer soils. As can be expected, guidelines on identifying similar buildings have to be provided to the end user for proper categorization. To develop such guidelines, different combinations of building and region-specific parameters need to be investigated and cases resulting in similar hazard-loss relationships should be identified. Such kind of investigations is conducted in Chapter 5.

Table 2.7 Sample grouping of buildings with respect to building parameters and soil variations over the region

Parameter Range → Group Id ↓	Number of stories	Story height (ft)	Floor area (ft^2)	Soil Type	…	Percentage of buildings (%)
Group A	1-2	10-12	<2000	Rock		12
Group B	3-4	10-12	<2000	Stiff		23
Group C	3-4	12-16	4000-6000	Soft		11
Group D	>4	10-12	4000-6000	Soft		34
. . .						
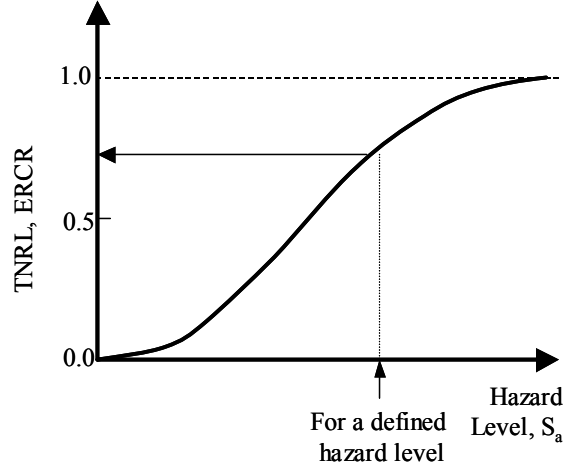
Figure 2.7. A typical hazard – loss relationship

After determining the correlated distribution of the building population, user can start the evaluation part of the methodology. This part mainly consists of determination of the expected loss for a defined hazard level by using the hazard – loss relationships provided for each building group. A typical hazard – loss relationship provides expected value of loss in terms of normalized replacement cost ratio, as illustrated in Fig. 2.7. This value corresponds to 0.0 for no damage or no hazard case and 1.0 for full damage or high hazard level. Calculations of expected replacement cost ratio, ERCR, and total normalized regional loss, TNRL, are further discussed in Chapter 5.

In mathematical terms, the total expected loss in each building group can be calculated as follows:

$$TLG_i(S_a) = ERCR_i(S_a) \times TBA_i \times MVPA \tag{2.9}$$

where, TLG_i = for a defined level of hazard, S_a, the total expected loss in the ith building group.

$ERCR_i$ = for a defined level of hazard, the expected value of the replacement cost ratio for the ith building group.

TBA_i = total building area in the ith building group.

MVPA = monetary value per unit area of buildings over the analysis region.

From this calculation the total loss over the region can be computed as:

$$TRL(S_a) = \sum_{i=1}^{n} TLG_i \tag{2.10}$$

where, $TRL(S_a)$ = total regional loss for a defined hazard level.

n = number of building groups used in the analysis.

The seismic risk for a given hazard level, also known as the scenario-based risk evaluation, can be determined by multiplying the calculated loss with the probability of occurrence of the assumed level of hazard, Eq. 2.11.

$$SR(S_a) = TRL(S_a) \times P(Hazard = S_a) \tag{2.11}$$

where, $SR(S_a)$ = seismic risk for a defined level of hazard.

$P(Hazard = S_a)$ = probability of occurrence of a hazard with level equal to S_a.

The summation of seismic risk for different levels of hazard gives the total seismic risk over the region.

2.6 Concluding remarks

A background on main aspects of seismic risk assessment methodologies is introduced. The differences between building specific and regional risk investigation studies are highlighted. The key ideas that can be utilized to develop regional risk assessment tools are introduced. Among such, the total risk and the scatter reduction concepts are utilized in the rest of the report to develop the key relationships for the proposed regional loss/risk assessment methodology. The following chapters provide technical knowledge on unreinforced masonry buildings and present analytical investigations that will simplify the proposed methodology and provide the necessary guidelines and tools.

CHAPTER 3 MODELING DAMAGE STATES FOR INDIVIDUAL UNREINFORCED MASONRY BUILDINGS

3.1. General

Cost effective construction and durability have made masonry one of the preferred construction types in the history of civilizations. In the United States, masonry has been frequently used since the early 19th century. Unlike more recent construction types, such as reinforced concrete and steel, masonry structures have been built before the development of modern building codes. In the early stages, the sizing of building components and detailing of the connections were typically based on certain guidelines and primarily constructed to carry static gravity loads (Lavicka 1980). Design for gravity loads resulted in buildings that were built with plain masonry. In other words, typical construction practice was unreinforced masonry. The concept of structural reinforcement for lateral loads did not enter into practice until after the 1933 Long Beach earthquake. In this earthquake, more than half of the damaged buildings were unreinforced masonry (Bruneau 1995). After the Long Beach experience, the state of California prohibited the construction of unreinforced masonry buildings and adopted seismic resistant design regulations. Even though a dramatic shift had taken place in the construction practice of masonry buildings in California, regions where earthquakes occur infrequently, continued the traditional practice for many years. In these regions, unreinforced masonry construction still constitutes a significant portion of the existing building population.

As a structural system, masonry buildings resemble a box system where, diaphragms distribute gravity loads to the exterior walls and exterior walls transfer these loads to the foundation, as illustrated in Fig. 3.1. Typically, walls perpendicular to the shortest side supports diaphragm joists and are named as the load-bearing walls. Walls perpendicular to the bearing walls primarily carry their own weight and therefore are commonly known as non-load-bearing walls. Depending on the direction of the lateral loads, walls are also categorized as in-plane or out-of-plane walls. In-plane walls are parallel to the direction of the lateral load and provide the main lateral resistance through in-plane deformations. Out-of-plane walls are perpendicular to the direction of the lateral loads. These walls do not significantly contribute to the lateral load resistance of the building.
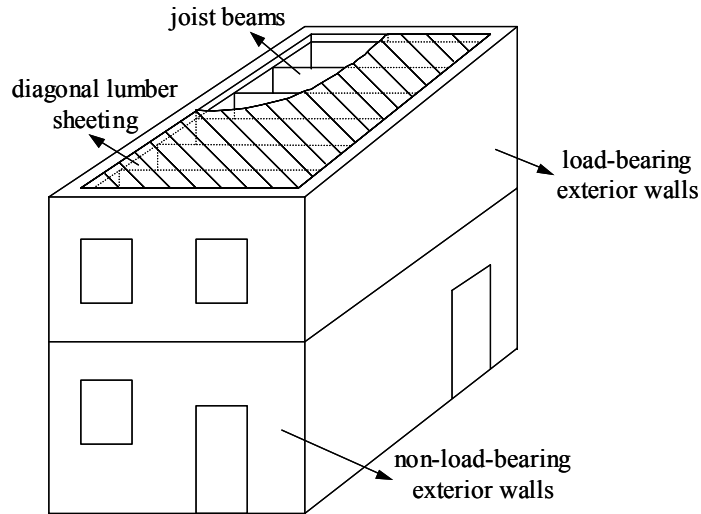
Figure 3.1. Typical components of an unreinforced masonry building

Diaphragm loads are usually distributed to the external walls through a wood joist system that runs from one side to the other. Joist beams are typically simply supported in "pockets" that are left open during construction of the load-bearing walls, see Fig 3.2. Attaching a wood ledger along the length of the bearing wall and connecting the joist beams to that ledger is also another common approach in supporting the joist. Figure 3.2 shows typical details of each connection type. In addition to end supports, joist beams, especially for longer span lengths, are also supported by intermediate gravity columns. However, as the name implies these components do not contribute to the lateral load resistance of the building. The diaphragm surface is formed by covering the joist beams with plywood or lumber sheeting. Figure 3.1 shows a typical diagonal lumber sheeting over the joist beams. These plywood and lumber sheets are basically nailed to the joist beams and the wood ledger that runs along the supporting wall. Unlike joist beams, the diaphragm sheeting is also attached to non-load-bearing walls through a wood ledger as shown in Fig. 3.2.

One characteristic feature of these wood diaphragms is their low in-plane stiffness due to inadequate shear transfer mechanism between plywood or lumber sheets. Unlike reinforced concrete floor systems, these wood diaphragms are usually treated as flexible in distributing the lateral loads and deformations to the supporting components. The low in-plane stiffness of wood diaphragms results in longer building periods and amplified floor displacements during seismic shaking. Amplified deformations impose higher demands on components

30

especially that are perpendicular to the direction of seismic shaking such as the out-of-plane walls. To improve the performance of out-of-plane walls under such deformation demands, anchor rods are typically used to tie the two opposing walls to the diaphragm and to each other. In the absence of anchor ties, nailing is the only source to provide strength to the diaphragm-wall connection. In case of load-bearing walls the friction between the beam joists and the masonry also adds to the strength of the connection. For this reason and the benefits of axial compressive stress, non-load-bearing walls are usually more vulnerable to out-of-plane actions.
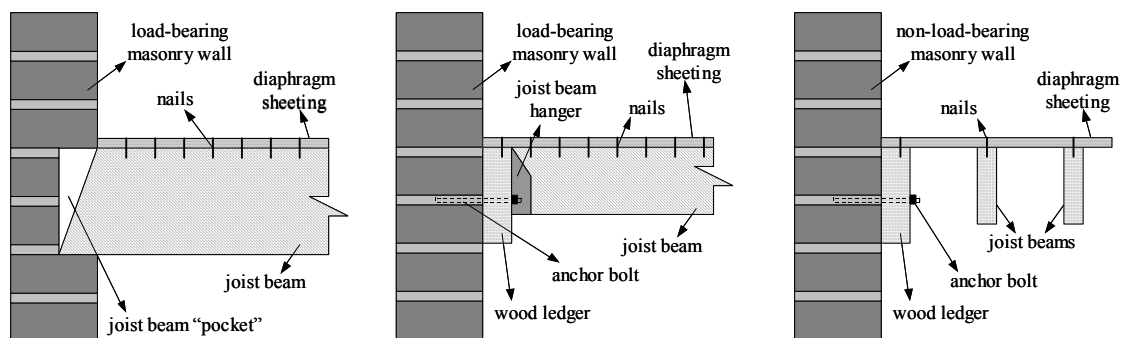
Figure 3.2. Typical diaphragm-wall connections

3.2. Damage mode and models

3.2.1 Observed damage modes

Existing unreinforced masonry buildings are highly vulnerable to earthquakes since most of these buildings were not designed for the level of seismic loads that we use in current practice. Therefore, even for moderate earthquakes, one may observe damage in these buildings. Previous post-earthquake reconnaissance investigations have provided detailed information about possible damage patterns in unreinforced masonry buildings for different levels of shaking. In view of investigations by Bruneau (1995 and 1994) and Holmes *et. al.* (1991), and Lizundia *et. al.* (1993) observed damage patterns in unreinforced masonry buildings can be classified into three categories:

1) In-plane

2) Out-of-plane

3) System level

The first two categories classify damage with respect to the direction of seismic actions that causes the damage. The remaining category basically represents system level damage patterns. System level damage patterns occur as a consequence of damage that is classified in the first two categories.
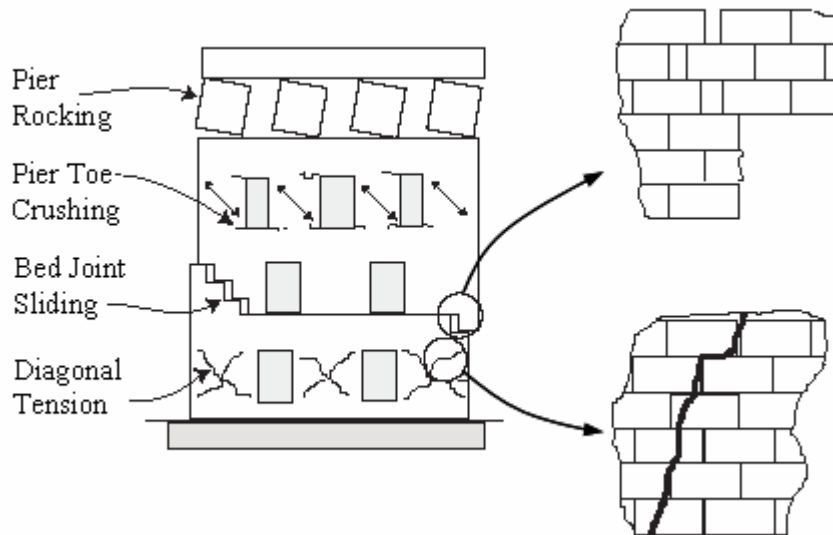
Figure 3.3. In-plane damage patterns (Figure taken from FEMA-306 1998)

Typical in-plane damage patterns and possible locations over the wall surface are shown in Fig. 3.3. These damage patterns are typical to walls that run parallel with the direction of shaking. Due to their orientation, these walls provide the lateral load resistance of the building and undergo in-plane deformation and stresses. The resulting form of damage is a function of axial compressive load level, wall aspect ratio, and quality of the mortar in components that comprises the wall. Depending on these factors, in-plane damage may take the form of diagonal, stair stepped, and horizontal (flexural) cracks. Diagonal and stair stepped cracks are more typical to stocky components, such as long shear walls. For high axial load and strong mortar combinations, stocky walls tend to fail in diagonal tension resulting in cracks going through masonry units. For low axial load and weak mortar combinations masonry units slide horizontally on each other forming a stair-stepped diagonal crack along the joints. Horizontal (flexural) cracks typically occur on the top and the base of the slender components. These cracks may also take place at the base of a stocky shear wall

under moderate axial load and strong mortar combination. In such case, a crack initially starts as a flexural crack and then extends along the length of the wall as sliding takes place at the base.

Typical out-of-plane damage patterns are shown in Fig. 3.4. Out-of-plane actions, such as displacements and accelerations, are primary causes of this damage category. Therefore, walls that are perpendicular to the direction of shaking are typically vulnerable to this kind of damage. The form of the damage may range from a single horizontal flexural crack to total collapse of a wall or a parapet. Out-of-plane actions are typically caused by excessive response of flexible diaphragms and by transverse inertial loadings. Damage is commonly observed at floor or roof levels or at mid-height of a wall. Under this damage category, one may also put anchorage failure of wall-diaphragm connection, which usually takes place at the verge of out-of-plane collapse of a wall.

Cracking   Out-of-plane failure
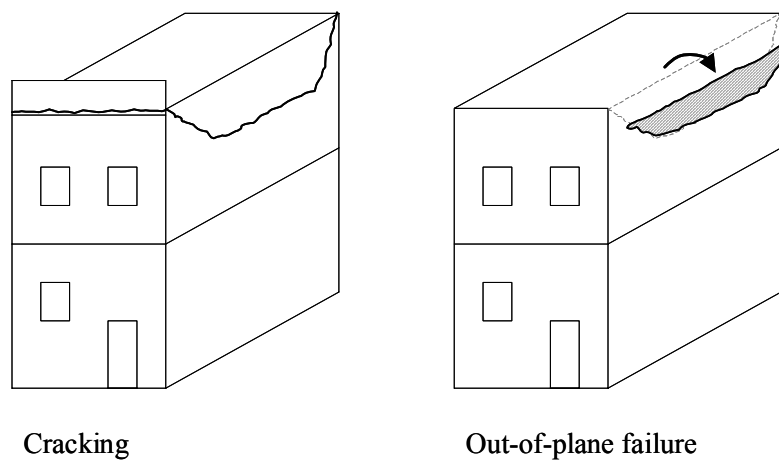
Figure 3.4. Typical out-of-plane damage patterns

System level damage patterns involve cases that are related with the global damage state of the whole building. Typical forms of damage may include soft story, roof/floor collapse, corner damage, and other non-structural failures. As mentioned earlier, system level damage patterns are caused by combinations of different damage patterns that can be described by the first two categories. Soft story damage mode is a typical example. Piers of a particular story lose their stiffness as they undergo in-plane deformations or rock, thus causing a very weak story over the height of the building, see Fig 3.5a. Similarly the collapse of a load-bearing out-of-plane wall may lead to a successive failure of the roof or the floor that used to be

carried by the wall, see Fig. 3.5b. As can be seen from these examples the system level damage patterns are localized damages that significantly affect the safety of the whole building.
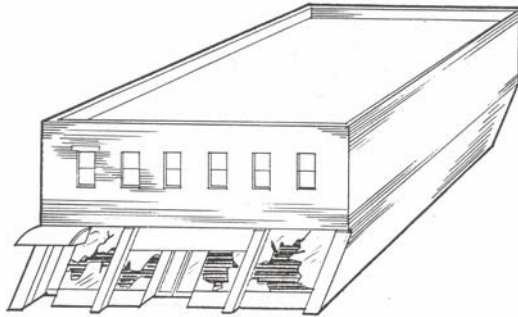
Figure 3.5a. Soft story failure (Figure taken from Holmes *et. al.* 1990)
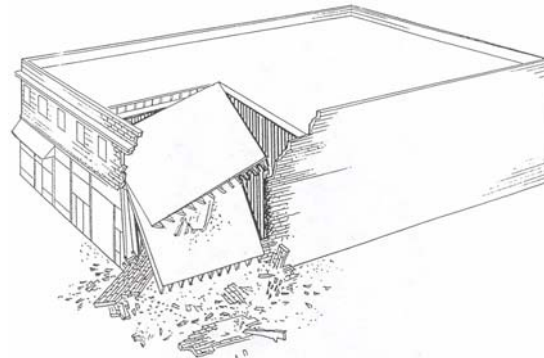
Figure 3.5b. Floor collapse due to out-of-plane failure (Figure taken from Holmes *et. al.* 1990)

3.2.2. Damage quantification models

The primary purpose of any building evaluation is to identify possible damage states for various levels of shaking and structural properties. As introduced in the previous sections, damage levels are typically expressed in verbal terms to describe the building condition. Post-earthquake reconnaissance investigations are highly valuable in understanding patterns and possible causes of damage. However, results of such investigations are specific to particular building configuration and shaking level. Mathematical relationships have to be defined between the observed damage and the building response parameters that have strong correlation with damage. The process of analytical correlation between observed damage and system response parameters is called "damage quantification".

In the literature, many different damage models have been proposed for different construction types. Among these damage models, ones based on displacement have been widely accepted and adopted in design and evaluation documents (e.g. FEMA-356). One main characteristic of these damage models is that damage is quantified in terms of peak response parameters, i.e. degradation of system performance due to cyclic effects are ignored. Numerous laboratory experiments (Abrams and Shah 1992, Costley and Abrams 1997, Franklin *et. al.* 2001, Erbay and Abrams 2002, Yi *et. al.* 2002) have shown that, unless the damage is of brittle nature, the

length and the size of cracks remain constant till the structure is pushed to a higher displacement level than the previous excursions. Hence the damage state does not change until the building experiences a higher displacement demand.
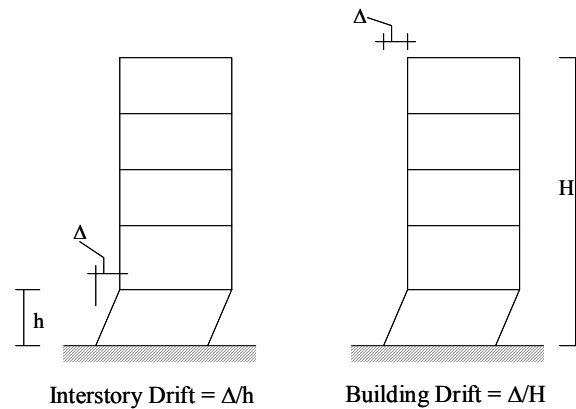
Figure 3.6. Interstory versus building drift calculations

Typical response parameters that are used in displacement-based damage models include interstory and building drifts. Depending on the building deflected shape, both measures may provide the same result. However, interstory drift captures failure modes that are insensitive to building drift. For example, consider a soft story failure mode where most of the building deformation is localized at the ground story, see Fig 3.6. For this case, building and ground story drifts are quite different. Building drift averages the concentrated deformation through the height of the building and returns a smaller value than ground story drift. Damage states calculated with this measure may underestimate the actual level of damage.

The comparison of estimated drift parameters with predefined threshold values determines the damage state in the components of the building (Abrams 2002). From component damage one may estimate the system level damage state. As discussed earlier, the key point is the definition of these threshold values. Table 3.1 summarizes various threshold values that are assigned for different damage states of unreinforced masonry buildings. In this table, damage scales used in other studies are interpreted in terms of the FEMA-356 performance levels: Immediate Occupancy (IO), Life Safety (LS), and Collapse Prevention (CP). An additional performance level, Total Collapse (TC), is added, as this level of damage state is not addressed in the FEMA-356 document.

Table 3.1. Damage scale and associated threshold building or interstory drift values (%)

Source	IO	LS	CP	TC
FEMA-356, Table C1-3, (2000)	0.3	0.6	1.0	
Abrams *et. al.* (1997)	0.1		1.0[*]	2.0
Calvi (1999)	0.1	0.3	0.5	

[*] This drift value corresponded a damage state that is in between LS and CP

Table 3.2. Component threshold drift values (%) for bed-joint sliding or sliding

Source	Details	IO	LS	CP
FEMA-356 (2000)		0.1	0.3	0.4
Abrams & Shah (1992)	W1, 75psi, h_{eff}/L=0.5	0.1	1.35	1.80
Erbay & Abrams (2002)	S1, 90psi, h_{eff}/L=0.5	0.1	0.21	0.28
Erbay & Abrams (2002)	S2, 130psi, h_{eff}/L=0.5	0.1	0.15	0.20

The threshold drift values suggested by Calvi (1999) are significantly smaller than the values suggested by the first two references. The main difference comes from the experimental results utilized in each reference. Calvi's investigation was based on stocky shear wall experiments conducted at Pavia and Ispra (Magenes and Calvi 1997). Even though the values suggested by Calvi are in good agreement with other stocky wall component tests (Table 3.2), they yield conservative estimates of threshold drift values for perforated unreinforced masonry walls. The presence of more deformable components, such as slender piers (Table 3.3), provides additional drift capacity to perforated walls. The higher drift values suggested by FEMA-356 and Abrams *et. al.* seem to capture this behavior and therefore are considered in this study.

Table 3.3. Component threshold drift values (%) for rocking

Source	Details	IO	LS	CP
FEMA-356 (2000)		0.1	$0.3h_{eff}/L$	$0.4h_{eff}/L$
Abrams & Shah (1992)	W1, 50psi	0.1	0.5 ($0.5h_{eff}/L$)	0.6 ($0.6h_{eff}/L$)
Costley & Abrams (1996)	S1, 33-40psi	0.1	1.0 ($0.5h_{eff}/L$)	1.3 ($0.7h_{eff}/L$)
Costley & Abrams (1996)	S2, 40-48psi	0.1	0.8 ($0.3h_{eff}/L$)	1.1 ($0.4h_{eff}/L$)
Franklin *et. al.* (2001)	F1, 25psi	0.1	1.5 ($0.8h_{eff}/L$)	1.9 ($1.1h_{eff}/L$)
Franklin *et. al.* (2001)	F2 , 42psi	0.1	0.9 ($0.5h_{eff}/L$)	1.2 ($0.7h_{eff}/L$)
Franklin *et. al.* (2001)	F6b, 85psi	0.1	1.5 ($0.8h_{eff}/L$)	1.9 ($1.1h_{eff}/L$)

In view of the values suggested in Table 3.1 and component test results presented in Tables 3.2 and 3.3, threshold drift values given in Table 3.4 are used to identify damage states. It should be noted that values in Table 3.4 represent in-plane damage to masonry walls. Damage due to out-of-plane actions should also be addressed in order to properly evaluate the overall damage state of masonry buildings.

Table 3.4. Damage categorization drift values

Damage Scale	IO	LS	CP	TC
Threshold building and interstory drift values	0.1	0.6	1.0	2.0

As discussed in the preceding sections, stability of walls and parapets is primarily a concern for actions in transverse direction. Damage states for these walls significantly affect the overall condition of the building. Stability of out-of-plane walls depends on wall thickness, wall height, axial compressive load applied to a wall, capacity of the connection with the diaphragm, and tensile strength of the mortar. Recent shake table tests at the University of

Illinois have shown that as long as there exists good connection between the diaphragm and the wall, out-of-plane failure can be prevented (Simsir *et. al.* 2002). However, many existing buildings have poor or no such connections.
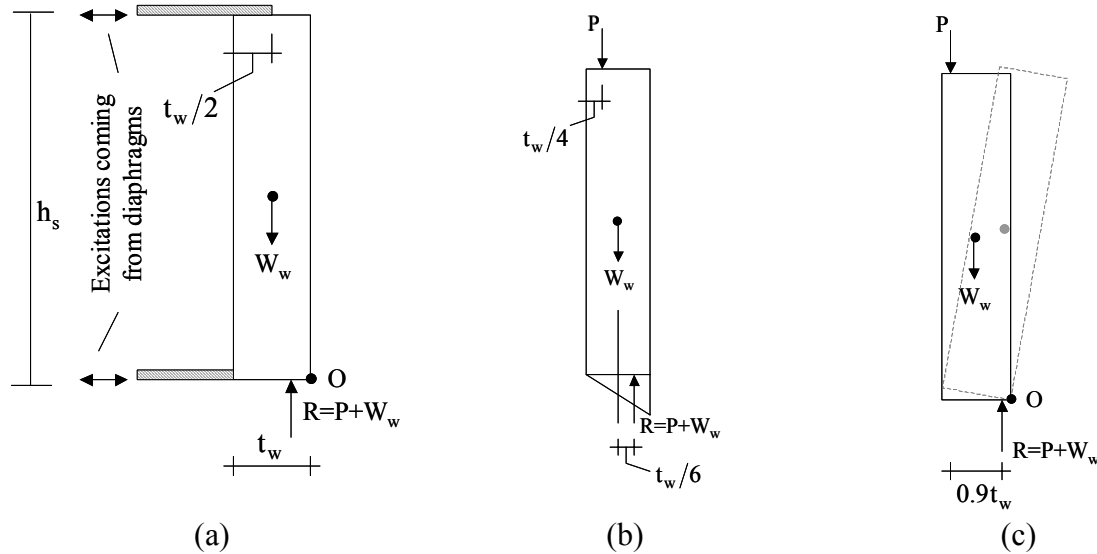
Figure 3.7. Analytical modeling of out-of-plane walls

The damage state of out-of-plane walls can be expressed by two failure modes: cracking and total collapse.   Per FEMA-356, Section 7.4.3.3, the onset of cracking is considered as threshold for immediate occupancy (IO) damage state. Furthermore, depending on wall type, the onset of wall instability is considered as threshold for collapse prevention (CP) in non-load-bearing walls and total collapse (TC) in load-bearing walls.   Response parameters associated with each damage state can be determined by simplifying the diaphragm-wall assembly as shown in Fig. 3.7a. Here the main assumptions are:

- the out-of-plane wall at the top story is the most critical component.

- the variation of acceleration over the height of the wall is uniform and is equal to the average of floor accelerations at top and bottom of the wall.

- connection between the diaphragm and the out-of-plane wall is rigid until failure.

- the out-of-plane wall rotates as a rigid body around point O.

- the effect of vertical accelerations on vertical stresses is ignored.

The cracking state is reached when the tensile stress at the extreme fiber exceeds the tensile strength, as shown in Fig. 3.7b. The equilibrium of moments around point O, yields the magnitude of the critical acceleration that is uniformly distributed along the height of the wall. Eqs. 3.1a and 3.1b express critical accelerations for non-load-bearing and load-bearing walls, respectively. The only difference in these equations is that there is no axial compressive load on non-load-bearing wall other than its own weight, W_w. In these calculations the tensile strength of masonry is neglected, therefore the equations provide a lower bound to critical response parameters.

$$a_{cr,nlb} = \frac{1}{3}\left(\frac{t_w}{h_s}\right)g \tag{3.1a}$$

$$a_{cr,lb} = \left[\frac{5}{6}\frac{P}{W_w} + \frac{1}{3}\right]\left(\frac{t_w}{h_s}\right)g \tag{3.1b}$$

Total collapse state is reached when the base reaction moves out of the wall thickness and the diaphragm-wall connection fails, see Fig. 3.7c. Unlike cracking, the value of the floor acceleration is not sufficient enough to identify the stability of the wall. Instead, displacement and acceleration has to be considered at the same time. For example, accelerations may be large enough to cause connection failure; however, they may not generate excessive displacements necessary for failure.

One way to check this state is utilizing the energy balance approach suggested by Housner (1963, as referenced in Aydin (2001)) and Paulay and Priestley (1992). In this energy approach, kinetic energy at the time of connection failure is compared with the potential energy (due to forces acting on the wall) that is necessary to reach collapse. The wall fails if, the kinetic energy of the wall is greater than the potential energy required for failure. In this study, friction is assumed to be the only form of connection between the diaphragm and the wall. The out-of-plane capacity of ledger type connections is ignored due to the fact that the nailing in these connections is usually random and typically not provided for lateral capacity. In view of these assumptions and with reference to Figs. 3.8a and 3.8b, the kinetic energy of the wall, (KE_w), and the potential energy of the external forces (PE_f) can be expressed as follows:

$$KE_w = \frac{1}{24}\frac{W_w}{g}\left[(V_t - V_b)^2 + (V_t + V_b)^2\right] \qquad (3.2a)$$

$$PE_{f,lb} = \frac{W_w}{2}\left[\frac{P}{W_w}\left(0.9\frac{3}{4}\frac{t_w^2}{h_s} + \mu_k t_w\right) + 0.45\frac{t_w^2}{h_s}\right] \qquad (3.2b)$$

$$PE_{f,nlb} = \frac{W_w}{2}\left[0.45\frac{t_w^2}{h_s}\right] \qquad (3.2c)$$
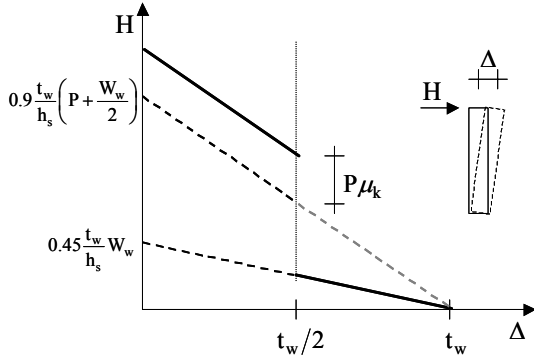
Fig 3.8a. Out-of-plane force-deflection curve for bearing and non-bearing walls
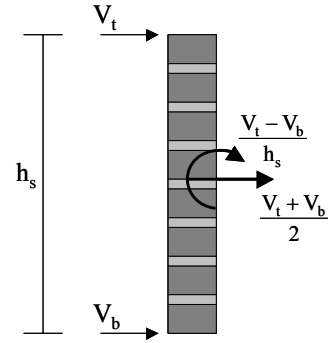
Fig 3.8b. Velocities at top and base of the wall at the time of connection failure

Diaphragm-wall connection failure of load-bearing walls can be determined by equating the inertia force to the friction force between the diaphragm and the wall. From this equality the critical acceleration, a_{con}, beyond which the connection starts to slide, can be expressed as:

$$a_{con} = \frac{F_{friction}}{m_w/2} = \left(\frac{P\mu_s}{W_w/2}\right)g \qquad (3.3)$$

Note that for non-load-bearing walls, the axial compressive force is very low and therefore frictional force is ignored. In these walls, the critical acceleration associated with cracking can be taken as the threshold value to identify the connection failure. Once the connection fails, the stability of the wall can be checked by comparing kinetic and potential energy terms provided in Eqs. 3.2a, 3.2b, and 3.2c. In Eqs. 3.2b and 3.3, μ_k and μ_s are respectively the kinetic and the static coefficient of friction between masonry and timber.

3.3. Loss quantification from a given damage state

In addition to relationships that relate system response to building damage states, a relationship defining building loss as a function of damage states has to be identified to estimate loss in each building. Threshold values and equations for response-based damage categorization procedure are defined in previous sections. In this section the focus is given to define parameters that identify damage-loss relationship. As discussed in Chapter 2 damage-loss relationships are typically identified in empirical terms. ATC-38 was one of the first attempts to investigate such a relationship through a field survey after the 1994 Northridge earthquake. As part of this investigations two field investigations were conducted. The initial survey was conducted right after the event and collected estimates of building repair costs. One year after the first survey a second survey was conducted. At the time of the second survey, most of the damage was repaired and data on actual repair costs were available. The results of the second survey were utilized to update the results of the first survey. Distribution of replacement cost ratios for different damage states is shown in Fig. 3.9.
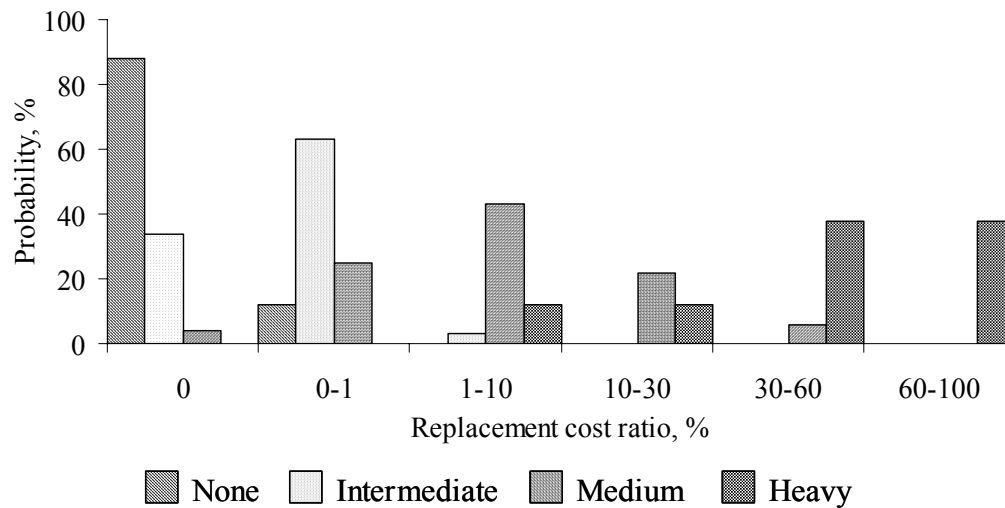
Figure 3.9. ATC-38 survey results showing distribution of replacement cost ratios for different levels of building damage states (Graph values are adopted from Abrams and Shinozuka, 1997).

The data shown in Fig. 3.9 show that for a given damage state, one may get wide range of replacement cost ratios. Such as, for intermediate damage state, the replacement cost ratio may take any value from 0% to 10%. Using the distributions associated with each damage

state one may calculate an expected value of replacement cost ratio for each damage interval. To do that, median values suggested by ATC-13 for each replacement cost ratio category are utilized. These median values are 0%, 0.5%, 5%, 20%, 45%, and 80%, respectively for replacement cost ratio categories shown in Fig. 3.9. Figure 3.10 shows the variation of expected replacement cost ratio values for each damage state. To be compatible with response-damage relationships, values are provided in terms of the FEMA-356 damage states. These damage states are introduced in Chapter 2, but for quick reference, NO, IO, LS, CP, and TC corresponds to No Damage, Immediate Occupancy, Life Safety, Collapse Prevention, and Total Collapse, respectively. In addition to ATC-38 results, replacement cost ratios suggested in two other investigations are also provided in Fig. 3.10. Solid, black colored data shows values that are utilized in this study. These values are determined from data collected in the first three investigations. More bias is given towards ATC-38 results, as these values were based on actual field investigations.
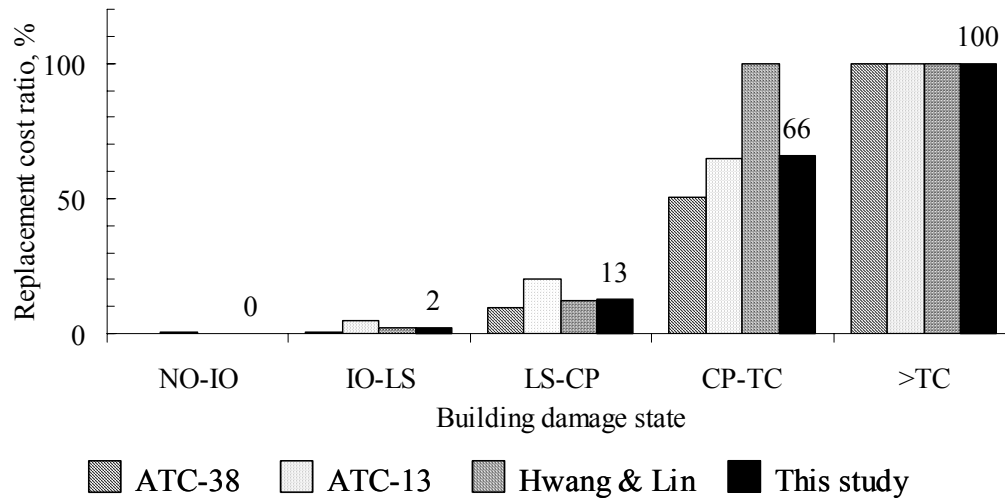
Figure 3.10. Expected value of replacement cost ratio for different intervals of building damage states.

3.4. Analytical idealization method

Response of unreinforced masonry buildings to earthquake loadings is difficult to idealize because of the complex mechanisms. Unlike skeletal frame buildings, absence of distinct structural elements makes it difficult to discretize the system into small components. In cases, where detailed information about building response is desired, the full three-dimensional

finite element idealization can be the only option. Even though conducting such analysis is possible, it may not be feasible as the number of analyses gets larger and information about building properties becomes scarce. On the contrary, if the goal is to capture some of the global response behavior one may resort to simpler models. Costley and Abrams 1996, Tena-Colunga and Abrams 1992, Tomazevic 1987 have shown that, by representing the stiffness and strength of each story with lumped spring elements, one may accurately estimate overall system response. Such simplification reduces the computation time and more importantly idealizes the system with less number of parameters. Representation of system response characteristics with a fewer number of parameters is highly desirable.
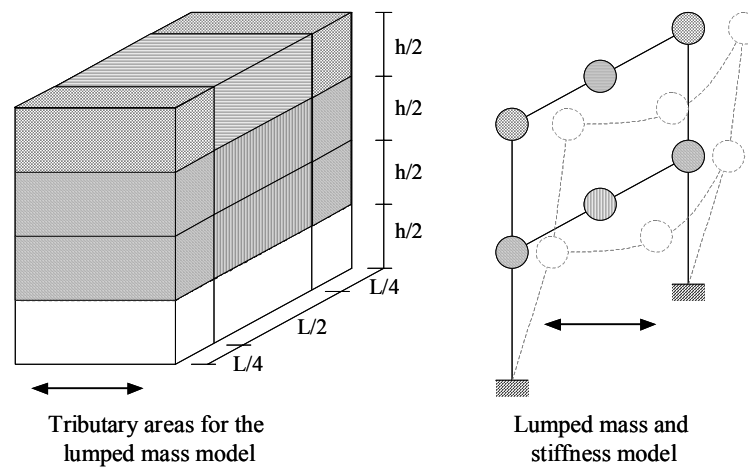
Figure 3.11. Analytical idealization of two story building

In this study, an analytical model similar to the one suggested by Costley and Abrams is utilized. As an example, Fig. 3.11 shows idealization of a two-story unreinforced masonry building. In this model the stiffness and strength of each story is represented with two non-linear spring elements, one for each wall. The mass associated with each wall is lumped at the nodes. Flexible diaphragms are modeled with elastic beams and are attached to the wall degrees of freedom at each story level. The properties of the elastic beam elements are adjusted so that they produce the same mid-span deflection as the diaphragm components (see upcoming sections for calculation of diaphragm stiffness). Shearing deformations are considered in calculating the in-plane stiffness of the diaphragms. The lumped mass of the diaphragm includes the tributary mass of the floor and the mobilized mass of the out-of-plane wall, see Fig. 3.11.

With some assumptions one may derive simple equations to estimate the properties of the lumped mass model. The simplifying assumptions made in this study are presented in Fig. 3.12 and listed in Table 3.5.

Table 3.5. Simplifying assumptions utilized in this study

Assumptions

---

1. buildings have rectangular plan shape.
2. gravity loads are only carried by load-bearing walls and interior gravity columns.
3. the number of piers are equal on each side of load-bearing walls, for non-load-bearing walls the number of piers may be different.
4. the walls parallel to the x-direction are load-bearing walls.
5. exterior walls of the building are the only components that resist lateral loads.
6. in each direction, length of piers are equal.
7. the out-of-plane walls do not contribute to lateral stiffness and strength of the building.
8. rocking and sliding are the primary failure modes in piers.
9. inelastic actions only take place in wall components. Diaphragms are assumed to respond in the elastic range.
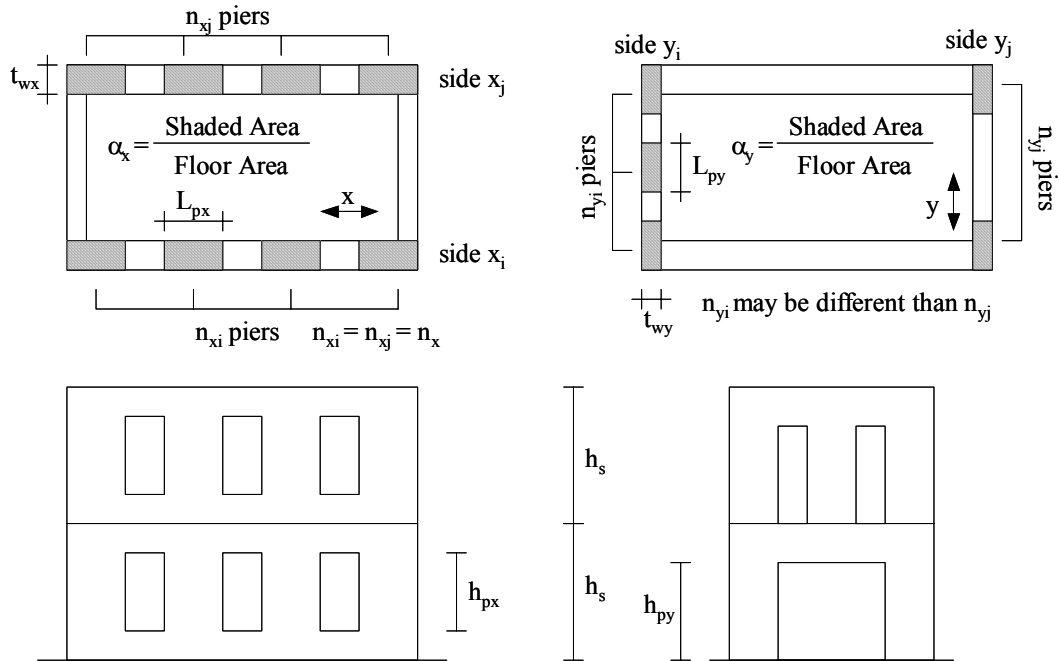
Figure 3.12. Assumptions and parameters to calculate structural properties of each story

Among these assumptions, the first three items are actually representing common construction characteristics of unreinforced masonry buildings that were built at the beginning of this century. Recent buildings show deviations from these assumptions however, they are typically reinforced and, therefore, beyond the scope of this study.

The fourth item is a definition rather than an assumption. This definition is used in deriving equations representing buildings' strength and stiffness in either direction. As will be discussed in the upcoming sections, due to size and connection differences of components, structural properties of unreinforced masonry buildings are different in each orthogonal direction.

The fifth assumption is a conservative one, as the additional lateral strength and stiffness due to presence of intermediate gravity piers and partition walls is ignored. However, the assumption is not too conservative as these intermediate components usually do not have proper shear connection with the floor diaphragm thus are ineffective in contributing building resistance in the lateral direction.

The sixth item is assumed to simplify the calculations. In general buildings consist of piers with different lengths. Due to this difference, the lateral stiffness and strength of components differs from each other. Shorter components tend to have less stiffness and strength as opposed to longer ones. However, the overall story stiffness and strength is not significantly affected by the variation in component lengths. If the goal is to estimate the global stiffness and strength of buildings (which is the case in this study) then, a constant average length is sufficient.

The seventh assumption on neglecting the contribution of out-of-plane walls in calculating building stiffness and strength results in conservative estimates. However, as analytically and experimentally observed by Yi *et. al.* (2003), the level of underestimation is negligible and is around 5-8%.

The assumption on in-plane failure modes of piers is based on experimental investigations by Epperson and Abrams (1989), Shah and Abrams (1992), Costley and Abrams (1997), Franklin *et. al.* (2001), Erbay and Abrams (2002), and Yi *et. al.* (2003). In theory, other failure modes are possible however; they are statistically insignificant especially for regional loss calculations.

The final assumption is based on the fact that the floors of old unreinforced masonry buildings were typically constructed out of wood. As compared to stiff masonry walls, wood construction results in flexible diaphragm response. Due to this relative flexibility, by the time walls reach their nonlinear state, diaphragms still respond in their elastic range. Typically, nonlinearity takes place at the wall-diaphragm interface. Such kind of nonlinearity is not considered in this study except for checking the out-of-plane stability of load-bearing-walls. These discussions are also experimentally observed by Peralta *et. al.* (2002).

In view of these assumptions and with reference to Fig. 3.12, the stiffness and strength properties of the lumped mass model can be calculated as follows:

Story stiffness:

Several parameters influence the in-plane stiffness of a wall. These parameters may include the size of the openings, number of piers, the thickness of the wall, aspect ratio of the piers, and elastic properties of the masonry. Among these parameters, the primary factor that affects the overall wall stiffness is the flexibility of the individual piers between openings. The story deformations mainly take place in these components as, the other parts of the wall remains relatively rigid. Therefore, story stiffness can be expressed as the summation of stiffnesses for individual piers (Abrams 2000). Considering flexural and shear deformations, the in-plane stiffness of a single pier can be expressed as follows:

$$k_p = \frac{t_w E_m}{\left(\dfrac{h_p}{L_p}\right)\left[\beta\left(\dfrac{h_p}{L_p}\right)^2 + 3\right]} \tag{3.4}$$

here, E_m = elastic modulus of masonry.

β = a constant to represent boundary conditions, $\beta = 1$ for fixed-free, $\beta = 4$ for fixed-fixed.

In deriving this expression, the shear modulus is taken as 40% of the elastic modulus of masonry. For practical ranges of h_p/L_p (0.5-2.0) and β (1-4), Eq. 3.4 can be further simplified into Eq. 3.5. The only difference between Eqs. 3.4 and 3.5 is that the square bracketed term is replaced by a constant.

$$k_p = 0.20 t_{wx} E_m \frac{L_p}{h_p} \qquad (3.5)$$
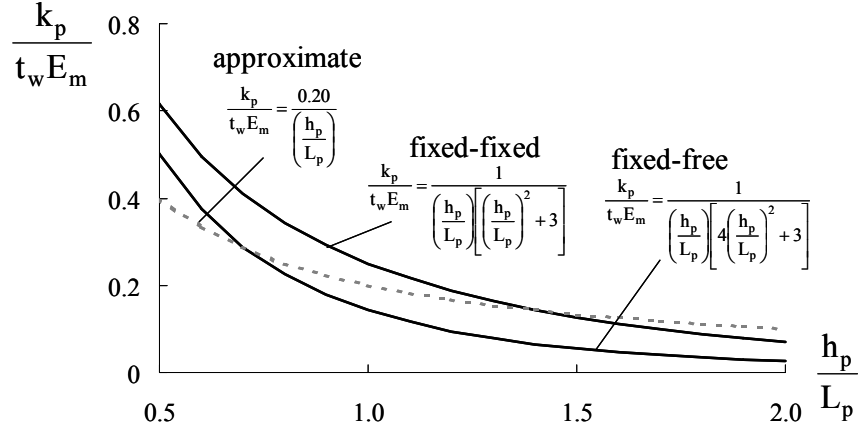
Figure 3.13. Variation of stiffness for different β values (adopted from Abrams 2000)

Fig. 3.13 plots normalized stiffness, $k_p / t_w E_w$, for different values of β. In this plot, the estimates calculated with Eq. 3.5 is also provided. As can be seen from this figure the approximate relationship on the average matches well with the original equations. It can be observed that, for large h_p / L_p the estimate approaches to fixed-fixed curve where as for small h_p / L_p the estimate approaches to fixed-free curve. Both observations are acceptable when the true behavior of piers is considered.

Eq. 3.5 can be used to calculate the rigidity of each pier in a wall. The story stiffness can be approximated as the summation of individual pier stiffness. With reference to the parameters defined in Fig. 3.12 and the listed assumptions in Table 3.5, Eq. 3.5 can be rearranged to express story stiffness as follows:

$$k_{x,y} = 0.20 \alpha_{x,y} \frac{E_m A_f}{h_{px,y}} \qquad (3.6)$$

here, A_f = floor area.

   $\alpha_{x,y}$ = effective wall area to floor are ratio in the x or y direction.

47

$h_{px,y}$ = average effective pier height in the x or y direction.

Eq. 3.6 is derived based on the assumption that the number of piers is equal on either side of the wall. This assumption is not valid for asymmetric buildings where stiffness of opposing walls is different. This is very typical for store buildings where the front of the building has a large opening compared to the back. This situation can be addressed by assigning a percentage to each wall in terms of their contribution to the overall story stiffness. With this modification, the stiffness associated with each wall on either side can be calculated as follows:

$$k_{xi,j} = 0.2\alpha_x\gamma_{xi,j}\frac{E_m A_f}{h_{px}} = \gamma_{xi,j}k_x \qquad (3.7a)$$

similarly for the y-direction

$$k_{yi,j} = 0.2\alpha_y\gamma_{yi,j}\frac{E_m A_f}{h_{py}} = \gamma_{yi,j}k_y \qquad (3.7b)$$

where, $\gamma_{xi,j}$ = percentage of story stiffness coming from side i and j for the x-direction

$\gamma_{yi,j}$ = percentage of story stiffness coming from side i and j for the y-direction

In this study, the load-bearing walls are assumed to have the same properties on either side (i and j), therefore a value of 0.5 is assigned to γ_{xi} and γ_{xj}. The values for γ_{yi} and γ_{yj} are determined as the ratio of the number of piers in each direction.

$$\gamma_{yi} = \frac{n_{yi}}{n_{yi} + n_{yj}} \qquad (3.8a)$$

$$\gamma_{yi} = \frac{n_{yi}}{n_{yi} + n_{yj}} \qquad (3.8b)$$

where, n_{yi} and n_{yj} = number of piers in either side of the walls in the y-direction. As will be discussed in the upcoming section, a relationship (see Fig. 3.17) is derived to estimate the number of piers for a given direction in terms of the global building parameters.

Diaphragm stiffness:

The in-plane stiffness of flexible diaphragms is a function of diaphragm thickness, support conditions, density of nailing, shear modulus of wood, and aspect ratio of the diaphragm. Typically, in-plane deformations take place in the form of bending, shear, and slippage of the nailing. As suggested by Tena-Colunga and Abrams, one may calculate a lower bound for the in-plane stiffness of a diaphragm by only considering shear flexibility. In this approach, the ignorance of flexibility due to nail slippage is assumed to be counter balanced by the ignorance of rigidity due to edge elements such as chord beams and masonry walls. Figure 3.14 shows assumed deformation shape to calculate the in-plane stiffness of a flexible diaphragm. In reference to parameters defined in this figure in-plane stiffness can be expressed as follows:

$$k_{dx} = 4G_d\alpha_d \qquad\qquad (3.9a)$$

$$k_{dy} = 4G_d\frac{1}{\alpha_d} \qquad\qquad (3.9b)$$

here, k_{dx} and k_{dy} = in-plane diaphragm stiffness in the x and y direction, respectively

α_d = diaphragm aspect ratio

G_d = effective diaphragm shear modulus
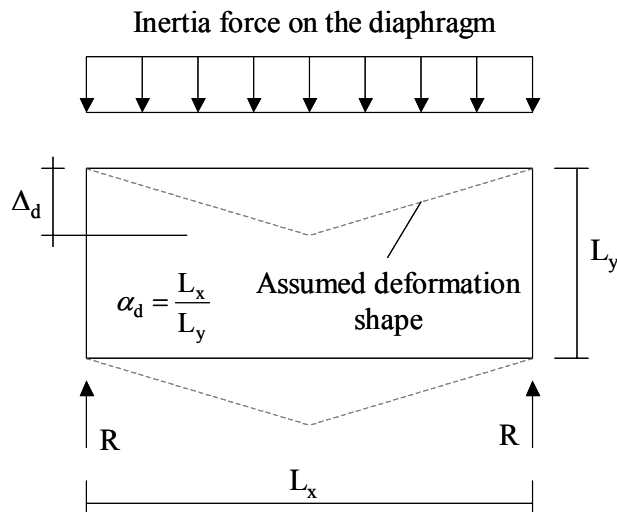
Figure 3.14. In-plane deformation shape for flexible diaphragms

Story strength:

In-plane shear capacity of walls primarily depends on aspect ratio of the piers, axial load on story, and strength of masonry. As discussed in previous sections, certain combinations of these parameters result in different failure modes and strength capacities. Among these, rocking and sliding shear modes are considered in this study. Similar to stiffness calculations, the summation of individual pier strengths can be used to calculate the shear strength of the story. As the name implies the rocking mechanism is basically the rotation of the pier around the toe region. Strength associated with this shear mode can be calculated by summing moments of external forces around the toe region as shown in Fig. 3.15. The solution of the moment equilibrium yields the following equation for rocking strength:

$$H_{rp} = 0.9 \frac{L_p}{h_p} P_p \qquad (3.10)$$

where, P_p = axial force on the pier
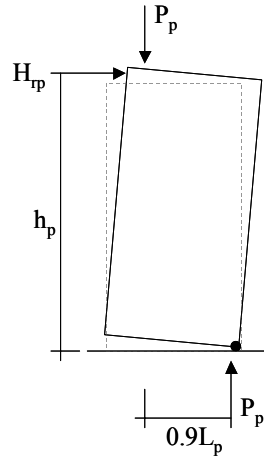
Figure 3.15. External forces on a rocking pier (Adopted from Abrams 2000)

In sliding shear mode, the masonry units slide either along the joints or at the base of a pier. Capacity associated with this mode can be estimated through a Mohr-Coulomb shear friction model. The following expression is provided in the FEMA-356 for sliding shear capacity:

$$H_{sp} = \left(\frac{3}{8} \tau_c + \mu_{sld} \sigma_p \right) A_p \qquad (3.11)$$

here, $\tau_c =$ cohesion between units, typically ranges between 20-60psi (Epperson and Abrams 1989, Calvi and Magenes 1997, Moon *et. al.* 2003, Yi *et. al.* 2003).

$\mu_{sld} =$ coefficient of friction between mortar and units, typically ranges between 0.20-0.80 (Epperson and Abrams 1989, Drysdale *et. al.* 1994, Calvi and Magenes 1997).

$\sigma_p =$ axial compressive stress on the pier

$A_p =$ cross sectional area of the pier.

In this study, average values for cohesion and coefficient of friction are utilized. Based on typical ranges of these parameters, values 40psi and 0.5 are assumed for cohesion and coefficient of friction, respectively. Figure 3.16 shows the normalized rocking and sliding shear strength, $H/A_p\sigma_p$, for different levels of axial compressive stress, σ_p.
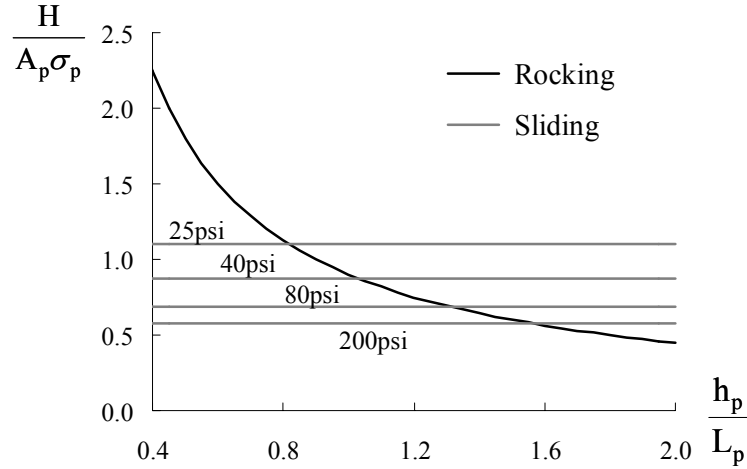
Figure 3.16. Comparison of rocking and sliding shear strengths

The lowest value obtained from Eqs. 3.10 and 3.11 is the shear strength of a pier. Shear strength estimate for a pier can be multiplied with the number of piers to calculate the shear strength corresponding to a story. This statement assumes that all piers have equal lengths and effective heights. Eq. 3.12a and 3.12b gives the expressions for story shear strengths:

$$H_{sr} = 0.9 \frac{L_p}{h_p} P_p m \qquad (3.12a)$$

$$H_{ss} = \left(\frac{3}{8} \frac{\tau_c}{\sigma_p} + \mu_{sld} \right) P_p m \qquad (3.12b)$$

where, H_{sr} = story shear strength associated with rocking mode of failure

H_{ss} = story shear strength associated with sliding mode of failure

m = number of piers effective in the direction of shaking

For equal pier lengths, the multiplication $P_p m$ is equal to the axial load on the story, P_f. Also from the same argument, the pier compressive stress, σ_p, can be replaced with the compressive stress at story level, σ_f. Story compressive stress can be expressed as P_f / A_w, where A_w is the effective wall area in the direction of shaking $(= \alpha_{x,y} A_f)$. Substituting these terms in Eqs. 3.12a and 3.12b gives:

$$H_{sr} = 0.9 \frac{L_p}{h_p} P_f \qquad (3.13a)$$

$$H_{ss} = \left(\frac{3}{8} \frac{A_f}{P_f} \alpha_{x,y} \tau_c + \mu_{sld} \right) P_f \qquad (3.13b)$$

In Eq. 3.13a, terms L_p and h_p are local parameters. With some assumptions they can be expressed in terms of the global system parameters. The variable h_p can be written as a percentage of the story height, h_s, Eq. 3.14.

$$h_p = \alpha_h h_s \qquad (3.14)$$

where α_h = percentage of pier height in terms of story height.

The variable L_p can be expressed in terms of diaphragm aspect ratio, α_d, floor area, A_f, wall area to floor area ratio, $\alpha_{x,y}$ and average width of openings in the wall, L_o. From α_d and A_f, it is possible to determine the planar dimensions of the floor, Eqs. 3.15a and 3.14b.

$$L_x = \sqrt{\alpha_d A_f} \qquad (3.15a)$$

$$L_y = \sqrt{\frac{A_f}{\alpha_d}} \qquad\qquad\qquad (3.15b)$$

here, L_x and L_y = x and y dimensions of the floor, respectively.

Deduction of total wall length from the length of the floor gives the total length of openings on either side of a wall, L_{ox} and L_{oy}, Fig. 3.17.

$$L_{ox} = L_x - \frac{L_{wx}}{2} = L_x - \frac{\alpha A_f}{2t_{wx}} \qquad\qquad (3.16a)$$

$$L_{oy} = 2L_y - L_{wy} = 2L_y - \frac{\alpha_y A_f}{t_{wy}} \qquad\qquad (3.16b)$$

As can be noted, for the x-direction total length of openings is calculated only for one side, compared to the y-direction, where total length of openings is calculated for both sides. This is due to the assumption that walls on the x-direction have the same number of piers as compared to possibly asymmetric y-direction. Therefore, investigation of only one side is enough to estimate the number of piers in the x-direction. Figure 3.17 demonstrates the meaning of parameters.
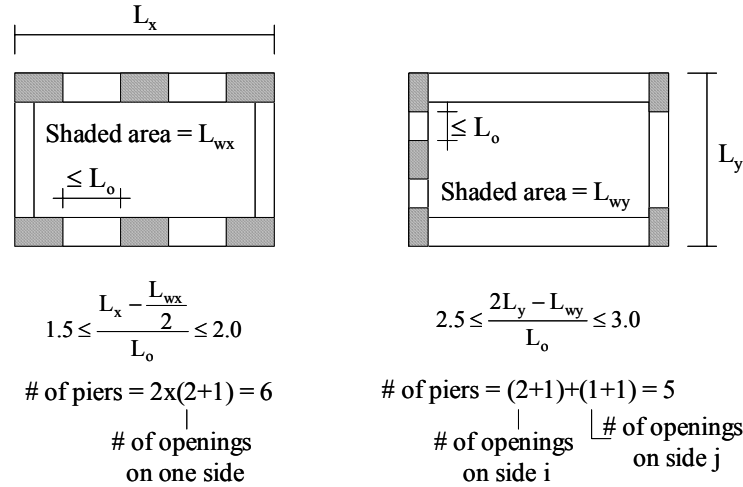
Figure 3.17. Estimation of number of piers in a story

Rounding up the ratio of Eqs. 3.16a and 3.16b to L_o, average width of openings in the wall, gives the number of openings in a wall. A ratio less than 1.0 means that there is only one

opening in between two piers. Number of piers is one larger than number of openings, as demonstrated in Fig. 3.17. Once number of piers is estimated, length of piers, L_p, can be calculated as follows:

$$L_{px.y} = \frac{L_{wx,y}}{n_{x,y}}$$ (3.17)

where, $n_{x,y}$ = number of piers in the x or y direction, respectively.

This derivation completes the representation of h_p and L_p in terms of global building parameters. The only remaining term in Eq. 3.13a and 3.13b is the axial load over story piers, P_f. This term has two parts: 1) self-weight of walls and 2) diaphragm load carried by walls. For non-load-bearing walls, self-weight is the only term that contributes to the axial story load.
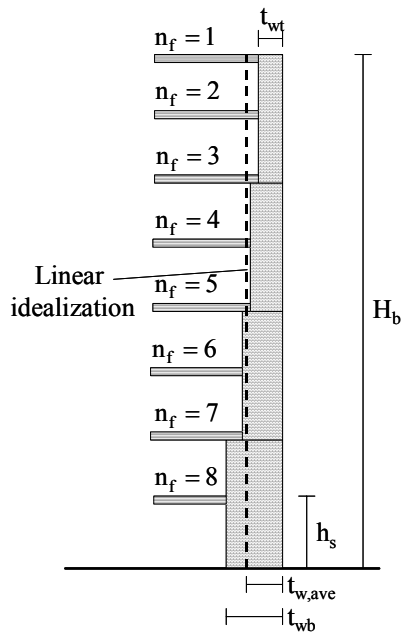
Figure 3.18. Tapered wall construction

Typically, walls of masonry buildings are tapered construction, see Fig. 3.18. Such shape reduces the self-weight of walls and creates more efficient load carrying system. For calculation purposes one may assume average wall thickness throughout the height of a wall,

54

as indicated by the dotted line in Fig. 3.18. With this assumption, the self-weight of a wall at each story can be expressed as:

$$P_{fsx,y} = n_f \gamma_m \alpha_{x,y,ave} A_f h_s \qquad (3.18)$$

where, $P_{fsx,y}$ = axial compressive load on story piers in x or y direction due to self-weight.

n_f = number of stories including and above the story being concerned, see Fig. 3.18.

γ_m = specific gravity of masonry, typically ranges between 125-140pcf

$\alpha_{ave} = \dfrac{\alpha_b}{2}\left(1+\dfrac{t_{wt}}{t_{wb}}\right)$, average wall area to floor area ratio along the height of the building.
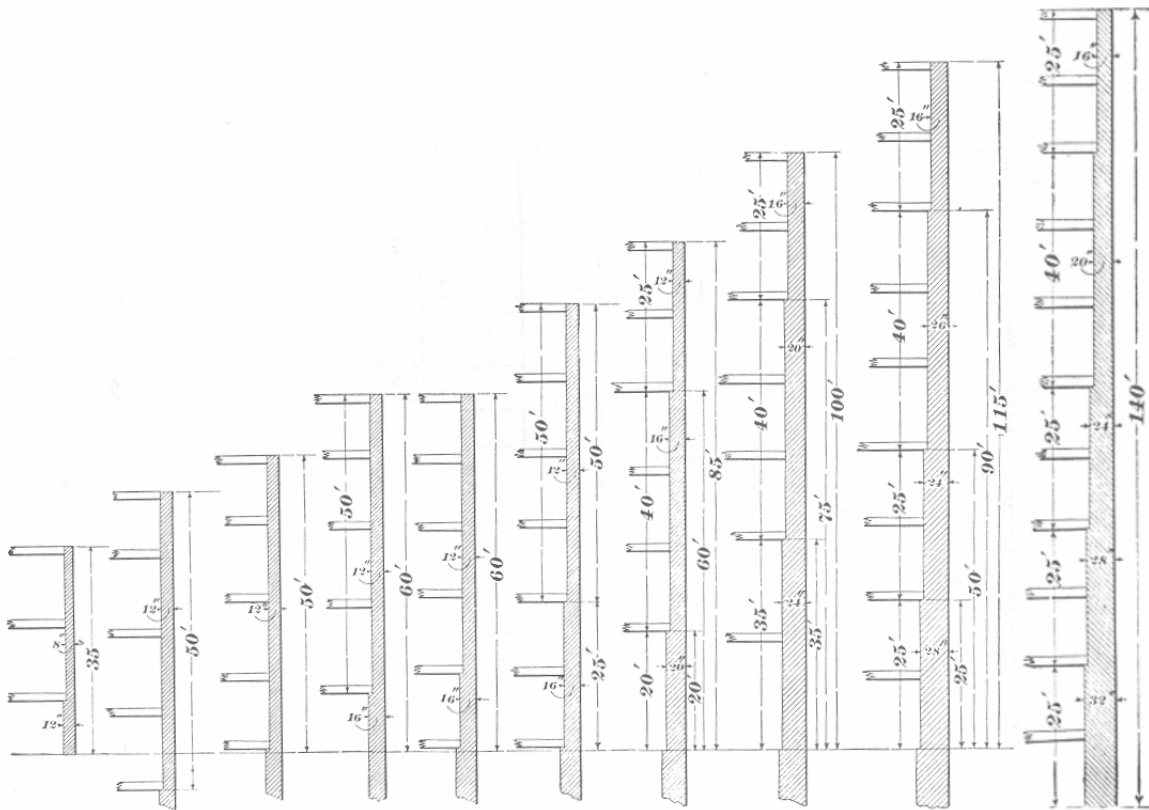
Figure 3.19 Standard thicknesses of masonry walls for dwelling houses per the building law of New York (figure taken from Lavica 1980)
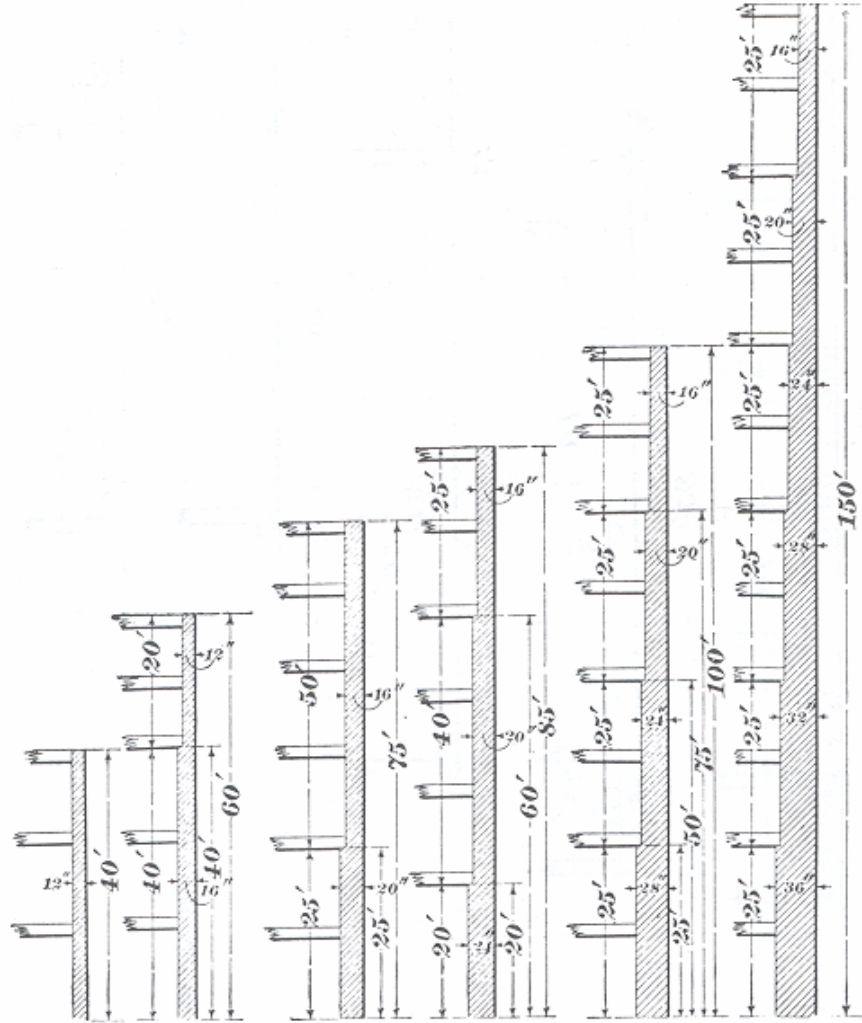
Figure 3.20. Standard thicknesses of masonry walls for warehouses and factories per the building law of New York (figure taken from Lavica 1980)

Lavicka (1980) provides standard thickness of masonry walls in proportion of their height per the building law of New York, as shown in Figs. 3.19 and 3.20. As noted by the author, the building law of New York can be taken as representative for the whole United States. The standard wall thickness values provided in Fig. 3.19 are utilized to estimate the wall thickness for the load-bearing walls considered in this study. The values in Fig. 3.20 are provided for reference and are not used, since the primary focus in this study is concentrated on residential type masonry construction. The thickness of non-load bearing walls are taken as 1-wyhte (4.0in) less thick than the thickness of load-bearing walls, as given by Eq. 3.19.

$$t_{wy} = t_{wx} - 4.0in \qquad (3.19)$$

56

Different than non-load-bearing walls, load-bearing walls also carry loads that are coming from floors. Axial load in load-bearing walls due to floor loads can be calculated as follows:

$$P_{fdx} = n_f \alpha_q q_f A_f \qquad (3.20)$$

here, P_{fdx} = axial compressive load on story piers due to uniform diaphragm loads. Note that this load only exists over load-bearing walls (= walls parallel to the x-direction).

q_f = uniformly distributed floor load.

α_q = percentage of floor load carried by exterior load bearing walls.

Figure 3.21 shows the estimation of α_q. In this figure, L_s represents typical span length of joists between adjacent vertical load supporting elements. Note that interior gravity columns only carry the vertical load. Their contribution to lateral strength and stiffness is negligible and ignored in this study.
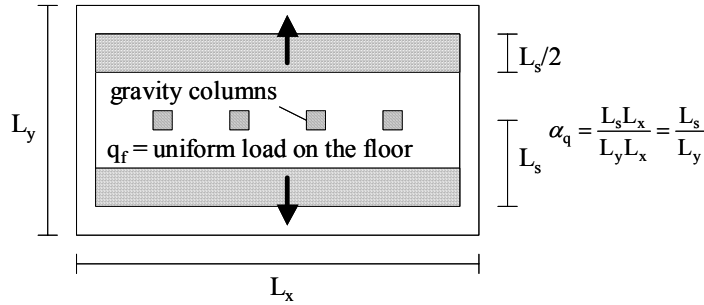
Figure 3.21. Percentage of floor load carried by exterior load-bearing walls

Eq. 3.18 and 3.20 can be combined to calculate the total axial compressive load on load-bearing walls:

$$P_{fx} = n_f A_f \left[\gamma_m \alpha_{x,ave} h_s + \alpha_q q_f \right] \qquad (3.21a)$$

for non-load bearing walls,

$$P_{fy} = n_f A_f \left[\gamma_m \alpha_{y,ave} h_s \right] \qquad (3.21b)$$

Once stiffness and strength associated with each wall are determined, non-linear spring properties can be determined. Depending on failure modes of walls, the response curves presented in Fig. 3.22a and 3.22b are used in this study. The first curve represents rocking

failure mode and it is bi-linear elastic. The second curve is bi-linear inelastic and represents the sliding failure mode. Energy dissipated within the loops mimics the energy dissipation through sliding of wall surfaces. In each response curve, post-elastic stiffness is taken as close to zero. This assumption is in agreement with various experimental investigations (Erbay and Abrams 2002, Franklin *et. al.* 2001, Costley and Abrams, Abrams and Shah 1992, Epperson and Abrams 1989). The initial stiffness and strength of springs are equal to story level stiffness and strength of walls.
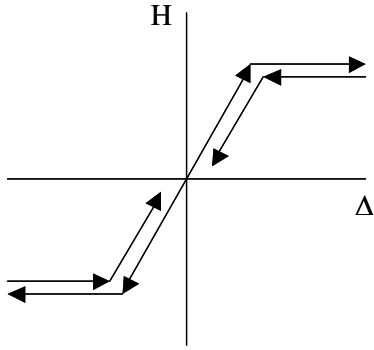
Figure 3.22a. Non-linear elastic response curve for rocking mode
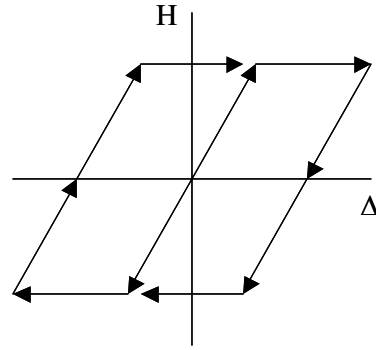
Figure 3.22b. Non-linear inelastic response curve for sliding mode

Dynamic mass:

Dynamic mass associated with each degree of freedom in the lumped mass model can be calculated with reference to Fig. 3.11. It is assumed that half of top and bottom wall masses are concentrated at a story level. This mass is distributed to analytical model degrees of freedoms as shown in Fig. 3.11. In terms of global building parameters, equations for mass calculations can be expressed as:

$$m_{dx} = \frac{1}{g}\left[L_y t_{wy} h_s \gamma_m + \frac{1}{2} A_f q_f\right] \tag{3.22a}$$

$$m_{dy} = \frac{1}{g}\left[L_x t_{wx} h_s \gamma_m + \frac{1}{2} A_f q_f\right] \tag{3.22b}$$

$$m_{wx} = \frac{1}{g}\left[\left(\frac{1}{2}L_y t_{wy} + L_x t_{wx}\right)\gamma_m h_s + \frac{1}{4} A_f q_f\right] \tag{3.23a}$$

$$m_{wy} = \frac{1}{g}\left[\left(\frac{1}{2}L_x t_{wx} + L_y t_{wy}\right)\gamma_m h_s + \frac{1}{4}A_f q_f\right]$$ (3.23b)

where, m_{dx} and m_{dy} = dynamic mass associated with diaphragm degree of freedoms for shaking in x and y directions.

m_{wx} and m_{wy} = dynamic mass associated with wall degrees of freedoms for shaking in x and y directions. Dynamic mass on opposing walls is equal to each other.

g = gravitational acceleration.

3.5. Steps of seismic evaluation procedure followed in this study

Previous sections introduced damage quantification and analytical idealization models to represent global response characteristics of unreinforced masonry buildings. The main objective of the modeling is to capture main dynamic response characteristics of an unreinforced masonry building with limited global building parameters. The damage quantification procedure links estimated global response parameters to different levels of damage states. Threshold values to categorize damage are defined and expressed in terms of global response parameters.

This section summarizes the steps of the seismic evaluation procedure that is followed in this study. Diagrammatic representation of the steps is laid out in Fig. 3.23.
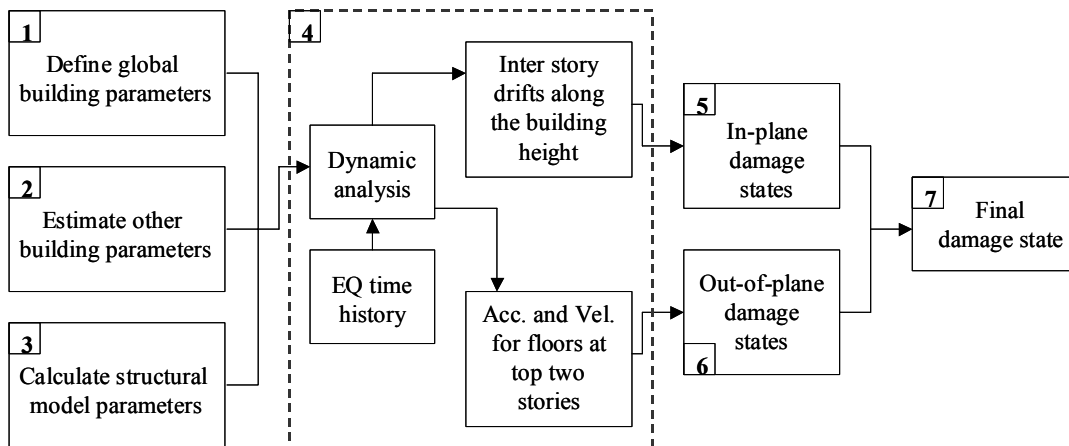
Figure 3.23. Steps of the seismic evaluation procedure

Steps:

1. <u>Define global building parameters:</u>

   - n_s, A_f, $\alpha_{x,y}$, α_d, α_h, q_f, h_s, E_m, G_d, L_o, and L_s

2. <u>Estimate remaining building parameters:</u>

   - t_{wx} and t_{wy} $\rightarrow$ Fig. 3.19 and Eq. 3.19

   - h_p $\rightarrow$ Eq. 3.14

   - L_x and L_y $\rightarrow$ Eqs. 3.15a and 3.15b

   - α_q $\rightarrow$ Fig. 3.21 and Eq. 3.20

   - n_x and n_y $\rightarrow$ Eqs. 3.16a and 3.16b

   - L_{px} and L_{py} $\rightarrow$ Eq. 3.17

   - γ_{yi} and γ_{yj} $\rightarrow$ Eqs. 3.8a and 3.8b

3. <u>Calculate structural model parameters:</u>

   - P_f $\rightarrow$ Eqs. 3.21a and 3.22b

   - a_{cr} $\rightarrow$ Eqs. 3.1a and 3.1b

   - a_{con} $\rightarrow$ Eq. 3.3

   - $PE_{f,lb}$ or $PE_{f,nlb}$ $\rightarrow$ Eqs. 3.2b and 3.2c

   - k_{wx}, k_{wyi}, and k_{wyj} $\rightarrow$ Eqs. 3.6, 3.7a and 3.7b

   - k_{dx} and k_{dy} $\rightarrow$ Eqs. 3.9a and 3.9b

   - m_{wx} and m_{wy} $\rightarrow$ Eqs. 3.23a and 3.23b

   - m_{dx} and m_{dy} $\rightarrow$ Eqs. 3.22a and 3.22b

   - H_{sr} and H_{ss} $\rightarrow$ Eqs. 3.13a and 3.13b

4. <u>Conduct dynamic analysis</u>

Compute the dynamic response of the building for x and y direction. From response history, calculate:

- Maximum inter story drift, ISD.

- Maximum diaphragm accelerations and velocities for the top two stories.

5. <u>Identify in-plane damage state:</u>

Compare the calculated ISD values with the threshold limits given in Table 3.4. Categorize the damage state for both shaking directions.

- ISD<0.1% → No damage, NO

- 0.1%<ISD<0.6% → Immediate Occupancy, IO

- 0.6%<ISD<1.0% → Life Safety, LS

- 1.0%<ISD<2.0% → Collapse Prevention, CP

- 2.0%<ISD → Total Collapse, TC

6. <u>Identify out-of-plane damage state:</u>

Compare the floor accelerations and velocities with the critical values.

- Averaged acceleration at top two floors $= (a_t + a_{t-1})/2 > a_{cr}$ → walls cracked in the out-of-plane direction → check the stability of the non-load-bearing walls.

- Acceleration at the top floor $= a_t > a_{con}$ → sliding takes place at the diaphragm wall connection → check the stability of the load-bearing walls.

- if no cracking takes place → No damage, NO

- if cracking takes place but no collapse → Immediate Occupancy, IO

- if collapse takes place in non-load-bearing walls → Collapse Prevention, CP

- if collapse takes place in load-bearing walls → Total Collapse, TC

7. Assign final damage state to the building:

The final damage state of the building is determined by comparing the damage states assigned to in-plane and out-of-plane component. The higher damage state in either direction governs and set equal to the final damage state of the building in that shaking direction. For example, if a building has IO level of in-plane damage and CP level of out-of-plane damage, then the final damage state of the building is CP. Similarly, if a building has LS level of in-plane damage and IO level of out-of-plane damage, then the final damage state of the building is LS.

3.6. Example building evaluation

Seismic evaluation steps that are outlined in Section 3.5 are demonstrated on a half-scale two-story building. Particular reason in selecting this building is that it has configuration and construction characteristics that are similar to its full-scale counterparts in typical urban regions of the United States. Furthermore, it was dynamically tested on the shaking table of the Construction Engineers Research Laboratory at the U.S.-Army Engineering Research and Development Center located in Champaign, IL. This test provides measured response data that can be compared with the analytical estimates.

3.6.1. Test building

A three-dimensional view of the building is shown Fig 3.24. Figure 3.25 presents elevation and plan drawings. The building consists of two stories with square floors. Walls are constructed out of half scale clay bricks and floors are constructed from wood. Floor joists are carried by walls A and B, making these walls load-bearing. As can be noticed from Fig. 3.25, walls A and B are mirror image of each other. This results in symmetrical building properties in the x-direction. Walls in the y-direction consist of openings that are asymmetrical on both sides of the building. This results in different stiffness and strength properties for either side of building in the y-direction. Lead bricks were added on wall surfaces as well as on floor diaphragms in order to compensate the non-proportional reduction of gravity stresses due to half scale model.
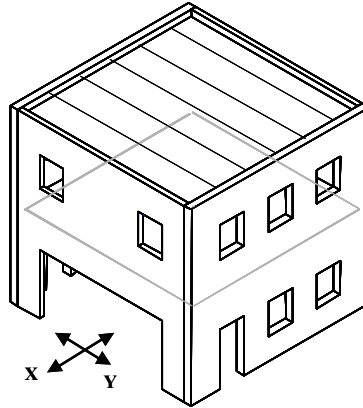
Figure 3.24. Three-dimensional view of the building
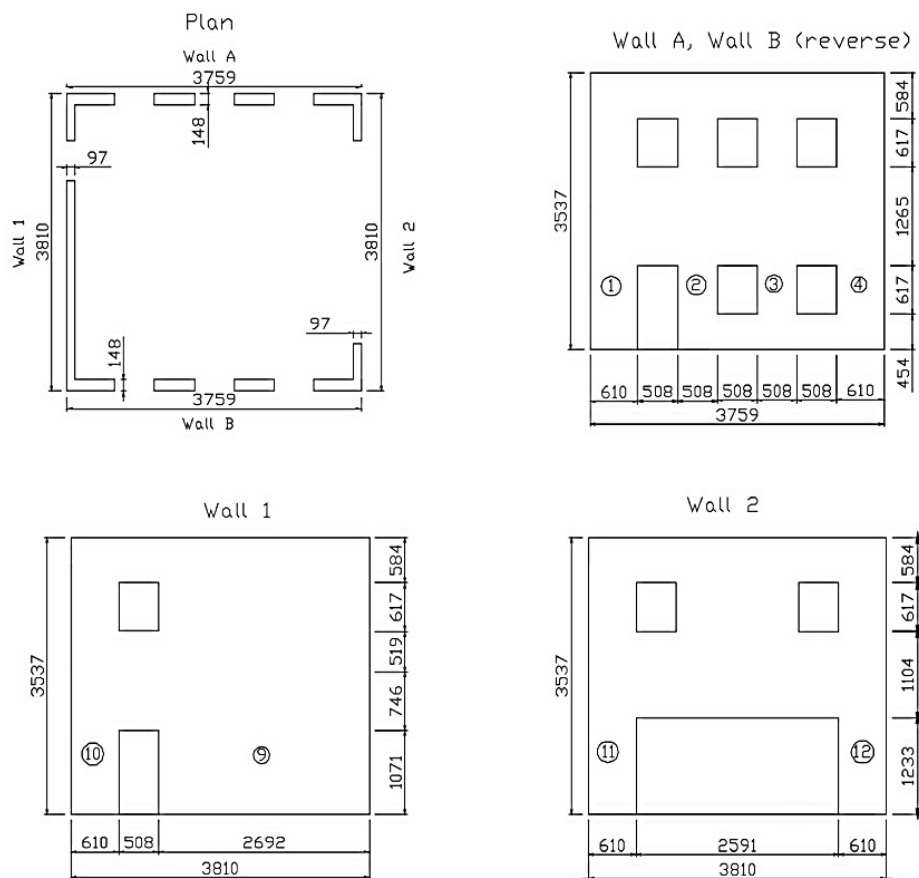
Figure 3.25 Elevation and plan layouts of the building (dimensions are in millimeters)

(drawings are taken from Orton *et al.* 1999)

Shaking table tests were conducted for both orthogonal directions of the building. Nahanni (23 December 1985, Component = 280, M = 6.8) acceleration time record was used to simulate base earthquake. The time component of the earthquake motion was condensed by a factor of $\sqrt{2}$ to account for the half scale test structure. Figure 3.26 shows the acceleration time-history that was applied as the input motion to the shake table and the acceleration time-history that was measured at the surface of the shake table. As can be noticed, the input and the output data is slightly from each other. The test structure was exposed to the acceleration time-history that was measured at the surface of the shake table. For this reason, the analyses were conducted using this time-history data. The response spectrum of the acceleration time-history measured at the surface of the shake table is shown in Fig. 3.27.
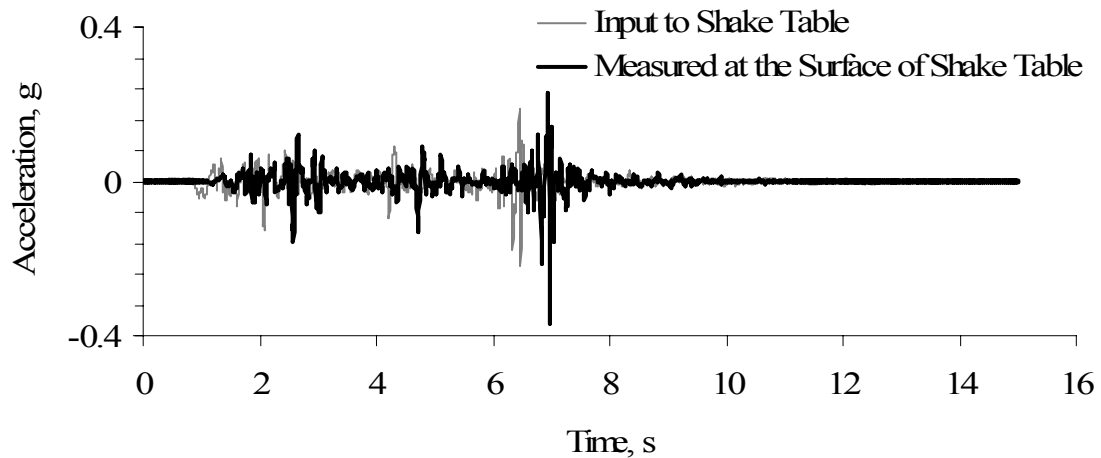
Figure 3.26 Acceleration time-history of the base excitation
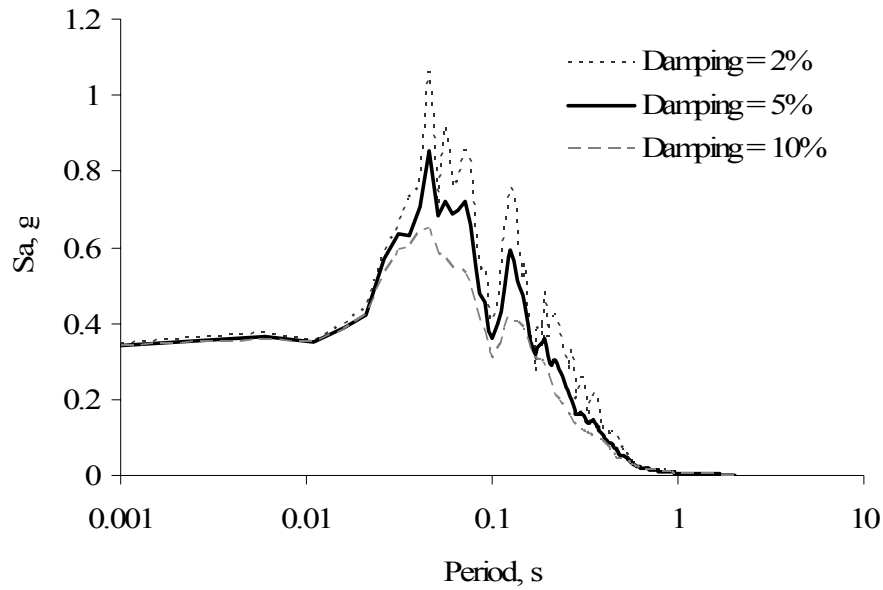
Figure 3.27 Response spectrum of the base excitation

The structural properties of the test building are listed in Table 3.6. The values provided in the second row of the table were used in the analytical idealization and evaluation.

Table 3.6 Measured and used values for some of the building parameters

	E_m, ksi	G_d, kip/in	Damping, ξ, %	Cohesion, τ_c, psi	Sliding friction, μ_{sld}
Measured range	200-530	25-50	5-12	-	-
Values used in analyses	250	35	5	40[*]	0.5[*]

[*] Values are assumed for type O mortar.

3.6.2. Evaluation

The building is evaluated under a ground motion with a PGA level of 0.2g in the x-direction. For this evaluation, walls A and B respond in the in-plane direction whereas walls 1 and 2 respond in their transverse direction. Following the steps that are outlined in Section 3.4:

Step 1. Define global building parameters:

$n_s = 2$

$A_f = 12.3 \times 12.5 = 154.2 \text{ ft}^2$

$q_f = 22 \text{ lb/ft}^2$

$\gamma_m = 200 \text{ lb/ft}^3$ (this value is selected to account for additional steel weights that are attached on wall surfaces)

$\alpha_x = A_w / A_f = 7.12/154.2 = 0.046$

$\alpha_d = 12.3/12.5 \cong 1.0$

$\alpha_h = \dfrac{3 \times 20 \times 24.3 + 1 \times 20 \times 42.2}{4 \times 20} \cdot \dfrac{1}{6 \times 12} = 40\%$ (using weighted average with respect

to pier lengths)

$h_s = 6.0\text{ft}$

$L_o = 20\text{in}$

$L_s =$ there are no intermediate gravity columns, therefore a value larger than the dimensions of the building is assumed.

Step 2. Estimate remaining building parameter:

Referring to Fig. 3.19 and Eq. 3.19 thickness of each wall can be estimated as:

$t_{wx,1} = 6\text{in}$ and $t_{wx,2} = 4\text{in}$

$t_{wy,1} = 4\text{in}$ and $t_{wy,2} = 4\text{in}$

Note that half of the estimated thickness values are taken since the building is a half scale model. As can be noticed, estimated values agree well, especially at the first floor, with actual wall thickness values that are used in the building.

$h_p = 0.40 \times 6 \times 12 = 28.8\text{in}$

$\alpha_q = 1.0$ (since, there are no gravity columns in between walls A and B)

$$L_x = L_y = \sqrt{154.2} = 12.4\text{ft}$$

$$L_{ox} = L_x - \frac{L_{wx}}{2} = 12.4 - \frac{0.046 \times 154.2}{2 \times 0.5} = 63.3\text{in}$$

$$3.0 < \frac{L_{ox}}{L_o} = \frac{63.3}{20} = 3.2 < 3.5 \;\rightarrow\; n_x = 2 \times (3+1) = 8 \;\;(4 \text{ piers on either side})$$

$$L_{px} = \frac{L_{wx}}{n_x} = \frac{0.046 \times 154.2}{8 \times 0.5} \times 12 = 21.3\text{in}$$

Step 3. Calculate structural model parameters:

$$\alpha_{x,ave} = \frac{L_{wx} t_{wx,ave}}{A_f} = \frac{14.2 \times (6+4)/2 \times 1/12}{154.2} = 0.038$$

$$P_{fx,1} = 2 \times 154.2 \times [200 \times 0.038 \times 6 + 1.0 \times 22] \times \frac{1}{1000} = 20.8\text{kips}$$

$$P_{fx,2} = 1 \times 154.2 \times [200 \times 0.038 \times 6 + 1.0 \times 22] \times \frac{1}{1000} = 10.4\text{kips}$$

$$a_{cr,nlb} = \frac{1}{3}\left(\frac{t_{wy}}{h_s}\right)g = \frac{1}{3}\left(\frac{4}{6 \times 12}\right)g = 0.02g$$

$$a_{con} = a_{cr,nlb} \;\;(\text{for non-load-bearing walls})$$

$$W_{wy} = \gamma_m h_s t_{wy,top} L_y = 200 \times 6 \times \frac{4}{12} \times 12.4 \frac{1}{1000} = 4.96\text{kips}$$

$$PE_{f,nlb} = \left[0.45 \frac{t_{wy}^2}{h_s}\right]\frac{W_{wy}}{2} = \left[0.45 \frac{4^2}{6 \times 12}\right]\frac{4.96}{2} = 0.248\text{kip} - \text{in}$$

$$k_{wx,1} = 0.20 \times 0.046 \frac{250 \times (154.2 \times 12^2)}{28.8} = 1773\text{kips/in} \;\;(1^{\text{st}} \text{ story stiffness})$$

$$k_{wx,2} = 0.20 \times \left(\frac{4\text{in}}{6\text{in}} \times 0.046\right)\frac{250 \times (154.2 \times 12^2)}{28.8} = 1182\text{kips/in} \;\;(2^{\text{nd}} \text{ story stiffness})$$

$$k_{dx} = 4G_d \alpha_d = 4 \times 35 \times 0.25 \times 1.0 = 140\text{kips/in}$$

$$m_{wx,1} = \frac{1}{g}\left[\left(\frac{1}{2}L_y t_{wy,1} + L_x t_{wx,1}\right)\gamma_m h_s + \frac{1}{4}A_f q_f\right]$$ (mass corresponding to each

opposing wall on the first story)

$$= \frac{1}{386.1}\left[\left(\frac{1}{2}\times 12.4 \times \frac{4}{12} + 12.4 \times \frac{6}{12}\right)\times 200 \times 6 + \frac{1}{4}\times 154.2 \times 22\right] = 27.9 \mathrm{lb}\cdot\mathrm{s}^2/\mathrm{in}$$

$m_{wx,2} = 21.5\mathrm{lb}\cdot\mathrm{s}^2/\mathrm{in}$ (2nd story wall mass on either side)

$$m_{wy,1} = \frac{1}{386.1}\left[\left(\frac{1}{2}\times 12.4 \times \frac{4}{12} + 12.4 \times \frac{4}{12}\right)\times 200 \times 6 + \frac{1}{4}\times 154.2 \times 22\right] = 21.5 \mathrm{lb}\cdot\mathrm{s}^2/\mathrm{in}$$

$m_{wy,2} = m_{wy,1} = 21.5\mathrm{lb}\cdot\mathrm{s}^2/\mathrm{in}$

$$m_{dx,1} = \frac{1}{g}\left[L_y t_{wy,1} h_s \gamma_m + \frac{1}{2}A_f q_f\right]$$ (diaphragm mass at the 1st story)

$$= \frac{1}{386.1}\left[12.4 \times \frac{4}{12}\times 6 \times 200 + \frac{1}{2}\times 154.2 \times 22\right] = 17.2\mathrm{lb}\cdot\mathrm{s}^2/\mathrm{in}$$

$m_{dx,2} = m_{dx,1} = 17.2\mathrm{lb}\cdot\mathrm{s}^2/\mathrm{in}$ (diaphragm mass at the 2nd story)

$$H_{sr,1} = 0.9\frac{L_{px}}{h_p}P_{fx,1} = 0.9 \times \frac{21.3}{28.8}\times 20.8 = 13.8\mathrm{kips}$$

$$H_{sr,2} = 0.9 \times \frac{21.3}{28.8}\times 10.4 = 6.9\mathrm{kips}$$

$$H_{ss,1} = \left(\frac{3}{8}\frac{A_f}{P_{fx,1}}\alpha_{x,1}\tau_c + \mu_{sld}\right)P_{fx,1} = \left(\frac{3}{8}\frac{(154.2 \times 12^2)}{20.8 \times 1000}\times 0.046 \times 40 + 0.5\right)\times 20.8 = 25.7\mathrm{kips}$$

$$H_{ss,2} = \left(\frac{3}{8}\frac{(154.2 \times 12^2)}{10.4 \times 1000}\times 0.030 \times 40 + 0.5\right)\times 10.4 = 15.2\mathrm{kips}$$

Comparison of H_{sr} and H_{ss} show that the story strength associated with rocking is smaller than the story strength corresponding to sliding. Therefore, the governing failure mode for each story is rocking. From this statement, the base shear coefficient of the building can be calculated as 0.27.

This step is carried out using the computer program Drain-2DX (Prakash *et al.* 1993). The calculated parameters and the idealization model, shown in Fig. 3.11, were used to build the numerical model of the building. The acceleration time history data that was measured on the surface of the shaking table is used as the input motion to analyze the model. Actual measurements have shown that damping ranged from 5% to 6% for the x-direction and 10% to 12% in the y-direction. For analysis a damping level of 5% is assumed.
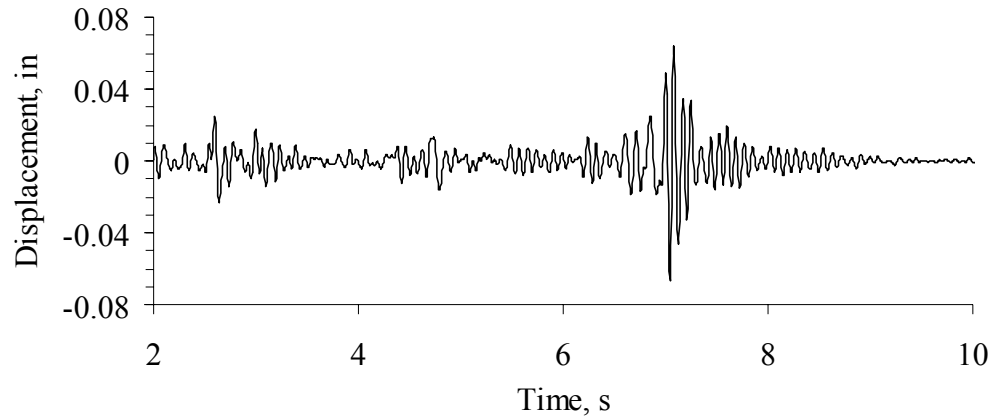

Figure 3.28. Calculated displacement time history at the mid-span of the second floor diaphragm
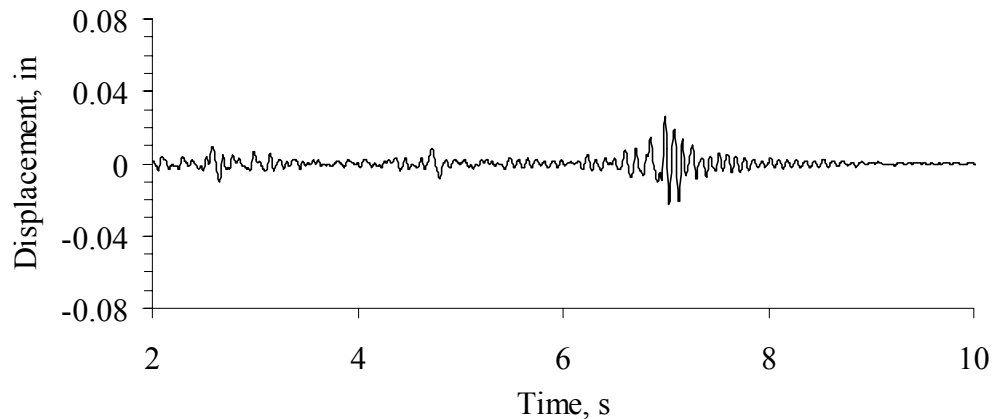

Figure 3.29. Calculated displacement time history at the top of the second story walls

Figures 3.28 and 3.29 show displacement time histories at mid-span of the second story floor and at the top of the second story walls. It can be noticed that diaphragm displacements are

approximately 2.5 times greater than wall displacements. Calculated fundamental period of the building for the x-direction is 0.085s.

Step 5. Identify in-plane damage state:

The maximum interstory drift happens at t = 7s and is equal to 0.02%. Based on this value and with reference to Table 3.4, the in plane damage of the building can be categorized as "no damage", NO, since 0.02% < 0.1%.

Step 6. Identify out-of-plane damage state:

Cracking acceleration level, $a_{cr,nlb}$, was reached at an earlier part of the time history analyses. However, continuous calculations for stability check revealed that transverse walls remained in their position. Therefore, damage state in out-of-plane direction is categorized as immediate occupancy, IO.

Step 7. Assign final damage state to the building:

Comparison of damage states for in-plane and out-of-plane directions yields and immediate occupancy, IO, damage state to the building for a shaking in the x-direction. This damage state corresponds to a PGA level of 0.20g.

3.6.3. Comparison with test results

Both estimated damage state and calculated response agree well with the measured and observed response of the building, especially considering the simplicity in the analytical model.

Calculated building period, 0.085s, is about the same as the measured one, which is 0.089s. It should be noted that calculated period value depends on assumed values for masonry elastic modulus and diaphragm shear stiffness. However, period calculations for different parameter combinations have shown that the variation is on the order of 10% (calculated values ranged from 0.080s-0.110s).

Figs. 3.30 and 3.31 compares the measured and calculated acceleration time histories at the top of the second story wall and at the mid-span of the diaphragm. As can be seen, both frequency content and general trend of response show good match with measured data. Difference between estimated and measured peak values for accelerations are on the order of

30%. To some degree, this difference can be attributable to damping level that was used in computations.

The amplitude ratio of diaphragm and wall response is approximately equal to 3.0 for measured response. For calculated response, this ratio is about 2.5. This claims that response amplification due to flexible diaphragms is well captured with the analytical model.
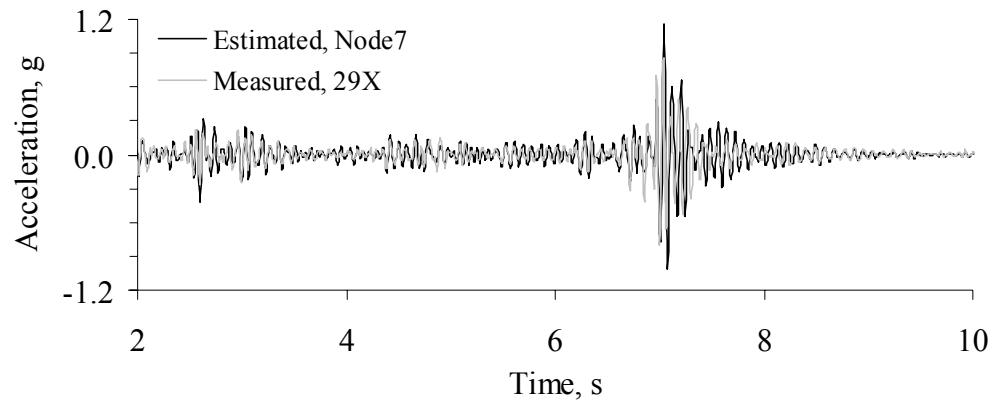

Figure 3.30. Comparison of acceleration time histories measured and computed at the mid span of the second floor diaphragm
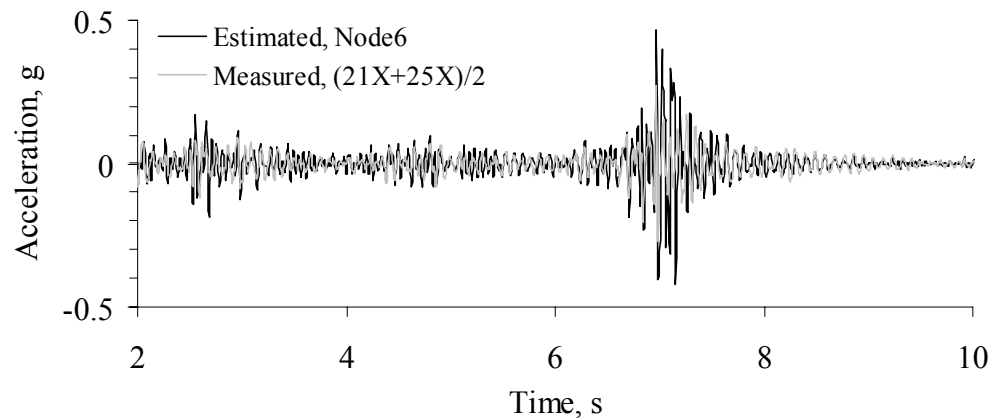

Figure 3.31. Comparison of acceleration time histories measured and computed at the top of second story walls (measured data is the average of measurements at two opposing walls)

CHAPTER 4 PARAMETERS THAT DEFINE POPULATIONS OF UNREINFORCED MASONRY BUILDINGS IN URBAN REGIONS

4.1. Introduction

The objective of this chapter is to define parameter distributions for a generic building population that represents characteristics of buildings in urban regions. Field surveys on unreinforced masonry buildings at Urbana, Carbondale, Memphis, and San Francisco, are investigated and distributions, on the average, representing building parameters of these populations are defined. These distributions are utilized to generate building populations for various ranges and combinations of parameters. Generated building populations are used in Chapter 5 to investigate the sensitivity of regional risk/loss estimates on global building parameters.

Table 4.1. Essential parameters for seismic evaluation of unreinforced masonry buildings.

Primary	Secondary
• Number of stories, n_s • Floor area, A_f • Story height, h_s • Floor aspect ratio, α_d • Wall area to floor area ratio, $\alpha_{x,y}$ • Average pier height as a percentage of story height, h_p • Uniform load over story, q_f • Elastic modulus of masonry, E_m • Equivalent in-plane shear modulus of wood floor, G_d	• Average length of openings, L_o • Average spacing between gravity load carrying members, L_s + Masonry wall thickness over the building height, t_w + Specific gravity of masonry, γ_m + Static coefficient of friction between wood and masonry, μ_s + Kinetic coefficient of friction between wood and masonry, μ_k

• Random parameters
+ Deterministic parameters

Table 4.1 summarizes essential building parameters that are necessary to evaluate seismic performance of unreinforced masonry buildings. Parameters are grouped into two: primary and secondary. Primary parameters are the main focus of sensitivity investigations that are conducted in Chapter 5. Secondary parameters are assumed to be of higher order for regional

risk investigations. Among them only the first two are investigated in Chapter 5, while remaining ones are treated deterministically.

4.2. Field investigations on building parameters in urban regions

To understand the variation of unreinforced masonry building parameters in urban regions, four field investigations that were conducted in different parts of the United States are analyzed. Table 4.2 summarizes general characteristics as well as types of data collected from each building population. In general, investigations conducted at Urbana and Carbondale represent building properties for small communities, whereas investigations conducted at Memphis and San Francisco represent building properties for large communities. As can be seen from Table 4.2, the building databases provided information primarily on four parameters, number of stories (n_s), floor area (A_f), story height (h_s), and floor aspect ratio (α_d). Additional field investigations were conducted in downtown Urbana to understand typical ranges for other parameters.

Table 4.2. Databases on unreinforced masonry building properties at urban regions.

City	Source	Number of buildings	Available variables
Urbana, IL	City of Urbana and Wu (2001)	54	n_s, A_f, α_d, $(h_p, L_o)^*$
Carbondale, IL	Wu, Crelling, Olshansky, (2001)	72	n_s, A_f
Memphis, TN	Abrams and Shinozuka, (1997)	517	n_s, A_f, $(h_p, L_o, \alpha_p)^*$
San Francisco, CA	Holmes *et. al.*, (1990)	2007	n_s, A_f, h_s, α_d

[*] The variables in parentheses represent the parameters that are measured in some buildings.

Distribution of building properties for each location is presented in Figs. 4.1 and 4.2. Each figure shows the variation of a particular parameter together with a representative distribution that is utilized in this study. Representative distributions are developed by considering individual as well as averaged distributions for each parameter. Averaged distributions are calculated through simple and weighted averaging of percentages corresponding to each

parameter interval. The number of buildings in each database is used to calculate "weights" for weighted averaging. Weighted averaging biased distributions towards larger communities, since the database associated with these communities contains more buildings. In statistical terms, such bias is acceptable, because the credibility of distributions gets better as the number of sample size gets larger. It should also be noted that, in general, regardless of the size of the community, each parameter showed highly similar distributions for each town.

(a)

(b)

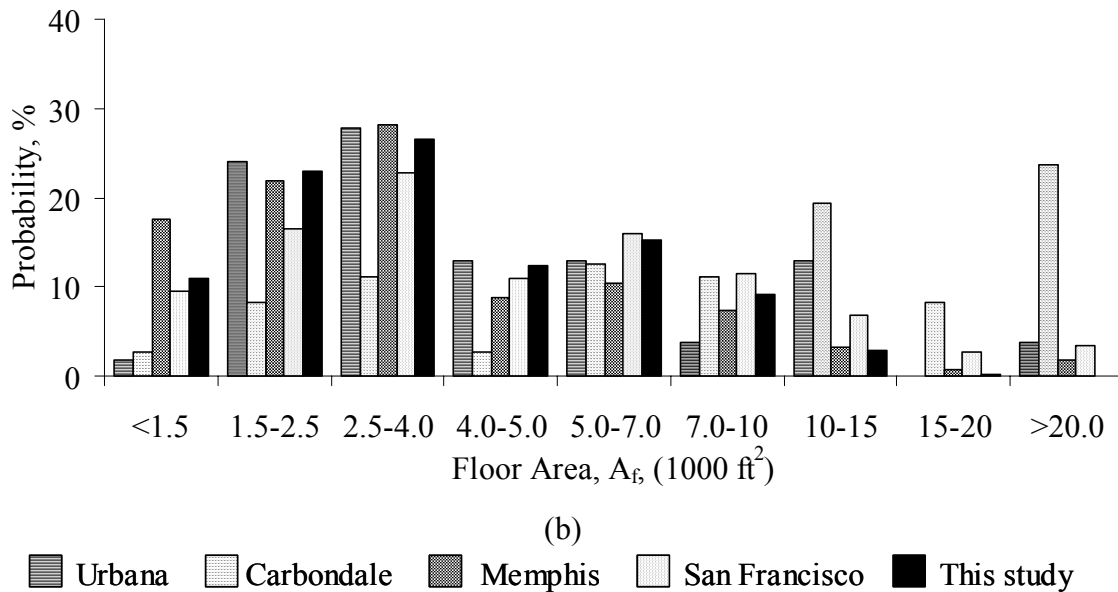Urbana   Carbondale   Memphis   San Francisco   This study
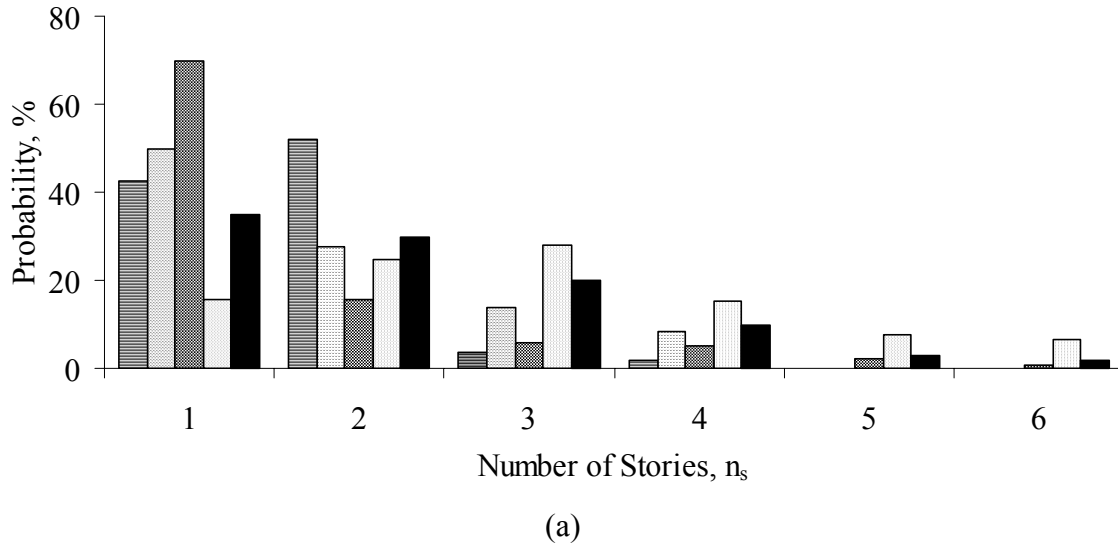
Figure 4.1. Variation of number of stories and floor area

According to the variation in number of stories it can be seen that about 90% of the building population, for each town, consists of one to four story buildings, see Fig 4.1a. The overall

trend of distributions in each town is similar to each other except the building population in San Francisco, where the frequency of observed three to four story buildings is about the same as the frequency of observed one to two story buildings. This pattern can be primarily attributable to construction practices in San Francisco rather than the size of the building population, since the building population in Memphis does not show a similar trend. In each town the building population contains buildings that are more than six stories; however, these buildings are statistically insignificant. Therefore, six stories can be taken as the statistical upper bound for each population. In view of these observations, a discrete distribution is defined to represent the variation of number of stories in urban regions, see Figs. 4.1a and 4.3a. The defined distribution on the average fits with 2.0% significance level to observed distributions.

As is in the case of number of stories, the variation of floor area, in general, is highly similar for different locations regardless of the size of the community, see Fig 4.1b. The different, shifted, distribution associated with buildings at Carbondale can be considered as site-specific and, therefore, can be taken out from the statistical investigation. Unlike number of stories, the floor area is a continuous variable. To capture this nature of the parameter, a continuous distribution is utilized to represent the variation. In this study a beta distribution is used to represent continuous variables. The main advantage of the beta distribution is that one may limit the possible values of a variable to specified ranges. Such bounding is essential to ensure realizations that are physically meaningful. Figures 4.1b and 4.3b respectively show discrete and continuous forms of the fitted beta distribution to observed floor area data. Representative beta distribution on the average fits with 2.5% significance level to the observed distributions.

The only database that provided information on story heights of buildings is the database associated with buildings in San Francisco. The variation of this parameter is shown in Fig. 4.2a. Additional investigations conducted in downtown Urbana confirmed that the distribution observed for downtown buildings in San Francisco can be considered as representative of story height distributions also in smaller communities. As is in the case of floor area, the variation of story height is represented by a continuous beta distribution. The resulting distribution fits with 10% significance level to the observed distribution, see Figs. 4.2a and 4.3c.
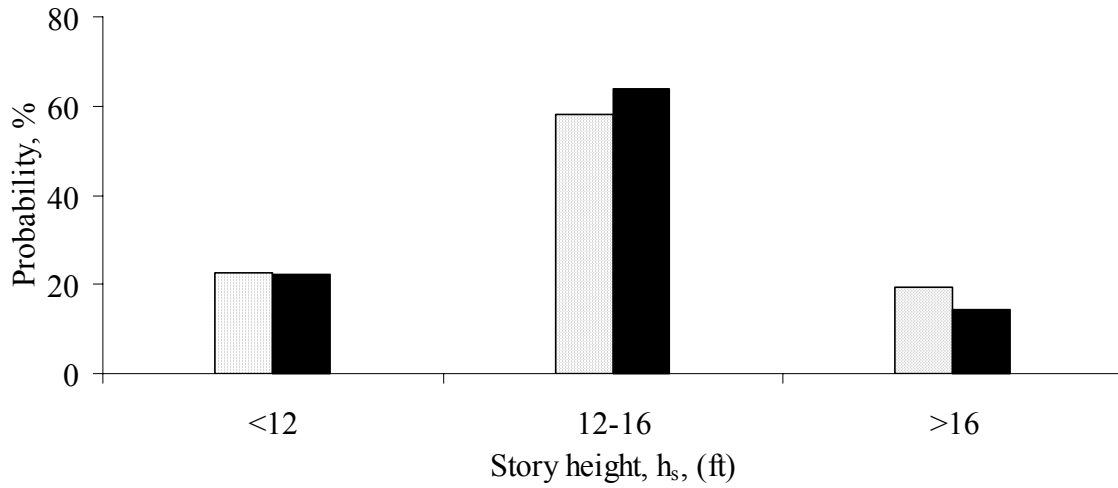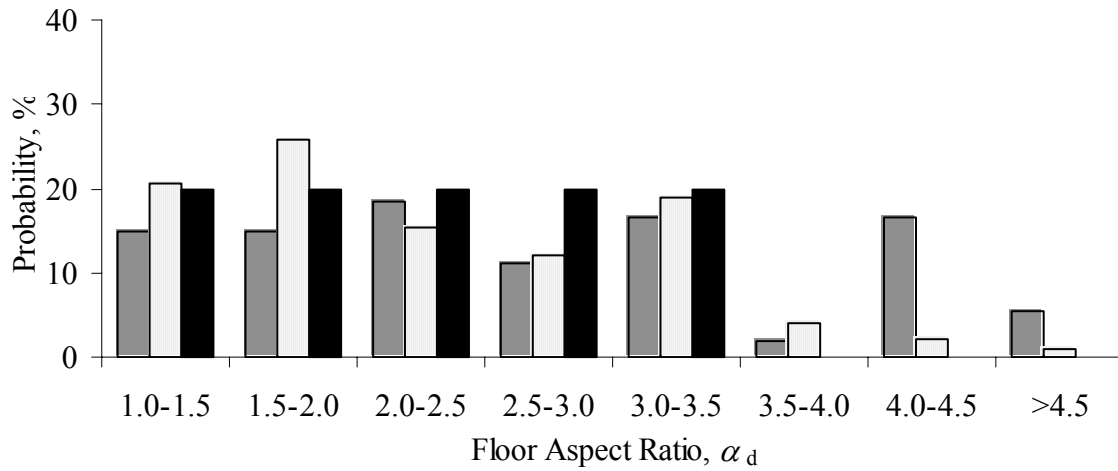
Figure 4.2. Variation of story height and floor aspect ratio.

Investigations in buildings in Urbana and San Francisco provided data on the variation of floor aspect ratio. In general, the variation of the parameter is uniform for both locations, see Fig 4.2b. For San Francisco more than 90% and for Urbana more than 75% of the building population lies in the range of 1.0 to 3.5. Relying more heavily on the data from San Francisco, a value of 3.5 can be taken as the statistical upper bound for floor aspect ratio of downtown buildings. Base on these observations a uniform distribution is assumed to represent this parameter. The continuous form of the distribution is shown in Fig. 4.3d and for comparison a discrete form is provided in Fig. 4.2b.
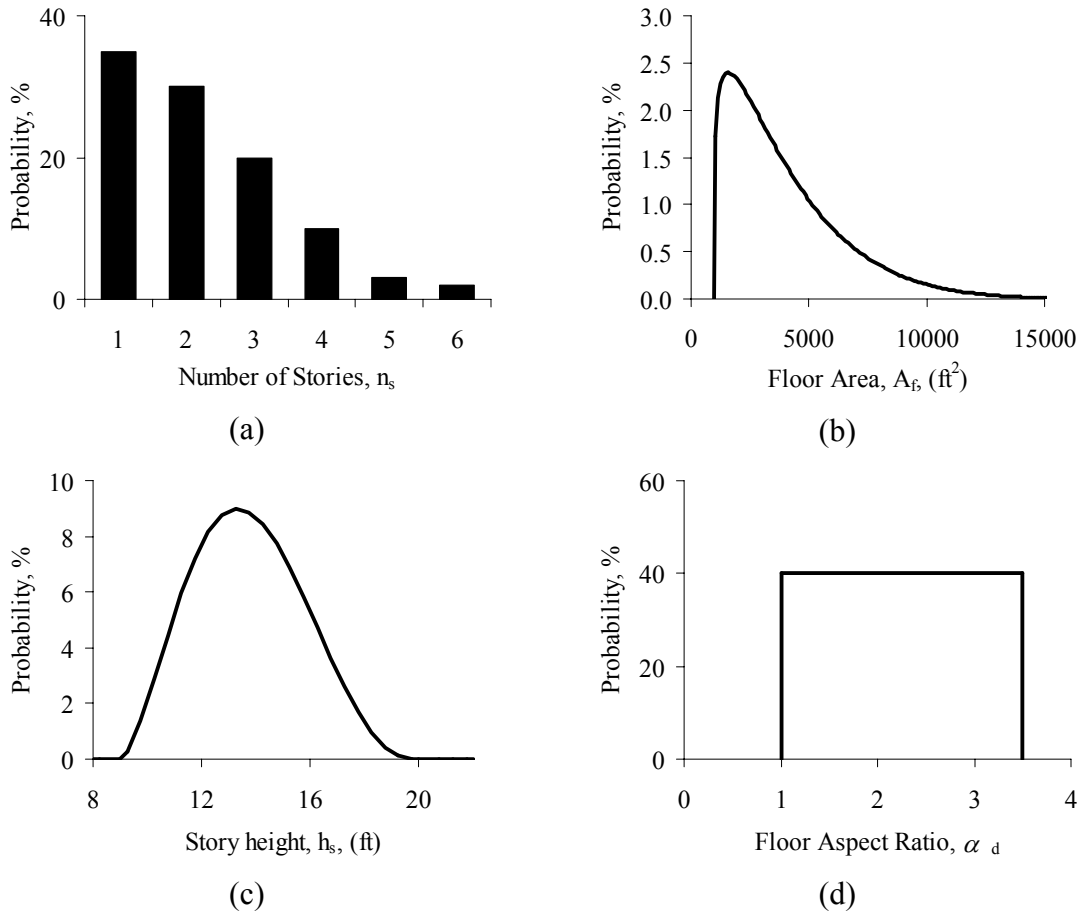
Figure 4.3. Representative distributions assumed for number of stories, floor area, story height, and floor aspect ratio.

So far, all the distributions are investigated with the assumption that the variation of each parameter is independent from the value of the other parameters. In statistical terms, the parameters are assumed to be statistically independent and uncorrelated. To investigate this assumption data from downtown Urbana is plotted for different discrete values of parameters. Figures 4.4a and 4.4b show the variation of floor area and floor aspect ratio for one story and two story buildings. As can be seen from these graphs the distributions associated with floor area and floor aspect ratio for different values of number of stories is, in general, are very similar to each other. With respect to this observation one may assume that floor area and floor aspect ratio are statistically independent from the number of stories. Figures 4.4a and 4.4b also show the variation of representative distributions that are assigned to each

parameter. As can be seen, in general, there is a good agreement with the observed data even though they are plotted for different number of stories.

(a)

(b)
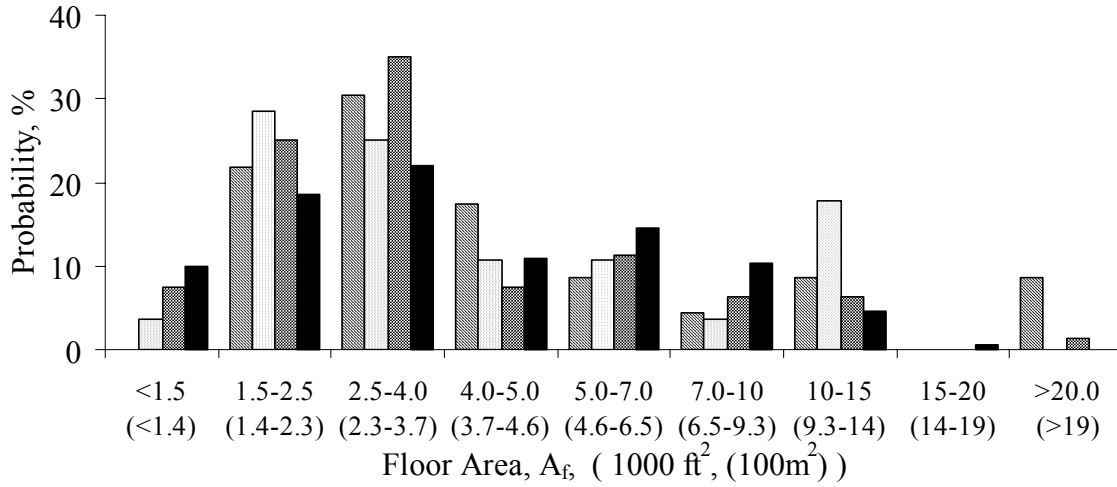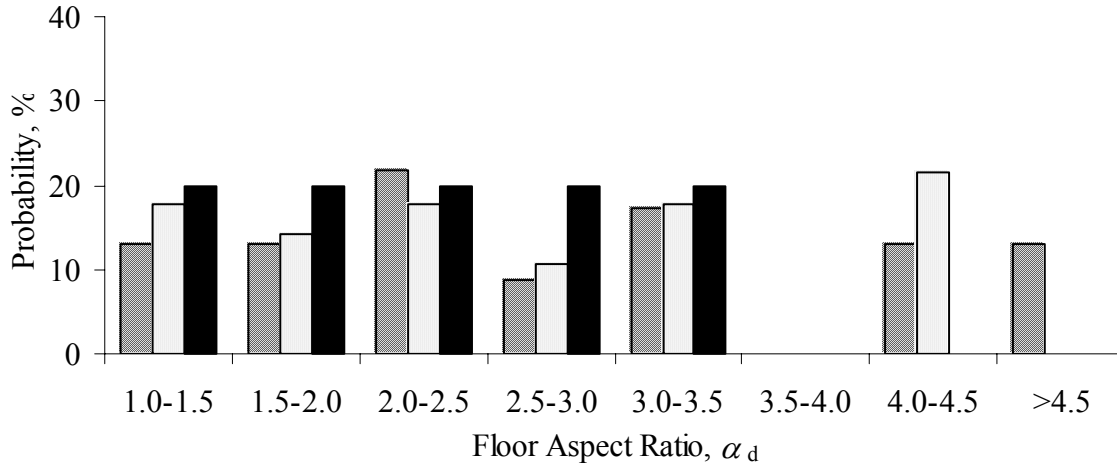
Figure 4.4. Variation of floor area and floor aspect ratio for different number of stories in Urbana and Memphis.

To investigate the statistical dependence between floor area and floor aspect ratio the distribution of floor area is plotted against two ranges of floor aspect ratio for the data from Urbana. The reason in selecting two ranges to discretize floor aspect ratio is to ensure statistically meaningful population size for each range. For this purpose the median value of 2.5 is selected to be the boundary between two ranges, 1.0 – 2.5 and 2.5 – 3.5. Figure 4.5

shows the variation of floor area for these two ranges. As can be seen from this graph, the distributions are similar to each other and show good agreement with the representative distribution that is assigned for floor area. This observation supports the assumption of statistical independence of floor area and floor aspect ratio.
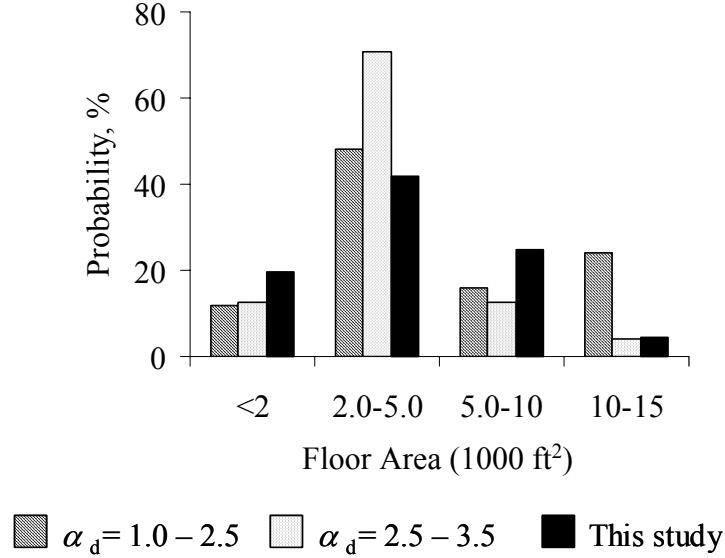

Figure 4.5. Variation of floor area for different ranges of floor aspect ratio in downtown Urbana.

Until now, the distributions associated with first four parameters in Table 4.1 are discussed. The remaining parameters are also essential for the seismic evaluation of unreinforced masonry buildings. However, none of the databases introduced so far contains field data on these remaining parameters. To overcome this problem, typical range of values that are measured in experimental studies as well as values suggested in design and evaluation documents are investigated. Based on these investigations, the ranges provided in Table 4.3 are assumed to represent typical values of the remaining building parameters in Table 4.1. For each parameter, the number of data points is not enough to define a probability distribution. Therefore, in order to be unbiased a uniform distribution is assumed to represent the randomness in each parameter.

Table 4.3. Ranges for parameters that are utilized in seismic evaluation of unreinforced masonry buildings.

Parameter	Source	Range	Used range
L_o (in)	Personal investigations at downtown Urbana Yi, Moon, Leon, and Kahn (2001) Abrams and Shinozuka (1997) Tena-Colunga, Abrams (1992)	40-120 35-140 36-120 36-150	40-120
L_s (ft)	Personal discussions with practicing engineers	15-25	15-25
h_p (% story height)	Personal investigations at downtown Urbana Yi, Moon, Leon, and Kahn (2001) Abrams and Shinozuka (1997) Tena-Colunga, Abrams (1992)	50-80 40-60 50-80 40-80	50-80
q_f (psf)	Tena-Colunga and Abrams (1992) Personal discussions with practicing engineers	40-55 40-50	40-50
$\alpha_{x,y}$ (%)	Abrams and Shinozuka (1997)	1-5	1-5
E_m (ksi)	Watertown tests (Baker, 1909) Watertown tests (Baker, 1909) University of Illinois tests (Baker, 1909) Erbay and Abrams (2001) Franklin *et. al.* (2001) Epperson and Abrams (1989)	770-1400[*] 605-1100[*] 550-1870[*] 550-765 300-1600 330-600	500-1200
G_d (kips/in)	FEMA-356 (2001) Peralta, Bracci, Hueste (2003)	2-18 0.4-5.3	1-5
t_w (in)	Lavicka (1977)	Function of number of stories	Fig. 3.17
γ_m (pcf)	Baker (1909) Lavicka (1977) Hudson (1946)	100-145 120 100-165	130
μ_k, μ_s	Brick Industry Association Tech Note 24G Elert (2003)	0.5-0.6 0.6	0.5, 0.6

[*] Values are calculated from compressive strength values by using the $E_m=550f'_m$ relationship.

Among these parameters, wall density ratio, $\alpha_{x,y}$, is represented by a slightly different parameter, $\alpha_{wx,y}$, in population randomizations. This parameter is defined as follows:

$$\alpha_{wx,y} = \frac{\alpha_{x,y}}{\max(\alpha_{x,y})} \qquad (4.1)$$

where, $\max(\alpha_{x,y}) = \dfrac{2L_{x,y}t_{wx,y}}{A_f} = $ maximum possible wall density that may physically exist in a building with wall thickness of $t_{wx,y}$, plan dimension (in the direction of shaking) of $L_{x,y}$, and floor area of A_f.

According the definition in Eq. 4.1, $\alpha_{wx,y}$ can be regarded as percentage of maximum possible wall density ratio for given building dimensions. As can be noticed, an arbitrarily selected wall density ratio, $\alpha_{x,y}$, may result $\alpha_{wx,y}$ values grater than 100%. This means either wall thickness or building dimension has to increase in order to physically fit that amount of wall area into building. Wall thickness values are taken from design guidelines by Lavica (1980), therefore they are assumed to be fixed for a given number of stories. Similarly building dimensions are function of floor aspect ratio and the floor area, and these parameters are discussed to be independent from each other. Therefore, in order to generate buildings that are physically meaningful the wall density ratio has to be correlated with other parameters. The new parameter defined in Eq. 4.1 does this correlation. Calculation of $\alpha_{wx,y}$ for real buildings revealed values from 50% to 90%. In building generations, this interval range is utilized to randomize $\alpha_{wx,y}$. Like other parameters, a uniform distribution is assumed to represent the randomness of this parameter. Once $\alpha_{wx,y}$ is randomized, actual wall density ratio, $\alpha_{x,y}$, is back calculated from Eq. 4.1.

4.3. Sampling procedure

Distributions associated with building parameters can be utilized to generate random building populations that represent characteristics of unreinforced masonry buildings in urban regions. To do that, a sampling procedure has to be utilized. In general, the concepts of sampling are well established and implemented in various commercial software packages, such as

MATLAB and Mathematica. Among available sampling methods the Monte Carlo Sampling is the most commonly utilized one. The basic idea in this method is to generate uniformly distributed random numbers between 0 and 1.0. These randomized numbers are used to calculate sample data from a known distribution that represents randomness of a given variable. The formulation of algorithms for generating uniform random numbers is beyond the scope of this study. A complete discussion can be found in Ang and Tang (1990). However, to provide some background for upcoming discussions, the calculation of sample data from a known distribution and uniformly generated random numbers is summarized in the following paragraphs. This summary is based on discussions in Ang and Tang (1990).

Let, X be the random variable with a known distribution and has a cumulative probability distribution of $F_X(x)$. Then for a given value of cumulative probability, u, the value of X can be determined as:

$$x = F_X^{-1}(u) \tag{4.2}$$

where, u = uniformly distributed random variable between 0 and 1.0.

The cumulative probability distribution for U is

$$P(U \le u) = F_U(u) = u \tag{4.3}$$

Eq. 4.3 can be used to derive cumulative distribution for variable X that is sampled through Eq. 4.2 as follows:

$$P(X \le x) = P\left[F_X^{-1}(U) \le x\right] \tag{4.4a}$$

operating with $F_X(x)$ to both sides of the expression in square brackets, Eq. 4.4a can be re-expressed as follows:

$$P(X \le x) = P\left[U \le F_X(x)\right] \tag{4.4b}$$

The right hand side of the equation is nothing but the probability of variable U being smaller than $F_X(x)$ and can be expressed in terms of Eq. 4.3

$$P(X \le x) = F_U\left[F_X(x)\right] = F_X(x) \tag{4.34}$$

82

Equality in Eq. 4.4c shows that for a uniformly distributed variable U, values obtained for variable X through Eq. 4.2 will have the same cumulative probability distribution as the variable X. It should be noted that the same conclusion couldn't be made if the variable U had a distribution that is different than a uniform distribution. The generation of X can be graphically seen in Fig. 4.6.
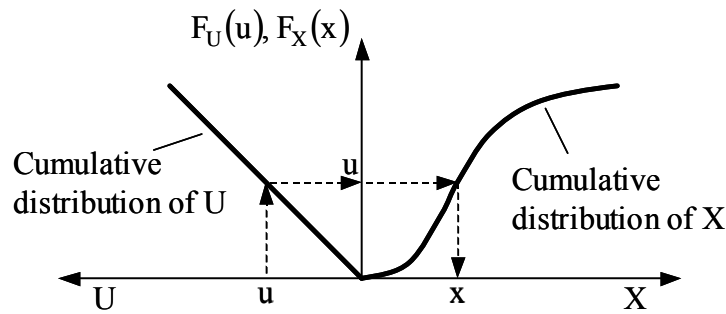

Figure 4.6. Generation of X from a uniformly distributed variable U. Figure adopted from Ang and Tang (1990).

The size of sample data to produce an acceptable level of representation for random variable X highly depends on the rate at which the uniformly distributed variable, u, approaches to uniform distribution in terms of the sample size. In most of the cases, large number of sampling is required to achieve the acceptable representation. To improve the convergence with smaller sample sizes, a constrained sampling scheme can be implemented into the Monte Carlo Sampling approach that was discussed above. This form of Monte Carlo Sampling is commonly known as the Latin Hypercube Sampling, LHS, (Wyss and Jorgensen, 1998).
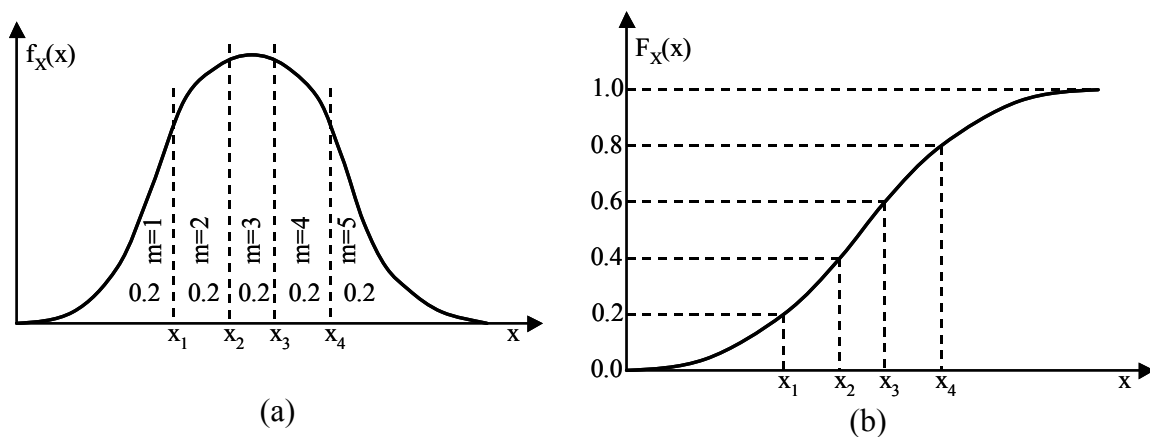

Figure 4.7. Selection of n=5 intervals with equal probability.

In this approach, the distribution associated with a random variable, X, is divided into n non-overlapping intervals on the basis of equal probability. An example division for n=5 intervals is demonstrated in Figs. 4.7a and 4.7b. In this example each interval corresponds to 20% probability. As can be noticed, even though the areas are equal in each interval, the interval range gets larger towards descending portions of the distribution.

The intervals are used to identify the boundaries from which equal number of samples is selected. As can be expected, for n=1, the approach becomes identical to regular Monte Carlo Sampling approach. However, as the number of intervals gets higher, the sample size that is required to properly represent distribution of X gets smaller. Once n equal intervals are selected, n times k uniformly distributed random numbers are generated, where k is the number of realizations that will be sampled from each interval. At this point the transformation equation, Eq. 4.5, is applied to generated random numbers. The purpose of this transformation is to ensure assignment of k random numbers to each interval. These numbers are utilized with Eq. 4.2 to calculate the corresponding x values.

$$u_{mi}^* = \frac{1}{n} u_{mi} + \frac{m-1}{n} \quad (i = 1, 2, \ldots, k \text{ and } m = 1, 2, \ldots, n) \qquad (4.5)$$

here, $u_m^* = $ cumulative probability associated with interval number m.

$u_m = $ cumulative probability randomly generated for interval m

n = total number of intervals

m = interval index

i = random number index

Figure 4.8 shows the influence of this modified approach on representing a standard normal distribution with different sample sizes. In this example, number of bins is taken as 10% of the sample size, i.e. 10 intervals are used for a sample size of 100. The probability distributions in Fig. 4.8a are generated through regular Monte Carlo Sampling approach, whereas the probability distributions in Fig. 4.8b are generated using the LHS method. As can be noticed, LHS more rapidly converges to the real distribution as the number of sample size increases.
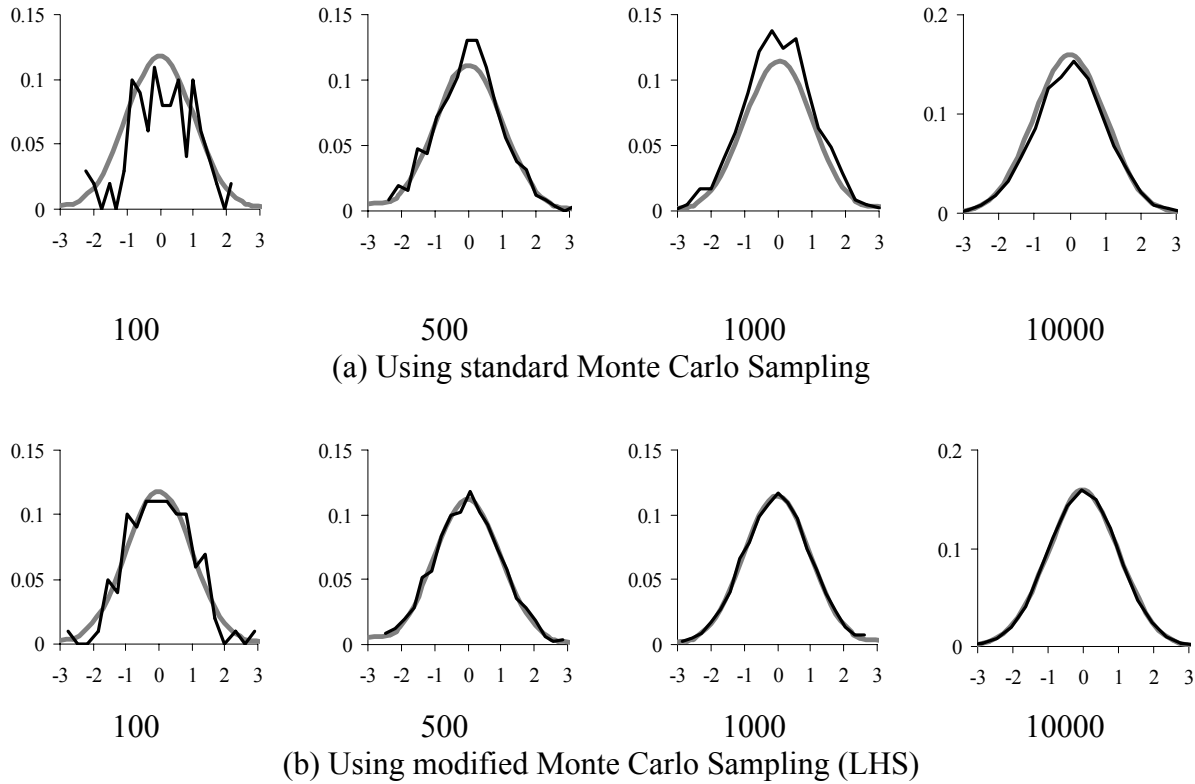
(a) Using standard Monte Carlo Sampling

(b) Using modified Monte Carlo Sampling (LHS)

Figure 4.8. Degree of representation with respect to sample size

4.4. Concluding remarks

The sampling procedures and defined distributions for parameters are utilized to generate random populations that represent building populations at urban regions. Due to its efficiency, LHS method is used to generate the populations. The generated populations are used as input to sensitivity investigations in Chapter 5. To illustrate the outcomes of this chapter, two building populations with 500 and 50 buildings are generated. Based on analytical idealization introduced in Chapter 3, some of the building structural parameters are calculated. Histograms representing assumed and calculated building parameters are presented in Figs. 4.9 and 4.10.
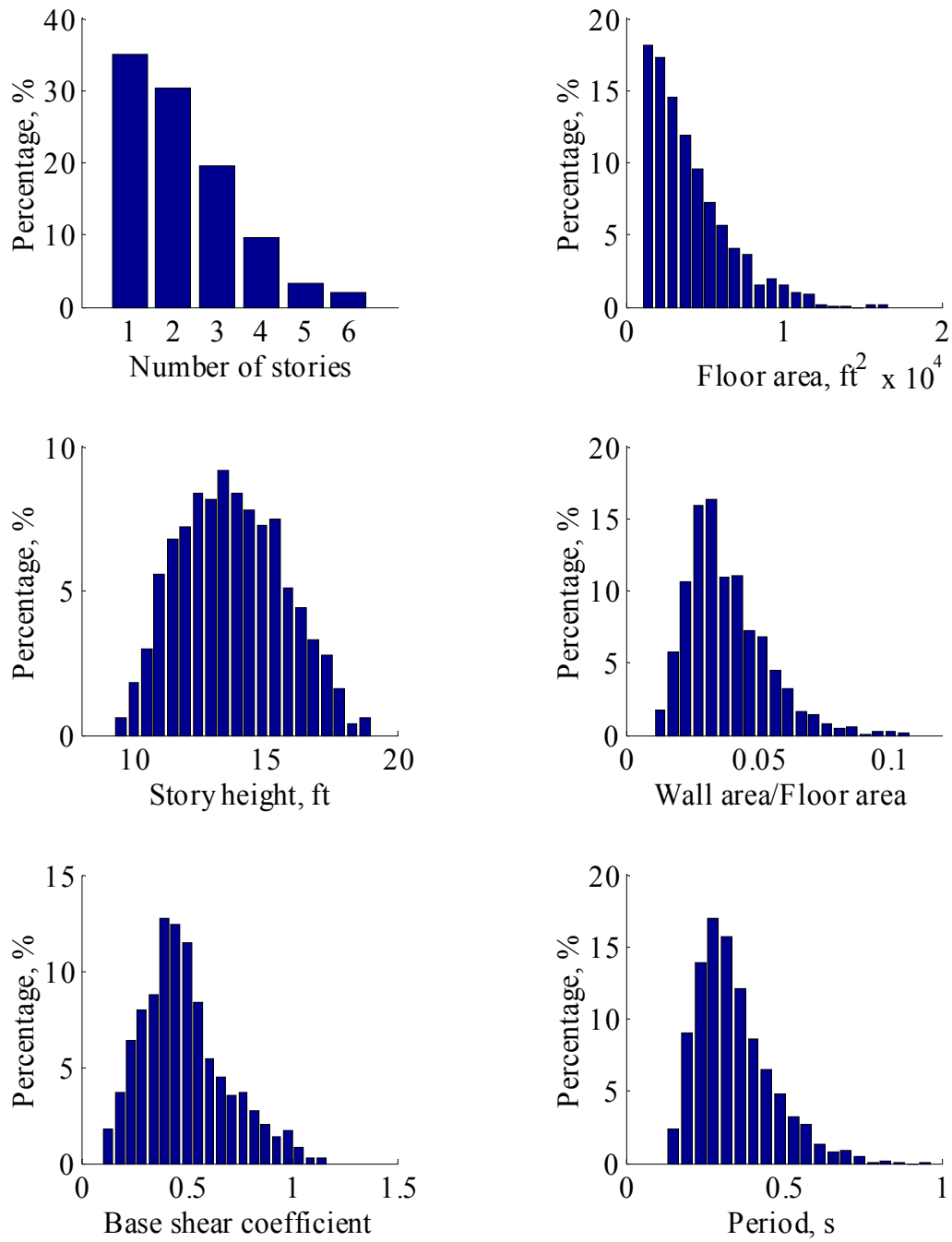
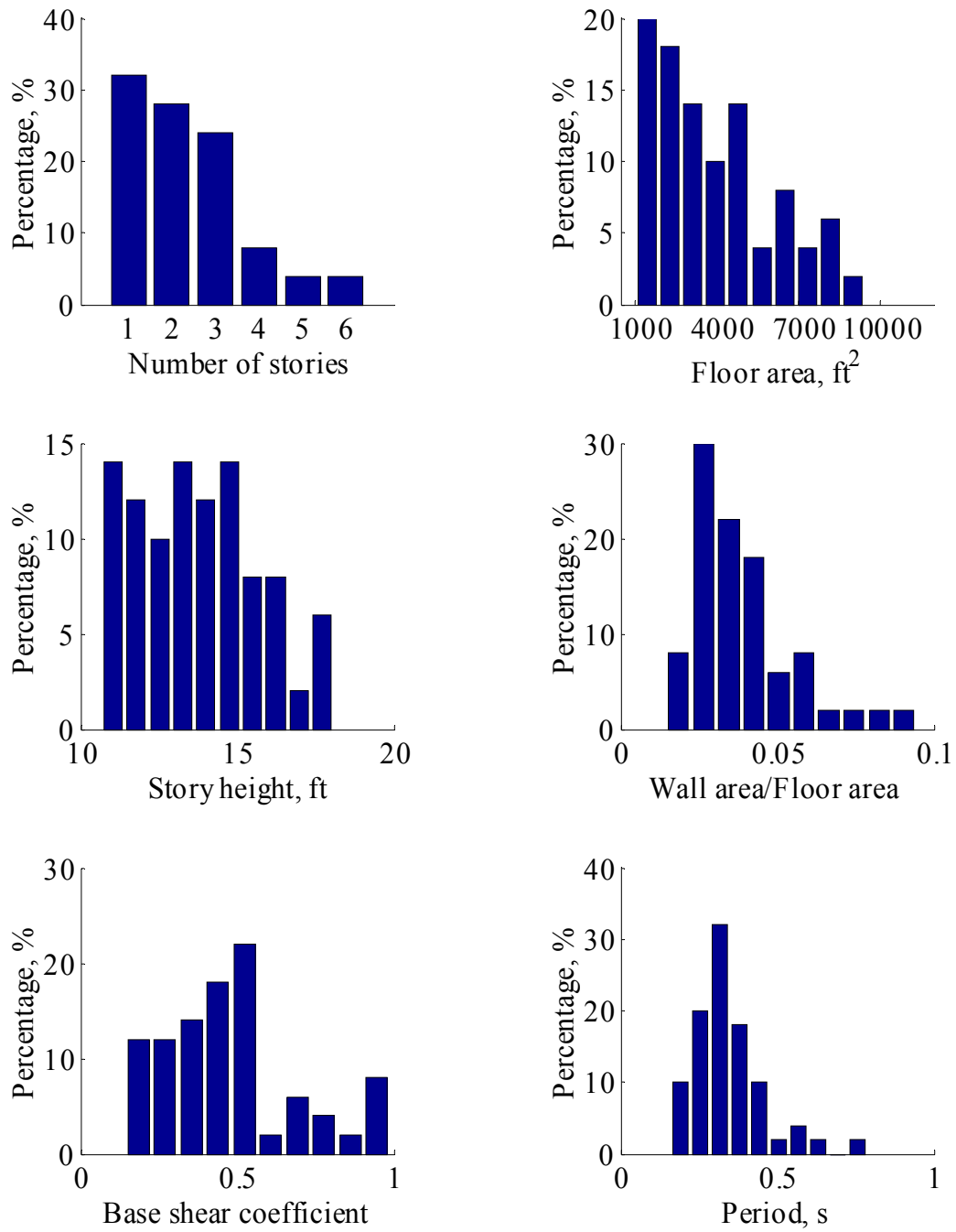Figure 4.9. Generated and calculated building parameters for a population size of 500 buildings

Figure 4.10. Generated and calculated building parameters for a population size of 50 buildings

CHAPTER 5 SENSITIVITY INVESTIGATIONS ON TOTAL REGIONAL LOSS

5.1 Introduction

The goal of this chapter is to investigate the sensitivity of regional loss and risk estimates to different categories of ground motions and building parameters. Incremental dynamic time history analysis is used to estimate vulnerability of unreinforced masonry buildings. The primary motivation in estimating response through time history analyses, rather than using static procedures, is to represent the dynamic response interaction between flexible diaphragm and relatively stiff exterior walls. As discussed in Chapter 3, this interaction is typical for unreinforced masonry buildings and critical in determining the overall damage state. Damping level is selected to be 5% and is introduced in the form of proportional damping in all analyses. Sensitivity investigations for different levels of damping is conducted and discussed in section 5.6.

Building populations on which sensitivity analyses are conducted are generated through the procedure outlined in Chapter 4. Randomizations of parameters are carried out on distributions that are defined in Chapter 4. These distributions are defined to represent building populations in urban regions. Even though the same distributions are used to generate building parameters, arbitrary combination of randomized values resulted in building populations that are different from each other.

The randomization process also resulted in building populations having different monetary values. In order to be able to compare estimated losses for different populations the generated hazard-loss curves are normalized with respect to the total value of populations. The normalization procedure is explained in the next section.

To clearly present differences between calculated hazard-loss curves for different parameter combinations, results are also provided as "difference-plots". Typically, a difference-plot is generated by subtracting the hazard-loss curve for the parameter that is being compared from hazard-loss curves for the remaining parameters. Difference-plot calculations that are specific to certain cases are explained when necessary.

5.2 Calculation of building and regional loss

In loss calculations, replacement cost of buildings is assumed to be proportional with number of stories and floor area. The constant of proportionality is assumed to be the same for each building regardless of its location and occupancy type, *i.e.* cost variations due to special locations and contents of buildings are not modeled in this study. With these assumptions, building replacement cost can be mathematically expressed as follows:

$$RC = \kappa n_s A_f \tag{5.1}$$

where, RC = replacement cost of a building

κ = constant of proportionality

n_s = number of stories

A_f = floor area

The monetary loss associated with each damage range is calculated by multiplying appropriate damage – loss conversion constant, replacement cost ratio (RCR), with the replacement cost (RC) of the building. Replacement cost ratios, associated with different ranges of damage for unreinforced masonry buildings were defined in Chapter 3. As stated in Chapter 3, each damage range represents damage variation between two consecutive damage states, such as IO-LS and, CP-TC. Using Eq. 5.1, the monetary loss for the ith damage range can be expressed as:

$$BL_i = \left(RCR_i\right) \times \left(RC\right) \tag{5.2}$$

where, BL_i = building loss for the ith damage range.

RCR_i = representative replacement cost ratio that is associated with the ith damage range.

RC = replacement cost of a building

The expected value of the monetary loss is calculated by multiplying the building loss, BL_i with the probability corresponding to that damage range:

$$EBL_i = \left(BL_i\right) \times P\left(DS^k \le Damage < DS^{k+1} \mid Hazard = S_a\right) \tag{5.3}$$

where, EBL_i = expected building loss for the ith damage range.

$P(DS^k \leq Damage < DS^{k+1} \mid Hazard = S_a)$ = probability of damage being within the ith damage range given that hazard level is equal to S_a.

DS^k and DS^{k+1} = consecutive damage states that define the ith damage range.

Summation of EBL_i for all damage ranges gives the total expected building loss for hazard level S_a. Mathematically:

$$TEBL(Hazard = S_a) = \sum_{\substack{for\ all \\ damage \\ ranges}} EBL_i \qquad (5.4)$$

where, TEBL = total expected building loss for a given hazard level

Total regional loss for a particular hazard level, scenario-based regional loss, is calculated as the summation of TEBL for all buildings. In expression form:

$$TRL = \sum_{\substack{for\ all \\ buildings}} TEBL \qquad (5.5)$$

where, TRL = total regional loss

In sensitivity analyses, effects of different parameters on TRL are investigated. For this purpose, different building populations are used. These populations are generated through the randomization process explained in Chapter 4. The randomization process results in buildings populations whose monetary values are different from each other. In order to compare total regional loss estimates for different parameters, the calculated hazard-loss relationships are normalized with the total value of each building population. For example, a value of 0.4 in a normalized hazard-loss relationship means that the real monetary loss is equal to 40% of the total value of the building population. In expression form, this normalization can be stated as follows:

$$TNRL = \frac{TRL}{TVR} \qquad (5.6)$$

where, TNRL = total normalized regional loss, ranges from 0.0 to 1.0

TRL = total regional loss

$$TVR = \sum_{\substack{\text{for all} \\ \text{buildings}}} RC = \text{total value of the region}$$

If the normalization is performed on a hazard-loss relationship that is specific to narrow range of parameters, then the normalized result is called the expected replacement cost ratio, ERCR, for that parameter range.

5.3 Selection, categorization, and scaling of ground motions

A suite of 18 ground motions is selected to carry out dynamic time history analyses. The goal of the selection process is to some extent represent structurally important features of acceleration time histories, such as frequency content, impulsive or cyclic characteristics, and predominant period. Various factors influence characteristic features of ground motions. These factors include distance from the epicenter, magnitude, local soil conditions, and duration.

To systematically consider the effects of all these factors, the ratio of peak ground acceleration, PGA, to peak ground velocity, PGV, a measure suggested by Zhu et. al. 1998, is used. This ratio combines ground motion characteristics for high frequencies, primarily represented by accelerations, with lower frequencies, mainly represented by velocities, into a single measure. In general, the measure tends to get higher as the distance to the epicenter gets closer and/or the magnitude of the event gets higher and/or the stiffness of the local soil gets higher. In this regard, PGA/PGV ratio not only reflects the effects of soil media but also implicitly contains information about near/far field characteristics of the ground motion and the magnitude of the event (Elnashai and McClure 1996). Even though the main focus is given to PGA/PGV ratio, a balanced distribution for individual parameters, such as magnitude, distance, and soil conditions, is targeted in finalizing the ground motion data set.

Table 5.1 Ground motion categories

Category name	Definition	PGA/PGV interval (g.s/m)[*]
High	Ground motions possessing many large-amplitude, high frequency oscillations. Near field – rock to firm soil.	> 1.40
Medium	Ground motions exhibiting significant energy over a broad range of frequencies. Medium stiff soil – medium epicentral distance.	1.40 – 0.80
Low	Ground motions in which the significant energy is contained in a few long-duration acceleration pulses. Far field – soft soil.	< 0.80

[*] in this expression "g" stands for the unit of gravitational acceleration

In order to investigate the effect of ground motion characteristics on regional loss/risk estimates, selected ground motions are grouped into three categories. Qualitative definitions provided by Zhu et. al. 1998, and quantitative values given in National Building Code of Canada (referenced from Elnashai and McClure 1996) are utilized to define ground motion categories in this study. Table 5.1 lists the main characteristics of each category together with assigned PGA/PGV ranges. The properties of selected ground motions are provided in Table 5.2. It can be noticed that there exist a good correlation between PGA/PGV values and the soil conditions at the recording site. In general, stiffer soils tend to result higher PGA/PGV values whereas softer soils tend to result lower values.

Figure 5.1 shows the elastic response spectra of the ground motions at 5.0% damping. PGA value of each ground motion is scaled to 0.1g. The spectra curves are grouped according to PGA/PGV categories that are defined in Table 5.1. As can be noticed, higher PGA/PGV values are associated with ground motions having higher energy in the short period range. Furthermore, as the value of the ratio gets lower the predominant period of ground motions increase. Acceleration time histories and response spectra for each ground motion are separately provided in Appendix A.

Table 5.2. Properties of selected ground motions

Name	Id[+]	Date	M	Soil Type[*]	Dist. (km)	Comp.	PGA/PGV (g.s/m)
San Fernando	H1	02/09/71	6.6	A	23	291	3.33
Kozani	H2	05/13/95	6.5	A	14	252	2.12
Northridge	H3	01/17/94	6.7	D	44	206	1.91
Kalamata	H4	10/13/97	6.4	A	48	35	1.73
Imperial Valley	H5	10/15/79	6.5	B	20	147	1.54
Whittier Narrows	H6	10/01/87	6.1	C	48	N196	1.44
Ano Liosia	M1	09/07/99	6.0	C	8	N70	1.38
Loma Prieta	M2	10/18/89	7.0	A	3	0	1.30
Coalinga	M3	05/02/83	6.5	C	64	0	1.14
Northridge	M4	01/17/94	6.7	C	26	N090	0.95
Superstation Hills	M5	11/11/87	6.6	D	27	315	0.91
Spitak	M6	12/07/88	6.7	C	20	EW	0.88
Loma Prieta	L1	10/18/89	7.0	D	34	0	0.80
Dinar	L2	10/01/95	6.4	D	1	EW	0.78
Landers	L3	06/28/92	7.3	A	73	90	0.73
Manjil	L4	06/20/90	7.4	D	67	N57E	0.62
Imperial Valley	L5	10/15/79	6.5	D	14	N140	0.57
Imperial Valley	L6	10/15/79	6.5	C	7	2	0.56

[*] USGS soil categorization: A-B = rock to stiff soil ($v_s > 360$ m/s), C = medium stiff soil (360 m/s $> v_s > 180$ m/s), D = soft soil ($v_s < 180$ m/s) where, v_s = shear wave velocity
[+] H = High, M = Medium, and L = Low PGA/PGV category
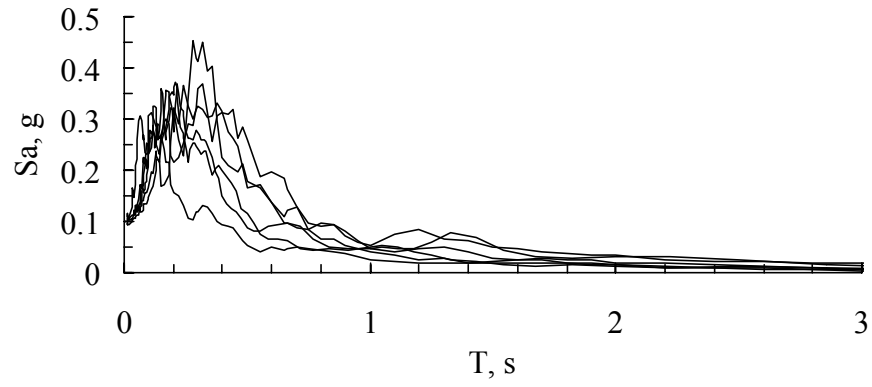
(a) Ground motions in high PGA/PGV category, H1-H6
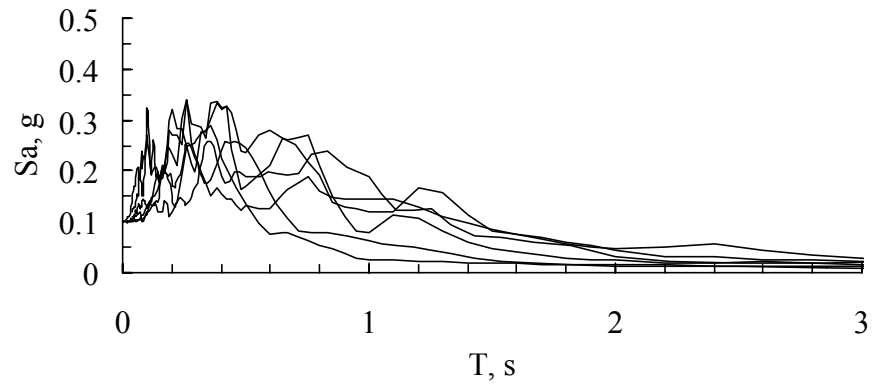
(b) Ground motions in medium PGA/PGV category, M1-M6
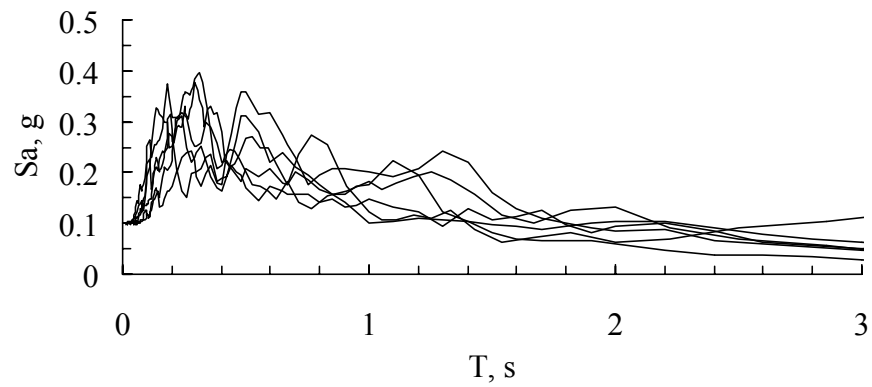
(c) Ground motions in low PGA/PGV category, L1-L6

Figure 5.1. 5.0% damped elastic response spectra of the ground motion set (PGA normalized to 0.1g)

Ground motions are scaled up and down to represent different levels of hazard. Elastic spectral acceleration at the fundamental period of buildings is used to represent different levels of hazard. Hence, each ground motion is scaled to give the same spectral acceleration at the fundamental period of a building that is under consideration. Due to variations in fundamental period of buildings, the level of scale differed from building to building. The range of building periods calculated as a function of assumed building parameters were presented in Chapter 4 and a sample variation was depicted in Figs. 4.9 and 4.10.

5.4 Sensitivity to population size

As discussed in Chapter 2, the number of buildings in a given population directly affects the level of uncertainties in total loss/risk estimates. In order to investigate the variability of total loss/risk estimates under this parameter, building populations having different number of buildings are generated by using distributions and sampling techniques defined in Chapter 4. Each building parameter is randomized in its full range, i.e. no bias is considered towards a smaller parameter interval. A total of 42 different building populations are generated. The distribution of generated populations with respect to population size is shown in Fig. 5.2. Buildings in each population are analyzed for 18 different hazard levels and for all ground motions in the ground motion data set. From these analyses, hazard-loss curve for each building is calculated. The building specific hazard-loss relationships are used to compute, as explained in section 5.2, the total normalized regional loss for each building population.
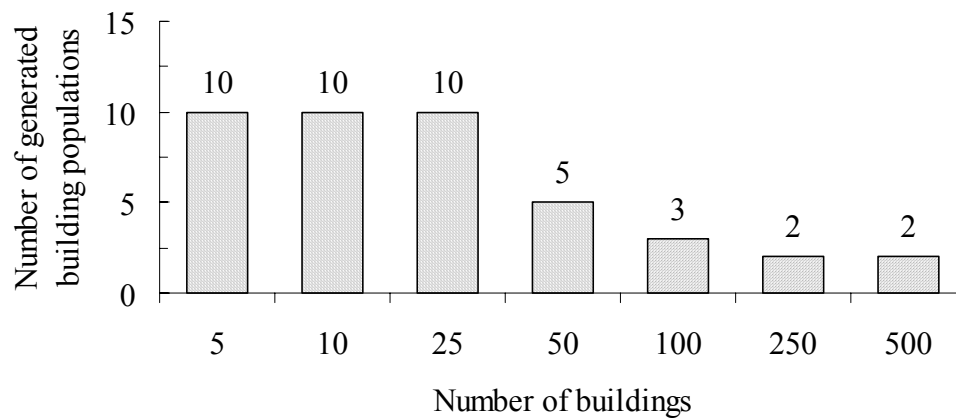
Figure 5.2. Distribution of generated populations with respect to population size

Figure 5.3 shows the variation of total normalized regional loss for building populations having 50 or less number of buildings. As can be seen the scatter in the curves gets smaller as the number of buildings gets higher in a given population. Furthermore, the curves approach to a single value as the level of hazard approaches either to 0g or to 3g. This is something expected since, for no hazard (S_a = 0g) there is no damage and loss on the contrary for high level of hazard (S_a = 3g in this case), all buildings are totally damaged resulting in total loss.

(a) Number of buildings = 5 (b) Number of buildings = 10

(c) Number of buildings = 25 (d) Number of buildings = 50
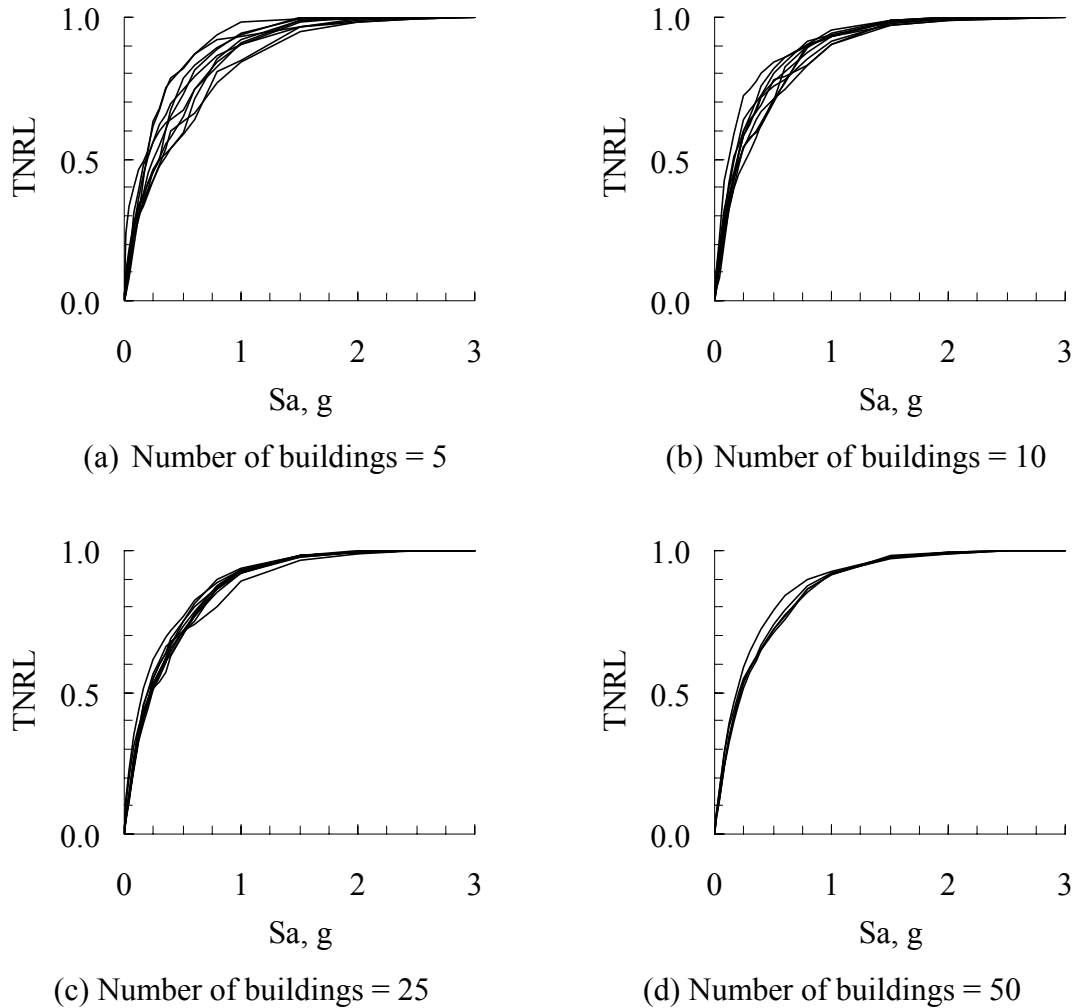
Figure 5.3. Variation of total normalized regional loss for building populations with 5, 10, 25, and 50 buildings.

Further increase of population size generates almost identical curves. The results for 100, 250, 500 building populations are provided in Fig. 5.4. It should be noted that each curve

96

represents loss variation in a different building population. Even though the distributions that are used to generate building parameters are the same, the arbitrary combination of parameters generates building populations that are different from each other. Based on this statement, Fig. 5.4 suggests that even though populations have different properties, regional loss can be represented by a single curve if the size of the building population exceeds 25 buildings.
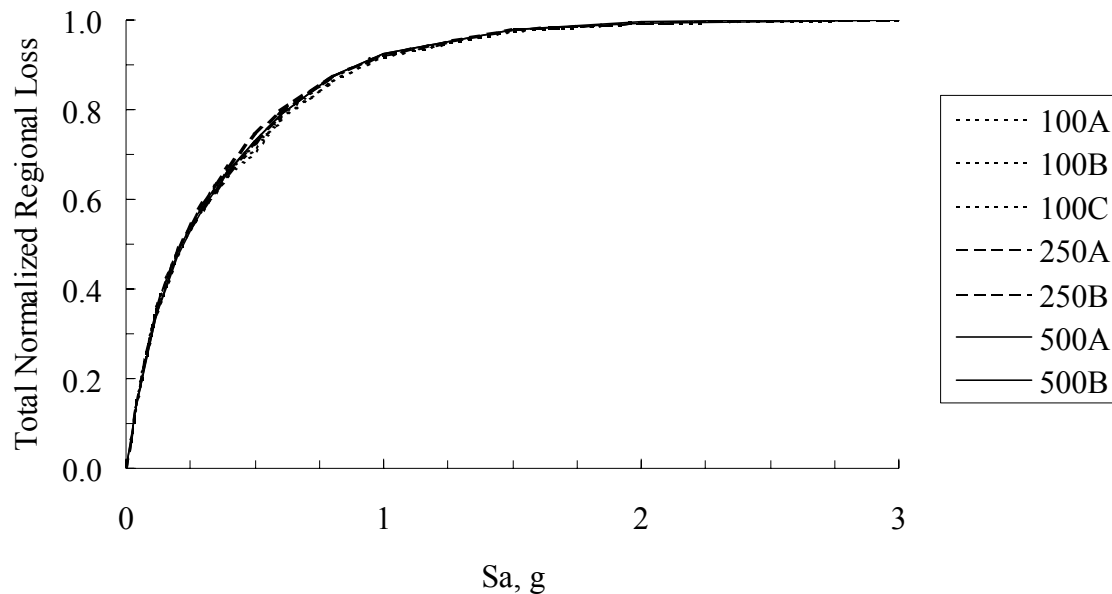
Figure 5.4. Variation of total normalized regional loss for building populations with 100, 250, and 500 buildings.

The reduction of scatter can be better presented by showing the results relative to the TNRL curve associated with building population size of 500 buildings. This is shown as difference-plot in Fig. 5.5. In this figure, the curve corresponding to population size of 500 buildings is subtracted from the upper and lower bounds of TNRL curves for building populations with less number of buildings. As can be seen, for populations with 25 or more buildings the difference gets smaller than 10% for all hazard levels.
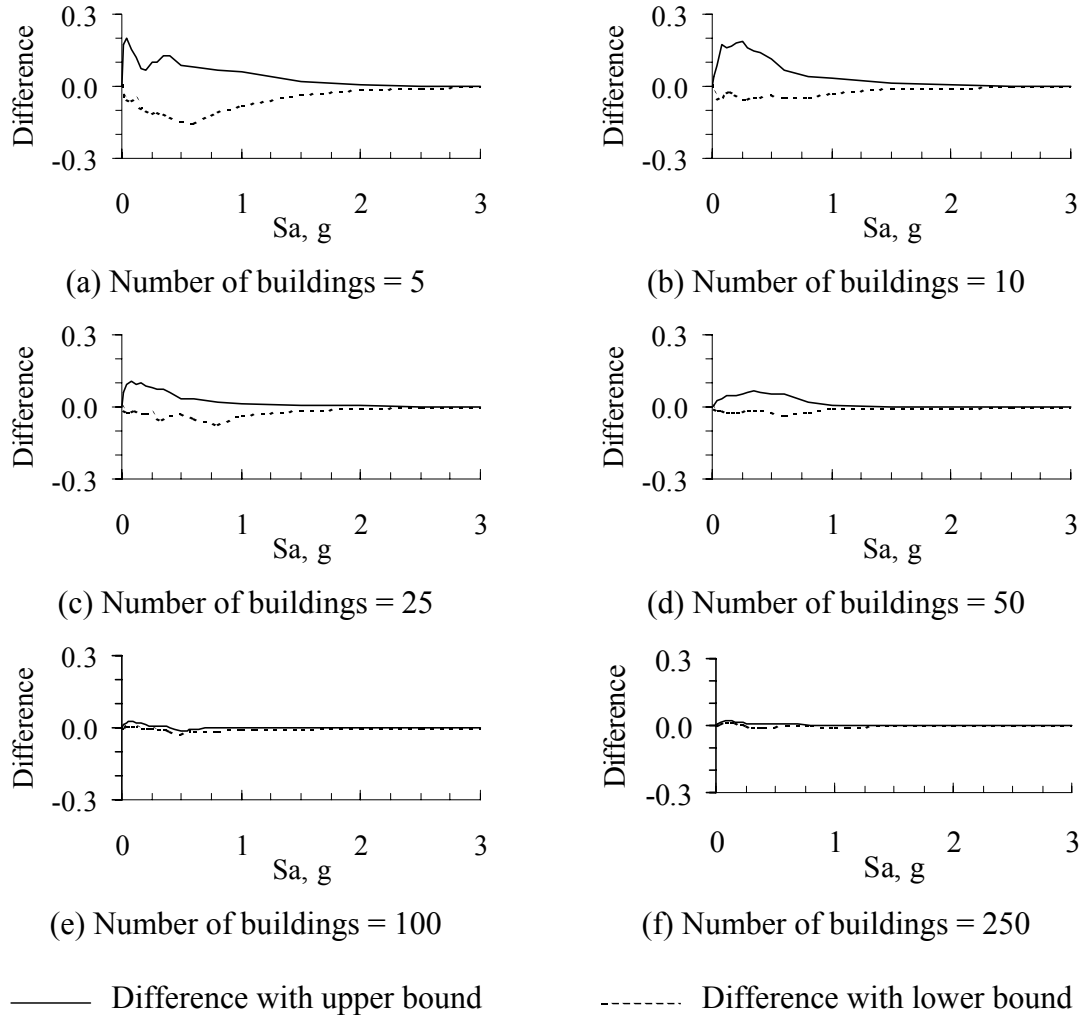
Figure 5.5. Difference between TNRL curve for building population with 500 buildings and TNRL curves for building populations with less number of buildings

5.5 Sensitivity to ground motion set

The variation in ground motion properties is represented, to some extent, by 18 different acceleration time histories that are listed in the ground motion set. In order to investigate the sensitivity of TNRL estimates to the selection of ground motions, a different set of acceleration time histories is selected to represent the variation of ground motion properties. The new ground motion set is selected from the list of acceleration time histories that was utilized in the FEMA-307 document. The only constraint that is considered in selecting ground motions is to assemble ground motion set that has similar PGA/PGV distribution as the ground motion set that is utilized in this study. Based on this constraint, 15 records are

selected from 18 records that were used in FEMA-307. Properties of the new ground motion set are listed in Table 5.3. Figure 5.6 shows 5% damped elastic response spectra for the new ground motions.

Table 5.3. Properties of alternative ground motion set

Name	Id[+]	Date	M	Dist. (km)	Comp.	PGA/PGV (g.s/m)
Whittier Narrows	A1	10/01/87	6.1	18	90	4.38
Central Chile	A2	03/03/85	7.8	60	010	1.78
Big Bear	A3	06/28/92	6.6	12	360	1.56
Loma Prieta	A4	10/17/89	7.1	28	360	1.23
Spitak	A5	12/07/88	6.9	57	360	1.21
Central Chile	A6	03/03/85	7.8	26	070	1.17
Imperial Valley	A7	05/18/40	6.3	12	180	1.09
Landers	A8	06/28/92	7.5	15	360	0.98
Loma Prieta	A9	10/17/89	7.1	8	90	0.96
Northridge	A10	01/17/94	6.7	19	360	0.88
Tabas	A11	09/16/78	7.4	<3	344	0.85
Imperial Valley	A12	10/15/79	6.6	27	140	0.74
Northridge	A13	01/17/94	6.7	19	360	0.61
Landers	A14	06/28/92	7.5	42	250	0.53
Hyogo-Ken Nambu	A15	01/17/95	7.2	11	360	0.51
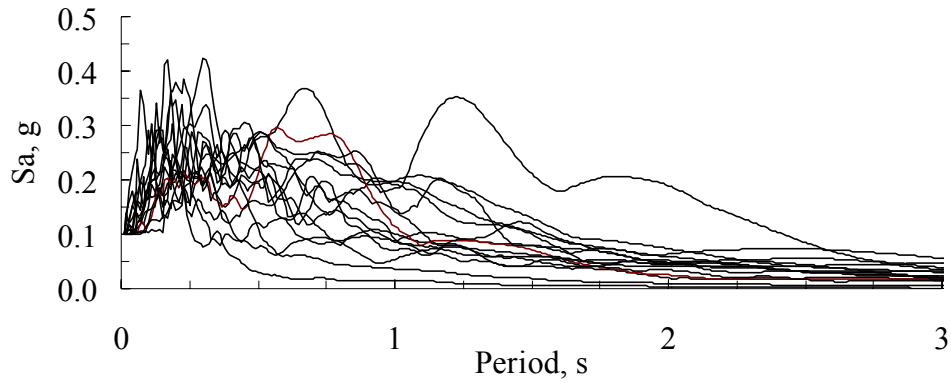
Figure 5.6. 5.0% damped elastic response spectra of the alternative ground motion set. PGA scaled to 0.1g

Three different building populations with 100 buildings are analyzed by using the new set of ground motions. Resulting TNRL curves are shown in Fig. 5.7. For comparison, the TNRL curve that is calculated from the first set of ground motions is also provided in the same plot. As can be seen from Fig. 5.7 as well as from the difference-plot presented in Fig. 5.8, curves shows good agreement for all levels of hazard, maximum deviation is less than 3.0%. From this observation it can be stated that as long as the selected ground motions have uniformly distributed PGA/PVG values, the ground motion set has minor influence on regional loss estimates.
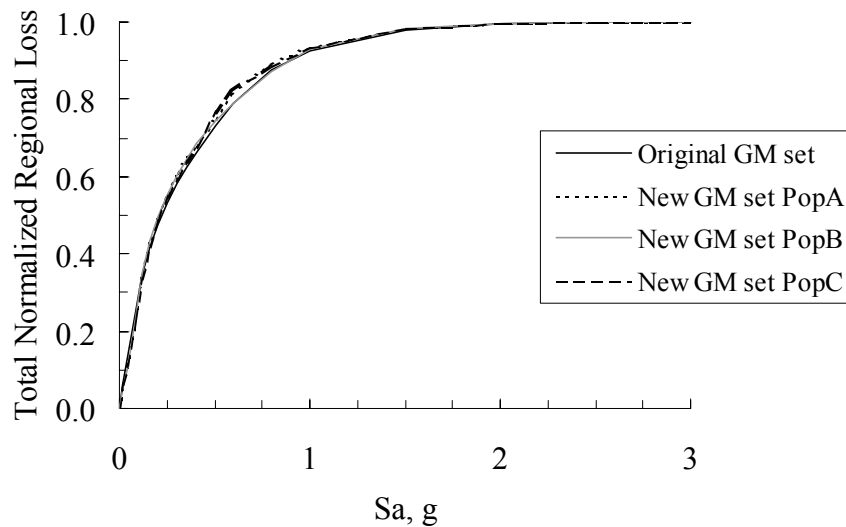
Figure 5.7. TNRL curves that are calculated from alternative set of ground motions

100
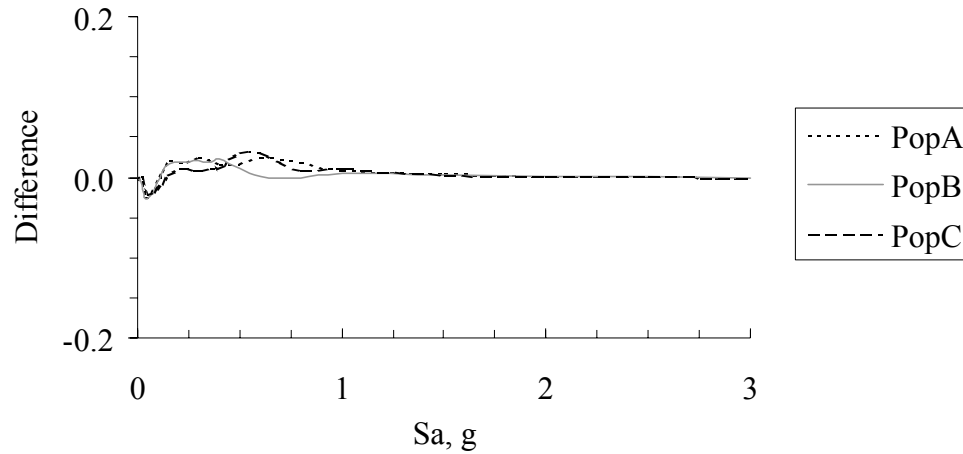
Figure 5.8. Deviation of TNRL curves for new set of ground motions from TNRL curve corresponding to original set of ground motions

5.6 Sensitivity to ground motion categories

In regional loss/risk estimations the variation of soil conditions and ground motion characteristics play an important role as the response of buildings are highly influenced by the signature of the ground shaking. As explained in previous sections the selected ground motions are categorized into three groups according to their PGA/PGV values. Four different building populations are analyzed to investigate the influence of different ground motion categories. In order to eliminate variations due to population size, the sensitivity investigations are conducted on building populations with 100 buildings.

Each building population is subjected to acceleration time histories from three ground motion categories. The results are shown in Fig. 5.9. Calculated TNRL curves for each building population are very similar to each other. Therefore, only the average curves are provided for each ground motion category. The "mean" curve is provided for comparison purposes. This curve represents the hazard-loss relationship of a building population that is evenly distributed over different site conditions, i.e. there is no bias on ground motion properties.
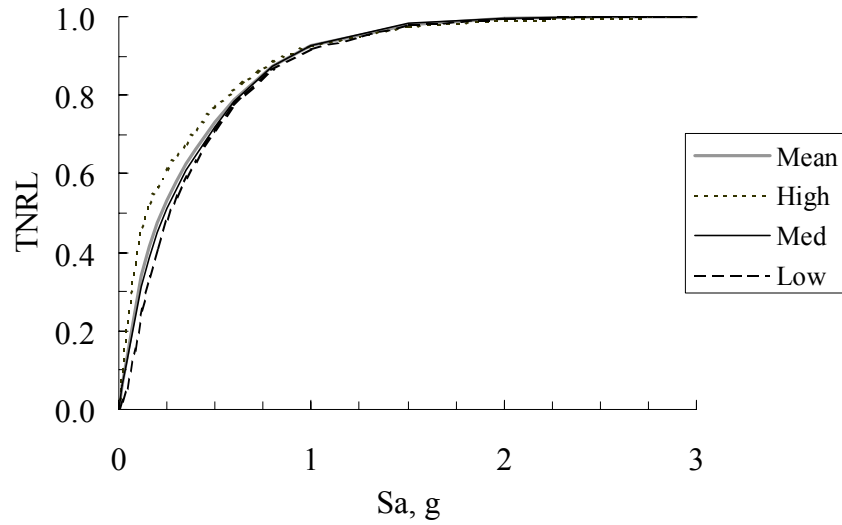
Figure 5.9. Variation of TNRL for three categories of ground motions

Figure 5.9 suggests that, regional loss estimates are moderately sensitive to ground motion categories. The largest deviation from the "mean" curve occurs for the "high" ground motion category. Deviations for all ground motion categories can be better seen in difference-plot as shown in Fig. 5.10. In this plot, the "mean", unbiased, curve is subtracted from TNRL curves for each ground motion category.
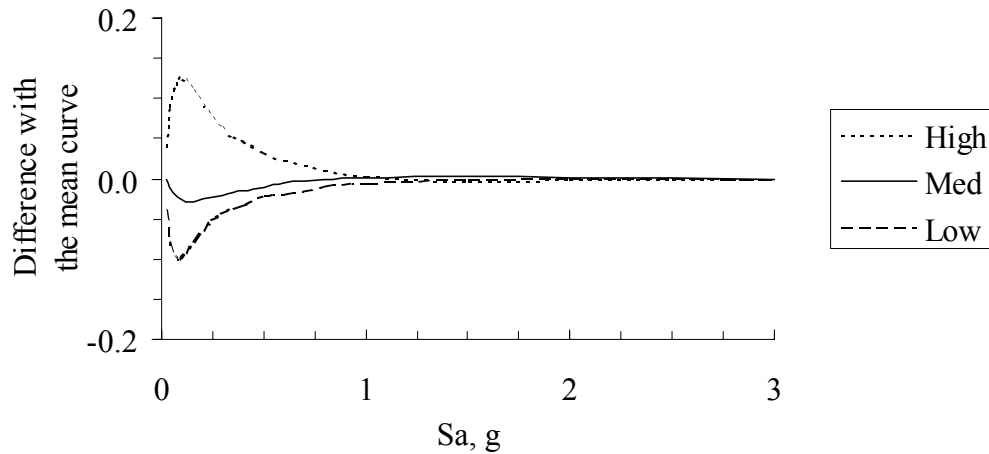
Figure 5.10. Difference with the mean TNRL curve

The "medium" ground motion category seems to agree well with the unbiased TNRL curve. The "medium" and the "low" ground motion categories result in very similar curves. The maximum deviation for all categories is less than 15%. It should be noted that these results

are valid only if the properties of a given building population follows the distributions that are defined in Chapter 4. For example, if some of the building parameters have bias towards a certain range, deviation of TRNL curves for different ground motion categories can be different then the ones shown in Fig. 5.10. However, as long as the distribution of building parameters agrees well with the distributions in Chapter 4, the TNRL estimates by using unbiased, "mean", hazard-loss curve will have an error less than 15%. The sensitivity of TNRL curves to biased building properties are investigated in upcoming sections.

5.7 Sensitivity to damping level

In all analyses, a damping level of 5% is used. The sensitivity of TNRL calculations on selected damping level is investigated for three additional damping levels, 10%, 15%, and 20%. For each damping level the associated damped elastic response spectra is used to calculate the spectral acceleration at the fundamental period of buildings. In order to eliminate the effect of population size, building populations with 100 buildings are utilized in this investigation. The resulting TNRL curves are presented in Fig. 5.11. Figure 5.12 shows deviations of each curve from the TNRL curve for 5% damping.
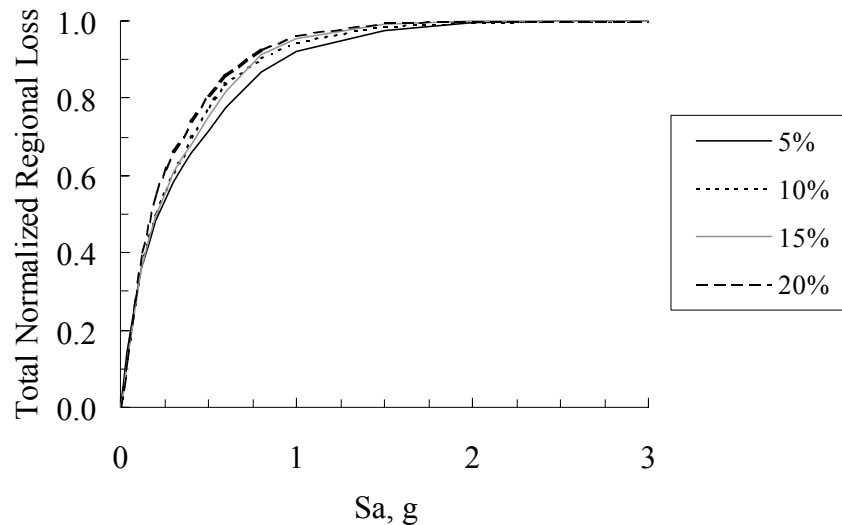
Figure 5.11 Variation of TNRL for different levels of damping

As can be seen from Figs. 5.11 and 5.12, TNRL curves for higher damping levels agrees well with the TNRL curve for 5% damping. The similarity is primarily attributable to the scaling method that is used in analyses. Ground motions are scaled according to the elastic response

spectra at the damping level that is used in the analyses. This resulted in higher scaling factor for higher damping ratios. In other words, even though building response parameters are reduced due to higher damping levels, the higher scaling factors counterbalanced the difference and yielded comparable building response. From this observation it can be stated that as long as the hazard level is defined from an elastic response spectra, which has the same damping level as the building population, the error in TNRL estimates will be less than 10%.
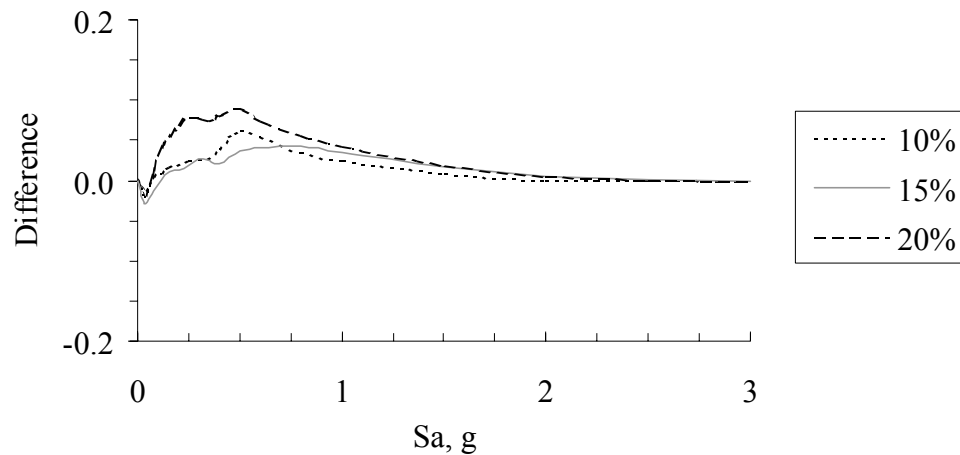
Figure 5.12. Deviation of TNRL curves for higher damping from TNRL curve for 5% damping

5.8 Sensitivity to building properties

The sensitivity investigations for building parameters are carried out at two levels. The first level investigation is conducted to identify the parameters that have the highest significance on regional loss estimates. In this preliminary investigation, each parameter is assigned two extreme values while other parameters randomized according to their associated distributions. Values corresponding to 10th and 90th percentiles are taken as the extreme values for each parameter.

Sensitivity investigations in which parameters are simultaneously biased towards a certain interval are carried out in second order analyses. These investigations are conducted on parameters that are determined to be significant in the first level investigation. The parameters that are categorized to be of second order are randomized according to their assigned distribution. Building populations are generated for all possible combinations of

intervals for each parameter. The hazard-loss relationship calculated for each combination is compared to identify correlations among parameters.

The results of both sensitivity analyses are utilized to identify the ranges and combinations of different parameters that show similar hazard-loss relationships. Each parameter range and combination is represented by a single hazard – loss relationship.

5.8.1 First order analysis

The first order analysis is intended to identify building parameters that have lower significance to regional hazard-loss relationships. Parameters that are determined to have higher significance are further investigated in the next section.

In first order analyses, building parameters are investigated one at a time. Each parameter is assigned two extreme values, 10th and 90th percentile, according to its distribution and rest of the parameters are fully randomized and arbitrarily shuffled. A new building population is generated for each extreme value. This resulted in two building populations for each parameter. Only for "number of stories", since it is discrete, sensitivity is carried out for each possible value resulting in six building populations. A total of 24 building populations are generated to represent all possible cases for ten different parameters. These parameters were listed in Table 4.1 of Chapter 4.

In order to keep the number of biased parameters to one, the TNRL curves are calculated for the full ground motion set. This eliminated the bias in ground motion categories and provided relationships that only reflect the effect of the selected parameter.

With reference to sensitivity investigations in section 5.4 and considering the bias in one parameter, building populations with 50 buildings are assumed to be sufficient to eliminate the variation of hazard-loss relationships due to population size. To verify this assumption, the variation in hazard-loss relationships for arbitrarily selected two parameters is investigated for five different building populations with 50 buildings. Figure 5.13 shows the resulting hazard-loss relationships together with difference plots. In this case, the difference plots are generated by subtracting the mean curve from the upper and the lower bounding curves. As can be seen, the variations are less than 3.0% for both parameters at each hazard level, confirming the assumption on population size.
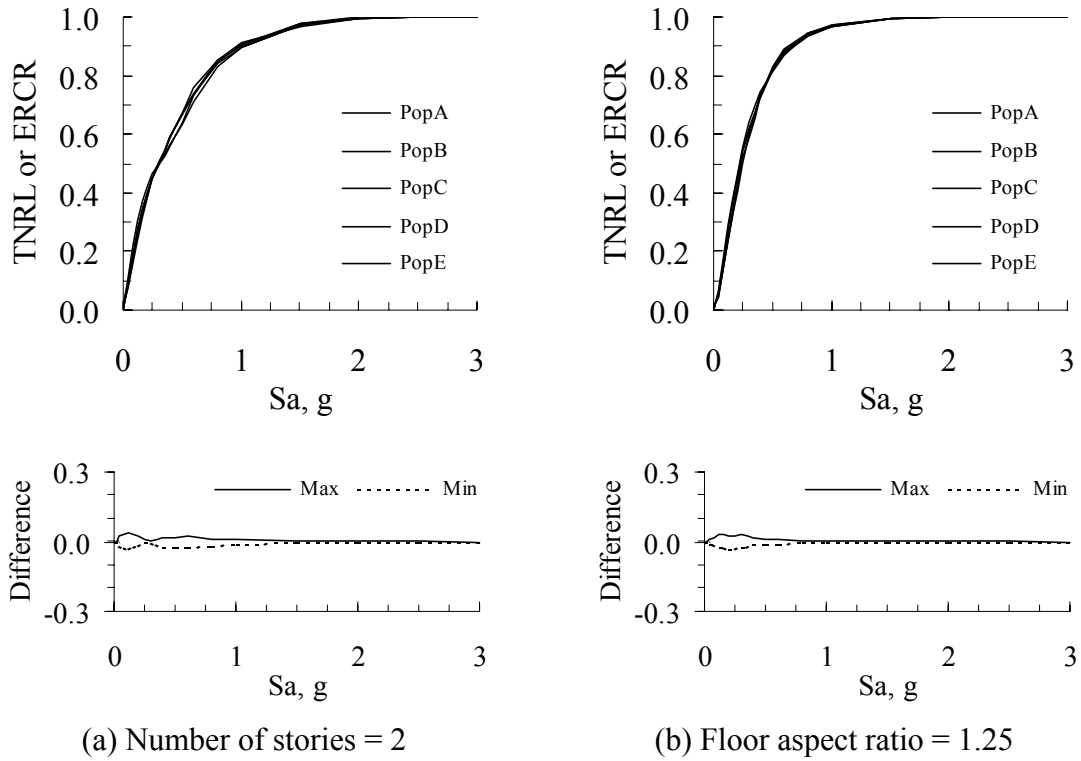
Figure 5.13. Variation of TNRL for 2-story buildings and buildings with floor aspect ratio of 1.25. Analyses are carried out on populations with 50 buildings.

Figure 5.14 shows the results of sensitivity analyses for each building parameter. In each plot, the dotted curve represents the hazard-loss relationship that is calculated for building population with 500 buildings. This curve can be regarded as the unbiased hazard-loss relationship, since none of the parameters are constrained to a single value. The sensitivity of each parameter is evaluated by investigating the deviation of calculated hazard-loss relationships from the unbiased curve. As the deviation gets larger, the sensitivity of TNRL relationship to that parameter gets higher.
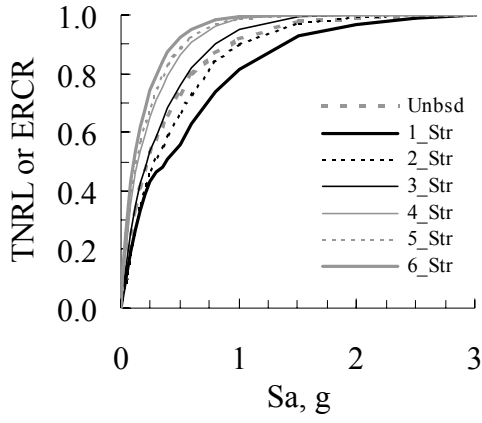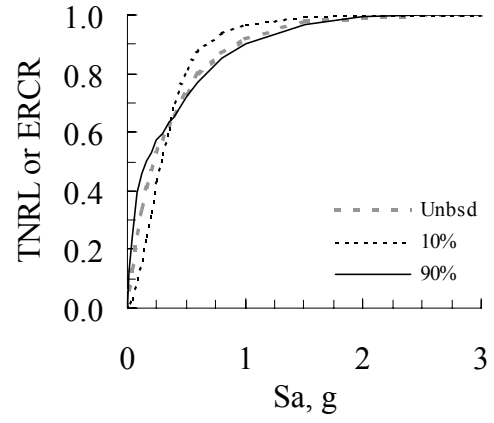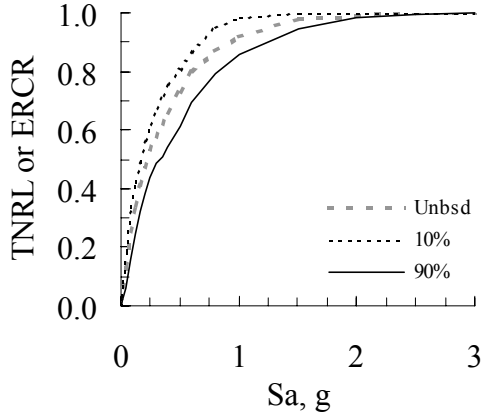
106

(a) Number of stories, n_s

(b) Floor aspect ratio, α_d

(c) Percentage of max wall-area-to-floor-area ratio, α_w
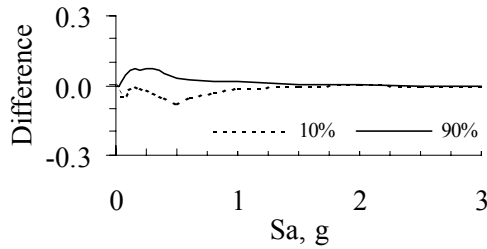
(d) Story height, h_s

(e) Elastic modulus of masonry, E_m

(f) Floor area, A_f

(g) Pier height ratio, α_h (h) Seismic mass on floors, q_f

(i) Average length of openings, L_o (j) Equivalent shear stiffness of floors, G_d
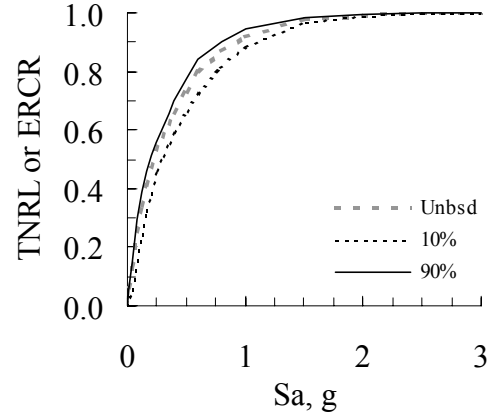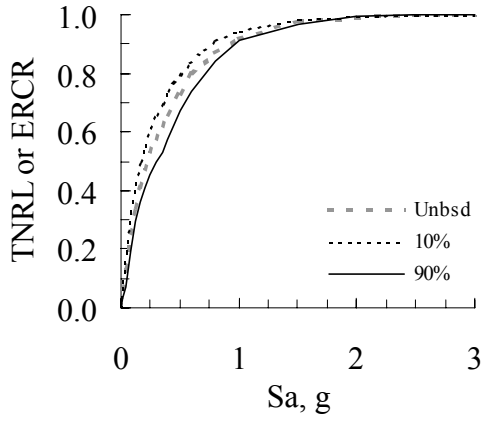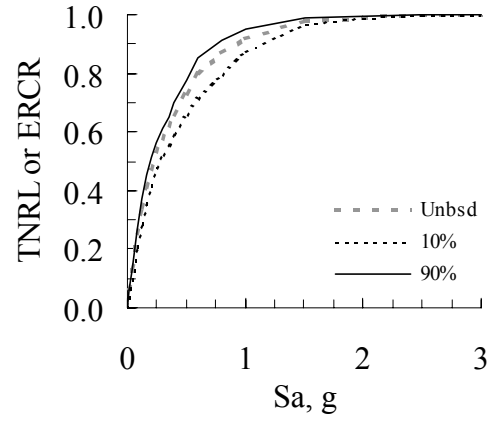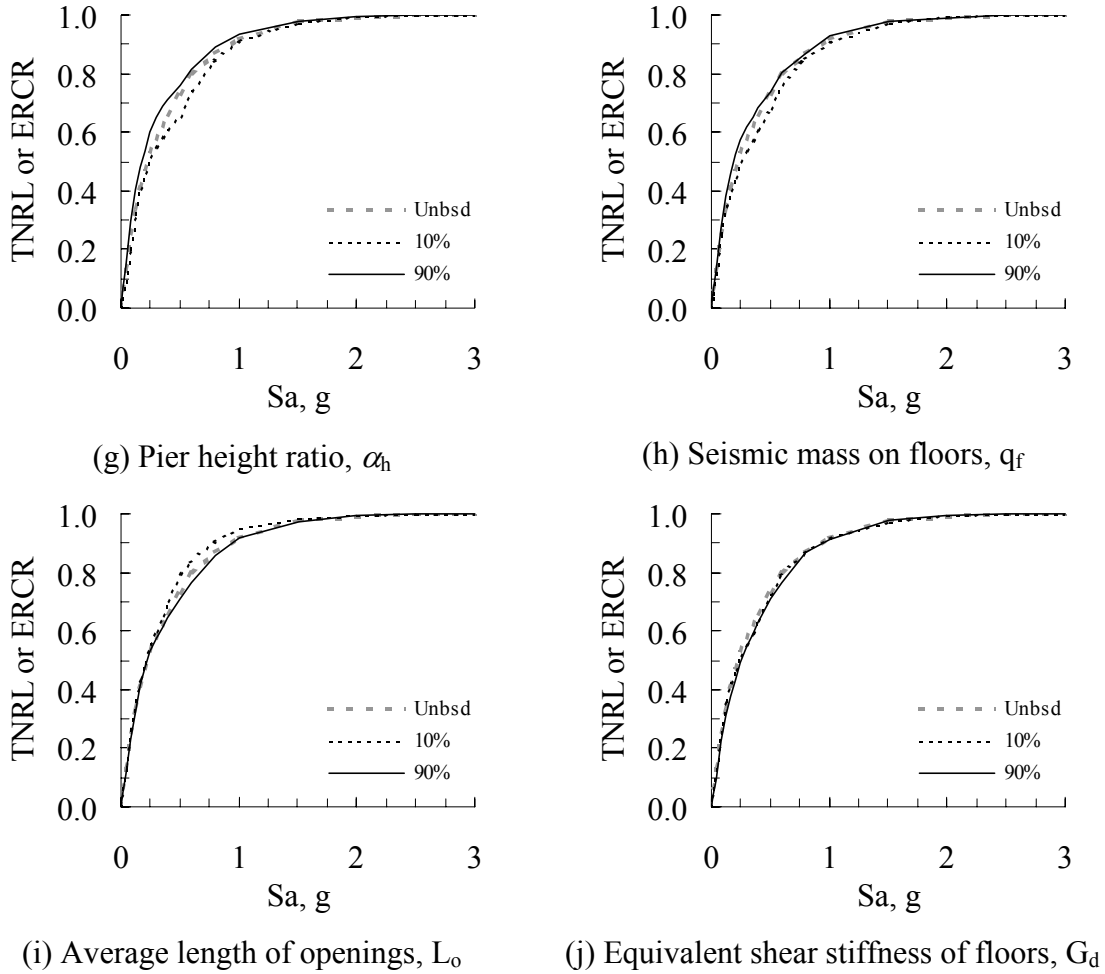
Figure 5.14. TNRL curves for biased values of building parameters

Figure 5.15 shows the same information as difference plots. In physical terms, the difference is the error in loss estimates when unbiased curve is utilized to calculate the regional loss in a biased building population. With considering the uncertainty or error margin in estimating hazard intensity and ground motion characteristics, a value of 10% difference is selected as the threshold value in identifying the building parameters that are of significant importance. In this regard, the last four parameters (average pier height ratio, seismic mass on floors, average length of openings, and in-plane effective shear stiffness of diaphragms) are categorized as second order.
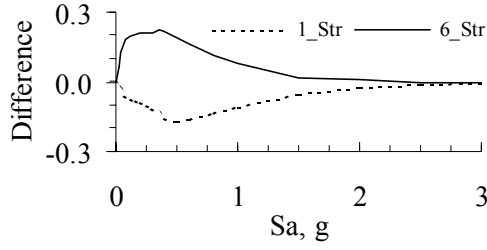
(a) Number of stories, n_s
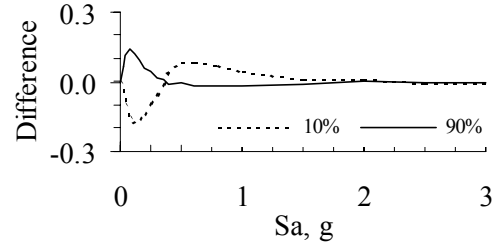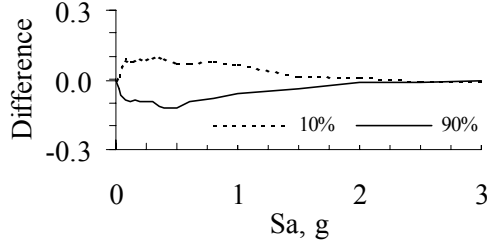
(b) Floor aspect ratio, α_d

(c) Percentage of max wall-area-to-floor-area ratio, α_w
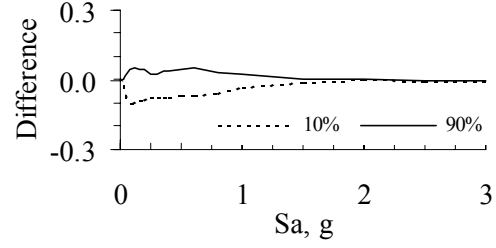
(d) Story height, h_s
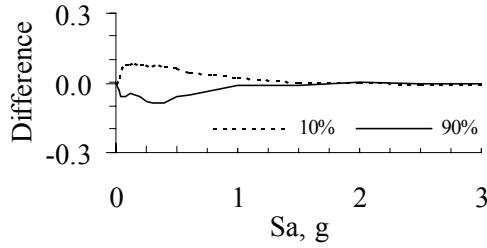
(e) Elastic modulus of masonry, E_m
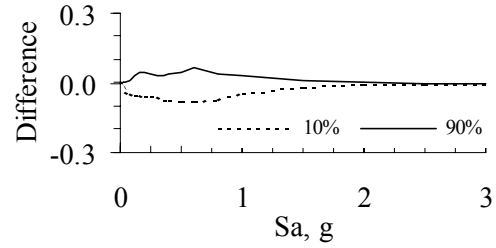
(f) Floor area, A_f

(g) Pier height ratio, α_h
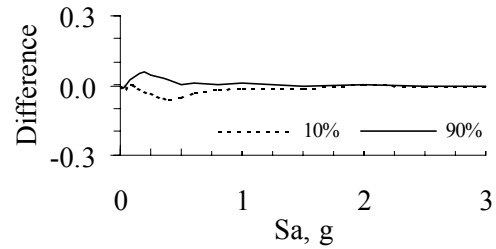
(h) Seismic mass on floors, q_f
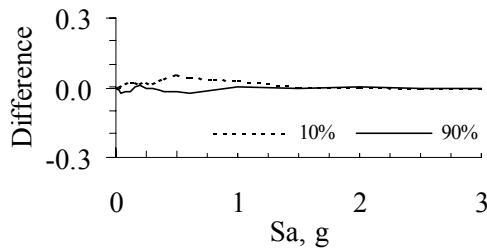
(i) Average length of openings, L_o
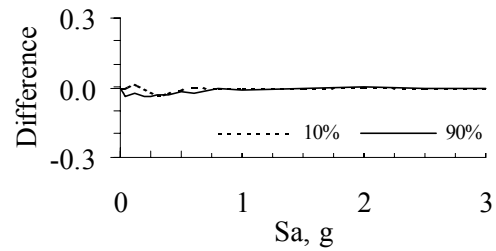
(j) Equivalent shear stiffness of floors, G_d

Figure 5.15. Difference plots with the unbiased hazard-loss curve

Among the remaining six parameters, the number of stories showed the largest deviation, 22%, from the unbiased curve. Comparison of TNRL curves in Fig. 5.14a suggests that the six curves corresponding to each number of stories can be represented by three curves. Curves for 4, 5, and 6 stories are grouped into first category, curves for 2 and 3 stories are grouped into second category, and curve for 1 story buildings placed into the third category. In second order analyses, these categories are used to discretize the parameter "number of stories".

The only parameter for which TNRL curves cross each other is the aspect ratio. This unique case is attributable to the influence of flexible diaphragm on the building response. For the same floor area, as the floor aspect ratio gets higher, the floor plan of the buildings becomes more rectangular for which the stiffness of the floor diaphragm gets smaller. The increased flexibility results in higher response amplification at the floor level, which puts more demand on walls in the out-of-plane direction. This explains the higher vulnerability associated with higher floor aspect ratios at lower levels ($S_a < 0.4g$) of shaking. For higher levels of shakings, the higher wall area in the long direction enhances the seismic capacity of buildings, since damage evaluation is carried out on both axes of buildings. Buildings that have floor shapes close to square tend to have similar capacities on either direction. If shaking in one direction starts to damage the building, there is a high probability that the shaking from the other direction will also damage the building. This is not always the case for buildings with rectangular shapes. Even though shaking in the short direction easily damage the building (high amplifications due to increased floor flexibility), the shaking in the long direction likely to cause limited or no damage to the building. This observation explains the reduced vulnerability for higher floor aspect ratio at higher levels ($S_a > 0.4g$) of shaking.

The remaining four significant parameters showed all positive or all negative deviations from the unbiased curve. When compared with the physical meaning of the parameters the sign of deviations from the unbiased curve are in the expected sense. For example, as the wall area gets higher, the seismic capacity of buildings gets higher, hence the vulnerability reduces. Likewise, increased floor area results in higher seismic mass, therefore, higher seismic demands and hence increases the vulnerability of buildings.

Elastic modulus, influences the stiffness of buildings, hence affects the response parameters. In general, especially for short-to-medium period range, as the stiffness gets smaller, (period gets longer) the response parameters tend to increase. Since, damage is categorized according to response parameters, the vulnerability of buildings gets higher as the elastic modulus gets lower. Similar observation can also be made for story height. This parameter, in addition to stiffness, influences lateral strength of buildings. For the same wall area, as story height gets higher stiffness and lateral strength of buildings get smaller. The increasing tendency of response parameters is also valid for decreasing lateral building strength. Therefore, it is expected to have higher vulnerability for higher story heights, as shown in Fig. 5.15d.

5.8.2 Second order, interaction, analysis

In sensitivity investigations for the first order analysis, only one parameter is biased and the rest of the parameters kept at their full range. This analysis identified the most significant parameters in regional loss estimates. To better understand the correlations among these

Table 5.4. Interval ranges for parameters investigated in second order analyses

Parameter	Range 1	Range 2	Range 3
Ground motion category	High	Medium	Low
Number of stories, n_s	1 story	2-3 stories	4-5-6 stories
*Floor aspect ratio, α_d	1.0-1.75 (1.4)[+]	1.75-2.75 (2.25)	2.75-3.5 (3.1)
Percentage of maximum wall-area-to-floor-area ratio, α_w, (%)	50-62 (56)[+]	62-78 (70)	78-90 (84)
*Story height, h_s, (ft)	9.0-12.5 (11.5)[+]	12.5-14.8 (13.6)	14.8-20 (16.0)
*Elastic modulus, E_m, (ksi)	500-710 (605)[+]	710-990 (850)	990-1200 (1095)
*Floor area, A_f, (ft^2)	1000-2300 (1680)[+]	2300-4750 (3320)	4750-30000 (6540)

* Parameters that are investigated only for the two extreme intervals.
[+] Median value associated with the interval

identified parameters and the loss estimates, sensitivity investigations are carried out for cases where parameters are simultaneously biased towards defined intervals. Three ranges are selected for each parameter. These ranges corresponding to upper 30th, medium 40th, and lower 30th percentile intervals on parameter distributions. Table 5.4 lists the investigated parameters together with defined intervals.

In order to keep the number of possible combinations low, some parameters are investigated only for the intervals corresponded to upper and lower 30th percentile. For these parameters, the hazard-loss curve associated with the medium interval is calculated through linear interpolation of hazard-loss curves corresponding to the two extreme intervals. A total of seven parameters are investigated in this section. Three parameters are investigated for all three intervals and the rest four parameters are investigated for only two intervals. The analysis is carried out in full matrix yielding 432 cases in total. When interpolated cases are included, the total number of combinations are add up to $3^7 = 2187$.

| Original distribution and associated cumulative distribution | Distribution segments for sub-intervals |
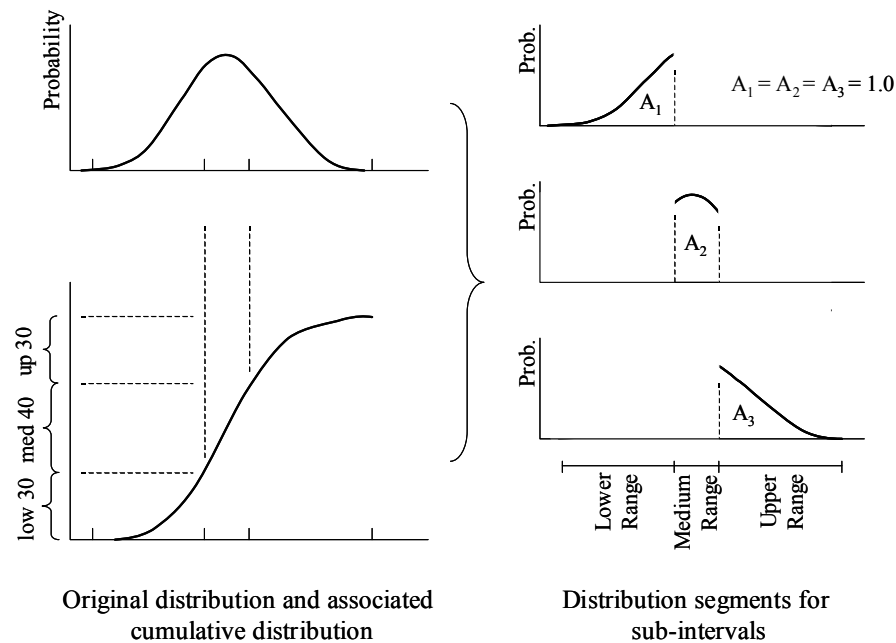
Figure 5.16. Determination of parameter distributions for sub-intervals.

Unlike representing each interval with singe value, which was done in the first order analysis, parameters are randomized in each interval and arbitrarily shuffled to generate building populations. Figure 5.16 demonstrates the generation of distributions that are utilized to

randomize parameters at their biased interval. In simple terms, the original distributions are divided into three sub-regions according to 30th and 70th percentile values of parameters. The resulting distribution segments are normalized to yield an area of unity at the range of each interval. As an alternative to this approach, a uniform distribution can be used to randomize parameters, however this would give equal importance to values that are less probable in the original (unsegmented) distributions.
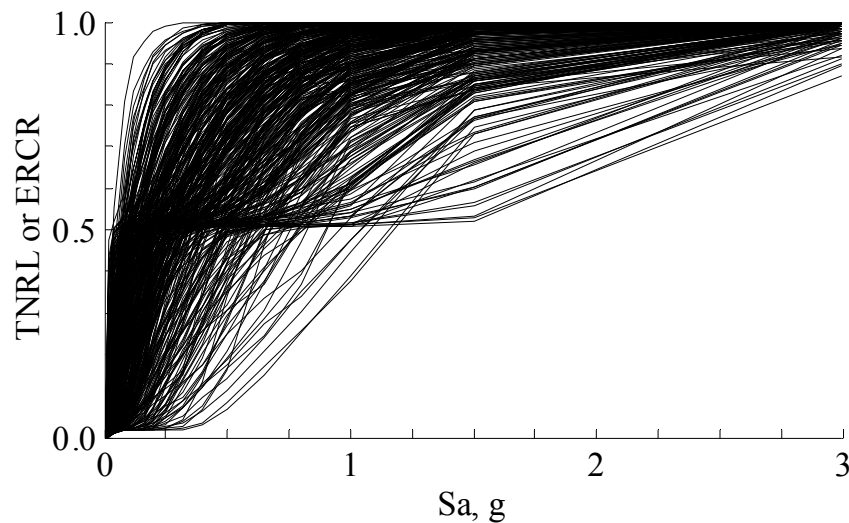
Figure 5.17 TNRL/ERCR curves for all 432 parameter combinations

Figure 5.17 shows the hazard-loss curves that are calculated for each parameter combination. As can be noticed, a high variation (standard deviation close to 20%) exists among calculated curves. This is something expected, as each curve represents a specific case for which parameters are randomized from smaller intervals. In other words curves represent the vulnerability of building populations with different characteristics. It should be noted that for building populations where building parameters follow the distributions that are defined in Chapter 4, the curves in Fig. 5.17 converges to "unbiased" curves of Fig. 5.4.

To investigate the correlation between parameters and their sensitivity on loss estimates, the calculated curves are clustered into subgroups according to their shape and relative difference. A value of 10% standard deviation is targeted in all groups and satisfied in almost all cases. In physical terms, this corresponds to an error level of 10% when the representative hazard-

loss curve for a group is utilized to estimate the regional loss in a building population that has similar characteristics with that group.

The groups are determined through a sequential procedure. First, the curves are clustered around the mean curve for the full set. Curves that have maximum deviation less than or equal to a certain threshold value, ε, are clustered as the first group. Trial calculations have shown that $\varepsilon = 0.2$ resulted in curves that have standard deviation on the order of 10%. Once the curves associated with the first group are determined, the remaining curves are divided into two groups, the ones that are consistently above and the ones that are consistently below the mean curve for the first group. Next, the same procedure that is followed to determine the curves for the first group is applied on the most recent two curve sets. This time the deviations are calculated from the mean curves that are associated with the new sets. This procedure is continued until all curves are grouped and have deviations less than or equal to $\varepsilon = 0.2$. After all curves are grouped, curves in each group are visually inspected to evaluate the similarity with respect to shape. Curves with different shapes are relocated to other groups that have better similarity. Relocation sometimes resulted in minor exceedance of the threshold value of $\varepsilon = 0.2$.

Table 5.5. Maximum standard deviation and difference from mean curve in each group.

	Full Set	Grp1	Grp2	Grp3	Grp4	Grp5	Grp6	Grp7	Grp8	Grp9	Grp10
Max Std. (%)	19.5	11.1	11.3	10.7	12.4	6.01	8.94	14.7	8.3	10.7	8.62
Ave. Std (%)	13.4	7.32	5.95	6.51	6.08	2.75	3.83	4.58	3.68	4.82	4.34
*Max Diff. (%)	61.8	22.6	22.3	21.4	27.9	14.7	27.5	28.2	24.5	27.1	14.5
*Ave. Diff (%)	35.2	15.4	12.8	13.7	11.6	6.31	9.14	9.13	7.46	10.1	7.15

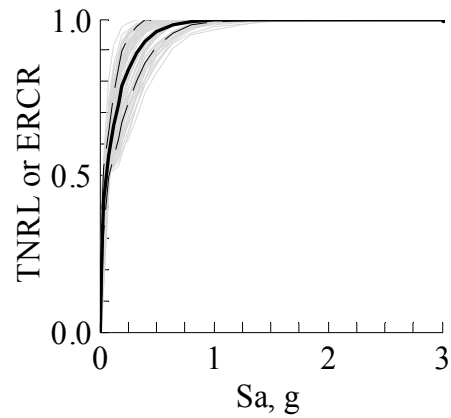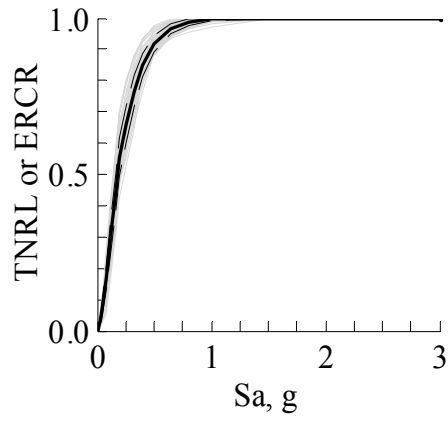* Difference is measured from the mean curve that is associated with each group
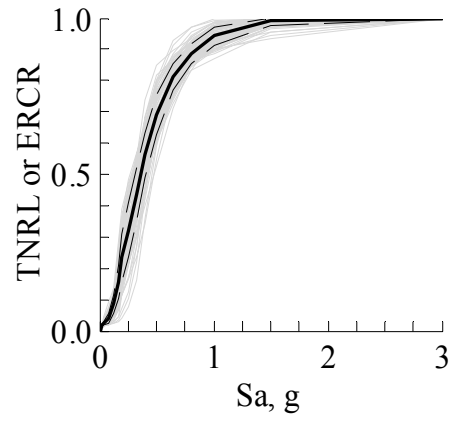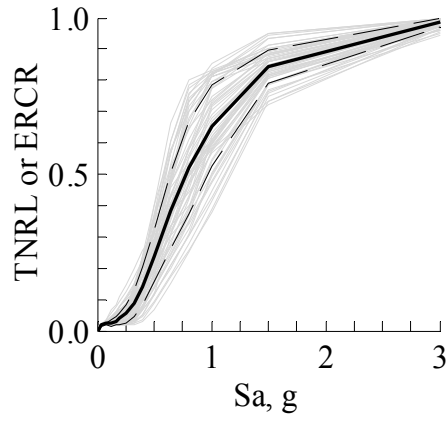
114

(a) Group 1

(b) Group 2

(c) Group 3

(d) Group 4

(e) Group 5

(f) Group 6

(g) Group 7

(h) Group 8

(i) Group 9

(j) Group 10

Figure 5.18 Variation of standard deviation in each group for different levels of hazard

The final categorization resulted in 10 different groups. The maximum deviation and standard error values in each group, as well as for the full set, are provided in Table 5.5. The average values of these quantities over the full range of hazard are also provided in this table. It should be noted that maximum values are calculated for the full hazard range. Typically, the error gets lower as the level of hazard approached to zero or to the maximum value. This variation is clearly demonstrated in Fig. 5.18 where the standard error associated with each group is plotted for different levels of hazard. As can be seen from this figure and from Table 5.5, the groups, in general, have standard error that is on the order of 10%. This error level can be reduced if number of groups is increased. However, considering the level of uncertainty in estimating the level of hazard and its variability over a given region, the 10% error range can be regarded as acceptable for loss calculations.

(a) Group 1

(b) Group 2

(c) Group 3

(d) Group 4

116

(e) Group 5

(f) Group 6

(g) Group 7

(h) Group 8

(i) Group 9

(j) Group 10

Figure 5.19 Groups representing cases with similar hazard-loss relationship

The hazard-loss curves associated with each group are presented in Fig. 5.19. Figure 5.20 compares the representative, mean, curves for each group in the same plot. In general, the

trend in each group agrees well with the parameter combinations that are included in that group. For example, parameter combinations that are expected to generate weaker buildings such as low wall area, high floor aspect ratio, high floor area, and large number of stories, tend to cluster in groups having rapidly increasing hazard-loss curves. Groups 2, 4, and 5 are typical examples of this case. Likewise, groups having softer hazard-loss curves, such as groups 3, 7 and 10, include parameter intervals that, typically, yield stronger buildings. Such parameter intervals may include high wall area, low floor aspect ratio, small floor area, and less number of stories.
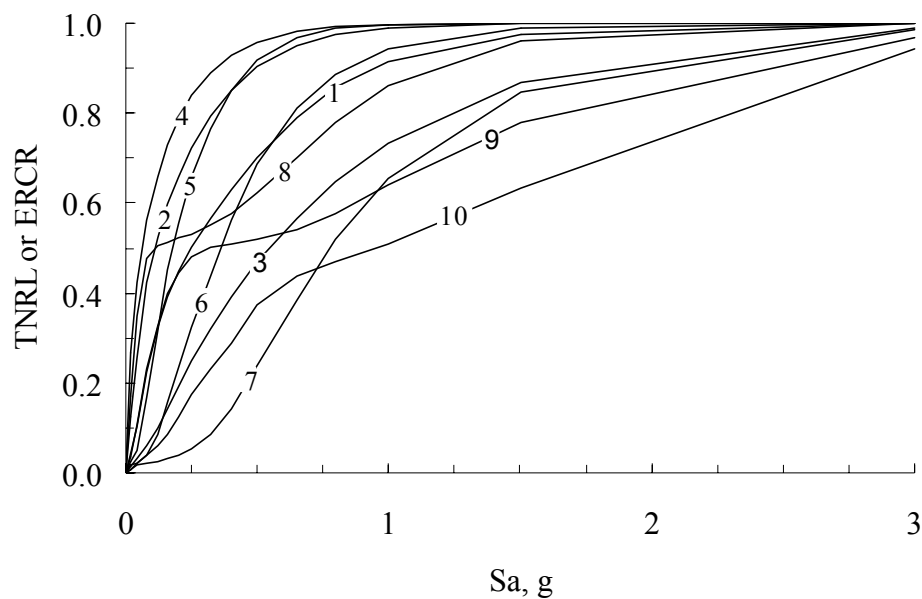
Figure 5.20. Representative (mean) TNRL/ERCR curves for each group.

Groups 1, 2, and 3 include almost 80% of all combinations. Among these groups, group 2 typically consists of buildings that are highly vulnerable to out-of-plane as well as in-plane failures. Parameter combinations include large number of stories with high story height, medium to high floor aspect ratio with large floor area, and low wall area in the in-plane direction. Large number of stories, high story height and high floor aspect ratio significantly affect the response amplification, especially in the out-of-plane direction. Likewise, low floor area in the in-plane direction directly reduces the base shear capacity of buildings. Demand increase in the out-of-plane and capacity reduction in the in-plane directions resulted in buildings that are highly vulnerable to seismic actions. Furthermore, buildings in group 2 are

118

primarily located on sites where ground motions have high to medium PGV/PGV values. This poses even higher demands on buildings since, frequency content of such ground motions, in general, matches well with the fundamental period of masonry buildings.

On contrary to group 2, buildings in group 3 included parameter combinations that enhance building vulnerability both in the in-plane and in the out-of-plane directions. Primarily, this group includes buildings with one story high and low story height, small to medium floor aspect ratio, small floor area and high wall area in the in-plane direction. Lower story height and less number of stories with squarer floor shape reduced the response amplification and increased the building capacity in the out-of-plane direction. Similarly, higher wall area in the in-plane direction and smaller floor area respectively increased the seismic capacity and reduced the seismic demands. All these factors combined to generate softer hazard-loss curves.

Group 1 can be considered to be in between group 2 and group 3. In general, the buildings in this group possess moderate parameter combinations, i.e. they do not include extreme cases. Therefore, the resulting hazard-loss curves are similar to the mean curve for all combinations.

The remaining groups, in general, include more specific parameter combinations. According to their similarities these groups can be categorized as special cases under the second and the third groups. In this regard, groups 4, 5, and 6 can be considered as part of group 2. Among these, group 4 possesses the worst combinations in the whole set. Different than group 2, the buildings in group 4 are subjected to ground motions with high PGA/PGV ratios. Furthermore, building parameters that enhance seismic performance are consistently low and parameters that increase seismic demands are consistently higher. These factors resulted in buildings that are more vulnerable than buildings in group 2. Groups 5 and 6 can be considered in the opposite side of group 2, i.e. groups included parameter combinations that resulted slightly less vulnerable buildings. Differences that enhance seismic performance include increased diaphragm stiffness due to square floor shapes, increased member capacity in the out-of-plane direction due to reduced story height, and, more importantly, reduced seismic demands due to different site conditions that generated ground motions having lower seismic energy in the short period range.

Groups 7 and 10 can be considered as special cases for group 3. Both groups show the lowest hazard-loss relationship among all groups. Primary differences between group 3 and 7 include the reduction of response amplification due to square floor shapes and increased in-plane shear capacity due to consistently higher wall areas. For group 10, even though the floor aspect ratio is consistently higher than group 3, small floor area and high in-plane wall area combination resulted in less vulnerable buildings especially at higher hazard levels, Fig. 5.20.

Groups 8 and 9 represent a specific case where the out-of-plane capacity is consistently weaker than the in-plane capacity of buildings. As a result of this combination, building populations reach 50% loss level at fairly low levels of hazard. This 50% loss is primarily attributable to out-of-plane damage, since vulnerability of buildings is evaluated in both directions, weak (shaking in the short side) and strong (shaking in the long side). The weak direction fails easily, but the strong direction resists higher demands. This explains the reduction in the rate of vulnerability, the slope of hazard-loss curves, after 50% loss level.

Table 5.6. Parameter intervals that are primarily dominant in each group

	GM	N_s	α_d	α_w	H_s	E_m	A_f
Group1	Uniform	1 to 2	2 to 3	Uniform	Uniform	1 to 2	1 to 2
Group2	1 to 2	3	Uniform	1 to 2	Uniform	1	Uniform
Group3	2 to 3	1 to 2	Uniform	2 to 3	Uniform	Uniform	1 to 2
Group4	1	3	1 and 3	1	3	1	3
Group5	2 to 3	2 to 3	1	1 to 2	Uniform	1	Uniform
Group6	2 to 3	1 to 2	1	Uniform	Uniform	2 to 3	Uniform
Group7	2 to 3	1	1	3	1 to 2	Uniform	1 to 2
Group8	1	1 to 2	3	1 to 2	Uniform	Uniform	Uniform
Group9	1	1	3	2 to 3	Uniform	Uniform	2 to 3
Group10	2 to 3	1	2 to 3	3	1 to 2	2 to 3	1

Detailed information about parameter combinations that are associated with each group is provided in Appendix B in the form of bar charts, Figs. B.2 through B.11. In these figures, each combination is expressed by a row of seven rectangles where each rectangle represents a parameter. The parameter intervals are defined through three different colors. Light gray represents range 1, darker gray represents range 2, and black represents range 3. The data is sorted sequentially with respect to each parameter. The parameters that are determined to have more significance are ordered first. Generic observations in each group are summarized in Table 5.6. In this table the numbers correspond to parameter ranges that are frequently observed in each group. The word "Uniform" is used to represent the case for which all three intervals are equally observed. As can be noticed from Table 5.6, the parameters that are determined to have medium significance in the first order analysis (h_s, E_m, A_f) tend to have full range representation in most of the groups. This observation further confirms the significance level that is assigned to these parameters in the first order analysis.

5.9. Concluding remarks

The primary objective of this chapter was to investigate the sensitivity of regional loss estimates for various building and region parameters. The results of sensitivity analyses are utilized to set the boundaries of parameters for which the loss in building populations can be represented with single hazard-loss relationship.

Based on the results of analyses the following conclusions and remarks can be stated:

- In a given region, buildings may have highly different hazard-loss relationships due to variations in site and building parameters. If the goal is to calculate regional loss, rather than building specific loss, those highly varying hazard-loss relationships that are associated with different buildings can be represented by few curves due to reduction of scatter in the summation process. This observation agrees well with the theoretical formulations for the total loss/risk concept that were presented in Chapter 2.

- If a given building population has building parameters similar to the ones defined for urban regions in Chapter 4, the hazard-loss relationship of this population can be represented by the unbiased curves of Fig. 5.4, provided that the population size is

equal to or larger than 25 buildings and site conditions are equally distributed among three ground motion categories. For this case, the estimation error is less than 10%.

- For building populations having less than 25 buildings, the loss estimates can be conducted either by using the unbiased curve, with accepting higher error level, or by using the appropriate biased hazard-loss relationships that have better fit with the parameter range of the population. Depending on characteristics of the building population, the later alternative may result in better loss estimates.

- For cases where building populations are located on regions with specific site conditions, appropriate hazard loss curves form Fig. 5.9 can be utilized to improve the estimations. If unbiased hazard-loss curves are used for these cases, the estimation error will be on the order of 15%.

- As long as selected ground motion set has uniformly distributed PGA/PGV values, the calculate hazard-loss relationships stay within 3.0% difference range.

- As long as hazard is defined from appropriate damped elastic response spectra, the calculated hazard-loss relationships stay within 10% difference range. Higher damping levels consistently result in higher loss estimates.

- First order sensitivity analyses on ten building parameters have shown that the loss estimates are less sensitive to average pier height ratio, seismic mass on the floors, average length of openings, and effective in-plane stiffness of diaphragms. The calculated deviations from the unbiased curve are less than 10%.

- Number of stories, floor aspect ratio, wall area, story height, elastic modulus of masonry, and floor area are determined to be the significant parameters. 10th and 90th percentile values for these parameters showed more than 10% variation from the unbiased hazard-loss relationship.

- Second order analyses on six building parameters and different ground motion categories have shown that different parameter combinations can be represented by 10 hazard-loss relationships. The resulting loss estimates have standard error on the order of 10%.

- Table 5.6 implies that ground motion categories, number of stories, floor aspect ratio and wall area are the most significant parameters in regional loss calculations.

- Some building populations may have properties that are consistently biased towards a certain interval. For these cases, end users may select hazard-loss curves from appropriate groups. Table 5.6 can be used as initial guidance in identifying suitable groups. For more specific combinations, bar charts, Figs. B.2 through B.11, can be referenced to make the selection.

CHAPTER 6 THE METHODOLOGY

6.1 Introduction

This chapter introduces a regional seismic loss/risk assessment methodology as developed through research presented in this report. The steps of the methodology are explained for use by a non-expert decision maker or stakeholder such as municipal officials, building owners, insurers or any other individual or group interested in estimating seismic losses for their conglomerate of unreinforced masonry buildings.

Extensive non-linear time history analyses on various building populations (Sections 4.2 and 5.8) have provided the basis to lay out these guidelines and to develop the tools of the methodology. Furthermore, the sensitivity investigations (Chapter 5) have helped to identify the most significant parameters that are necessary for regional loss/risk calculations. Comparison of these parameters with the ones listed in the preliminary methodology (Section 2.5) resulted in elimination of some parameters and hence simplified the overall data collection process.

Hazard-loss relationships included in the methodology are intended to estimate regional seismic loss/risk across vast building populations. They are not intended for evaluation of a single building.

Steps of the methodology are explained in this chapter. These steps are presented as independently as possible from the remainder of this report to stand alone for comprehension by a non-technical decision maker. Application of the methodology is demonstrated by estimating seismic risk for a small town in Italy that was shaken by two moderate earthquakes in October and November 2002. This demonstration is presented in Chapter 7.

6.2 The methodology: General layout and analysis tiers

In general, the methodology has three parts: 1) data collection, 2) grouping, and 3) evaluation. Fig 6.1 shows these three parts and their interaction among each other. In simple terms, the objective in the first part is to collect building and region specific data that will be utilized throughout the methodology. The collected information is used in the second part to identify the appropriate tools and relationships that represent the loss potential of the region or sub-regions. The outcomes of the first two parts are utilized in the final part to calculate the loss/risk estimate for the region.
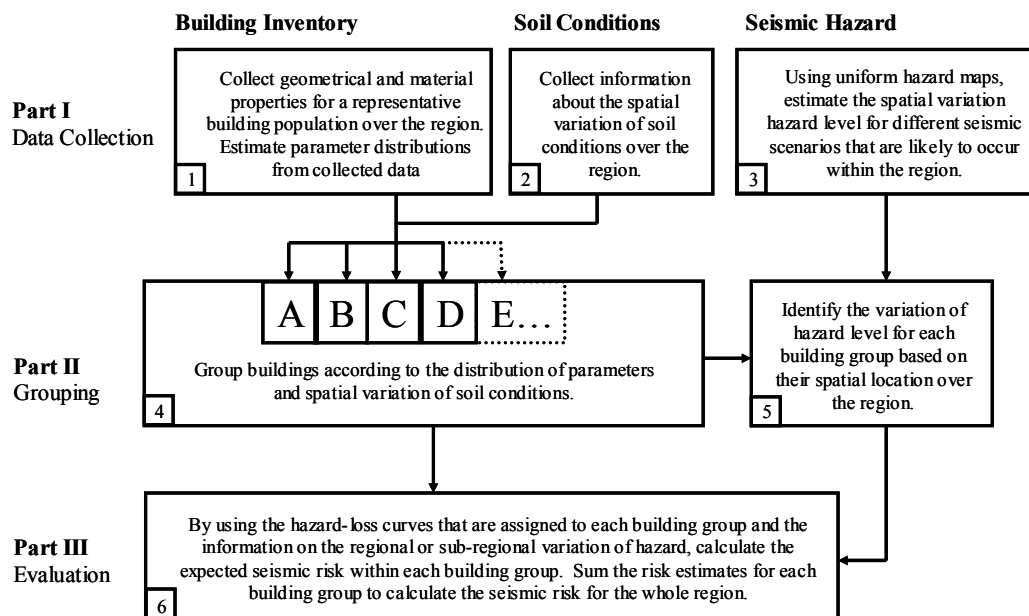
Figure 6.1. General layout and steps of the seismic risk/loss assessment methodology.

Depending on the region and building population properties, one or more steps of the methodology can be skipped to simplify the overall procedure. Four analysis tiers are provided to represent different combinations of region and building properties. The initial goal of the user is to identify the appropriate analysis tier by comparing the properties of analysis region with the properties of the "typical region". The typical region is defined to ease the data collection process and represents the properties of unreinforced masonry buildings in a typical urban region of the United States. The properties of the "typical region" are provided in Section 6.4.2.

	S_a and soil type variation is constant.	S_a and/or soil type variation is <u>not</u> constant.
Parameter distributions per Fig. 6.4 <u>and</u> population size is greater than 25 buildings.	**A**	**B**
Parameter distributions <u>not</u> per Fig. 6.4 <u>and</u> population size is greater <u>or</u> less than 25 buildings.	**C**	**D**

Figure 6.2. Tiers of the methodology.

Tiers	Information required	Action required
A	- Total floor area of the buildings. - Sa value and soil type. - Monetary value per unit area of buildings.	- Simple summation. - Can be carried out by a non-expert.
B	- Total floor area of the buildings in each soil and S_a category. - Representative S_a value and soil type in each S_a and soil category. - Monetary value per unit area of buildings.	- Integration of loss over sub-regions. - Can be carried out by a non-expert with some assistance from an engineering profession.
C	- Total floor area of the buildings. - Distributions for the building parameters that are listed in Table 6.1. - Sa value and soil type. - Monetary value per unit area of buildings.	- Field measurements from sample buildings to determine parameter distributions. - Grouping of buildings according to Figure 6.7. - Integration of loss over building groups. - Can be carried out by an engineering profession.
D	- Total floor area of the buildings in each soil and S_a category. - Representative S_a value and soil type in each S_a and soil category. - Distributions for the building parameters that are listed in Table 6.1. - Monetary value per unit area of buildings.	- Field measurements from sample buildings to determine parameter distributions. - Grouping of buildings according to Figure 6.7. - Integration of loss over building groups and sub-regions. - Can be carried out by an engineering profession.

Figure 6.3. Types of information and actions that are required for each analysis tier.

The region and building parameter combinations associated with each analysis tier are summarized in Fig. 6.2. In Figure 6.3, the required level of technical knowledge and expertise and the necessary types of information to complete the seismic risk evaluation are provided. In general, more time and more expertise are required with increasing tier letters (i.e. from A to D). Among analysis tiers, tier A represents the case for which the analysis region has properties that are similar to the properties of the "typical region" (the one assumed in the methodology). This analysis tier is the simplest of all as, user neither needs to collect inventory data nor needs to categorize buildings for different soil conditions and hazard levels. In analysis tier B, the regions in which the soil conditions changes with location are covered. As is in the case of analysis tier A, the properties of the building population are still similar to the properties of the building population for the "typical region". For analysis tier B, no building inventory data needs to be collected however, buildings need to be grouped according to the soil conditions. In analysis tiers C and D, the regions that have building properties different than the building properties of the "typical region" are represented. The primary difference between analysis tier C and D is that in analysis tier C the soil conditions and the variation of hazard level are constant over the region. In this regard, analysis tier D can be considered as the most generic case among other analysis tiers. In analysis tiers C and D, a sample building data needs to be collected in order to identify representative building properties over the region. Moreover, technical assistance from an engineering professional is required for both analysis tiers.

In order to decide which analysis tier to use, the user needs to identify the cases (see Fig. 6.2 for cases associated with different analysis tiers) that best represent the properties of the analysis region. In general, quick discussions with local engineers and city planners are sufficient to select the appropriate cases for the analysis region. The parameter distributions that are provided in Section 6.4.2 should be utilized to identify whether the properties of the building population is similar to the properties of the typical building population.

Once the analysis tier is selected, the specific steps associated with that analysis tier can be followed to complete the seismic risk evaluation process. The steps that are specific to each analysis tier primarily involves grouping of buildings over the region and assigning of hazard-loss curves to each building group. These steps are discussed in Section 6.5. Before going

into these discussions, the general steps for regional risk calculations and the supporting background information for the parameters of the methodology will be provided.

6.3 Calculation of regional loss/risk

Regional seismic risk is defined as the summation of expected losses due to all possible earthquakes within the region of the building population. In this methodology, the term "expected loss" corresponds to the average (most likely) value of the monetary losses due to direct structural damage. In reality, regional losses may include other factors, for example indirect economical losses due to business interruption. Those other types of losses are not represented in this methodology and may become 2-3 times higher than the losses due to direct structural damage.

For a particular seismic hazard (particular hazard level), the associated seismic risk is calculated as follows:

$$SR_i = EL_i \cdot P(H_i) \qquad (6.1)$$

where, SR_i = seismic risk associated with the ith seismic hazard.

EL_i = the expected (average) value of losses for the ith seismic hazard.

$P(H_i)$ = the probability (chance) of getting a seismic hazard with level equal to H_i.

Seismic risk for a particular event is also known as the "scenario-based" seismic risk. The summation of seismic risk for all possible scenarios gives the total seismic risk over the region. In the expression form:

$$TSR = \sum_{\substack{i=\text{for all} \\ \text{possible} \\ \text{events}}} SR_i \qquad (6.2)$$

where, TSR = the total seismic risk over the region.

In general, loss values get higher with increasing levels of hazard. On the contrary, the corresponding probabilities (chances) for higher levels of hazard become smaller. Due to this

trend, the product in Eq. 6.1 yields finite results; i.e. it is bounded. The same statement, therefore, is also true for the summation in Eq. 6.2.

The primary goal of this methodology is to provide the tools and the guidance to estimate the terms in Eq. 6.1. The term "hazard" is represented by the spectral acceleration, S_a, at a period that is representative of the fundamental periods of the buildings over the whole region or sub-regions. The estimation of the S_a value and its probability for a given region is discussed in Section 6.4.4. The term "loss" corresponds to the monetary losses due to direct structural damage in the building population. A normalized parameter, expected replacement cost ratio (ERCR), is used to represent the loss term. This term is defined in tabular form as a function of the hazard level, S_a, for various combinations of soil conditions, and properties of the building population. This tabular relationship between the hazard level and the loss parameter is named as the "hazard-loss" relationship in the methodology. By following the guidelines highlighted in Section 6.5, the user can group buildings with similar loss potential and identify corresponding ERCR values that represent the loss for each building group. A typical use of hazard-loss relationship is demonstrated in Section 6.4.5.

Once the ERCR values are identified, the total expected loss in each building group can be calculated as follows:

$$TLG_i(S_a) = ERCR_i(S_a) \times TFA_i \times MVPA \tag{6.3}$$

where, TLG_i = for a defined level of hazard, S_a, the total expected loss in the ith building group.

$ERCR_i$ = for a defined level of hazard, the expected value of the replacement cost ratio for the ith building group (the value read from the hazard-loss tables, see section 6.5).

TFA_i = total floor area of the buildings in the ith building group. For a single building, this value is equal to the floor area times the number of stories in that building.

$MVPA$ = monetary value per unit area of buildings over the analysis region.

From this calculation the total loss over the region can be computed as:

$$TRL(S_a) = \sum_{i=1}^{n} TLG_i$$
(6.4)

where, $TRL(S_a)$ = total regional loss for a defined hazard level.

n = number of building groups defined in the analysis region.

The seismic risk for a given hazard level, also known as the scenario-based risk evaluation, can be determined by multiplying the calculated loss with the probability of occurrence of the assumed level of hazard, Eq. 6.5.

$$SR(S_a) = TRL(S_a) \times P(Hazard = S_a)$$
(6.5)

where, $SR(S_a)$ = seismic risk for a defined level of hazard.

$P(Hazard = S_a)$ = probability of occurrence of a hazard with level equal to S_a.

The summation of seismic risk for different hazard levels gives the total seismic risk over the region.

6.4 Background information on the parameters and the tools of the methodology

6.4.1 Parameters of the methodology

As discussed in Section 6.2, different levels of information are required for different types of analysis tiers in the methodology. Table 6.1 lists the necessary type of information for the most generic case (analysis tier D). A list of resources that can be referenced to collect these data is also provided at the bottom of the Table 6.1. Even though information on the parameters listed in Table 6.1 is essential for tier D type analysis, a general idea on typical values of each parameter is necessary to identify type of the analysis tier that is appropriate for the region. As noted in Section 6.2, in addition to the references provided at the bottom of the Table 6.1 the user may consult local engineers and urban planners to get an estimate of the typical ranges for each parameter in the analysis region.

Among the parameters listed in Table 6.1, the ones essential for the selected analysis tier (see Fig. 6.3 for required types of information in each analysis tier) should be collected from a representative building population in the region. In collecting data, a survey form similar to the one provided in Appendix C can be utilized. Note that the form in Appendix C is designed for post-earthquake damage and building inventory data collection purposes. In data collection for pre-earthquake loss/risk investigations, the section "Damage Category" can be discarded.

Table 6.1. Building and region specific parameters that are used in the methodology.

Seismic Hazard and Soil Conditions	Building Parameters
• Elastic response spectra and its spatial variation within the building population. • Soil variation over the region	• Monetary value • Aerial location • Number of stories • Floor area • Floor aspect ratio • Normalized wall density index. • *Story height • *Elastic modulus of masonry
Possible resources	Possible resources
• USGS (2000) Hazard Maps (provide parameters to generate elastic response spectra for a given region and defined scenario).	• Existing city inventories • Tax assessor's or insurance database • Aerial photography • Field surveys

* These parameters are second order and can be neglected if necessary

The collected parameter data is used to identify the appropriate hazard-loss relationships that will be utilized to estimate the seismic risk of the region or sub-regions. The selection of such relationships will be discussed separately for each analysis tier in Section 6.5.

The building parameters that are listed in Table 6.1 are self explanatory except the "floor aspect ratio" and the "normalized wall density index". The floor aspect ratio is the ratio of the longer floor dimension to the smaller one. The wall density is defined as the ratio of total

effective wall area at the ground level to the floor area of the building. Normalized wall density index is calculated as follows:

$$\alpha_{wx} = \frac{\alpha_x}{\alpha_x'} \qquad \text{and similarly} \qquad \alpha_{wy} = \frac{\alpha_y}{\alpha_y'} \qquad (6.6)$$

where, $\alpha_{wx,y}$ = normalized wall density index in directions x or y

$\alpha_{x,y}$ = actual wall area-to-floor area ratio (wall density) in directions x or y

$$\alpha_{x,y}' = \frac{2L_{x,y} t_{wx,y}}{A_f} = \text{wall area-to-floor area index ratio with } t_{wx,y} = \text{sum of the wall}$$

thicknesses in directions x or y, $L_{x,y}$ = plan dimensions of the floor, and A_f = floor area.

x and y = directions orthogonal to the sides of the buildings

6.4.2 Building properties for the "typical region"

In general, building populations in urban regions of the United States have similar building properties. In this methodology, these similarities are identified to define parameter distributions that represent the characteristics of a "typical region" in the urban areas of the United States. The parameter distributions associated with such a "typical region" are provided in Fig. 6.4. These distributions are obtained through investigating the building inventory data that was collected for typical communities in the United States.

For some regions, the building properties may show deviations from these typical parameter distributions. The goal of the user is to identify whether such deviation exists in any of the parameters that are listed in Table 6.1. If deviations are identified, the user needs to conduct tier C or tier D type analysis to complete the seismic risk evaluation. As highlighted in the earlier sections, both analysis tiers C and D require definition of representative distributions for the parameters that show differences from the properties of the typical region.
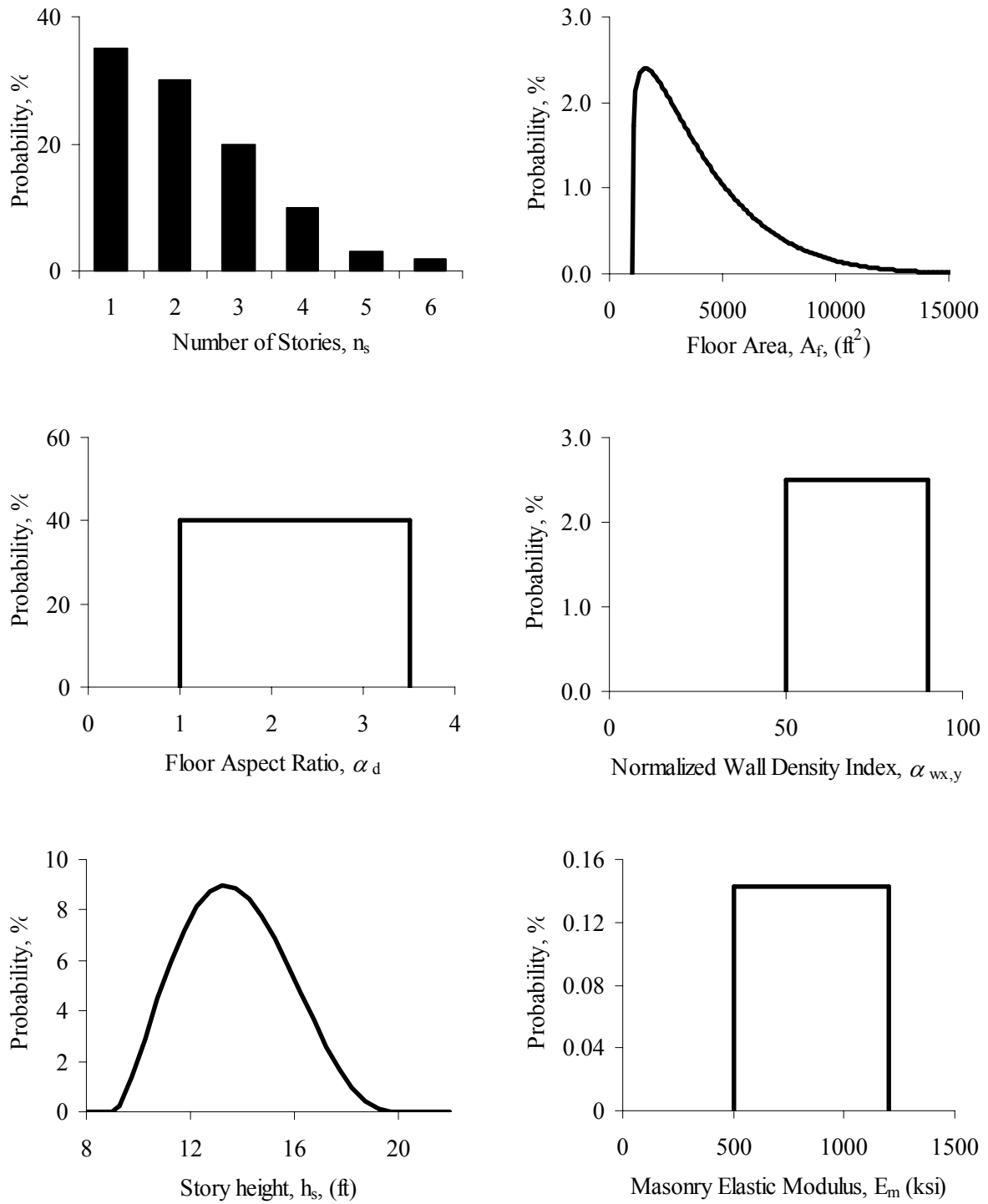
Figure 6.4. Parameter distributions for typical unreinforced masonry building populations in urban regions of the United States.

6.4.3 Soil conditions and soil categories

In this methodology, the possible variations in ground shaking characteristics due to site conditions are represented by three soil categories: 1) SC_A, 2) SC_B, and 3) SC_C. The task of the user is to identify the variation of the soil conditions in his/her region and identify sub-regions with similar soil categories. A regional map that shows the location of different soil types is useful for regions where the soil conditions vary significantly. Such kind of a soil map can be utilized to identify the building groups that have similar soil conditions.

Table 6.2. Properties of the soil categories.

Soil Category	SC_A	SC_B	SC_C
Soil Property (USGS Soil Class)[*]	Rock-Stiff Soil (A-B)	Medium Stiff (C)	Soft (D)

[*] USGS soil classes: A-B $= v_s >$ 1200 ft/s, C $=$ 1200 ft/s $> v_s >$ 600 ft/s, D $= v_s <$ 600 ft/s where, $v_s =$ shear wave velocity of the soil.

In Table 6.2, the properties of each soil category are provided. The definition of the soil categories are based on the USGS soil classes. The first category, SC_A, represents rock to stiff soils with shear wave velocities higher than 1200 ft/s. The second category, SC_B, represents medium stiff soils with shear wave velocities range from 600 to 1200 ft/s. The third category, SC_C, represents soft soils with shear wave velocities less than 600 ft/s.

6.4.4 Estimation of regional hazard and its probability

In the absence of region specific seismicity data, the United States Geological Survey (USGS) National Earthquake Reduction Program Maps (NEHRP, 2000) can be used to estimate spectral accelerations for a given zip code. NEHRP maps provide the parameters that can be used to generate elastic response spectra for seismic events with different return periods. The spectral acceleration corresponding to the plateau region (Fig. 6.5) of the elastic response spectrum can be taken as the representative hazard level for the region as, fundamental period of masonry buildings typically falls in this region. One may also use the procedure that is highlighted in the FEMA-356 document Section 1.6 to generate the full elastic response spectrum according to the parameters given in the NEHRP maps and use that curve to

estimate spectral acceleration values for various structural periods. However, as mentioned earlier such an approach is not necessary for almost all applications.
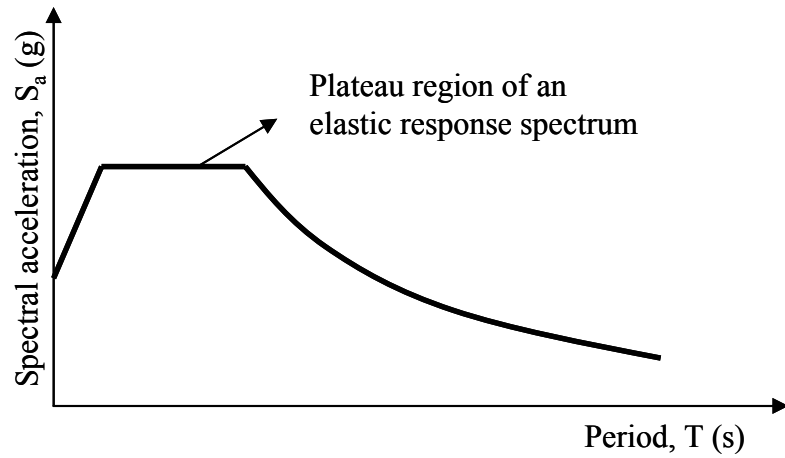
Figure 6.5. Elastic response spectrum.

Table 6.3. Acceleration scale factors for the soil categories (the scale factors are adopted from the FEMA 356 document (2000)).

Soil Category	Scale Factor, F_{SC}*				
	S_s** $< 0.25g$	$S_s = 0.5g$	$S_s = 0.75g$	$S_s = 1.0g$	$S_s > 1.25g$
SC_A	1.0	1.0	1.0	1.0	1.0
SC_B	1.6	1.4	1.2	1.1	1.0
SC_C	2.5	1.7	1.2	0.9	0.9

* Scale factor to account for ground motion amplification due to soil conditions.
** S_s is the spectral acceleration associated with the short period range. This value is taken from the NHERP hazard maps.

To calculate the spectral acceleration associated with the plateau region of the elastic response spectrum, obtain the short period (defined with symbol S_S in the NEHRP maps) spectral acceleration according to the zip code of the region. These values can also be digitally obtainable through USGS's web site, http://www.usgs.org/update.htm. Once the spectral acceleration for short period is obtained it should be multiplied with the corresponding scale factor to represent the ground motion amplification due to soil conditions. In Table 6.3, the scale factors for the three soil categories of the methodology are provided. These factors are used in Eq. 6.7 to estimate the spectral acceleration level.

$$S_a = F_{SC} S_S \tag{6.7}$$

where, S_a = spectral acceleration to be used in loss calculations (see Eq. 6.3)

F_{SC} = scale factor to account for the ground motion amplification due to soil conditions.

S_S = short period spectral acceleration that is obtained from NEHRP hazard maps.

The estimation of the probability associated with the selected hazard level is typically a complicated procedure. However, one may get a reasonable estimate by modeling earthquake occurrence as Poisson's distribution. With this assumption, the probability of single occurrence of a seismic event for a given return period, T_r, and for a given time interval of one year can be calculated by using Eq. 6.8. The calculated probabilities for the four hazard levels of NEHRP maps are provided in Table 6.4. The calculated probability can be directly used in Eq. 6.5 to estimate the annual seismic risk.

$$P\left(\text{Hazard Level} = S_a\right) = \frac{1}{T_r} \cdot e^{\left(\frac{1}{T_r}\right)} \tag{6.8}$$

where, S_a = spectral acceleration associated with the selected hazard level.

T_r = return period of the selected hazard level. The return periods for different hazard levels that are defined in the NEHRP maps are listed in Table 6.4.

Table 6.4. Return periods and probabilities associated with different hazard levels of the NEHRP maps.

Hazard level	Mean return period (years)	Probability of single occurrence of in a year (calculated per Eq. 6.8), %
50% / 50 years[*]	72	1.408
20% / 50 years	225	0.446
10% / 50 years	474	0.211
2% / 50 years	2475	0.0404

* The term "x% / y years" is directly taken from the NEHRP maps and means that there exists a "x" percent chance that the selected level of hazard will occur a least once in a period of "y" years. The severity of the hazard increases as one goes down in the provided list.

6.4.5 Definition and the use of the hazard-loss relationships

The hazard-loss functions are the key relationships of the methodology. They define the level of loss for a given hazard level of S_a. The loss is expressed in terms of a normalized quantity called expected replacement cost ratio, ERCR. This quantity is defined as the ratio of the actual loss amount due to structural damage to the actual replacement cost of the building. A typical hazard-loss curve is presented and its use is demonstrated in Fig. 6.6. As can be noticed, based on its definition, the ERCR takes the value of 0.0 for no damage or no hazard case and takes the value of 1.0 for full damage or high hazard level.
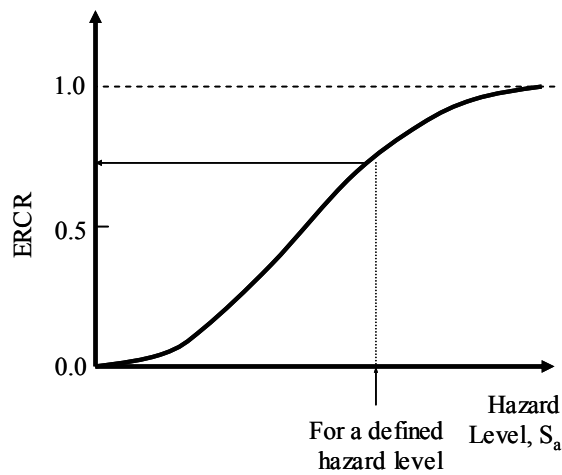
Figure 6.6. Typical use of hazard–loss relationships.

6.5 Data collection and grouping of buildings in each analysis tier

As discussed in the earlier sections, the primary objective in analysis tiers is to identify the building groups that have similar loss potential and assign those building groups a representative hazard-loss relationship. As laid out in Section 6.3, these hazard-loss relationships are used in Eq. 6.3 to estimate the loss level in each building group.

In order to complete the steps discussed in this section, the analysis tier should already have been selected and the necessary types of parameter data should already have been collected from the region. In the following sections, the additional steps that are required to complete the selection of appropriate hazard-loss curves for the building group or sub-groups will be

described. The values provided in hazard-loss tables can be linearly interpolated to calculate the loss values for intermediate hazard levels.

6.5.1 Analysis tier A

The analysis tier A corresponds to the simplest case as user neither needs to collect building inventory data nor needs to categorize buildings according to different soil conditions. For each soil category, the loss potential of the building population is represented by a single hazard-loss relationship. The hazard-loss relationships for each soil category are provided in Table 6.5. Also provided in Table 6.5 is the representative hazard-loss relationship for a region in which the building population is uniformly distributed over all three soil conditions. The regions in which to soil conditions are not uniform are addressed in Analysis tier B.

The task of the user is to enter the table with the S_a value and the soil category that are representative for the analysis region and calculate the ERCR value. The calculated ERCR value is used in Section 6.3 to complete the seismic risk calculations.

Table 6.5. Hazard-loss curves for uniform and for different soil categories. The building population has properties similar to the properties of the "typical region".

S_a, g	0.02	0.04	0.08	0.14	0.2	0.3	0.4	0.5	0.6	0.8	1.0	2.0	3.0
ERCR Uniform	0.06	0.13	0.25	0.38	0.47	0.58	0.66	0.73	0.79	0.87	0.92	0.99	1.00
ERCR SC_A	0.10	0.22	0.37	0.49	0.57	0.65	0.71	0.77	0.81	0.89	0.93	0.99	1.00
ERCR SC_B	0.06	0.12	0.23	0.35	0.45	0.56	0.65	0.72	0.78	0.87	0.93	1.00	1.00
ERCR SC_C	0.02	0.05	0.15	0.29	0.41	0.54	0.63	0.71	0.77	0.87	0.92	0.99	1.00

6.5.2 Analysis tier B

Analysis tier B is similar to the analysis tier A except that the buildings need to be grouped according to the variation of soil conditions and spectral acceleration over the region. The task of the user is to estimate the percentage of the total floor area of the buildings in each

group. In making this estimation, regional soil and hazard maps can be overlapped on to each other to identify zones with similar soil conditions and hazard levels. Once these zones are identified, the regional maps (or aerial photographs) that show the location of the buildings can be used to estimate the total floor area (or percentage of the total floor area in whole building population) of buildings in each zone. As a result of this estimation a table that is similar to Table 6.6 can be prepared to help the seismic risk calculations in Section 6.3.

Table 6.6. Example summary table

Group ID	Soil Category	Hazard Level, S_a (g)	Total floor area (% of the total floor area of the region)
1	A	0.3	3.5
2	C	0.6	27.4
3	A	0.1	45.0
.	.		.
.	.	.	.
.	.		.
n	B	0.4	2.0

Once a table similar to the Table 6.6 is completed, user can calculate the ERCR values by entering Table 6.5 with the assigned soil category and hazard level values for each building group. The calculated ERCR values are used in Section 6.3 to complete the seismic risk calculations.

6.5.3 Analysis tiers C and D

As noted in the earlier sections, analysis tier C is a special case of analysis tier D. However, as far as the type of steps involved, both analysis tiers are similar to each other. For this reason, they will be covered together in this section. Where necessary, differences will be highlighted during the text.

As for the previous analysis tiers, the primary task of the user is to group buildings that have similar loss potential. In this case, the grouping will be identified according to the properties of the building population as well as the variations in soil conditions and hazard level (for analysis tier D).

The initial step in identifying building groups is to determine the building parameters that have different distributions than the distributions of the building parameters for the "typical region" (Fig. 6.4). In the general case, one or more parameter distributions of the analysis region may not match with the ones provided in Fig 6.4, as these parameter distributions are generic and are defined for a typical unreinforced masonry building population. In particular, some parameters in the analysis region may have values that are shifted towards a certain range. For example, a region may primarily consist of 2 to 3 storey buildings with square floor plan shapes as opposed to 1 to 6 storey buildings with square to rectangular floor plan shapes.

Table 6.7. The three intervals that are assigned to each parameter.

Parameter	SC	n_s	α_d	α_w (%)	h_s (ft)	E_m (ksi)	A_f (100 ft^2)
Range 1	SC_A	1	1.00-1.75	50-62	9.0-12.5	500-710	10-23
Range 2	SC_B	2-3	1.75-2.75	62-78	12.5-14.8	710-990	23-48
Range 3	SC_C	4-5-6	2.75-3.50	78-90	14.8-20	990-1200	48-300

In the current methodology, three intervals are defined to represent possible biases in each parameter. These intervals are defined on the parameter distributions provided for the "typical region". Parameter values corresponding to lower 30, medium 40, and upper 30 percentiles are taken as the interval boundaries. The three intervals assigned to each parameter are listed in Table 6.7. Extensive investigations are conducted to compare hazard-loss relationships for various building populations with biased parameter distributions. The results of these comparisons have shown that with accepting 10% standard error, one may cluster the hazard-loss relationships for all parameter combinations into 10 hazard-loss categories. The parameter intervals that are primarily observed in each hazard-loss category are summarized in Fig. 6.7.

The tasks of the user include:

1) for the building parameters that have different distributions than the building parameters of the typical region: cluster the parameters in the sample building data

(that was collected from the analysis region) according to the parameter intervals defined in Table 6.7.

2) For analysis tier D, the buildings in the sample data are also need to be clustered according to the variations in the soil categories. This step is skipped for analysis tier C, as the soil variation is constant across the analysis region.

3) sort the clustered region and building parameters with respect to the interval ranges.

4) compare sorted data with Fig. 6.7 in order to identify building groups with similar hazard-loss potential. The sorted data can also be compared with the B2-B11 for more precise categorization. In Figures B2 through B11, the properties of all parameter combinations that are associated with each hazard-loss category are presented.

5) assign one of the ten hazard-loss relationships to each building group.

6) For analysis tier D, investigate the hazard variation in each building group to identify subgroups with the same hazard level. This step is skipped for analysis tier C, as the hazard variation is constant across the analysis region.

Hazard-Loss Category	SC	n_s	α_d	α_w	h_s	E_m	A_f
ID-1							
ID-2							
ID-3							
ID-4							
ID-5							
ID-6							
ID-7							
ID-8							
ID-9							
ID-10							

☐ All ranges   ☐ Range 1   ◼ Range 2   ■ Range 3

Figure 6.7. Parameter intervals dominant in each hazard-loss category.

Once each building group is identified and the associated hazard-loss category and the hazard level are assigned, the information can be summarized as shown in Table 6.8.

Table 6.8. Example summary table

Group ID	Hazard-Loss Category ID	Hazard Level, S_a (g)	Total floor area (% of the total floor area of the region)
1	1	0.2	20.5
2	4	0.6	7.4
3	5	0.5	15.0
.	.	.	.
.	.	.	.
.	.		.
n	4	0.4	12.0

After completing the information in Table 6.8, user can calculate the ERCR for each building group by entering Table 6.9 with the assigned hazard-loss category and the S_a value. The estimated ERCR values are used in Section 6.3 to complete the seismic risk calculations.

Table 6.9. Hazard-loss relationship associated with each group

S_a, g	0.02	0.04	0.08	0.14	0.2	0.32	0.4	0.5	0.65	0.8	1.0	1.5	3.0
ID-1	0.04	0.10	0.23	0.36	0.45	0.57	0.63	0.70	0.79	0.86	0.91	0.98	1.00
ID-2	0.12	0.26	0.42	0.56	0.66	0.79	0.85	0.90	0.95	0.97	0.99	1.00	1.00
ID-3	0.01	0.03	0.06	0.12	0.19	0.32	0.39	0.47	0.56	0.65	0.73	0.87	0.99
ID-4	0.27	0.42	0.56	0.69	0.78	0.89	0.93	0.96	0.98	0.99	1.00	1.00	1.00
ID-5	0.02	0.05	0.17	0.39	0.56	0.77	0.85	0.92	0.97	0.99	1.00	1.00	1.00
ID-6	0.02	0.02	0.04	0.12	0.23	0.44	0.56	0.69	0.81	0.89	0.94	0.99	1.00
ID-7	0.01	0.02	0.02	0.03	0.04	0.08	0.14	0.24	0.38	0.52	0.65	0.85	0.99
ID-8	0.17	0.35	0.48	0.51	0.52	0.55	0.58	0.62	0.70	0.78	0.86	0.96	1.00
ID-9	0.04	0.11	0.23	0.36	0.45	0.50	0.51	0.52	0.54	0.58	0.64	0.78	0.97
ID-10	0.01	0.02	0.04	0.07	0.12	0.23	0.29	0.37	0.44	0.47	0.51	0.63	0.94

CHAPTER 7 CASE STUDY: LOSS ESTIMATION IN S. G. D. PUGLIA, ITALY

7.1. Introduction

The primary objective of this chapter is to demonstrate the application of the loss assessment methodology that is developed in this study. Secondary objective is to compare the loss estimate (calculated through using the methodology) with real data that is collected from the field. Demonstration is carried out from a stakeholder point of view. For this application, a city decision maker is thought as the stakeholder.

In order to address both objectives of this chapter, a region with known building and site properties has to be selected. Furthermore, to be able to compare the loss estimates, the region has to have damage data from a past earthquake. Unfortunately, a survey among earlier reconnaissance investigations has revealed that these investigations, typically, include general information about the damage, but do not contain physical properties of buildings that undergo described damage. This makes it difficult to use damage observations from such reconnaissance investigations. An attempt to fill the gaps with judgment-based premises introduces additional uncertainties leading to misinterpretations. In order to overcome the issues related with incomplete datasets, a field trip is conducted to a small town, San Giuliano di Puglia (see Fig 7.1), in Italy. This town was recently shaken by two moderate size earthquakes. The reasons in selecting this town as a case study region can be listed as follows:

- The small size of the town is convenient to collect additional inventory data that is required by the methodology.

- The town has significant number of masonry buildings owing to the construction tradition over the region.

- Recent earthquakes on October 31 and November 1, 2002, caused damaged in masonry buildings. A damage survey on buildings can be compared with the loss estimates that are calculated from the proposed methodology.

- Town is closed to public entrance due to ongoing legal investigations on one of the collapsed buildings. This isolation preserved the damage state of the buildings right after the events to this date.

Next two sections provide information about general characteristics of the town, the earthquakes, and building inventory and damage data that was collected during the field investigations. Following sections utilize these data to demonstrate the application of the methodology and compare the loss estimates with the field observations.

7.2. General information about the region and the earthquakes

7.2.1. Region properties

S. G. D. Puglia, see Fig. 7.1, was built over the crest of a hill. The town has about 100-150 buildings with a population of around 1200 people. About 45-65% of the construction consists of two to three story residential engineered and non-engineered masonry houses. The masonry materials range from rubble stone to cut stone to hallow clay tiles. The floors are, in general, made out of wood or reinforced concrete. The wood diaphragm is more typical for old non-engineered construction.

Figure 7.1. San Giulinao di Puglia, Molise, Italy

7.2.2. Recent earthquakes of October 31 and November 1, 2002

On October 31 and November 1 two moderate size ($M_L = 5.4$ and 5.3) earthquakes shook the region. The epicenters of the earthquakes were about 5 km far from S. G. D. Puglia. Comparison of the local intensities with the historic events suggests that the recent events generated similar level of damage as the event that occurred on May 12, 1456 in the Bojano basin (Mola *et. al.* 2003). This suggests that the recent events may have a return period of about 500 years.
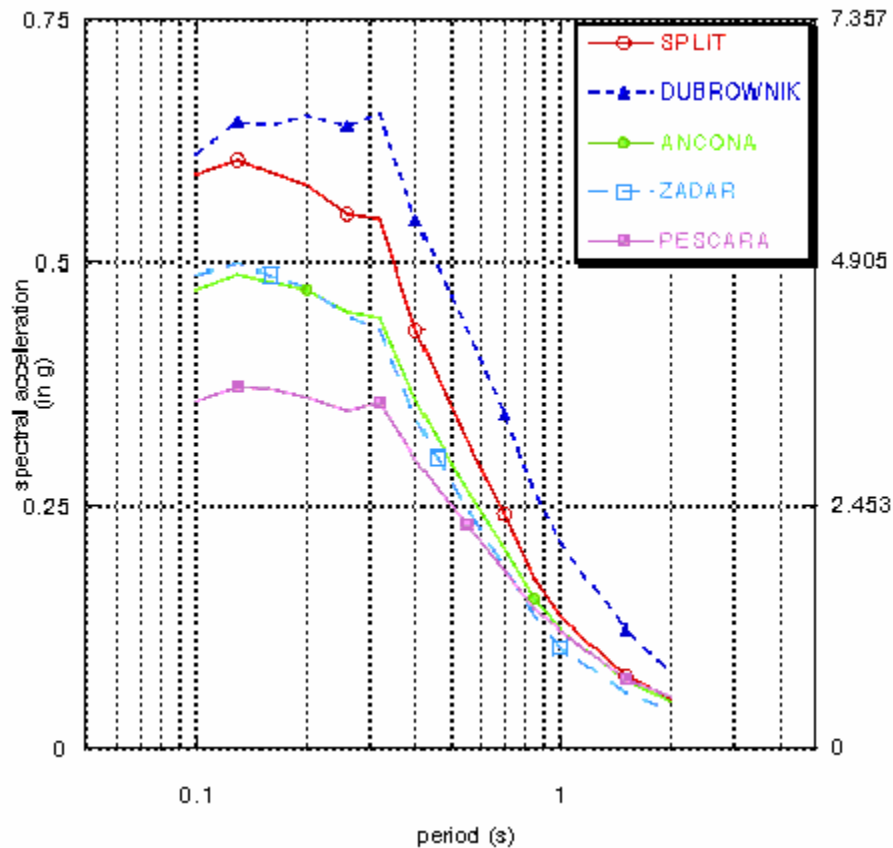

Figure 7.2. Uniform hazard spectra for events with 475 years return period (Slejko *et. al.* 1999, figure taken from Mola *et. al.* 2003)

Unfortunately there were no recording stations in the town. Therefore, the exact value of the hazard level is not known precisely. Based on region-specific attenuation relationships and measurements taken from close by recording stations, Mola *et. al.* estimates the peak ground accelerations in S. G. D. Puglia to be 0.36g for the first event and 0.17g for the second event. These values agree well with the uniform hazard spectra

145

(see Fig. 7.2) that is generated for the town of Pescara. Due to its close distance, this town can be considered to have similar hazard level as S. G. D. Puglia. Curves in Fig. 7.2 are generated for a return period of 475 years, which is on the same order as the estimated return period for the most recent events.

7.2.3. Site characteristics and region topography

The local soil conditions in S. G. D. Puglia ranged from limestone (for old part of the town) to talus and anthropic refillings (for more recent part of the town) (Mola *et. al.* 2003). Figure 7.3 shows the variation of soil conditions over the topographic map of S. G. D. Puglia. As can be noticed from densely spaced elevation contours, the town is constructed over the crest of a hill. Such kind of development is typical for other towns in that region.
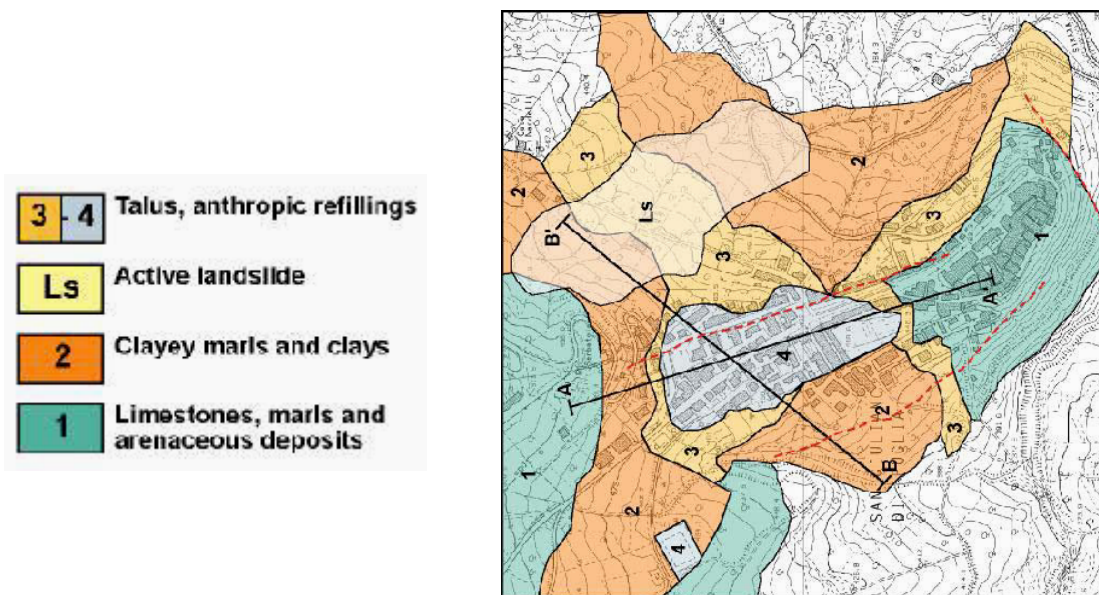

Figure 7.3. Soil variation over S. G. D. Puglia (picture taken from SSN web site, 2002)

In most of the cases, the topography is modified through fillings in order to allow more area to expand the towns. In S. G. D. Puglia, such modification corresponds to recently developed part of the town, zones 3 and 4 as shown in Fig. 7.3. The soil properties in these zones had an influence on the local amplification of the ground motions. This effect is clearly reflected as concentrated damage in this part of the town.

146

7.3. Building inventory and damage surveys

7.3.1 Building inventory

During field investigations, damage as well as inventory data were collected for the buildings in S. G. D. Puglia. A total of 66 unreinforced masonry buildings were investigated in the recently developed part of the town, see Fig. 7.4. The buildings in the older part of the town were discarded since these buildings have significantly different construction characteristics than the masonry building types that are addressed in this study.

Figure 7.4. Investigated buildings in S. G. D. Puglia (numbered buildings, map taken from the site engineer)

Figure 7.5. Aerial photo of S. G. D. Puglia (picture taken from the site engineer)

The collected data consists of damage state, story height, wall thickness, floor type, and the type of masonry material in each building. Additional parameters that are required by the methodology are estimated from building photos and the aerial photograph of the town, see Fig. 7.5. These parameters include floor area, floor aspect ratio, and size of the window/door openings in the buildings.
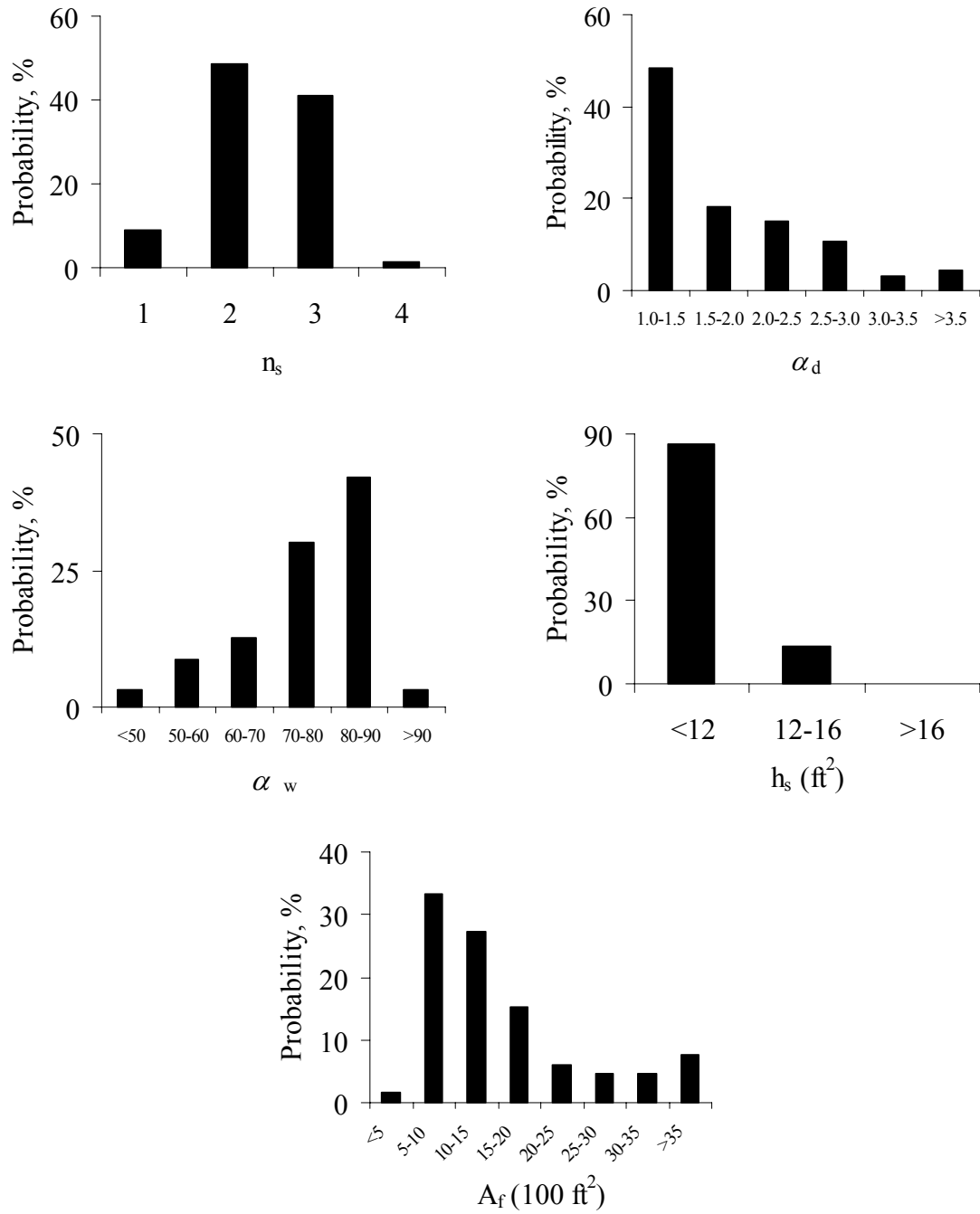

Figure 7.6. Distribution of building parameters in S. G. D. Puglia

Figure 7.6 shows the variation of parameters that are significant for the loss assessment methodology. As can be noticed from parameter distributions, the town mainly consisted of buildings with 2-3 stories high, almost square plan shapes, and high wall densities. During field investigations, the elastic modulus of masonry was not measured. However, visual inspections suggested that the materials are in the low quality range. A similar observation is also stated in Mola *et. al.* (2003).

7.3.2. Damage survey

Damage survey is conducted on all masonry buildings whether they are damaged or not. The goal is to have a complete set of damage data. Damage in buildings is visually inspected and categorized according to EMS-98 (1998) damage sketches for masonry buildings, see Fig. 7.7. As a result of these field inspections, each building is assigned one damage state among five damage states provided in EMS-98. The assigned damage states are converted to damage states that are defined in FEMA-356 document. Damage definitions associated with each scale are compared to convert data into FEMA-356 form. Table 7.1 provides the conversion that is used in this study.

| Grade 1 | Grade 2 | Grade 3 | Grade 4 | Grade 5 |

Figure 7.7 EMS-98 damage scale

Table 7.1. Conversion from EMS-98 damage states to FEMA-356 performance states

EMS-98 Damage States	FEMA-356 Performance States
Grade 1 – Negligible to slight damage	NO[*] to IO – No damage to Immediate Occup.
Grade 2 – Moderate damage	IO – Immediate occupancy
Grade 3 – Substantial to heavy damage	LS – Life safety
Grade 4 – Very heavy damage	CP – Collapse prevention
Grade 5 – Destruction	TC[*] – Total collapse

[*] These damage states are added to the primary performance states of FEMA-356

Damage distribution over the building population showed variation from minor to collapse. Figures 7.8, 7.9, and 7.10 shows examples of typical damage patterns observed in the field. The construction details and soil conditions were the two primary factors that affected the distribution of damage. The form of in-plane damage mainly consisted of bed-joint-sliding for solid unit construction and diagonal cracking for hollow unit construction. The out-of-plane damage typically observed for buildings where no floor anchors exist and typically occurred at the top story level. Figure 7.11 shows the distribution of damage for all masonry buildings in the town.

Figure 7.8. Good performing buildings

Figure 7.9. In-plane damage patterns, bed-joint-sliding and diagonal cracking

150

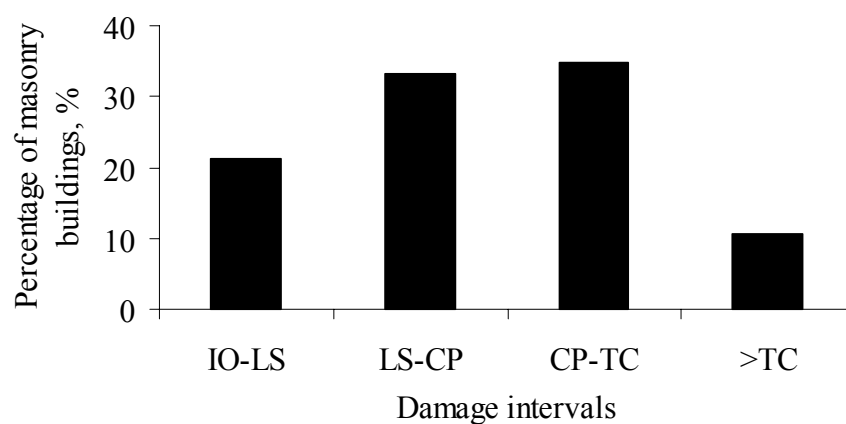Figure 7.10. Out-of-plane damage patterns

Figure 7.11. Damage distribution over masonry building population

7.4. Application of the methodology

In this section, the proposed methodology is applied to estimate the regional loss in S. G. D. Puglia. The steps of the methodology, Chapter 6, are followed to estimate regional losses.

The first step, Part I, is to gather information about hazard, soil distribution, and building inventory. In this case study, the hazard is defined by the events of October 31 and November 1. In general, hazard variation for future events can be determined from uniform hazard maps. It should be noted that the hazard-loss curves are generated for spectral acceleration at the fundamental period of buildings. Therefore, proper hazard definition requires estimation of building periods over the population and calculation of S_a level for each building. For period estimations, the empirical formula provided in

Chapter 6 (Eq. 6.2) can be utilized. In this case, fortunately, all buildings are in short period range corresponding to the plateau region of the response spectrum. This results in constant amplification factor, same S_a value, to each building. In this application, an amplification factor of 2.0 is used, resulting in a hazard-level of $S_a = 2 \times 0.36g = 0.72g$

The soil variation over the town is provided in Fig. 7.3. Overlapping of soil map, see Fig. 7.3, with the location map of the buildings, see Fig. 7.4, identifies the variation of soil over the building population. Such comparison is presented in Fig. 7.12. As can be seen from this figure, the variation of soil conditions is almost constant under the building population that is investigated in this case study. Typically, soil conditions correspond to artificially filled regions that are defined by zones 3 and 4.
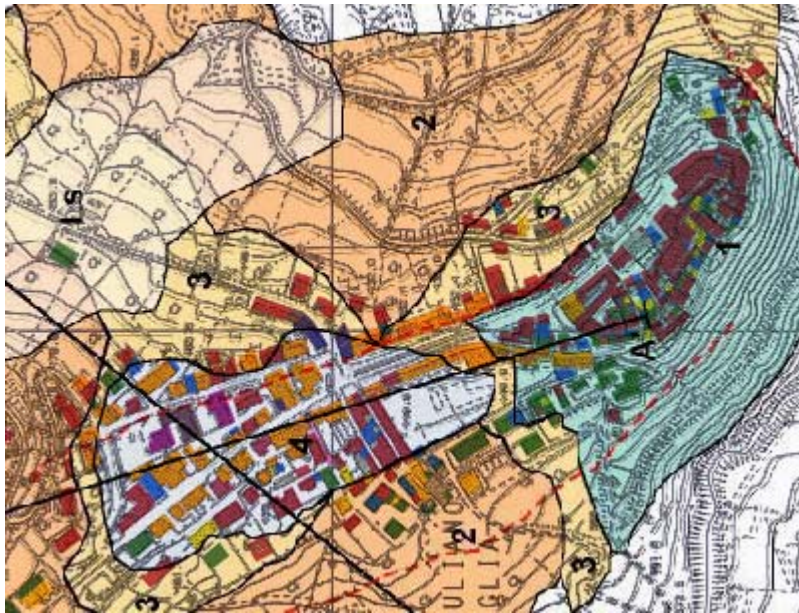

Figure 7.12. Overlapping of soil and building location maps

Essential building inventory data include distributions for number of stories, floor aspect ratio, wall density, story height, masonry elastic modulus, and floor area. Data corresponding to these parameters are collected from the field as well as estimated from aerial photo of the region. The resulting distributions were provided in earlier sections. These distributions are typically different than the ones that were provided in Fig. 6.2. Due to these differences a biased approach is utilized and buildings are categorized into

subgroups. If differences between parameter distributions were insignificant, no grouping would be necessary to estimate losses over the region.

The second step, Part II, of the methodology involves grouping of the building population with respect to variations in hazard, soil, and building parameters. As discussed in previous paragraphs, the hazard and soil are assumed to be constant over the region. Therefore, grouping is only done to address the bias, differences, in building parameter distributions. To do this, building parameters are assigned interval numbers according to the parameter ranges that are defined in Table 6.3. Once interval numbers are assigned, the data is sequentially sorted with respect to all parameters. Figure 7.13 shows the sorted data in the form of bar chart where colors define the interval range that is assigned to each building. In this figure, each row of rectangles represents one building in the population. Comparison of this figure with Figures B.2 through B.11 and Fig. 6.5 yields the groups that show good agreement with the characteristics of the building population. Buildings that are in the same group are highlighted in Fig. 7.13.
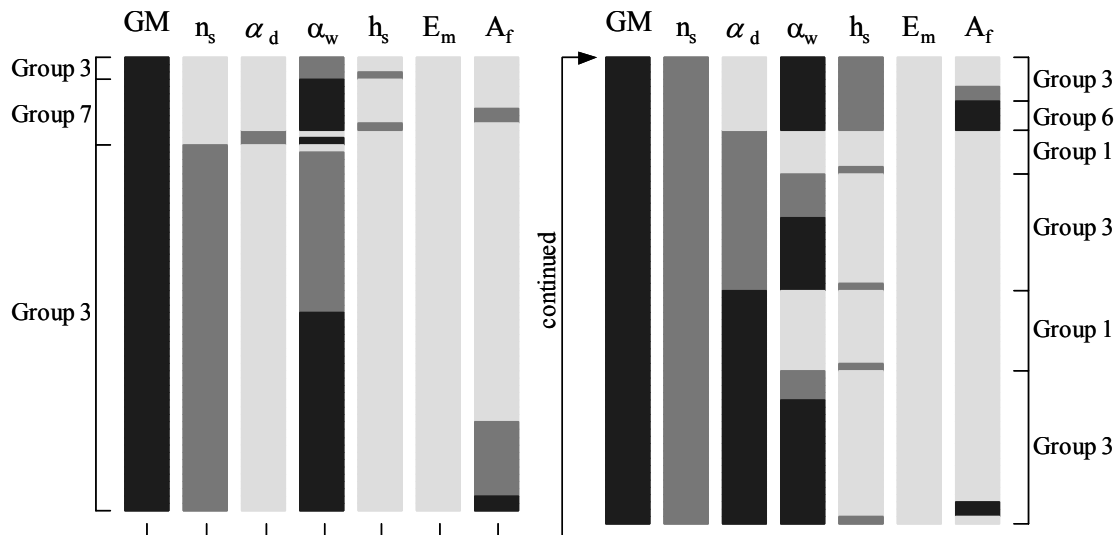

Figure 7.13. Region and building parameters that are essential for total loss estimates

As can be seen the region is divided into 4 subgroups. In this case, hazard-loss curves are taken from groups 1, 3, 6, and 7. To calculate the losses, the value of each building has to be known. Due to lack of field information, value of each building is determined according to the assumption that was stated in Section 5.2. Based on this assumption, the value of each building is calculated as the multiplication of the floor area with the

number of stories and normalized with respect to the total value of the region. First row in Table 7.2 provides normalized building value for each subgroup.

Table 7.2. Total normalized value, ERCR, and estimated loss in each subgroup

	Group A (1)[*]	Group B (3)[*]	Group C (6)[*]	Group D (7)[*]	Total
Value, %	6.5	79.7	10.2	3.6	100
ERCR	0.82	0.60	0.85	0.45	-
Loss, %	5.3	47.8	8.4	1.6	63.1

[*] Value represents the group number that is associated with that subgroup

The remaining two rows in Table 7.2 gives the ERCR and associated loss for each subgroup at a hazard level of $S_a = 0.72g$. Based on this calculation the total normalized loss is estimated to be 63% for the events of October 31 and November 1.

Using the estimated regional loss, the annual seismic risk can be calculated by using an appropriate probability distribution that can model occurrence of earthquakes in time. In this case, a Poisson's distribution is assumed to model earthquake occurrence. Using the estimated return period ($T_r \sim 500$ years) for the events, the annual risk is calculated as follows:

$$\text{Seismic Risk} = \text{TRL} \times P\left(n = 1 \middle| S_a = 0.72g\right)$$

$$= 63.1 \times \frac{\left(\frac{1}{500} \cdot 1\,\text{year}\right)^1}{1!} \cdot e^{\left(-\frac{1}{500} \cdot 1\,\text{year}\right)} = 12.5\% \, / \, \text{year} \qquad (7.1)$$

The result obtained from Eq. 7.1 means that each year there exits 12.5% loss potential due to a 500-year return period event in S. G. D. Puglia. It should be noted that the risk is calculated for exactly one occurrence of such an earthquake in one-year time. In general, there is a chance that this kind of event may occur more than once in a given year. However, it can be shown that the probability of such occurrence is very small when compared to the occurrence of one event. In this case, it does not affect the calculations, but for events with shorter return periods and longer time intervals, occurrence of more than one event should be considered in risk calculations.

7.5. Comparison of loss estimates with field data

At the time the field data was collected, no information about the repair cost of the buildings was available. Therefore, it was not possible to get an estimate of real loss amount due to building damage. To be able to compare analytical loss estimates, the regional loss is estimated according to damage survey results. To convert damage data into loss units, the conversion factors that were defined in Section 3.3 are used. Using these factors, the loss in each building is calculated. The summation over the building population yields 43% normalized loss. This value is about 30% lower than the analytical estimate. Uncertainty in estimating hazard level, differences in construction characteristics and material properties, and modeling errors in calculating hazard-loss relationships can be considered as the primary factors that contributed to the 30% deviation.

CHAPTER 8 SUMMARY AND CONCLUSIONS

8.1. Summary

The primary goal of this study was to develop a regional risk/loss assessment methodology that utilizes easily obtainable physical properties of unreinforced masonry buildings.

Research was focused towards old existing clay brick unreinforced masonry buildings that have material, configuration, and construction characteristics similar to the ones found in urban regions of the United States. In general, these buildings were constructed in the late 19th and in the early 20th century. Typically, these buildings contain wood floor construction that results in flexible diaphragm response. This flexible response increases demands on the walls that are oriented in the transverse direction to the shaking. Even though focus was concentrated on unreinforced masonry buildings the approach is general and can be applied to develop similar risk/loss assessment methodologies for other construction types.

Within the scope of this study, a comprehensive sensitivity investigation was conducted on building as well as region specific parameters. The main objective of these investigations was to identify the most significant factors for risk/loss estimations and hence reduce number of essential parameters that is required by the proposed risk/loss assessment methodology. The factors that were investigated for buildings included: (1) number of stories, (2) floor aspect ratio, (3) wall area, (4) story height, (5) floor area, (6) length of window/door openings, (7) average pier height over a story, (8) floor mass, (9) elastic modulus of masonry, and (10) diaphragm flexibility. Region specific factors included (1) variation of ground motion characteristics and (2) size of the building population.

To conduct these sensitivity investigations, a simple analytical model representing dynamic characteristics of unreinforced masonry building was developed. Closed form equations for calculating model parameters were derived so that buildings can be easily generated for parametric investigations. A procedure that utilizes response estimates from analytical calculations was provided to evaluate damage for in-plane and for out-of-plane actions.

Parameter distributions for global and local properties of unreinforced masonry buildings at urban regions of the United States were defined. These distributions were utilized to generate building populations on which the sensitivity investigations were conducted.

In sensitivity analyses, hazard level was represented by the magnitude of spectral acceleration at the fundamental period of buildings. A suite of ground motions was used to represent variations in ground shaking characteristics. These ground motions were selected from various combinations of PGA/PGV, distance, magnitude, and soil properties. Sensitivity of loss estimates for a different set of ground motions was also investigated.

The proposed methodology was demonstrated on a small town in Italy that was recently shaken by two moderate size earthquakes. From data collection to utilization of generated hazard-loss relationships, the steps of the methodology were demonstrated from the perspective a stakeholder. Estimated regional losses were compared with data that was collected from field investigations.

8.2. Conclusions

Total risk/loss concept was the thrusting idea in developing a simple regional risk/loss assessment methodology. Analytical derivations showed that as a result of this concept, hazard-loss relationships that are unacceptably scattered for individual building loss calculations can be utilized to estimate regional losses. This statement was proved to be valid especially for building populations that possess low-level correlation in terms of their dynamic response characteristics.

Sensitivity investigations on building and regional parameters have shown that as long as a building population has (1) similar distributions as the representative building population for urban regions, (2) more than 25 buildings, and (3) uniform spatial distribution over different ground motion categories (represented by PGA/PGV), a single hazard-loss relationship is enough to estimate regional losses. For a population size of 25 buildings, the maximum analytical scatter was calculated as 10%.

Among regional factors, variation of ground motion characteristics showed moderate significance on loss estimates. Maximum deviation from unbiased curve was observed for

high PGA/PGV category and it was about 13%. As ground motion properties shifted toward low PGA/PGV category, vulnerability of building populations reduced, resulting in lower loss estimates. This observation agreed well with expectations as short period unreinforced masonry buildings are more sensitive to ground shakings that contain more energy on higher frequencies.

Comparison of hazard-loss relationships that were developed for a different set of ground motions has shown less than 3.0% difference. The only constraint that was followed in selecting the alternative ground motion set was to have similar PGA/PGV distribution with the initial set. From this observation it can be stated that PGA/PGV is an effective index in selecting ground motion sets with comparatively balanced properties for regional loss calculations.

Hazard-loss relationships showed less than 10% variation for different damping levels. In developing these curves, ground motions were scaled from elastic response spectra that had the same damping level as the curves. This claims that, with 10% tolerance, hazard-loss relationship that is developed for a specific damping level can be used to estimate regional loss for a building population with different damping characteristics provided that hazard level is defined from an elastic response spectrum that has the same damping level as the building population.

First order sensitivity analyses have revealed that regional loss estimates are less sensitive to length of window/door openings, seismic mass, effective shear modulus of diaphragms, and pier height. Hazard-loss curves associated with these parameters showed less than 10% variation from unbiased hazard-loss curve.

Second order analyses on remaining 6 parameters and one region specific factor, ground motion category, have shown that number of stories, floor aspect ratio, wall density, and ground motion categories are the most significant parameters in regional loss estimates.

With accepting 10% standard error, it was possible to categorize 2187 different hazard-loss relationship into 10 groups. The group that has the worst vulnerability contains buildings with large number of stories, high aspect ratio, low wall area, high story height, and large

floor area. Furthermore, these buildings are subject to ground motions that have high PGA/PGV. The group that has the least vulnerability contains buildings with single story, square floor shape, high wall area, low story height, and small floor area. In general, buildings in this group are subjected to ground motions that have medium to low PGA/PGV. These observations confirm well with expected variations in vulnerability due to the factors listed above.

Comparison of loss estimates with the damage data that was collected from S. G. D. Puglia showed 30% deviation from the analytical estimate. This difference can be attributable to uncertainty in estimated hazard level, differences in construction characteristics and material properties, and modeling errors in utilized hazard-loss relationships. This observation implies that even though uncertainty associated with analytical calculations can be low, this does not necessarily mean that analytical results will have good match with actual values.

The suggested analytical idealization and damage categorization procedure was used to evaluate a two-story building. Estimated dynamic response as well as damage state of the building showed good correlation with test measurements. Both frequency content and general trend of response estimates were in good agreement with their measured counterparts. Calculated peak values for accelerations were consistently higher, about 30%, than measured ones. However, estimated relative response between floor and wall components showed good match with the measured ones. Based on these observations and with considering the level of simplifications, it can be stated that analytical idealization and damage categorization procedure can capture essential dynamic features of unreinforced masonry buildings.

8.3. Recommendations for future research

Comparison of loss estimates with collected data has shown the significant importance of validating analytical relationships before utilizing them in real life situations. This observation brings up the essential need for collection of complete damage data from real events. In data collection process, together with building damage states, building parameters that are found to be significant for loss estimates have to be collected. Only with such complete data sets, proper verification of analytical estimates can be done. A sample survey

form that can be utilized to collect post-earthquake damage and inventory data of unreinforced masonry building is suggested in Appendix C.

In order to evaluate different mitigation strategies, hazard-loss relationship that are similar to ones developed for unreinforced masonry buildings need to be developed for various rehabilitation schemes.

Investigating types of building failures has shown that unreinforced masonry buildings are as vulnerable to out-of-plane actions as they are for in-plane actions. In this study, a simple damage evaluation procedure for out-of-plane actions was developed. However, due to limited scope of the study, a detailed verification of the suggested procedure couldn't be performed. Based on the significance of such failure modes in loss estimates, more elaborate investigations need to be carried out to verify and if necessary to improve the suggested procedure for stability evaluation of walls in their transverse directions.

In analyses, the effects of vertical accelerations and soil-structure interaction are not considered. Both factors have the potential for altering capacity as well as response characteristics of buildings. Further investigations addressing those factors need to be conducted to improve the accuracy of analytical loss/risk estimations.

For practical applications, non-contact, remote, data collection tools and methods have to be developed to ease the effort associated with this step. Among evolving methods, ones based on aerial measurements seem to be the most applicable and promising for regional risk/loss assessment calculations.

REFERENCES

1. Abrams, D. P., A. S. Elnashai, J. E. Beavers, "A New Engineering Paradigm: Consequence Based Engineering," Submitted for publication in Earthquake Spectra, 2002.

2. Abrams, D. P., "Performance Based Engineering Concepts for Unreinforced Masonry Building Structures," Journal of Progress in Structural Engineering, Vol. 3, No. 1, pp. 48-56, 2001.

3. Abrams, D. P., "A set of Classnotes for a Course in: Masonry Structures," The Masonry Society, Boulder, CO, 2000.

4. Abrams, D. P., M. Shinozuka, "Loss Assessment of Memphis Buildings," National Center for Earthquake Engineering Research, NCEER, Technical Report 97-0018, Buffalo, NY, 1997.

5. Abrams, D. P., N. Shah, "Cyclic Load Testing of Unreinforced Masonry Walls," Advanced Construction Technology Center, Document No. 92-26-10, University of Illinois at Urbana-Champaign, Urbana, IL, 1992.

6. Ang, A. H-S., W. H. Tang, "Probability Concepts in Engineering Planning and Design: Volume II – Decision, Risk, and Reliability," John Wiley & Sons Inc., New York, 1990.

7. Ang, A. H-S., W. H. Tang, "Probability Concepts in Engineering Planning and Design: Volume I – Basic Principles," John Wiley & Sons Inc., New York, 1975.

8. ATC-13, "Earthquake Damage Evaluation Data for California," Applied Technology Council, Report No. ATC-13, 1985.

9. ATC-21, "Rapid Visual Screening of Buildings for Potential Seismic Hazard: A Handbook," Applied Technology Council Report No. ATC-21, 1988.

10. ATC-38, "Development of a Database on the Performance of Structures Near Strong-Motion Recording Sites: 1994 Northridge, California, Earthquake," Applied Technology Council, Report No. ATC-38, 2001.

11. Aydin, K., C. C. Tung, "Energy Balance Equation for Estimating Overturning Potential of an Unanchored Rocking Body Subjected to Earthquake Excitation," Earthquake Spectra, Vol. 17, No. 2, pp. 209-220, 2001.

12. Baker, I. O., "A Treatise on Masonry Construction," John Wiley & Sons Inc., New York, 1909.

13. Bazzurro, P., C. A. Cornell, "Seismic Hazard Analysis of Nonlinear Structures. I: Methodology," Journal of Structural Engineering, Vol. 120, No. 11, 1994, pp. 3320-3344.

14. Brick Industry Association, "Contemporary Bearing Wall Detailing," BIA Technical Notes on Brick Construction, Technical Note 24G, Reston, VA, 1987.

15. Bruneau, M., "Performance of Masonry Structures During the 1994 Northridge (Los Angeles) Earthquake," Canadian Journal of Civil Engineering, Vol. 22, pp. 378-402, 1995.

16. Bruneau, M., Lamontagne, M, "Damage from 20th Century Earthquakes in Eastern Canada and Seismic Vulnerability of Unreinforced Masonry Buildings," Canadian Journal of Civil Engineering, Vol. 21, pp. 643-662, 1994.

17. Bruneau, M., "State-of-the-art Report on Seismic Performance of Unreinforced Masonry Buildings," Journal of Structural Engineering, ASCE, Vol. 120, No. 1, pp. 230-251, 1994.

18. Calvi, G. M., "A Displacement-based Approach for Vulnerability Evaluation of Classes of Buildings," Journal of Earthquake Engineering, Vol. 3, No. 3, 1999, pp. 411-438.

19. Cornell, C. A., F. Jalayer, R. O. Hamburger, D. A. Foutch, "Probabilistic Basis for 2000 SAC Federal Emergency Management Agency Steel Moment Frame Guidelines," Journal of Structural Engineering, Vol. 128, No. 4, 2002, pp. 526-533.

20. Costley, A. C., Abrams, D. P., "Dynamic Response of Unreinforced Masonry Buildings with Flexible Diaphragms," National Center for Earthquake Engineering Research, NCEER, Technical Report 96-0001, Buffalo, NY, 1996.

21. Doherty, K., M. C. Griffith, N. Lam, J. Wilson, "Displacement-based Seismic Analysis for Out-of-plane Bending of Unreinforced Masonry Walls," Earthquake Engineering and Structural Dynamics, Vol. 31, pp. 833-850, 2002.

22. Drysdale, R. G., A. A. Hamid, L. R. Baker, "Masonry Structures," Prentice Hall, Englewood Cliffs, NJ, 1994.

23. Dumova-Jovanoska, E., "Fragility Curves for Reinforced Concrete Structures in Skopje (Macedonia) Region," Soil Dynamics and Earthquake Engineering, Vol. 19, 2000, pp. 455-466.

24. Dymiotis, C., A. J. Kappos, M. K. Chryssanthopoulos, "Seismic Reliability of RC Frames with Uncertain Drift and Member Capacity," Journal of Structural Engineering, Vol. 125, No. 9, 1999, pp. 1038-1047.

25. Dymiotis, C., A. J. Kappos, M. K. Chryssanthopoulos, "Seismic Reliability of Masonry-Infilled RC Frames," Journal of Structural Engineering, Vol. 127, No. 3, 2001, pp. 296-305.

26. Eguchi, R. T., S. E. Chang, "Losses Associated with Building Damage in Memphis," Proceedings of the 11th World Conference on Earthquake Engineering, Acapulco, Mexico, 1996.

27. EMS-98, "European Macroseismic Scale," European Seismological Commission, Luxemburg, 1998.

28. Eperson G. S., D. P. Abrams, "Nondestructive Evaluation of Masonry Buildings," Advanced Technology Research Center, Document No. 89-26-03, University of Illinois at Urbana-Champaign, Urbana, IL, 1989.

29. Erbay, O. O., D. P. Abrams, "Seismic Rehabilitation of Unreinforced Masonry Shear Walls," Proceedings of the 7th National Conference on Earthquake Engineering, Boston, MA, 2002.

30. FEMA-356, "Prestandard and Commentary for the Seismic Rehabilitation of Buildings," Federal Emergency Management Agency, Washington, D.C., 2000.

31. FEMA-306, "Evaluation of Earthquake Damaged Concrete and Masonry Wall Buildings: Basic Procedures Manual," Federal Emergency Management Agency, Washington, D. C., 1999.

32. FEMA-307, "Evaluation of Earthquake Damaged Concrete and Masonry Wall Buildings: Technical Resources," Federal Emergency Management Agency, Washington, D. C., 1999.

33. Fischer, T., M. Alvarez, J. C. De la Llera, R. Riddell, "An integrated Model for Earthquake Risk Assessment of Buildings," Engineering Structures, Vol. 24, 2002, pp. 979-998.

34. Franklin, S., J. Lynch, and D. P. Abrams, "Performance of Rehabilitated URM Shear Walls: Flexural Behavior of Piers," ST-6 Project Final Report, Mid-America Earthquake Center Publications, University of Illinois at Urbana-Champaign, Urbana, IL, 2001.

35. Gülkan, P., M. A. Sözen, "Procedure for Determining Seismic Vulnerability of Building Structures," ACI Structural Journal, Vol. 96, No. 3, 1999, pp. 336-342.

36. Gülkan, P., H. Sucuoğlu, O. Ergünay, "Earthquake Vulnerability Loss and Risk Assessment in Turkey," Proceedings of the 10th World Conference in Earthquake Engineering, Balkema, Rotterdam, 1992, pp. 539-543.

37. Hassan, A. F., M. A. Sözen, "Seismic Vulnerability Assessment of Low-Rise Buildings in Regions with Infrequent Earthquakes," ACI Structural Journal, Vol. 94, No. 1, 1997, pp. 31-39.

38. HAZUS, "Earthquake Loss Estimation Methodology," Federal Emergency Management Agency, FEMA, Washington D.C., 1999.

39. Holmes, W. T., B. Lizundia, W. Dong, S. Brinkman, "Seismic Retrofitting Alternatives for San Francisco's Unreinforced Masonry Buildings: Estimates of Construction Cost & Seismic Damage," Rutherford & Chekene Consulting Engineers, San Francisco, CA, 1990.

40. Holmes, W. T., "Seismic Evaluation of Existing Buildings: State of the Practice," Proceedings of the 11th World Conference on Earthquake Engineering, Acapulco, Mexico, 1996.

41. Holmes, W. T., "Risk Assessment and Retrofit of Existing Buildings," Proceedings of the 12th World Conference on Earthquake Engineering, Auckland, New Zealand, 2000.

42. Hudson, R. G., "The Engineer's Manual," John Wiley & Sons Inc., New York, 1945.

43. Hwang, H. H. M, J. W. Jaw, "Probabilistic Damage Analysis of Structures," Journal of Structural Engineering, Vol. 116, No. 7, 1990, pp. 1992-2007.

44. Hwang, H., Y. W. Lin, "Seismic Loss Assessment of Memphis City School Buildings," Proceedings of the 7th National Conference on Earthquake Engineering, Boston, MA, 2002.

45. Kishi, N. G., A. Yakut, J. S. Byeon, "Advanced Component Method (ACM) – An Objective Methodology for the Assessment of Building Vulnerability," Applied Insurance Research (AIR) Publication, Boston, MA, 2001

46. Kiremidjian, A. S., "Subjective Probabilities for Earthquake Damage and Loss," Structural Safety, Vol. 2, 1985, pp. 309-317.

47. Lang, K., H. Bachmann, "On the Seismic Vulnerability of Existing Unreinforced Masonry Buildings," To be published in the Journal of Earthquake Engineering.

48. Lavicka, W. L. (original text by anonymous authors), "Masonry, Carpentry, and Joinery: The Art of Architecture, Engineering, and Construction in 1899," Chicago Review Press, Chicago, IL, 1980.

49. Lizundia, B., W. T. Holmes, W. Dong, "Analysis of Unreinforced Masonry Building Damage Patterns in the Loma Prieta Earthquake and Improvement of Loss Estimation Methodologies: Technical Report to the USGS," Rutherford & Chekene Consulting Engineers, San Francisco, CA, 1993.

50. Mola E., Tsionis G., Pinto A., "The Molise (Italy) earthquakes of 31 October and 1 November 2002: Report and analysis from a field mission," European Laboratory for Structural Assessment, ELSA, Italy, 2003.

51. Moon, F. L., T. Yi, R. Leon, L. Kahn, "Large-scale Tests of an Unreinforced Masonry Low-rise Building," Proceedings of the 9th North American Masonry Conference, Clemson, SC, 2003.

52. Mwafy, A. M., A. S. Elnashai, "Static Push Over Versus Dynamic Collapse Analyses of RC Buildings", Engineering Structures, Vol 23, 2001, pp. 407-424

53. Orton, S. L., D. P. Abrams, and J. R. Hayes, "Performance of Rehabilitated Unreinforced Masonry Building Systems," Proceedings of the 9th Canadian Masonry Conference, Fredericton, New Brunswick, Canada, 1999.

54. Paulay, T., M. J. N. Priestley, "Seismic Design of Reinforced Concrete and Masonry Buildings," John Wiley & Sons, New York, 1992.

55. Pellissier, V., P. A. Jaccard, M. Badoux, "Decision Framework for Seismic Risk Management," Proceedings of the 12th European Conference on Earthquake Engineering, London, Britain, 2002.

56. Peralta D. F., J. M. Bracci, M. B. D. Hueste, "Seismic Performance of Rehabilitated Floor and Roof Diaphragms," ST-8 Project Final Report, Mid-America Earthquake Center Publications, Texas A&M University, TX, 2002.

57. Prakash, V., G. H. Powell, S. D. Campbell, "DRAIN-2DX base program description and user guide: version 1.10," UCB/SEMM-1993/17, Dept. of Civil Engineering, University of California, Berkeley, 1993.

58. Şimşir, C. C., M. A. Aschheim, D. P. Abrams, "Response of Unreinforced Masonry Bearing Walls Situated Normal to the Direction of Seismic Input Motions," Proceedings of the 7th National Conference on Earthquake Engineering, Boston, MA, 2002.

59. Singhal, A., A. S. Kiremidjian, "Method for Probabilistic Evaluation of Seismic Structural Damage," Journal of Structural Engineering, Vol. 122, No. 12, 1996, pp. 1459-1467.

60. SSN, Servico Sismico Nazionale, http://www.serviziosismico.it/, 2003.

61. Stehle, J., T. Jones, J. Schneider, D. Stewart, N. Corby, "Earthquake Vulnerability and Risk for Newcastle, Australia," Proceedings of the 7th National Conference on Earthquake Engineering, Boston, MA, 2002.

62. Tena-Colunga, A., D. P. Abrams, "Response of an Unreinforced Masonry Building During the Loma Prieta Earthquake," Structural Research Series, Report No. 576, University of Illinois at Urbana-Champaign, Urbana, IL, 1992.

63. Windeler, D. S., J. Bouabid, A. A. Nassar, "Seismic Risk Assessment for Residential and Commercial Buildings in San Francisco," Building to Last: Proceedings of Structures Congress XV, Portland, Oregon, 1997, pp. 1433-1437.

64. Wu, Y., I. Crelling, R. B. Olshansky, "Mitigation Action Plans,", SE-9 Project Data, Mid-America Earthquake Center, University of Illinois at Urbana-Champaign, Urbana, IL, 2001.

65. Wu, Y., "Seismic Risk Assessment for Typical Communities in Mid-America," Ph.D. Dissertation, University of Illinois at Urbana-Champaign, 2001.

66. Wyss, G. D., K. H. Jorgensen, "A User's Guide to LHS: Sandia's Latin Hypercube Sampling Software," Sandia National Laboratories, Risk Assessment and Systems Modeling Department, Report No. SAND98-0210, Albuquerque, NM, 1998.

67. Yi, T., F. Moon, R. Leon, L. Kahn, "Performance Characteristics of Unreinforced Masonry Low-rise Structure Before and After Rehabilitation," Proceedings of the 7th National Conference on Earthquake Engineering, Boston, MA, 2002.

68. Yi, T., F. Moon, R. Leon, L. Kahn, "Structural Analysis of a Prototype Unreinforced Masonry Low-rise Building," Proceedings of the 9th North American Masonry Conference, Clemson, SC, 2003.

69. Yun, S. Y., R. O. Hamburger, C. A. Cornell, D. A. Foutch, "Seismic Performance Evaluation for Steel Moment Frames," Journal of Structural Engineering, Vol. 128, No. 4, 2002, pp. 534-545.

APPENDIX A TIME HISTORIES AND ELASTIC RESPONSE SPECTRA FOR GROUND MOTIONS USED IN THE STUDY

A.1. San Fernando, US

Table A.1. Properties of the ground motion

Date:	February 09, 1971	Distance:	23km
Magnitude:	6.6	PGA:	0.130g
Soil Type:	A	PGV:	3.9cm/s
Component:	291	PGA/PGV:	3.3g.s/m
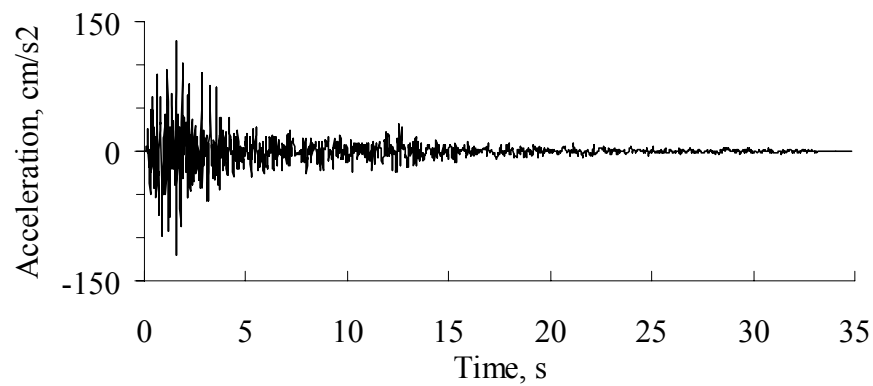
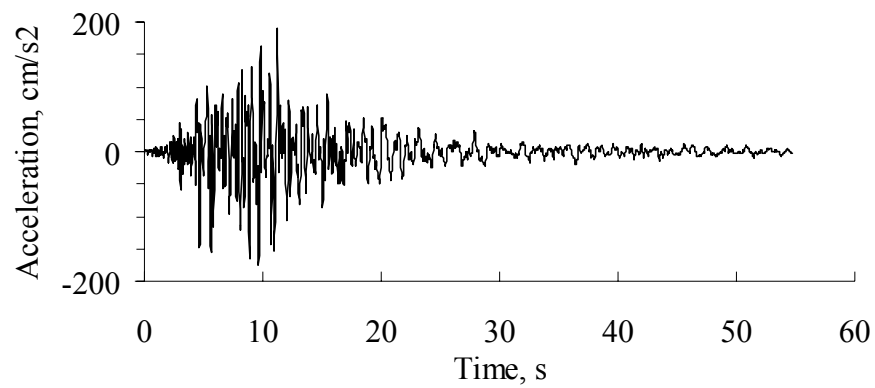Figure A.1. Acceleration time history of the original record
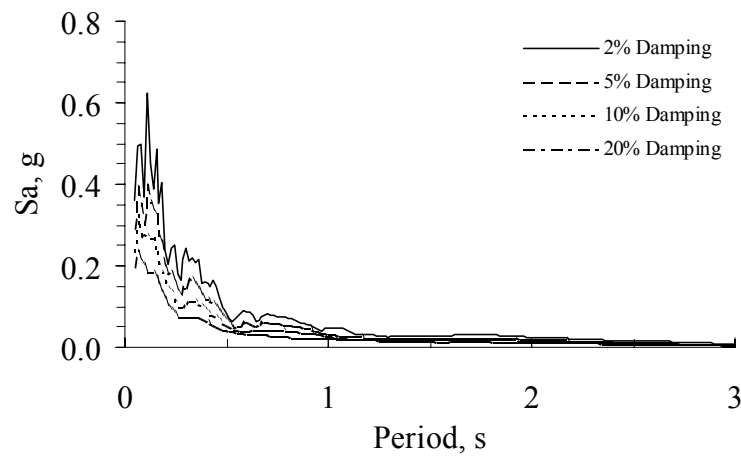
Figure A.2. Elastic response spectra

168

A.2. Kozani, Greece

Table A.2. Properties of the ground motion

Date:	May 13, 1995	Distance:	14km
Magnitude:	6.5	PGA:	0.140g
Soil Type:	A	PGV:	6.60cm/s
Component:	252	PGA/PGV:	2.12g.s/m
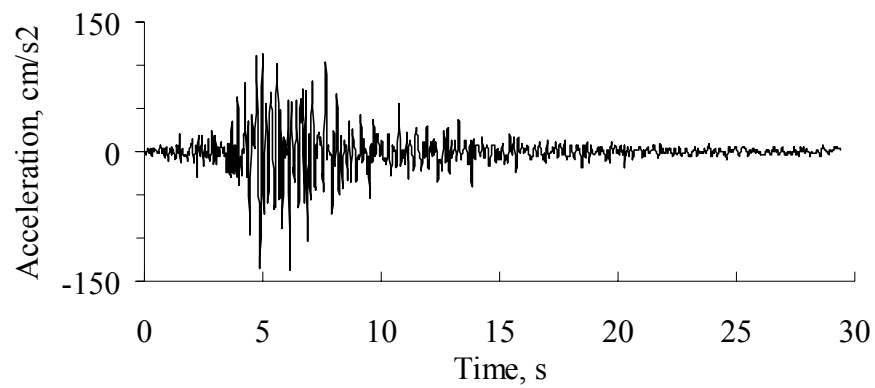
Figure A.3. Acceleration time history of the original record
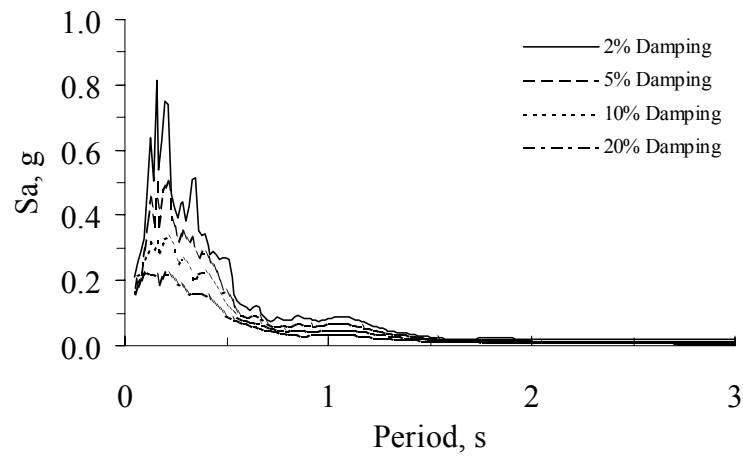
Figure A.4. Elastic response spectra

A.3. Northridge, US

Table A.3. Properties of the ground motion

|			
Date:	January 17, 1994	Distance:	44.2km
Magnitude:	6.7	PGA:	0.180g
Soil Type:	D	PGV:	9.4cm/s
Component:	206	PGA/PGV:	1.91g.s/m
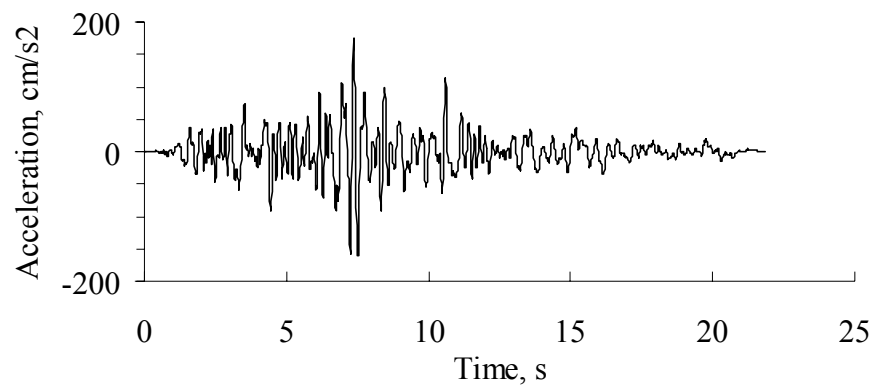
Figure A.5. Acceleration time history of the original record
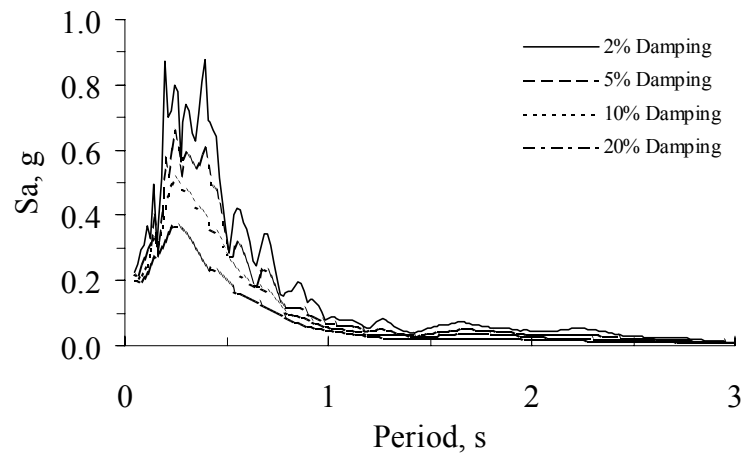
Figure A.6. Elastic response spectra

A.4. Kalamata, Greece

Table A.4. Properties of the ground motion

| Date:	October 13, 1997	Distance:	48km
Magnitude:	6.4	PGA:	0.121g
Soil Type:	A	PGV:	7.0cm/s
Component:	35	PGA/PGV:	1.73g.s/m
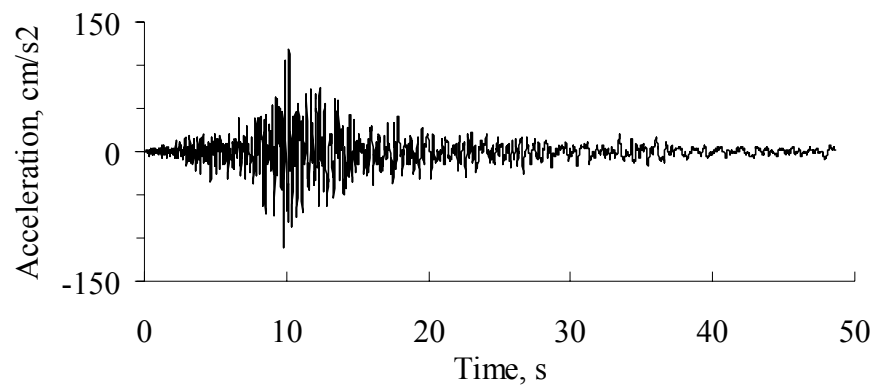
Figure A.7. Acceleration time history of the original record
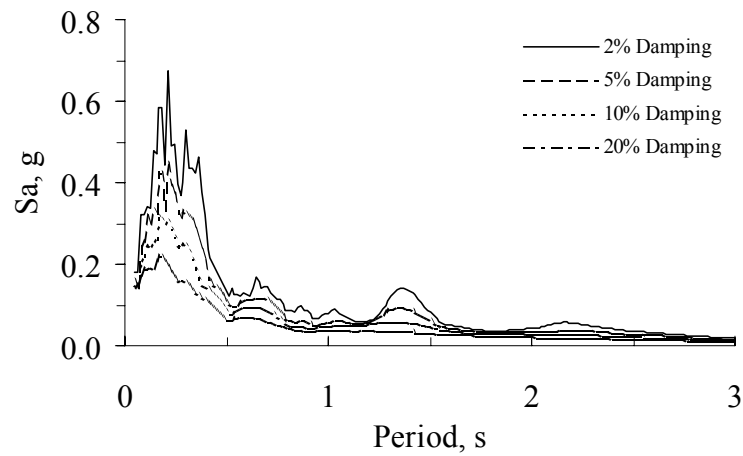
Figure A.8. Elastic response spectra

A.5. Imperial Valley, US

Table A.5. Properties of the ground motion

Date:	October 15, 1979	Distance:	20km
Magnitude:	6.5	PGA:	0.179g
Soil Type:	B	PGV:	11.6cm/s
Component:	147	PGA/PGV:	1.54g.s/m
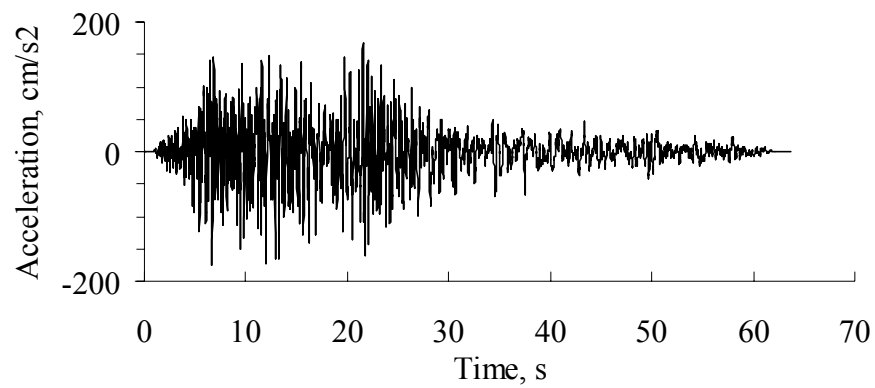
Figure A.9. Acceleration time history of the original record
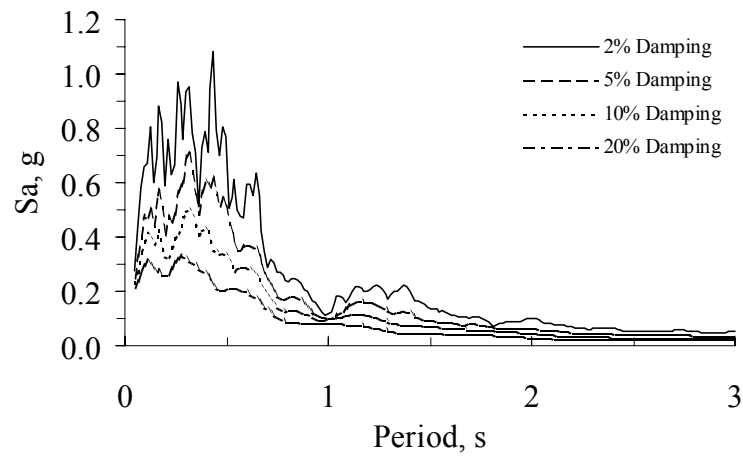
Figure A.10. Elastic response spectra

A.6. Whittier Narrows, US

Table A.6. Properties of the ground motion

|			
Date:	October 01, 1987	Distance:	48.4km
Magnitude:	6.1	PGA:	0.116g
Soil Type:	C	PGV:	8.1cm/s
Component:	N196	PGA/PGV:	1.44g.s/m
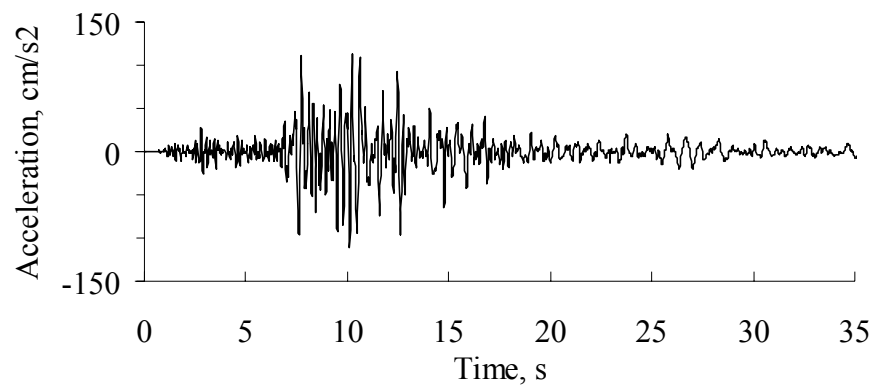
Figure A.11. Acceleration time history of the original record
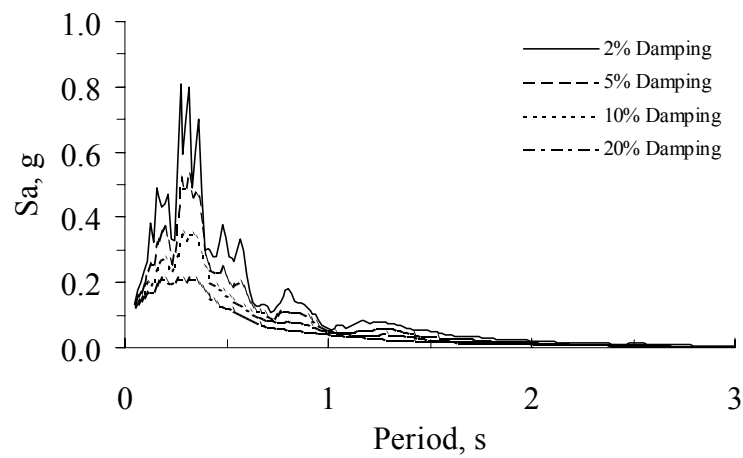
Figure A.12. Elastic response spectra

A.7. Ano Liosia, Greece

Table A.7. Properties of the ground motion

|			
Date:	September 07, 1999	Distance:	8km
Magnitude:	6.0	PGA:	0.120g
Soil Type:	C	PGV:	8.7cm/s
Component:	N70	PGA/PGV:	1.38g.s/m
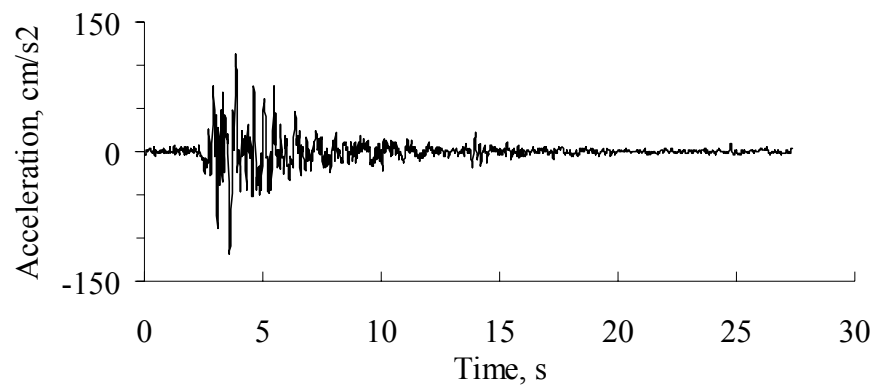
Figure A.13. Acceleration time history of the original record
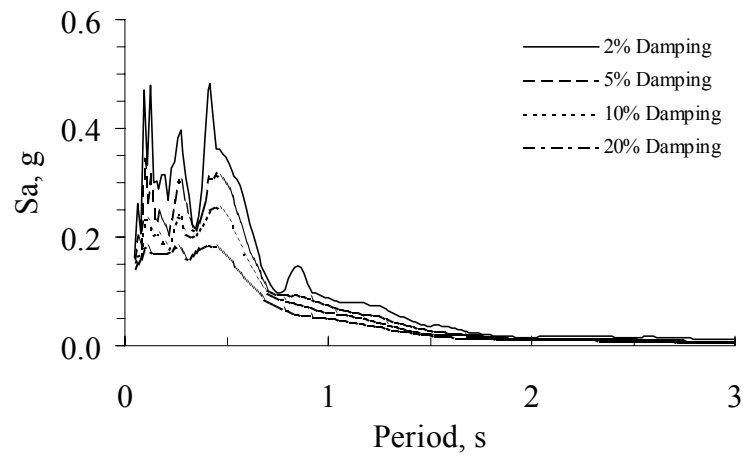
Figure A.14. Elastic response spectra

A.8. Loma Prieta, US

Table A.8. Properties of the ground motion

Date:	October 18, 1989	Distance:	2.8km
Magnitude:	7.0	PGA:	0.410g
Soil Type:	A	PGV:	31.6cm/s
Component:	0	PGA/PGV:	1.30g.s/m
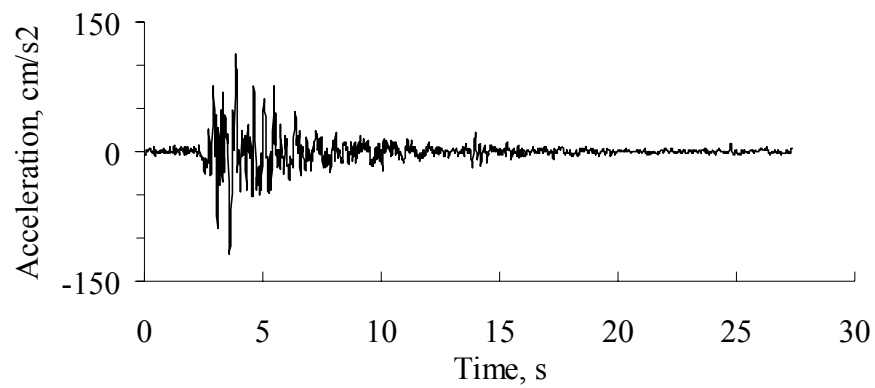
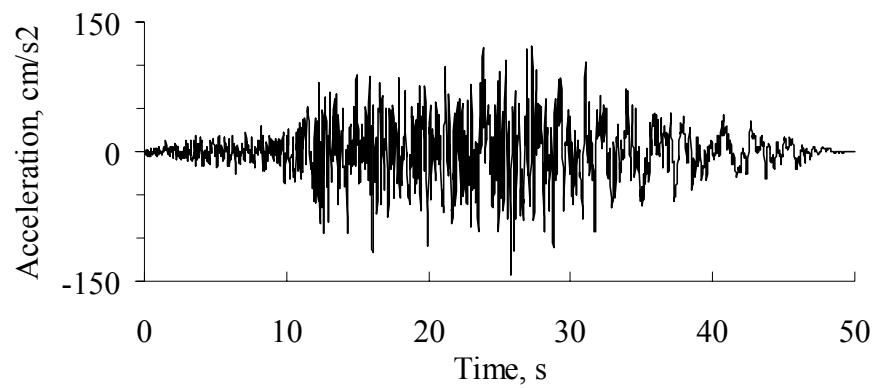Figure A.15. Acceleration time history of the original record
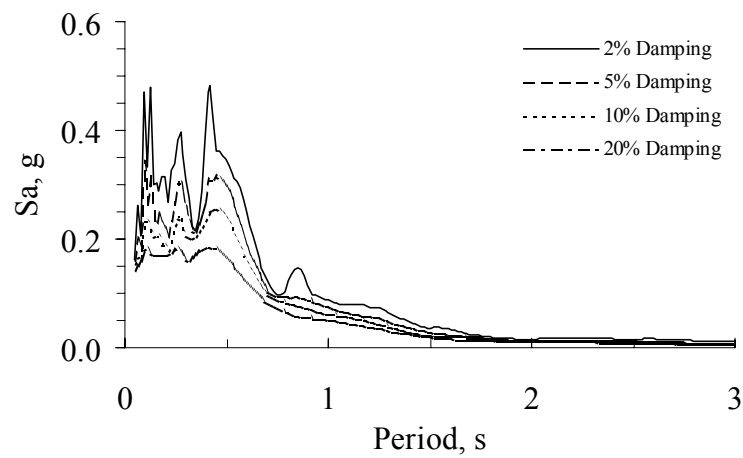
Figure A.16. Elastic response spectra

A.9. Coalinga, US

Table A.9. Properties of the ground motion

Date:	May 02, 1983	Distance:	63.5km
Magnitude:	6.5	PGA:	0.098g
Soil Type:	C	PGV:	8.6cm/s
Component:	0	PGA/PGV:	1.14g.s/m
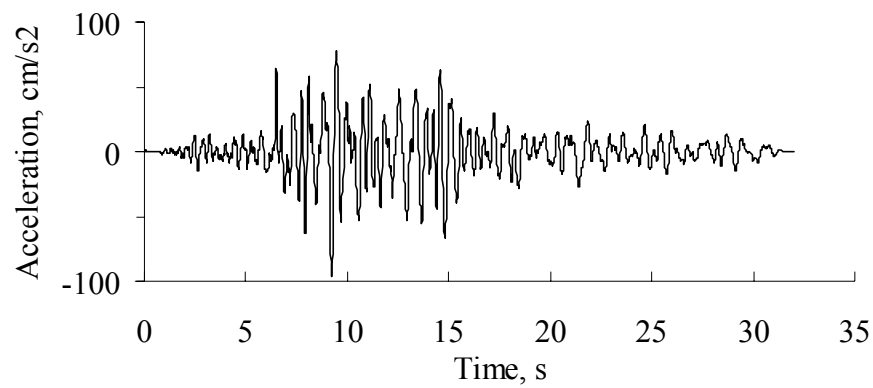
Figure A.17. Acceleration time history of the original record
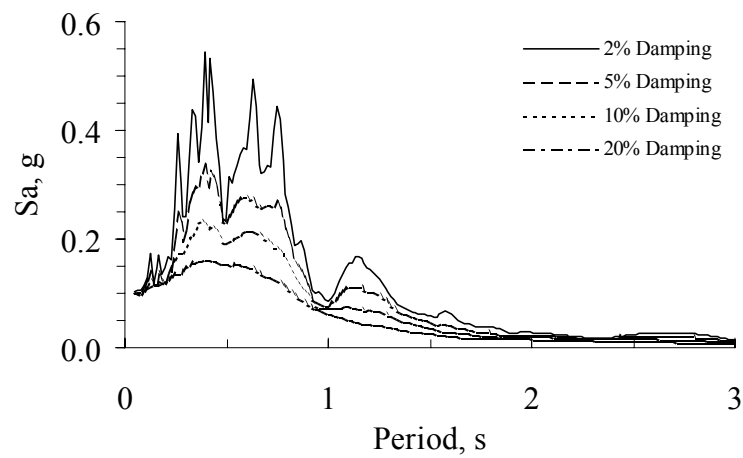
Figure A.18. Elastic response spectra

A.10. Northridge, US

Table A.10. Properties of the ground motion

|			
Date:	January 17, 1994	Distance:	26.4km
Magnitude:	6.7	PGA:	0.193g
Soil Type:	C	PGV:	20.4cm/s
Component:	N090	PGA/PGV:	0.95g.s/m

Figure A.19. Acceleration time history of the original record
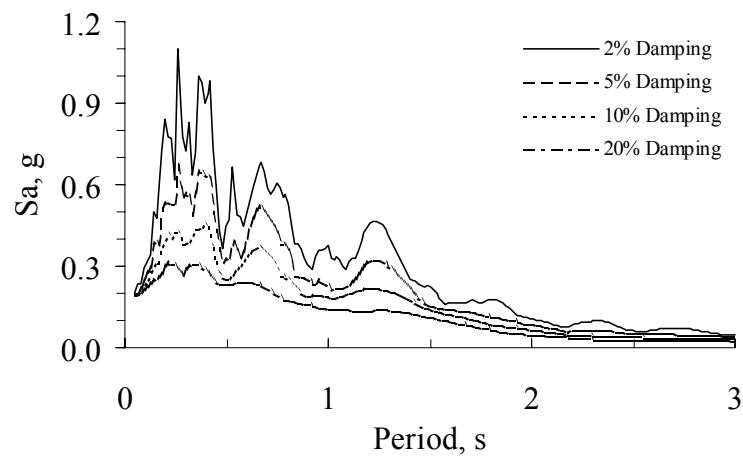
Figure A.20. Elastic response spectra

A.11. Superstition Hills, US

Table A.11. Properties of the ground motion

Date:	November 11, 1987	Distance:	27.1km
Magnitude:	6.6	PGA:	0.167g
Soil Type:	D	PGV:	18.3cm/s
Component:	315	PGA/PGV:	0.91g.s/m
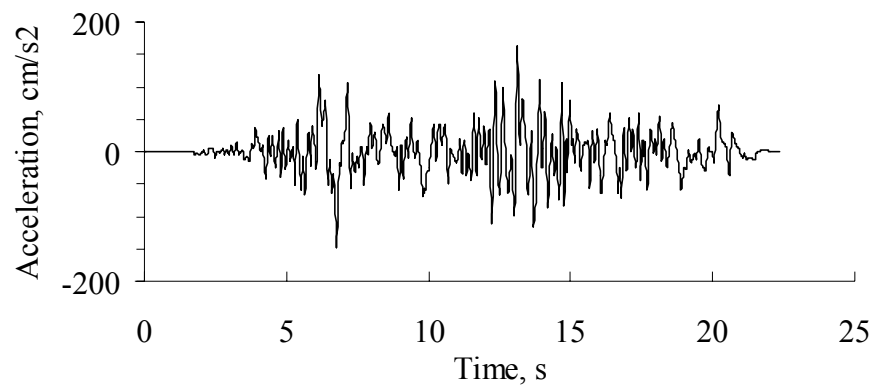
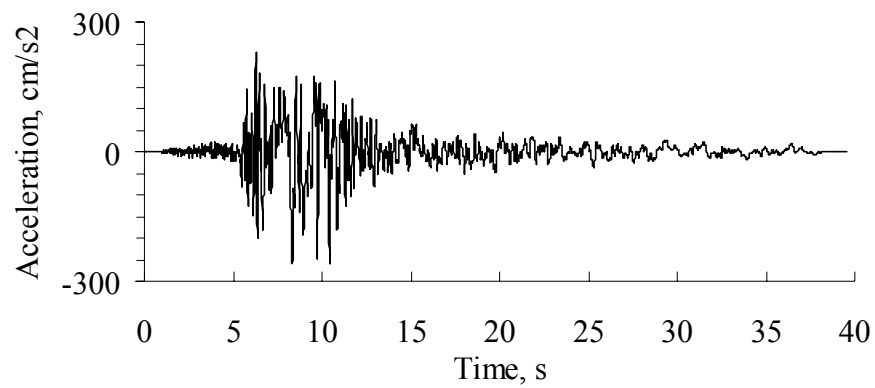Figure A.21. Acceleration time history of the original record
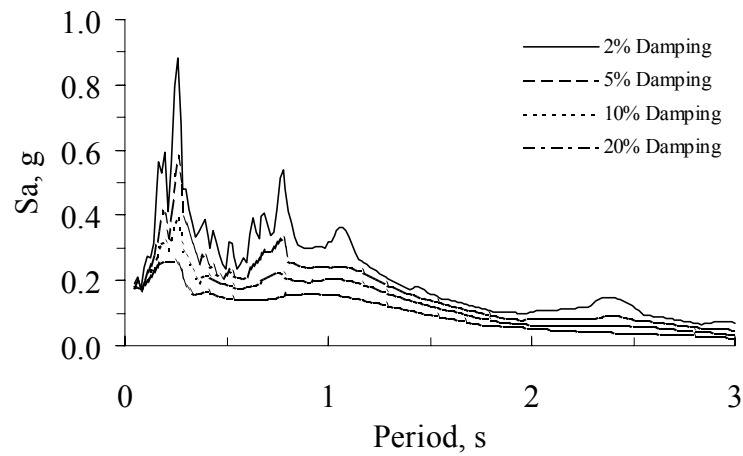
Figure A.22. Elastic response spectra

A.12. Spitak, Armenia

Table A.12. Properties of the ground motion

Date:	December 07, 1988	Distance:	20km
Magnitude:	6.7	PGA:	0.183g
Soil Type:	C	PGV:	20.7cm/s
Component:	EW	PGA/PGV:	0.88g.s/m
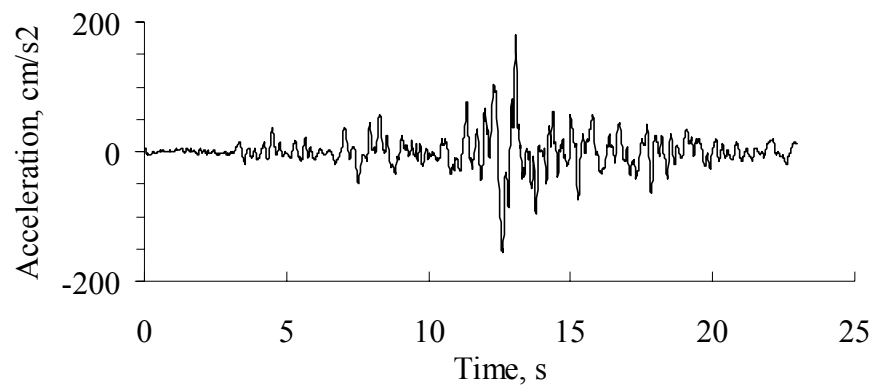
Figure A.23. Acceleration time history of the original record
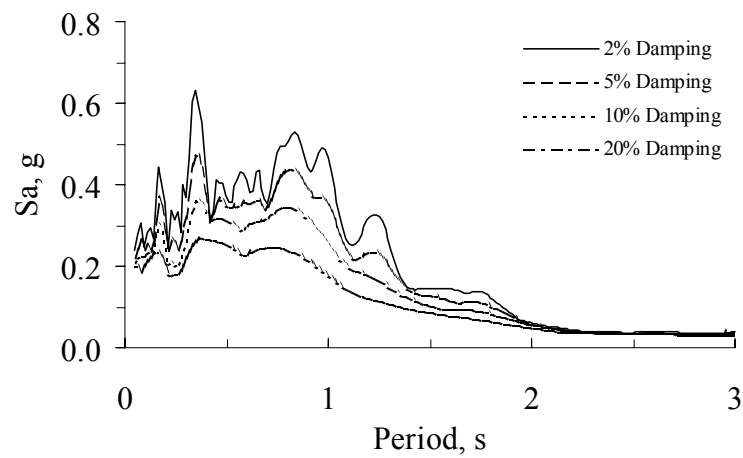
Figure A.24. Elastic response spectra

179

A.13. Loma Prieta, US

Table A.13. Properties of the ground motion

Date:	October 18, 1989	Distance:	34.3km
Magnitude:	7.0	PGA:	0.258g
Soil Type:	D	PGV:	31.8cm/s
Component:	0	PGA/PGV:	0.81g.s/m
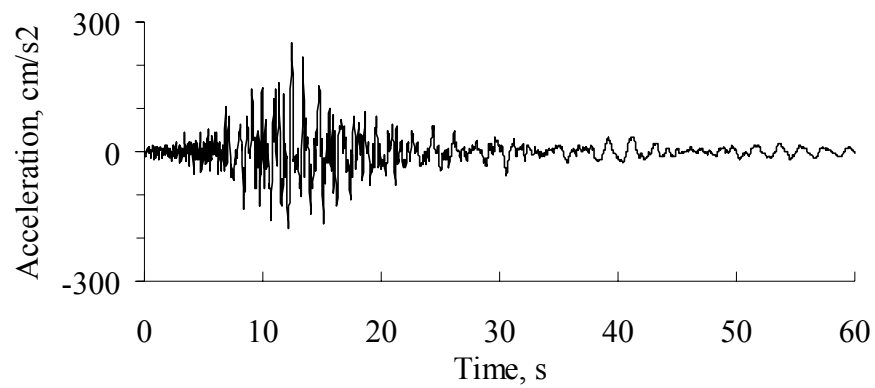
Figure A.25. Acceleration time history of the original record
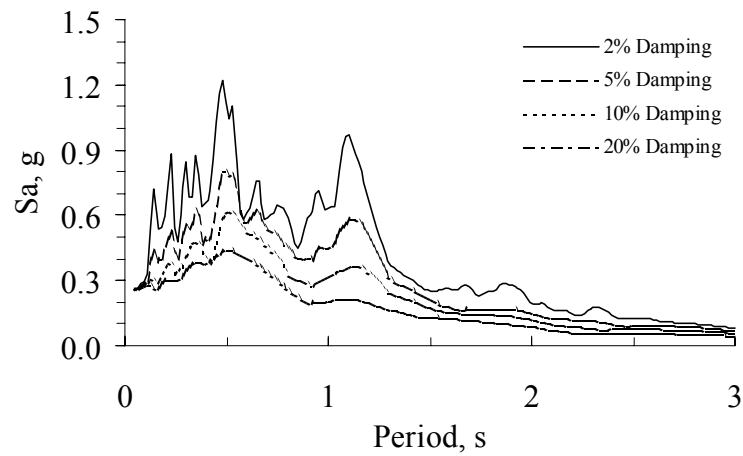
Figure A.26. Elastic response spectra

A.14. Dinar, Turkey

Table A.14. Properties of the ground motion

Date:	October 01, 1995	Distance:	1km
Magnitude:	6.4	PGA:	0.320g
Soil Type:	D	PGV:	40.8cm/s
Component:	EW	PGA/PGV:	0.78g.s/m
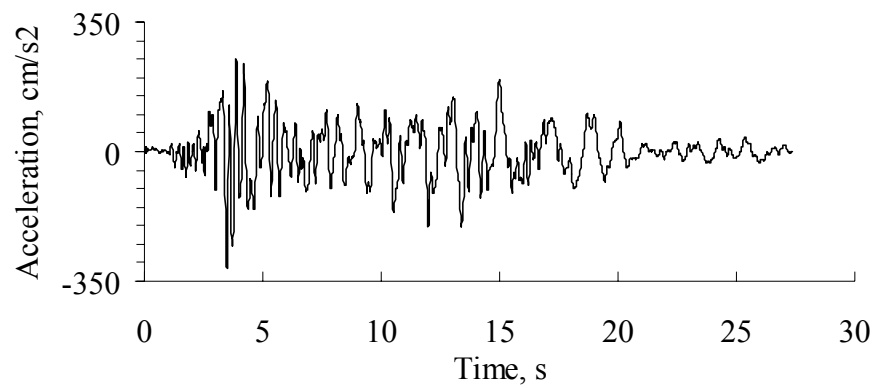
Figure A.27. Acceleration time history of the original record
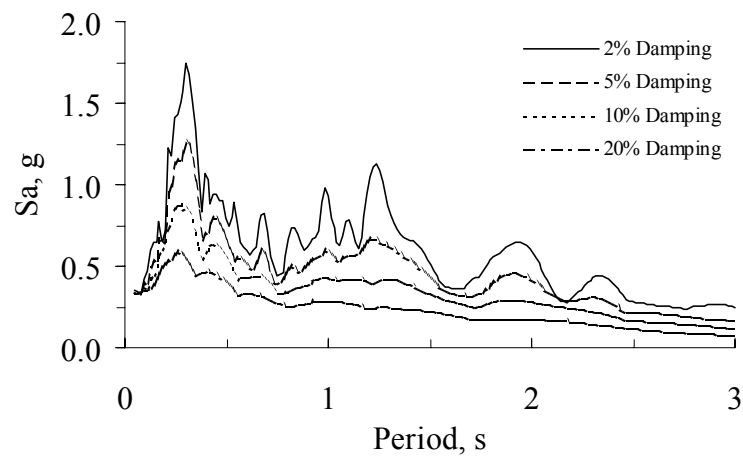
Figure A.28. Elastic response spectra

A.15. Landers, US

Table A.15. Properties of the ground motion

Date:	June 28, 1992	Distance:	73.2km
Magnitude:	7.3	PGA:	0.146g
Soil Type:	A	PGV:	20.0cm/s
Component:	90	PGA/PGV:	0.73g.s/m

Figure A.29. Acceleration time history of the original record
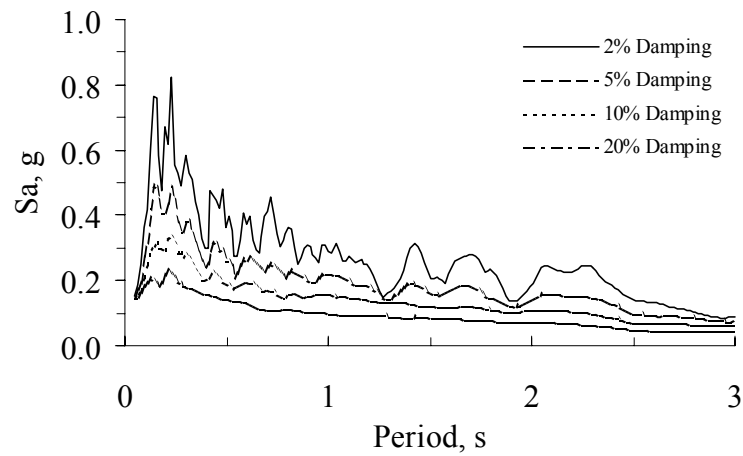
Figure A.30. Elastic response spectra

A.16. Manjil, Iran

Table A.16. Properties of the ground motion

Date:	June 20, 1990	Distance:	67km
Magnitude:	7.4	PGA:	0.132g
Soil Type:	D	PGV:	21.1cm/s
Component:	N57E	PGA/PGV:	0.62g.s/m
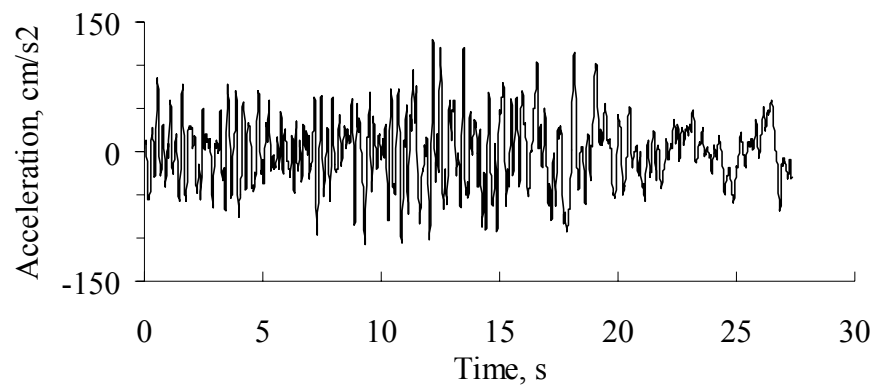
Figure A.31. Acceleration time history of the original record
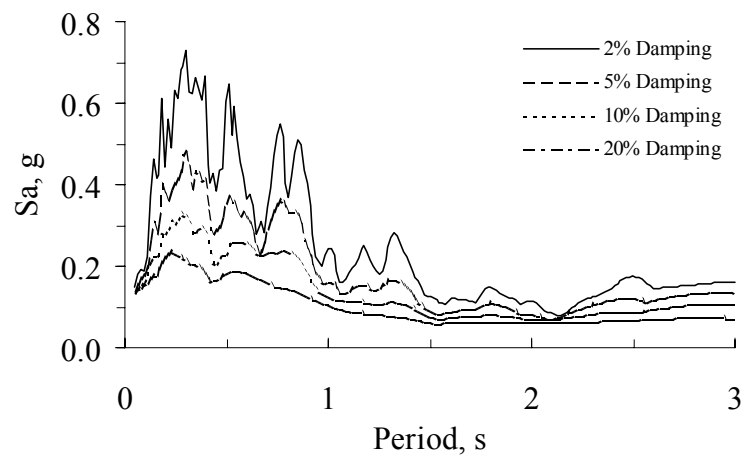
Figure A.32. Elastic response spectra

A.17. Imperial Valley, US

Table A.17. Properties of the ground motion

Date:	October 15, 1979	Distance:	13.8km
Magnitude:	6.5	PGA:	0.266g
Soil Type:	D	PGV:	46.8cm/s
Component:	N140	PGA/PGV:	0.57g.s/m

Figure A.33. Acceleration time history of the original record
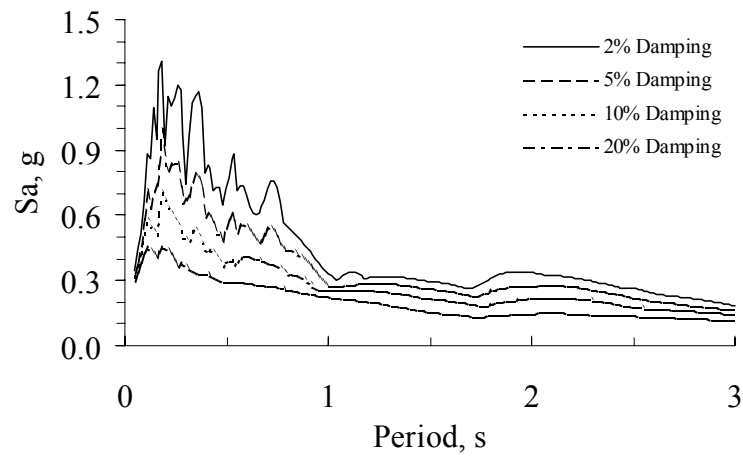
Figure A.34. Elastic response spectra

A.18. Imperial Valley, US

Table A.18. Properties of the ground motion

Date:	October 15, 1979	Distance:	6.6km
Magnitude:	6.5	PGA:	0.210g
Soil Type:	C	PGV:	37.5cm/s
Component:	2	PGA/PGV:	0.56g.s/m
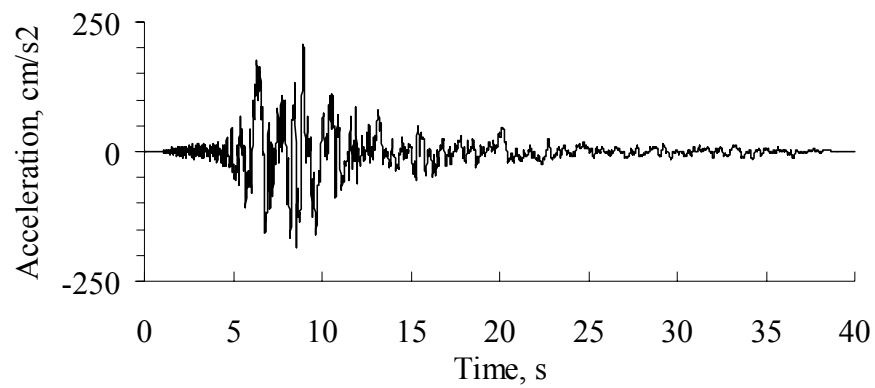
Figure A.35. Acceleration time history of the original record
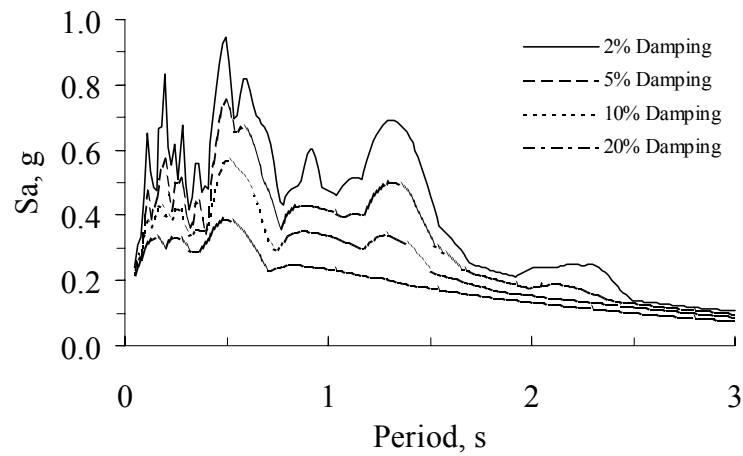
Figure A.36. Elastic response spectra

185

APPENDIX B COMBINATION OF PARAMETERS FOR EACH HAZARD-LOSS GROUP

B.1. Introduction

Second order sensitivity analysis resulted in 10 different hazard-loss groups. The parameter combinations that are associated with each group are provided in Figures B.2. through B.11. Bar charts are utilized to present the data. In these charts, each parameter combination is expressed by a row of seven rectangles where each rectangle represents a parameter. The parameter intervals are defined through three different colors. Light gray, darker gray, and black represents range 1, range 2, and range 3, respectively. The data is sorted sequentially with respect to each parameter. The parameters that are determined to have more significance are ordered first.

Figure B.1. demonstrates the usage of the charts. In this figure, lets assume the dashed rectangle represents one possible combination in a given group. According to the color variation of each rectangle the parameter intervals that are associated with that combination can be identified. For instance, the combination in the figure reads 1-3-3-2-1-3-1. In physical terms these numbers correspond to, with reference to Table 5., high PGA/PGV value, large number of stories (4-5-6), high floor aspect ratio (2.75-3.5), medium wall area (62-78%), low story height (9-12.5ft), high elastic modulus (990-1200ksi), and small floor area (1000-2300ft^2)
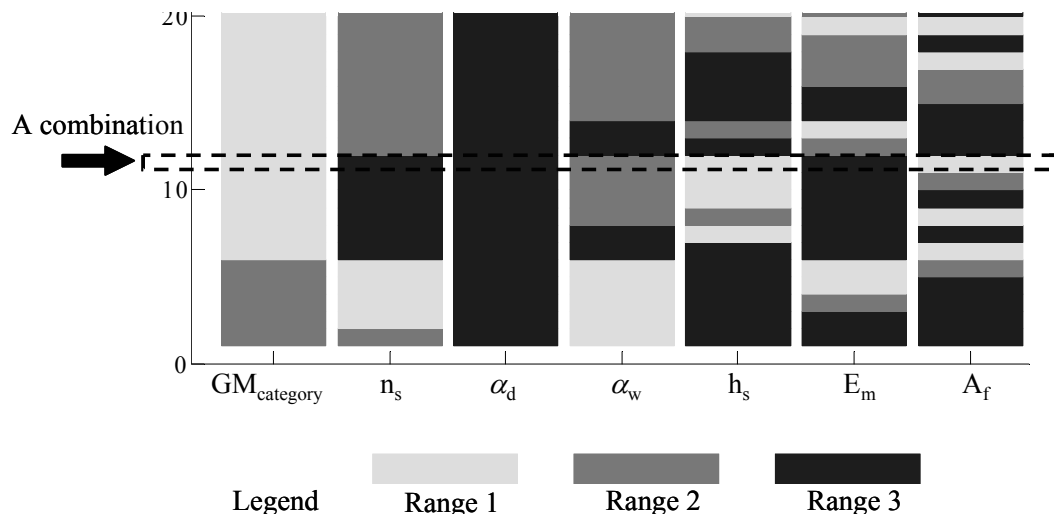
Figure B.1. How to use the charts?

186
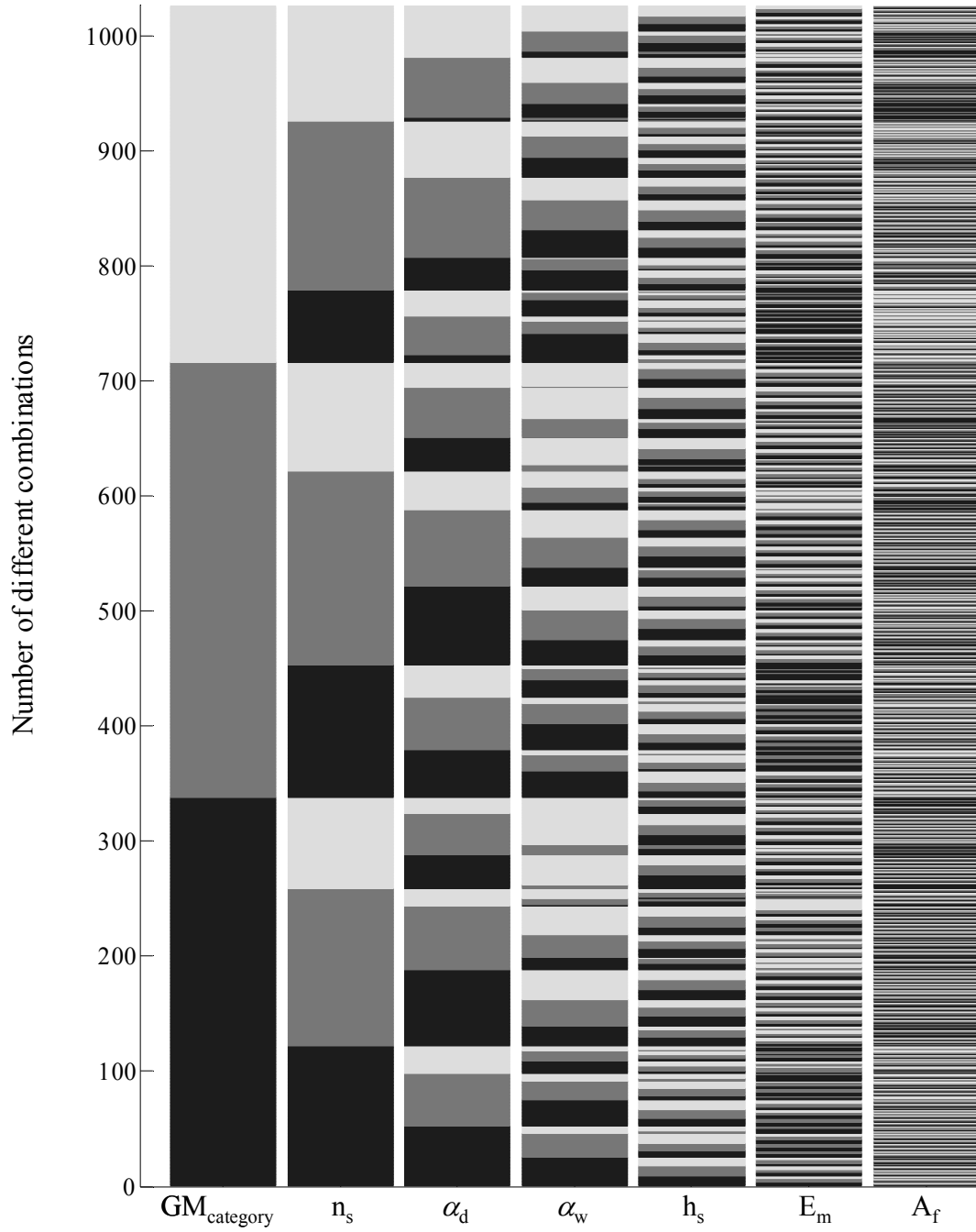
Figure B.2. Combination of parameters in group 1
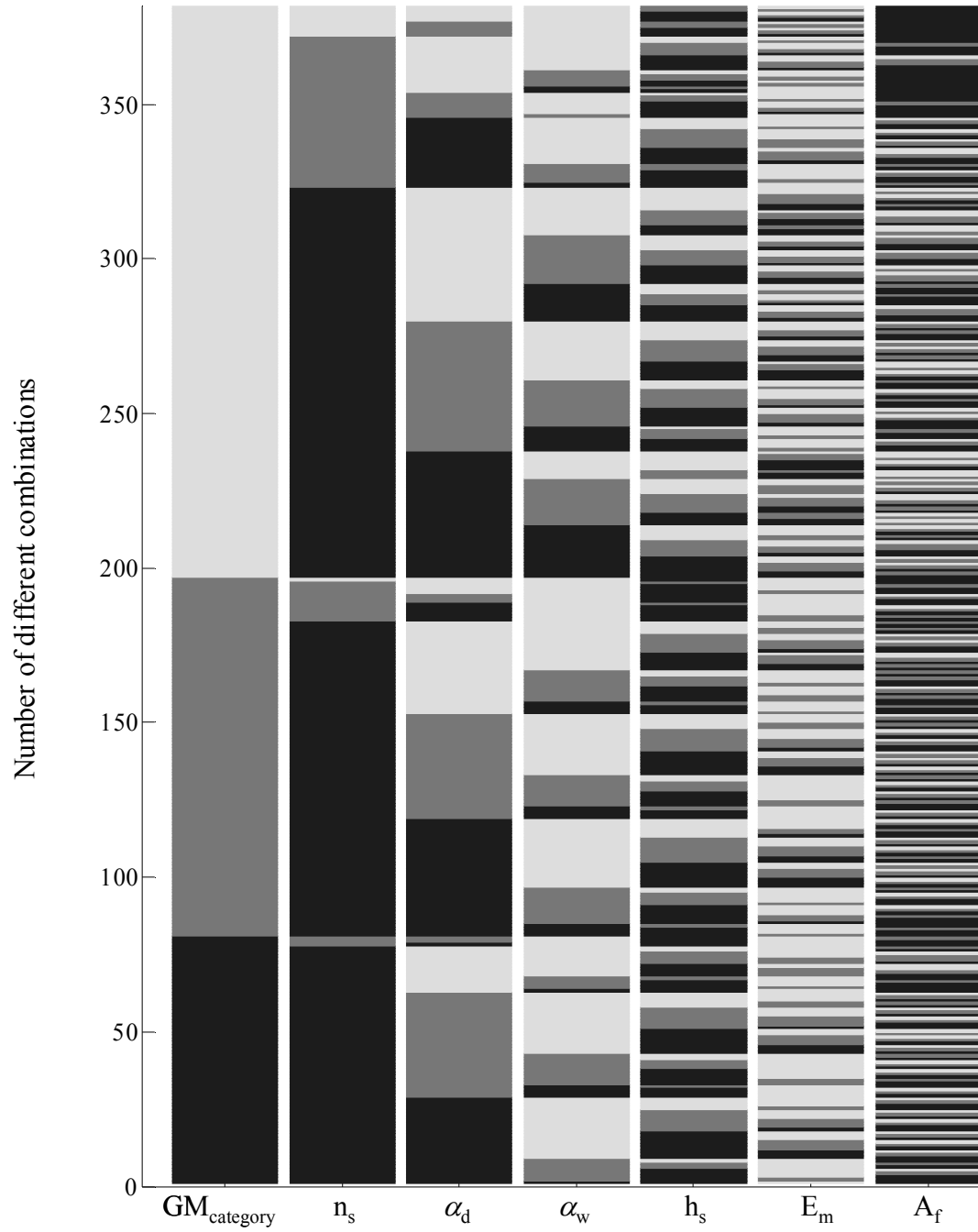
Figure B.3. Combination of parameters in Group 2

B.4. Group 3
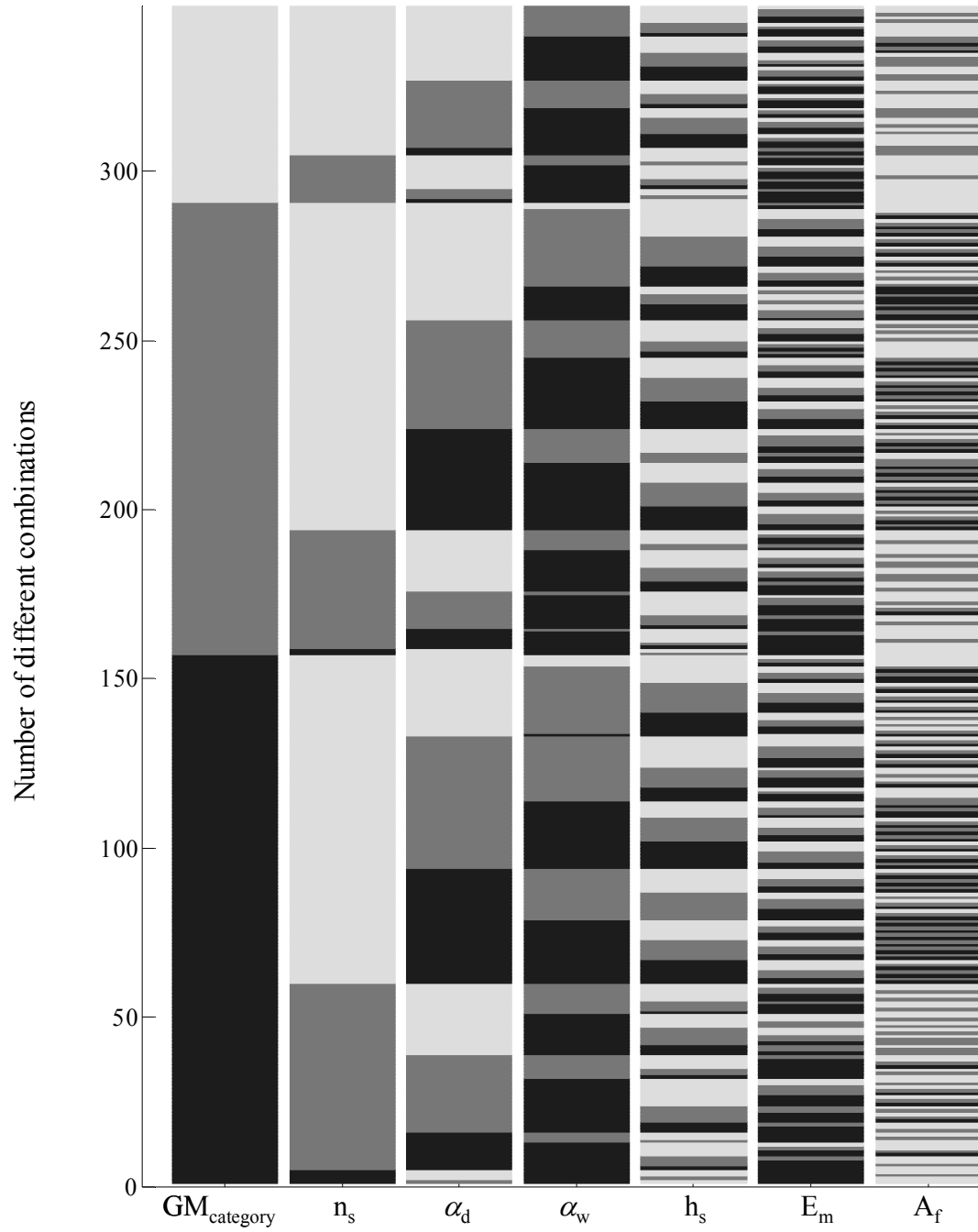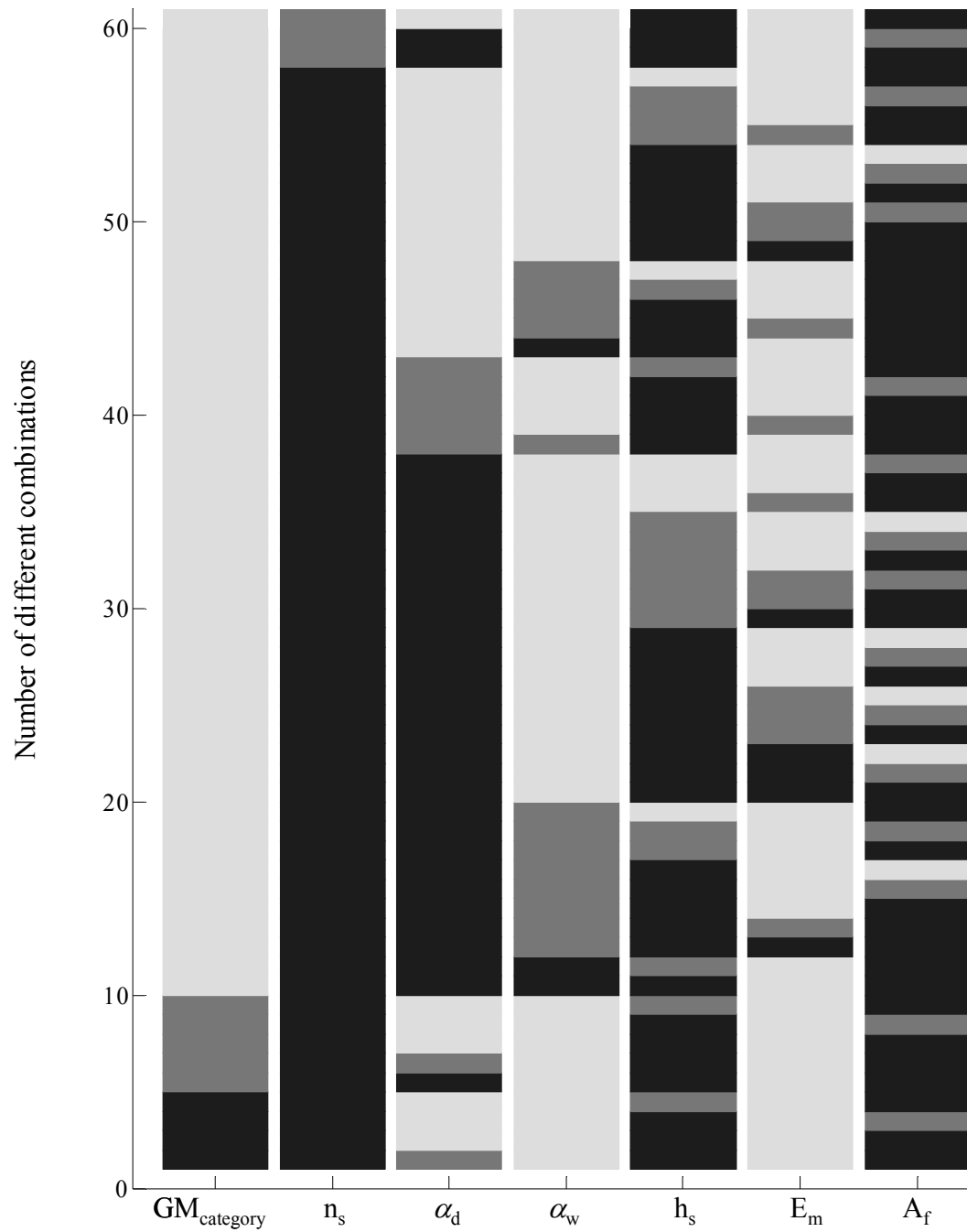

Figure B.4. Combination of parameters in Group 3

Figure B.5. Combination of parameters in Group 4
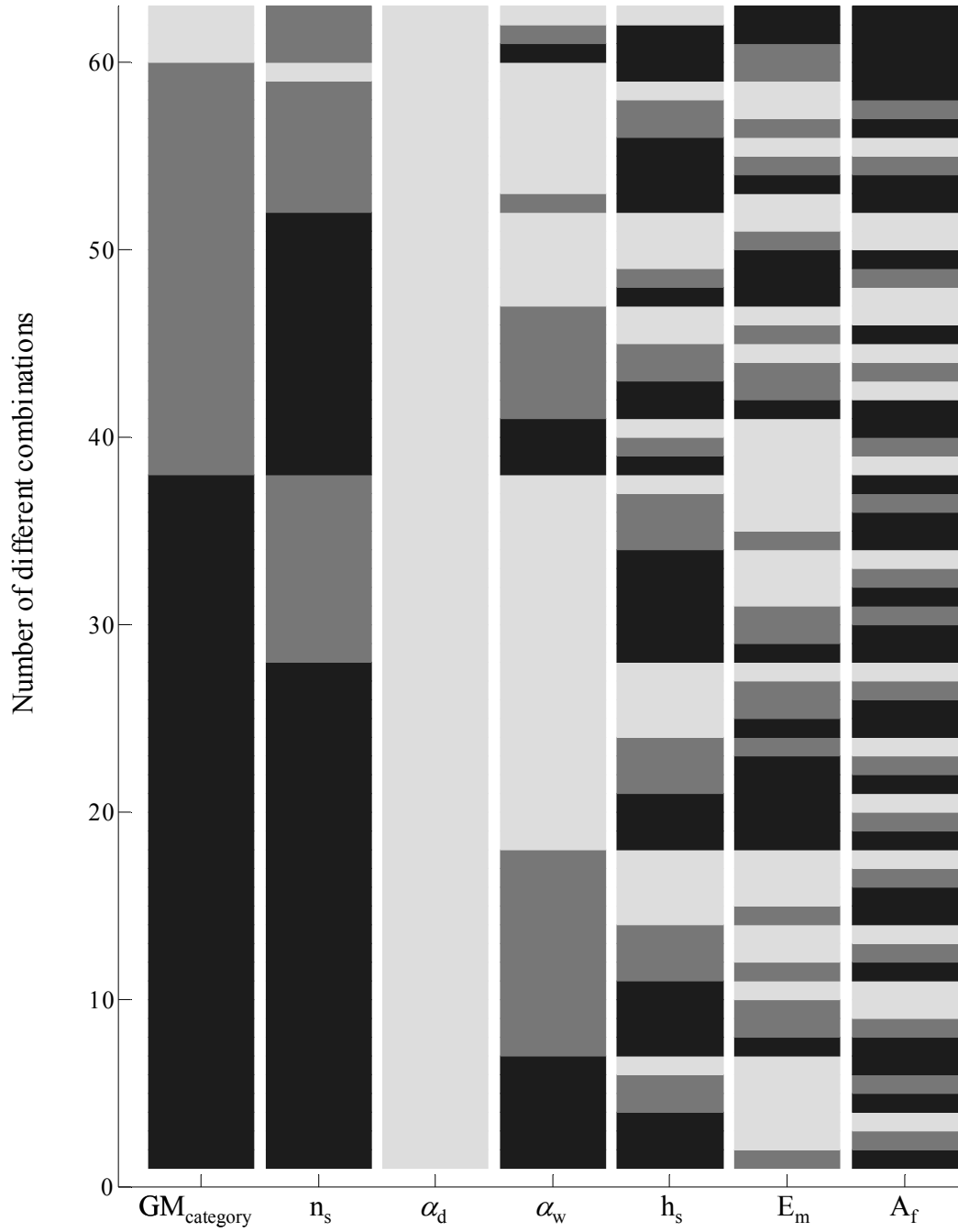
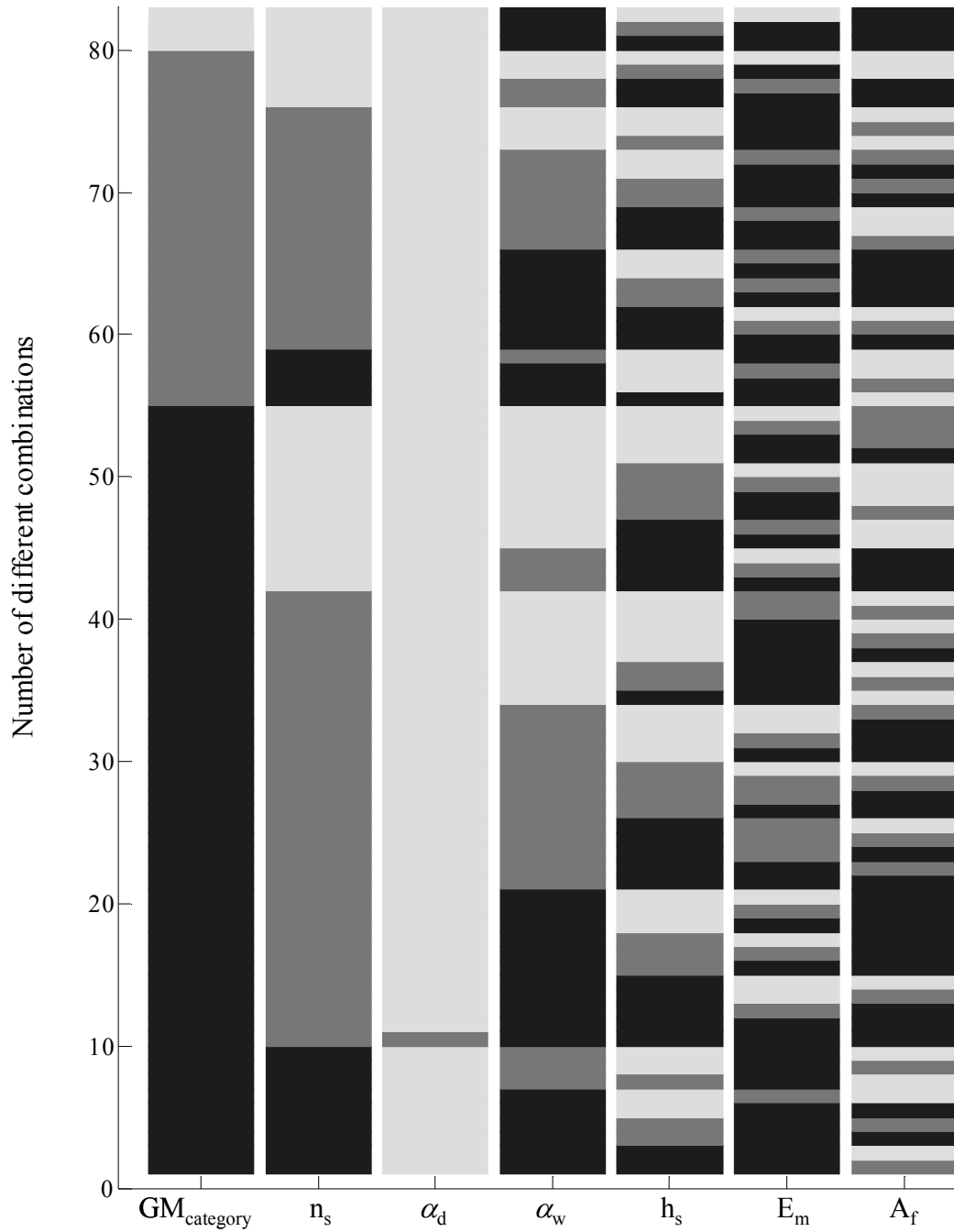Figure B.6. Combination of parameters in Group 5

B.7. Group 6
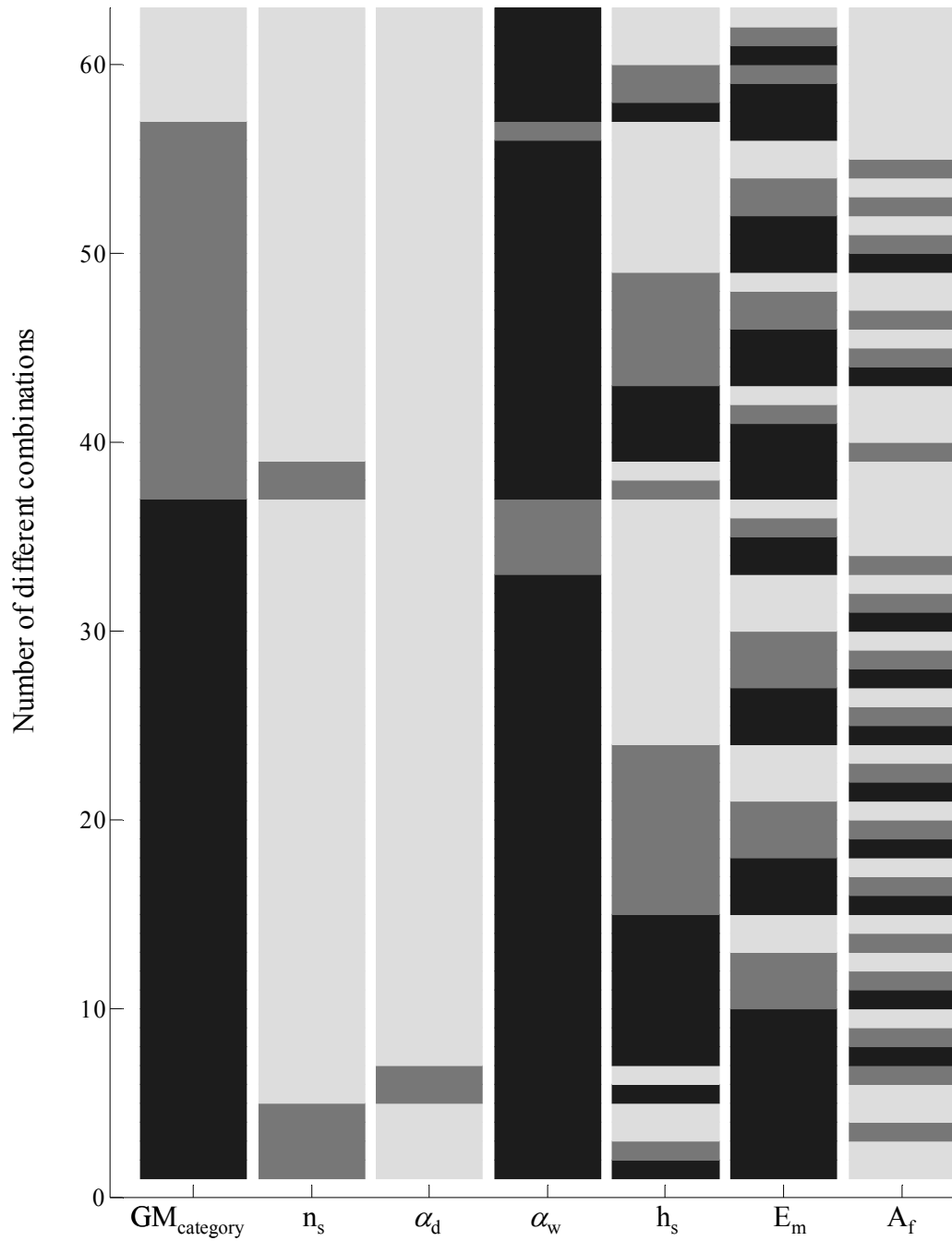

Figure B.7. Combination of parameters in Group 6

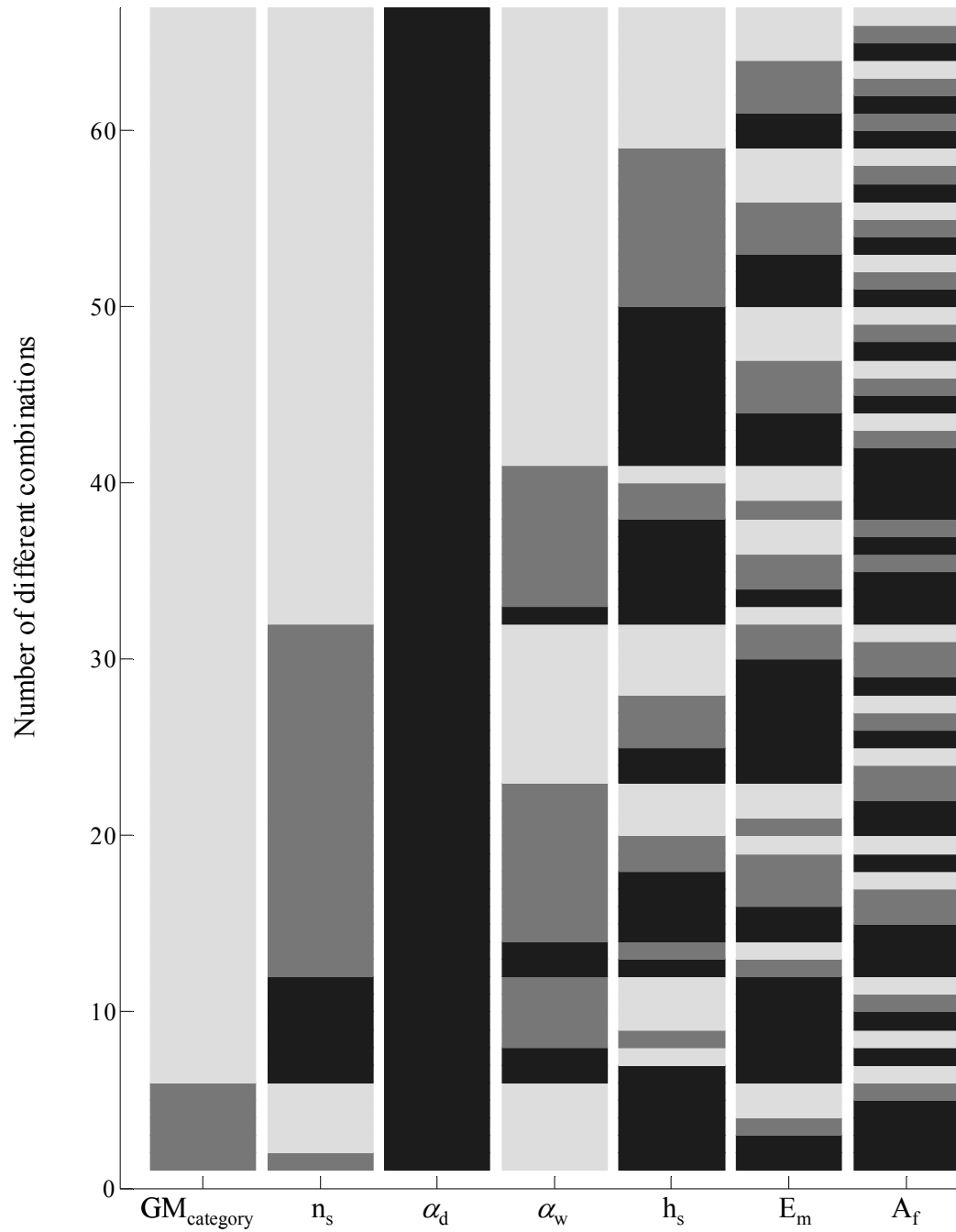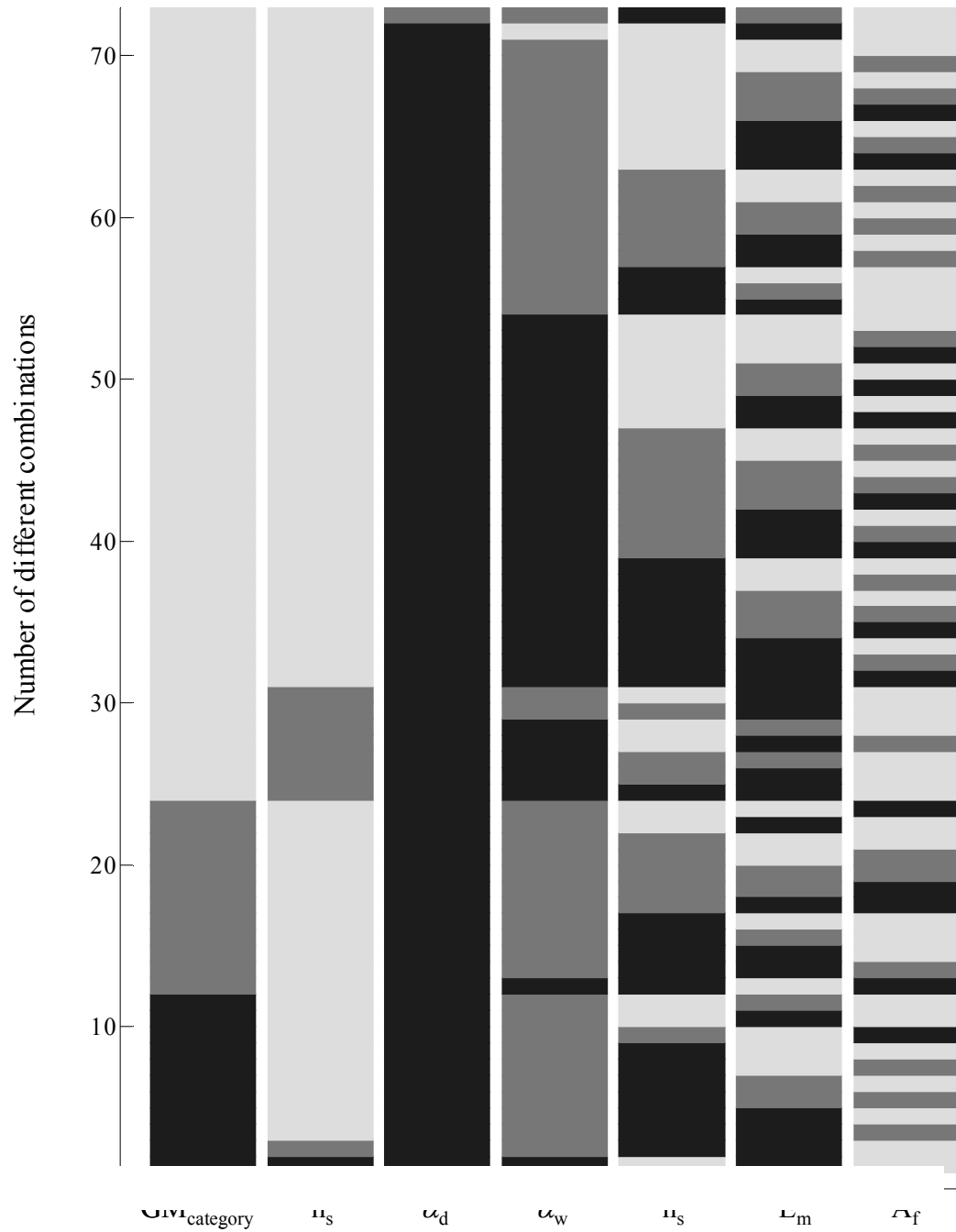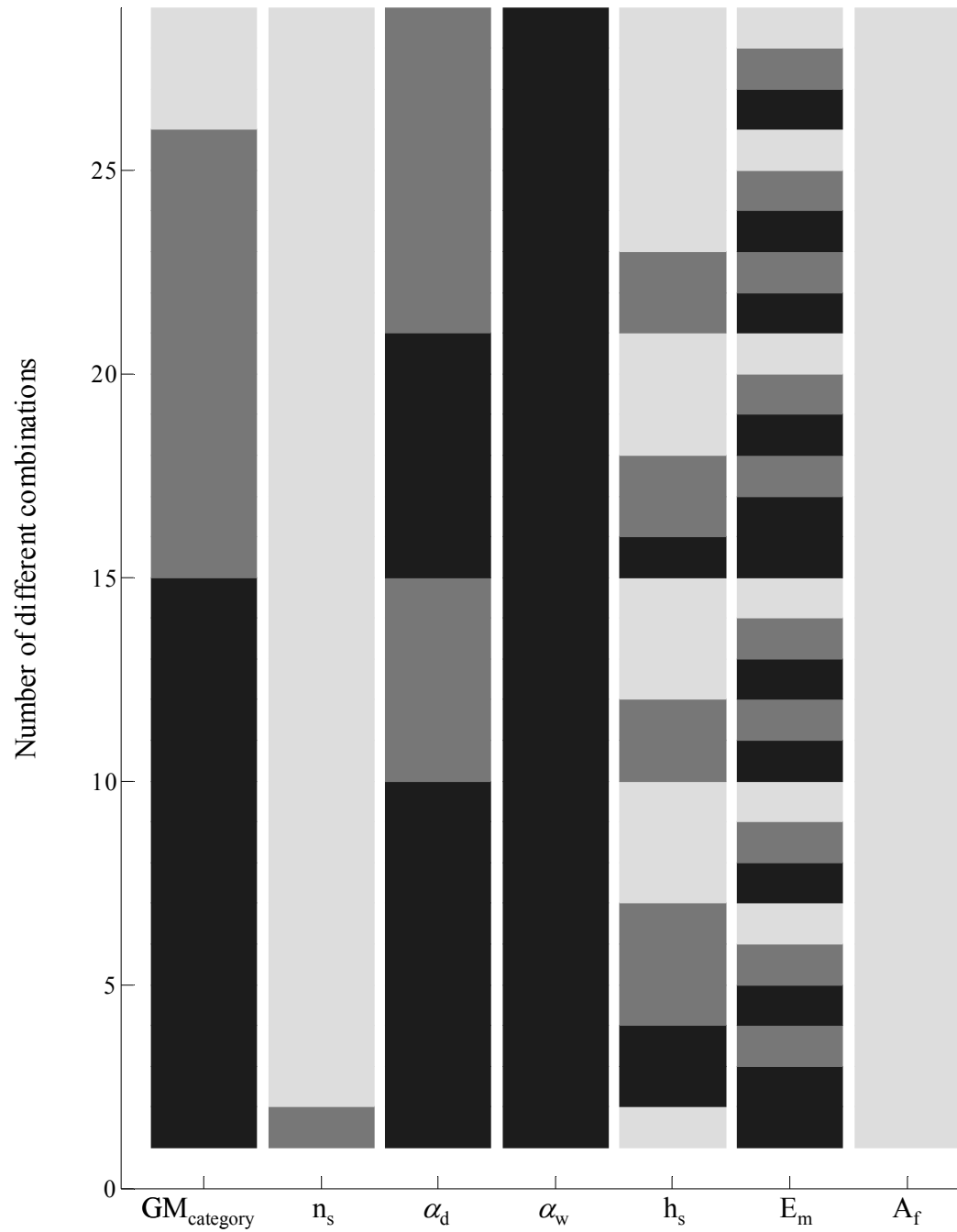Figure B.8. Combination of parameters in Group 7

B.9. Group 8

Number of different combinations

Figure B.9. Combination of parameters in Group 8

Figure B.10. Combination of parameters in Group 9

Figure B.11. Combination of parameters in Group 10

APPENDIX C A FORM TO BE USED IN COLLECTING POST EARTHQUAKE DAMAGE AND INVENTORY DATA OF UNREINFORCED MASONRY BUILDINGS

C.1 Introduction

As discussed in Chapters 4, 7, and 8, verification of analytical relationships is very important before utilizing them in real life applications. Such kind of verification requires complete data sets including not only the damage state but also the physical properties of buildings. Only with these kinds of data sets one can investigate the accuracy of analytical relationships and identify sections in the process that need further improvement.

To address the need of collecting complete data sets after earthquakes, a form is developed and presented in this section. The form is designed to include building parameters that are determined to be significant for regional loss calculations. Depending on other needs, additional parameters can be added to the form.

One form is used for one building. Each form consists of three sections. The first section is designed to gather general information about the building. Information includes use, location, value, and total floor area. Also included in this section are the building and the picture ids that are used for indexing purposes. The second section is designed to assign a damage state to the building. Schematic drawings from EMS-98 damage scale are provided to visually aid the categorization of damage. A verbal description of each damage state was provided in Table 2.5. The third section is designed to collect physical properties of buildings. Here, the investigator is given two options: 1) measure the actual value and record it, 2) assign a range to each value based on personal judgment through visual inspection.

It should be noted that the form is only designed to collect information about buildings. To complete the data set, the investigator should also gather information about the soil and geological conditions of the region. If available, ground motion data from the event that caused the damage should also be included in the data set. The best form of compiling data on soil conditions and hazard is through plotting them on the region map. These maps can be used together with building location data (coordinates) to estimate hazard and soil conditions under each building.

C.2 The form

GENERAL INFORMATION

Date: _____   Use[*]: ☐ Residential ☐ Commercial   ☐ Office
                                       ☐ Industrial   ☐ Pub. Assem. ☐ School

Building Id: _____   ☐ Govt. Bldg. ☐ Emer. Serv. ☐ Hist. Bldg.

Address: _____   Total floor area: _____

_____   Monetary value: _____

Photo Ids: _____   Location: _____ _____

[*]List is taken from ATC-21, 1988   Latitude   Longitude

DAMAGE CATEGORY[**]
[**]Figures taken from EMS-98, 1998

☐ Negligible   ☐ Moderate   ☐ Substantial   ☐ Heavy   ☐ Collapse
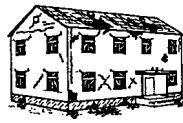
---

PARAMETERS

	Measured[+]	Estimated range based on judgment[+]				
Number of stories:		☐ —	☐ 1	☐ 2-3	☐ 4-6	☐ > 6
Floor area (ft²):		☐ < 1000	☐ 1000-2300	☐ 2300-4800	☐ 4800-30000	☐ > 30000
Floor aspect ratio:		☐ —	☐ 1.0-1.8	☐ 1.8-2.8	☐ 2.8-3.5	☐ > 3.5
Story height (ft):		☐ < 9	☐ 9-13	☐ 13-15	☐ 15-20	☐ > 20
Masonry elastic modulus (ksi):		☐ < 500	☐ 500-700	☐ 700-1000	☐ 1000-1200	☐ > 1200
Exterior wall thickness at the 1st floor (in), x:		☐ 2 wyhtes	☐ 3 wyhtes	☐ 4 wyhtes	☐ 5 wyhtes	☐ > 6 wyhtes
y:		☐ 2 wyhtes	☐ 3 wyhtes	☐ 4 wyhtes	☐ 5 wyhtes	☐ > 6 wyhtes

[+]Provide a measured value or select a range from the table based on judgment

Wall density[++] (%), x: _____
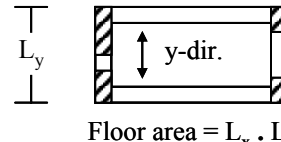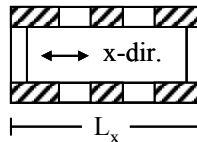
Wall density[++] (%), y: _____

[++]Ratio of shaded wall area to floor area

Floor area = $L_x \cdot L_y$

COMMENTS